University of Southampton

Optical micro-resonators in chalcogenide glass

By
Gregor Robert Elliott

Thesis submitted for degree of

Doctor of Philosophy

Faculty of Science, Engineering and Mathematics
Optoelectronics research centre

January 2009

Acknowledgements

I would like to thank my supervisor Prof. Dan Hewak for the opportunity to undertake this PhD, for suffering my interminable dyslexic first drafts with good grace, for his advice, support, and friendship, and for discussions about horse riding and keeping chickens. I have been very fortunate to have such a kindred spirit as a supervisor.

I would like to thank all of my colleagues at the Optoelectronics Research Centre and collaborators at other universities, Daniel Jaque, Deb Kane, Richard Curry, and John Rarity. Particular thanks go to Kenton Knight, Edwin Weatherby, Mark Lessey, Roger More, Andrew Webb, Fei Xu, for technical support. The assistance of Eleanor Tarbox has been of great help throughout the whole PhD.

Special thanks go to my family who have helped immeasurably to get me through some dark, dark times in a dark, dark lab. Particularly Kira and Torin who probably do not even know they helped, but one should not underestimate the ability of small children who do not care about your problems, to bring perspective. To my father who did a great job for 18 years and I still miss constantly. To my mother, my sisters Jaci and Fiona, my brother Duncan and all of their families, without whose help it would have certainly been a harder job.
Finally, I am very grateful to Fran for keeping me on the straight and narrow the past few months and to John for his help with the troublesome chapter 6.

University of Southampton

Faculty of Science, Engineering and Mathematics

Doctor of Philosophy

Optical micro-resonators in chalcogenide glass

Abstract

By Gregor Robert Elliott

This thesis focuses on the production of gallium lanthanum sulphide (GLS) microspheres and their potential uses. Microspheres, and micro-resonators in general, have attracted considerable attention because of their promise in all-optical-switching, micro-lasers, multiplexers and many other applications. In this thesis, several applications have been investigated, culminating in the demonstration of laser action in a neodymium doped GLS microsphere.

The method of microsphere production used here was to drop crushed glass through a vertical furnace purged with an inert gas, typically argon. Bulk glass was crushed to a suitable size and uniformity before microsphere production. The glass was crushed with a pestle and mortar, and sieved to achieve glass particles of the required size. Systems have been designed and developed for the production of microspheres and these have resulted in microspheres with diameters from 0.5µm up to 580µm being achieved. The failure to confirm spheres of a smaller size than this owes more to the equipment used to analyze the samples rather than a lack of spheres themselves. The material that has passed through the furnace will typically contain a mixture of particles that have melted into spheres and particles that have not. A system has been put in place to separate spherical particles from non-spherical ones. Together these production and separation systems have resulted in the reliable and reproducible production of microspheres in GLS as well as other types of glass.

The quality of a resonator is quantified in its Q-factor. This can be measured by coupling light into a microsphere and observing the spectral intensity of scattered light. Using this method GLS microspheres were shown experimentally to have a Q-factor of up to 1.2×10^5 at a wavelength of 1.5µm. It is also possible to calculate a maximum theoretical Q-factor for a given material, from its attenuation. By using data for the theoretical minimum attenuation of GLS /GLSO a maximum possible Q-factor has been calculated as over 4×10^{10} in GLSO at 3µm and 10^9 at 1µm. Similarly by using attenuation measurements made on state of the art GLSO a maximum Q factor of 10^7 at 1µm was calculated.

The possibility of using microspheres as ball lenses has been investigated and shown to be possible. Laser action was observed in a neodymium doped GLS microsphere. The laser had a threshold of 83mW of incident pump power, with a peak at 1082nm and a line width of <0.05nm.

TABLE OF CONTENTS

Table of figures

Tables

1 Introduction

Although the concept of making integrated optical devices using circular micro-resonators was first proposed in 1969 [1], the use of electrons rather than photons has dominated research and development in the field of integrated circuits. However, in recent years, all-optical networks have become the norm in long distance telecommunications, and there is increasing interest in trying to replace electrical components with their optical counterpart. Resonators are of particular interest for the design of optical components and systems, because of their ability to transmit very specific wavelengths of light and also because the intensity of light inside a resonator can be orders of magnitude higher than the incoming light. These properties could be potentially useful in a number of optical components.

This project is concerned with circular optical resonators, their production in chalcogenide glasses and their use. The aim of this project is firstly, to investigate production of resonators in chalcogenide glass, secondly to characterise the resonators and thirdly to look at possible applications for these resonators.

1.1 The motivation

Micro resonators have been proposed for the production of a variety of optical components. These include, but are not limited to, logic switches, routing switches (add drop multiplexing) and lasers. The fact that light will propagate through a suitably small resonator at only very specific wavelengths, is a key factor in their exploitation. For example, if broadband light travels through a waveguide next to a resonator, it will couple to the resonator through its evanescent field and a specific wavelength or wavelengths will resonate, while the rest of the broadband light in the waveguide will be almost unaffected. If the resonator is coupled to a second waveguide, then the resonating light can be coupled out. The same process works in reverse producing an add drop multiplexer or wavelength switch.

If the resonator is made of a non-linear material, a logic switch can be produced [2-4]. Through nonlinear effects, the refractive index can be changed by the intensity of light in the resonator. This changing refractive index will cause the resonant wavelength to vary, which can then in turn be used to switch a signal on or off, or tune the resonance for use at a specific wavelength.

The natural resonant properties of circular resonators can be utilized as a laser cavity [5] if the resonator incorporates a gain medium. This eliminates the need for using mirrors to provide

the feedback mechanism of the laser cavity, because the microsphere cavity is inherently resonant.

In addition to coupling to waveguides, micro-resonators can be coupled to other micro resonators or a series of resonators [6]. Microspheres are a three-dimensional form of micro-resonator, these spheres are able to be moved around [7-9] and could form the basis of reconfigurable circuitry. If a line of such resonators were constructed, light could be coupled from one to the next along the line, forming a whispering gallery mode waveguide [10]. The configuration of the spheres could then be changed such that light would follow a different path. Furthermore, micro-resonator lasers can be used to produce memory devices [11], by utilizing the difference between the clockwise and anticlockwise modes of circular resonance. Micro barcodes [12, 13] rely less on the resonant property of microspheres and more on their manoeuvrability, and the ability to make them from glass doped with rare earth ions or other dopants. The rare earth ions in the glass fluoresce at very specific wavelengths, and because of the manoeuvrability of microspheres they can be attached or printed onto items [12, 13]. All of these are highly useful applications. However it is quite probable that there are many other useful applications that may not yet have been considered. Therefore the study of resonators potentially carries considerable reward.

Glasses are widely used in optoelectronics, particularly silica glass. However as the use of glass has moved beyond basic transportation of light, the need has grown for more optically active materials, these glasses have become more exotic to meet this need. Chalcogenide glasses are noted for having high refractive indices and corresponding highly nonlinear properties, and could therefore be used in all-optical-switching. Their range of transmission reaches from the visible, well into the infrared, beyond the transmission range of more conventional oxide glasses [14]. Some chalcogenides such as gallium lanthanum sulphide glasses (GLS) can be readily doped with rare earth elements, making them useful for active optical devices, such as amplifiers and lasers [15].

This project focuses on gallium lanthanum sulphide (GLS) / gallium lanthanum sulphide oxide (GLSO) glasses, which are non-toxic (unlike many chalcogenides that contain arsenic), have a high melting temperature and many other useful properties [16]. The refractive index of GLS/GLSO is between 2.1 and 2.5 [17] depending on the composition and wavelength. Through *Miller's Law*, a high nonlinear index is expected and has been experimentally validated [18, 19]. This high nonlinearity is in part a motivating factor for the production of high Q GLS/GLSO micro-resonators.

In this report, evidence is presented of the first chalcogenide microspheres made by in-flight melting of crushed glass, the first chalcogenide microsphere laser, the quality (Q) values that have currently been measured and the Q-factor that these microspheres could potentially achieve, as well as investigations into their environmental robustness.

1.2 This report

This thesis is broken down into several chapters. Chapter 2 is concerned with the background to the topic, firstly the basic science of resonators, chalcogenide glass and associated optics are outlined, then possible fabrication methods are discussed, and finally potential applications are given. Chapter 3 contains a more in depth look at the theory and its application to GLS resonators. Chapter 4 describes the fabrication of microspheres, the various developments that have been made and goes on to discuss some characterisation methods of the microspheres. Chapter 5 contains the measurements that have been carried out to quantify the potential usefulness of these microspheres. In Chapter 6 the effects of rare earth doping and observations of laser action in GLS microspheres are described. Chapter 7 contains a discussion of potential future work that could be carried out with microspheres and planar devices.

2 Background

The background section looks at the science behind resonators and chalcogenide glass, and at the applications and devices that arise from them. All of these applications or devices could utilise chalcogenide micro-resonators, but currently none of them do. This is therefore a new and exciting opportunity for original research in the field.

2.1 Review of fundamental science

2.1.1 Circular resonators

In a circular body, it is possible for light to propagate in a mode of continuous total internal reflection, such that the light effectively travels round the surface of the circle. When light propagates in this fashion, it is said to exist in a whispering gallery mode (WGM), in some ways this is like the way sound travels around the whispering gallery in the dome of St Paul's Cathedral [20]. When this happens, the light travelling round the circle will cause interference, either constructively or destructively. This leads to only very specific wavelengths of light propagating within the whispering gallery mode.

The light frequency that can effectively fit an integer number of wavelengths into the circle will propagate, while light that has a non-integer number of wavelengths will destructively interfere.

Analysis of the spectrum of light in the whispering gallery mode will find sharp peaks where the light has an integer number of wavelengths fitting into the circle.

Each time the light circulates round the resonator it will interfere. So the more times the light travels round the resonator, the more precise the wavelengths of light that propagate in the whispering gallery mode become, i.e. the narrower the bandwidth of each spectral peak.

The quality factor (Q) of a resonator is a measure of how well the light travels round the resonator. A value for the quality factor of a resonator can be obtained from the ring down lifetime of the resonator (τ) and the angular frequency (ω) [21].

Equation 2.1

$$Q = \tau\omega$$

The quality factor of a resonator is limited by three factors, the internal or material losses, the radiation loss and the surface scattering. They are related by the equation

Equation 2.2

$$Q^{-1} = Q_{mat}^{-1} + Q_{surf}^{-1} + Q_{curv}^{-1}$$

Q factors in silica resonators can been obtained as high as 10^9 [22].
There are other forms of micro resonator such as droplets or hollow spheres[23], but these will not be discussed further.

2.1.2 Chalcogenide glass.

Glasses which incorporate any of the Chalcogen group of elements (e.g. sulphur, selenium, and tellurium) are known as the chalcogenides. This group of glasses is noted for having high refractive indices and, consequently, highly nonlinear properties. Their range of transmission reaches from the visible, well into the infrared, beyond the transmission range of more conventional oxide glasses [14].
The Novel Glass group at the University of Southampton primarily studies chalcogenide glass, particularly gallium lanthanum sulphide (GLS) and gallium lanthanum sulphide oxide (GLSO). GLS has the advantage of being non-toxic, unlike more common chalcogenide glasses containing arsenic. The glass has a refractive index of approximately 2.1-2 .5 [17], increased visible transmission over other chalcogenides and consequently it exhibits one of the highest levels of nonlinearity in a glass [18, 19], especially when the two photon absorption is taken into account Gallium lanthanum sulphide can hold very high dopant concentrations of rare earth ions (lanthanides) because the lanthanides bond into the glass matrix in a similar way to the lanthanum ions, this makes it a good host medium for any kind of fluorescent device.
Chalcogenides can be produced as fibres [24] thin films [25] and have also been used to make waveguides [26-30].

2.1.3 Glass production

All samples of glass used in this project were produced in-house at the ORC, from raw materials purified and synthesised in-house. Glasses were melted prior to the start of this project. However for completeness some mention should be made of the glass production procedures. These techniques were developed by Brady [31], Mairaj [32] and Hughes [33], whilst glass production has been carried out by Kenton Knight.
GLS glass is made from the raw materials gallium sulphide, lanthanum sulphide and lanthanum oxide in batches, with each batch given a number (e.g. LD984). The exact proportion of each raw material used can be varied to produce glasses from the heavier gallium lanthanum sulphide (GLS) through to the lighter gallium lanthanum sulphide oxide (GLSO). The purity of these raw materials is very important, as impurity ion concentrations as low as 1 ppm can result in strong absorptions [34].

The raw materials were not commercially available at the desired purities and were therefore produced in-house from precursor materials (gallium metal, lanthanum fluoride and gaseous H_2S). A system was developed to produce the raw materials by using flowing H_2S. The H_2S flows though a furnace where it passes over the heated gallium metal or lanthanum fluoride, the gas and solid react, leaving the solid resultant (lanthanum sulphide or gallium sulphide) in the furnace. The gaseous resultants are carried away, which prevents the same reaction happening in reverse [31-33].

Once the raw materials for glass production have been produced they are mixed into batches. This happens in a glove box, which is purged with dry nitrogen to avoid contamination. The moisture level in the glove box is monitored with a dew point meter and is kept below 1ppm. The raw materials are weighed and placed in a plastic bottle, which is rotated to achieve a uniform mixture. The mix is then placed in a vitreous carbon crucible and transferred to a furnace. The glass melt takes place at 1150^{o}C in a continuously purged argon atmosphere, which will carry away volatile impurities as well as preventing contamination. After melting, quenching takes place. The crucible is pushed out of the furnace into a silica water jacket, where it rapidly cools to form a glass, which can then be removed.

2.1.4 Rare earth doping / gain

Dopants are an important part of many active photonic systems, such as lasers and amplifiers. The spectroscopic properties of rare earth and transition metal dopants in GLS have been studied extensively in [34-46].

Rare earth ions are used in many lasers and amplifiers because of their useful absorption and emission bands. This allows them to be pumped at one wavelength and emit at another. The absorption and emission characteristics of the rare earths are well known. In GLS they are shifted to longer wavelengths than in oxide glasses because of the high refractive index [47]. When light passes through a sample of doped glass, light may be absorbed by one of the ions and cause an electron to become excited into a higher energy state. If absorption is observed the energy of the photon will correspond to the gap between two energy states[48].

Equation 2.3

$$h\upsilon = E_1 - E_2$$

If intensity I_0 of light is incident on an absorbing material, the intensity of light I_T that passes through a thickness l is governed by the Beer-Lambert law [33].

Equation 2.4

$$\alpha l = -\ln\left(\frac{I_T}{I_0}\right)$$

Where α is the absorption coefficient, usually given in units of cm^{-1}, which will be dependent on wavelength and absorbing species. This gives rise to absorption spectra, which are characteristic to a given type of absorbing species or combination of species (Figure 2.1).

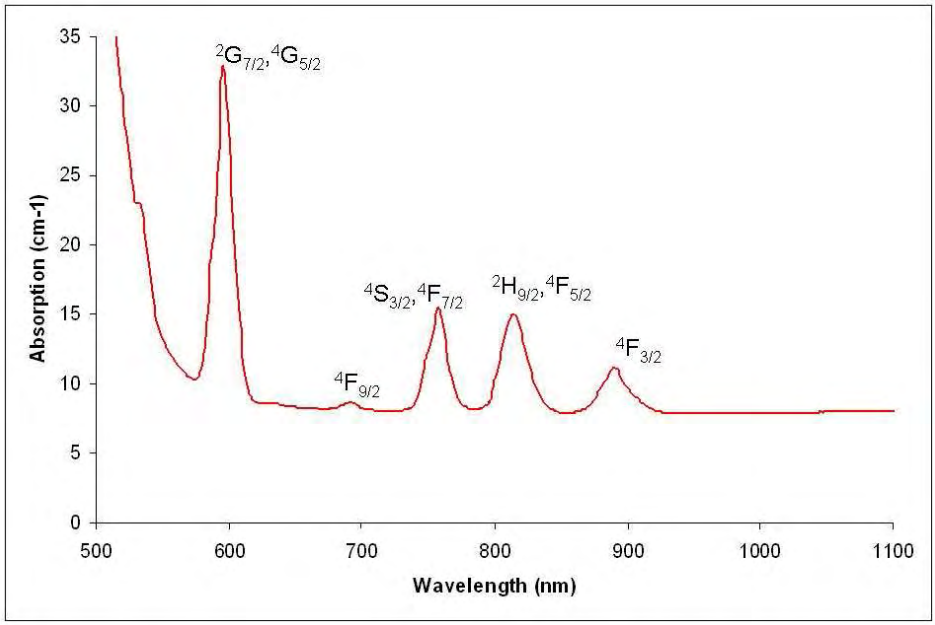

Figure 2.1 Absorption spectra from Nd:GLS with 1.5mol% dopant level

Once electrons are in an excited state they can decay to a lower state by a number of routes. The most useful route is via radiated decay, giving off a photon to reach a lower energy state. However they can also emit a phonon or, if the concentration of active ions is high, they can undergo cross relaxation [42]. The combination of these effects results in emission spectra with a number of peaks over a range of wavelengths when pumping occurs at only one wavelength (Figure 2.2).

Here the main purpose of observing rare earth fluorescence is to aid the design and construction of a laser. In neodymium doped GLS, laser action has been achieved by pumping in the 815nm band, or 890nm band, which results in lasing from the 1060-1090nm band [15, 49, 50].

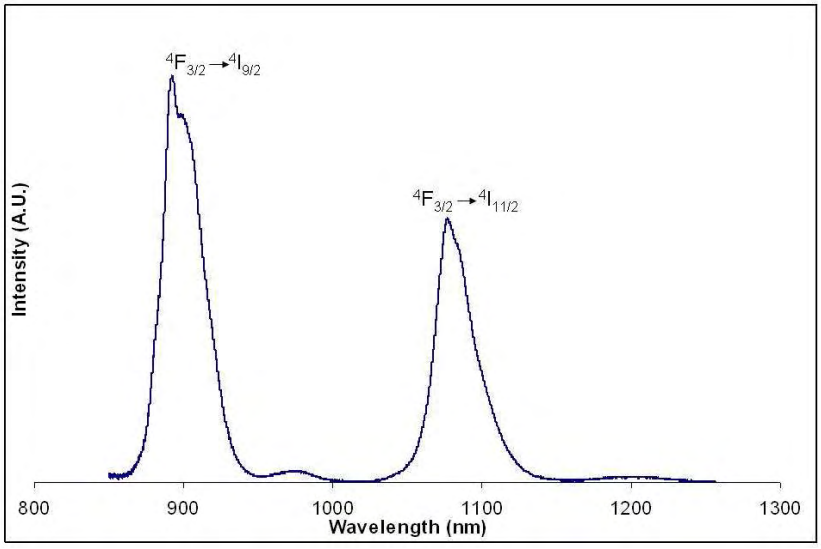

Figure 2.2 Emission spectra from Nd:GLS pumped at 808nm

The emission of a photon from an excited atom can occur by spontaneous emission or stimulated emission [48]. Spontaneous emission occurs when the electron decays from the excited state with no outside influence and in so doing it emits a photon. Stimulated emission occurs when a photon with the same energy as the excitation is present, this causes the excited electron to decay and emit a photon with the same energy, phase, polarisation and direction as the stimulating photon. These two photons can then go on to stimulate the emission of two more photons and so on, in a chain reaction, causing the original photon to be amplified. For stimulated emission to be the dominant process it is necessary for the upper energy level associated with the photon, to be more populated by electrons than the lower energy level (Figure 2.3 (b)). This is known as population inversion. If the opposite is true (Figure 2.3 (a)) then the dominant process, in the presence of radiation at the corresponding energy, will be absorption.

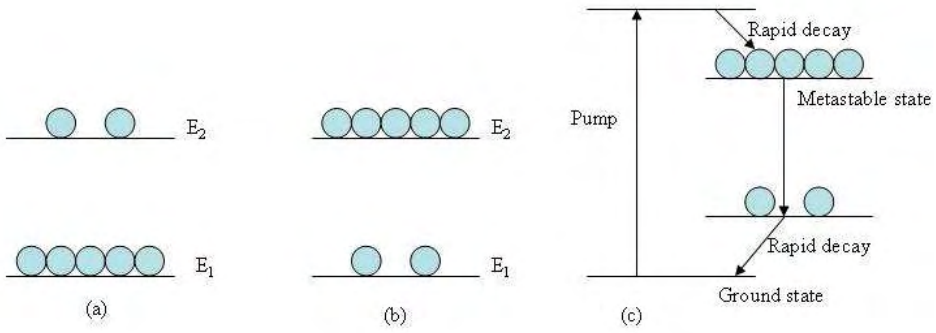

Figure 2.3 Energy levels of a system that will absorb (a), an inverted population (b), and a four level system to achieve population inversion (c).

To achieve a population inversion, a system of three or four levels is employed. In a four level system (Figure 2.3 (c)), such as Nd [50], electrons are pumped up to an excited state by

photons at one frequency, they then rapidly decay to a metastable state where the electron population can build up. From the metastable state they can decay to a lower energy level, emitting a photon of a different frequency from the pump. The electron will then decay rapidly back to the ground state. Because the metastable state has a longer lifetime than the lower level a population inversion will be allowed to occur, and stimulated emission can become dominant.

To make a laser it is necessary to have a resonator with a medium for stimulated emission inside of it. When a photon is spontaneously emitted in the correct direction it will resonate and be amplified. This will give rise to the lasers' characteristic light which is in phase, unidirectional and monochromatic.

2.1.5 Nonlinear effects

The classical view of light assumes that a medium will respond in a linear fashion when an oscillating electromagnetic field passes through it. At low powers this is held to be true but at higher powers other effects come into play [51]. The response of a material to the applied electrical field is given by

Equation 2.5

$$P = \varepsilon_0\left(\chi E + \chi^{(2)}E^2 + \chi^{(3)}E^3 + ...\right)$$

Where P is the polarisation, ε_0 is the permittivity of free space, χ is the linear susceptibility, $\chi^{(2)}$ and $\chi^{(3)}$ are the second and third order non-linear susceptibilities. The magnitude of χ is much greater than that of $\chi^{(2)}$ and $\chi^{(3)}$, which is why the nonlinear contribution is usually only noticeable with high amplitude electric fields (E). The second order nonlinear susceptibility ($\chi^{(2)}$) is zero in glasses because of their isotropy. This leaves $\chi^{(3)}$ as the main form of nonlinearity in glass.

Of particular interest to this work is the third order nonlinear refractive index change. This is an essential part of many nonlinear all-optical devices.

The polarisation in a glass can be written as

Equation 2.6

$$P = \varepsilon_0\left(\chi E(\omega) + \chi^{(3)}\left|E(\omega)\right|^2 E(\omega)\right) = \chi_{eff}E(\omega)$$

As the refractive index is a function of χ this gives rise to the intensity dependent refractive index [52].

Equation 2.7

$$n = n_0 + n_2 I$$

This can result in self focussing [14, 15, 52, 53] or bistability in resonators [54].

2.2 Sphere fabrication techniques

Three-dimensional resonators or microspheres can be made by a number of methods.
A common method of producing microspheres is to melt the tip of a glass filament [22] [55] (typically an optical fibre [56, 57]). This produces a single sphere which remains attached to the filament. The filament can then be used to position the microsphere wherever it is desired. This method is effective at producing individual high Q [57] microspheres which can be made into lasers. However as each microsphere has to be individually produced it would be impractical for use in devices where multiple spheres are required.
There are several methods of production that will produce a large number of spheres at once. These include pouring molten glass into liquid nitrogen [55], or onto a spinning disk [58, 59] which then flings out droplets that quench as they fly, and another is by passing crushed glass through a plasma [60]. It was reported that when pouring molten glass into liquid nitrogen, a poor quality surface was produced which had to undergo a chemical etch to produce a high Q sphere [55]; none of the other sphere production methods examined here had to undergo any kind of etch or polish. All of these methods will produce a large number of spheres with a range of sizes.
Microspheres made from optical fibres will have an extra step in the production process, compared to microspheres produced directly from bulk glass. To form an optical fibre, bulk glass will have to be drawn into a filament, which will then be melted to produce a microsphere. Therefore, this introduces another point at which contamination can occur, for these reasons the chalcogenide microspheres that we produce are made from crushed bulk glass.
Our preferred method of microsphere production is to drop crushed glass through a furnace [61], called the in flight melt-quenching method. Other methods were tried [61], such as chemical etching and rapid quenching of molten GLS in liquid nitrogen, but these were found to produce an inferior surface quality, compared to those produced by the drop furnace method.
In the preferred method the crushed glass melts as it drops through the furnace, surface tension pulls it into a sphere which quenches as it drops to the cooler region beyond the hot zone.

2.3 Review of prior art

As already mentioned the very sharp transmission lines that characterise WGM in micro-resonators make them useful for a number of applications, such as add-drop multiplexers, switches and lasers. In most cases the principle behind these devices will work for either spheres or disc resonators, because the devices exploit the WGM properties of circular resonators and both spheres and discs are types of circular resonator. Spheres, discs, rings etc. would be produced in different ways and would therefore have to be incorporated into devices and setups in accordingly different ways. Some of these potential uses are discussed here.

2.3.1 Wavelength filters/and drop multiplex

Micro-resonators are ideal for wavelength division, such as add drop multiplexing or wavelength filters, because of the very narrow band that will resonate. If the waveguide is coupled to the micro-resonator, broadband light can be passed through the waveguide and only very specific wavelengths will be diverted through the resonator. The off-resonance wavelengths of light will be unaffected [10] and will continue along the waveguide. If there is a second waveguide on the other side of the resonator, this method can be used to couple the light in and out of an analysis channel, thus making a simple wavelength specific add drop multiplexer or wavelength filter [1, 6, 62-64]. Several resonators can be coupled together to change the characteristics of the pass band [65]. The light then travels between the resonators via the evanescent field, in the same way that it does between the waveguide and the resonator in the one resonator system. If the add drop multiplexer is made out of chalcogenides glass, it will have all the associated advantages, such as a wider transmission window than is achieved with silica glass. However, to avoid the nonlinear effects associated with chalcogenides, the system would have to operate at low power.

2.3.2 All optical switching

The basic design of a circular resonator add drop multiplexer is very similar in structure to an all optical switch based on a circular resonator [4], but the resonator is made of a third order nonlinear material, so the refractive index is a function of the intensity of light. The resonant wavelength can be altered as the intensity in the resonator changes, and instead of the device passively diverting specific wavelengths, it will divert, or not divert, a wavelength as the intensity changes.

In recent years, micro-ring resonators [2, 3, 66, 67] and chalcogenide glasses [18, 19] have separately come under scrutiny for their potential to yield all-optical-switches. But to the best of our knowledge no one has yet combined these two fields.

It has long been thought that the increased intensity inside a resonator could be utilised for all optical switching and, in recent years, this has started to be achieved [2, 3, 66, 67]. In order for switching to occur in a circular resonator, the increased intensity inside the WGM has to trigger third order nonlinearities in the resonator medium, this causes the refractive index to change, which in turn changes the resonance of the resonator, causing the resonator to start or stop transmitting.

The ultimate goal of this field is to replace electronic microchip processors with optical processors. This requires the development of logic gates, which can be densely integrated onto an optical chip. Some optical logic gates have been developed [2, 3], but as yet no integrated system of optical switches or optical processor has been demonstrated.

2.3.3 Micro resonator lasers

As well as having potential uses in switching, micro-resonators are a natural choice for use as laser cavities [5, 68, 69], because by their very nature they are intrinsically resonant cavities thus eliminating the need for mirrors. A laser can be produced with a gain medium in the resonator and the relevant pump source, hence avoiding having to tune the cavity itself. Most microsphere lasers use rare earth doping as a gain medium [5, 55, 57-60, 70-72], but a Raman laser has been produced using a microsphere [56].

The coupling method used to pump the laser and collect the light will have a significant effect on the characterisation and performance of a microsphere laser. A number of methods have been used to couple a microsphere laser, including an angle polished fibre tip [72], a fibre taper [5, 56, 58-60, 71], a bulk prism [57] and free space coupling via a microscope objective [55, 70]. Each method has its advantages and disadvantages. Fibre taper coupling is widely used, it is efficient at coupling to a minimal number of modes and therefore maximising intensity in those modes. However fibre tapers are fragile and therefore unsuitable for integration into devices. Angle polished fibres are more robust than tapers, but their positioning relative to the microsphere is highly critical to achieving laser action. A bulk prism will be versatile but bulky. Free space coupling via a microscope objective is inefficient, but relatively simple in design.

All of these coupling methods are for laboratory examination of small numbers of spheres. For integration into robust devices it will most likely be necessary to couple using integrated waveguides.

2.3.4 Memory devices

Two ring lasers, coupled to a waveguide, can be used to make a memory device [11]. The system (Figure 2.4) has two stable states, corresponding to the clockwise (CW) and anticlockwise (ACW) lasing modes. In state a, a pulse of light sets Laser A lasing, the light from Laser A injection locks laser B, forcing it to lase only in the CW direction. In state b, a pulse of light sets Laser B lasing causing it to injection lock Laser A, forcing it to lase only in the ACW direction. The resonator state can be read by comparing light from the two ends of the waveguide and can be controlled with a pulse at the corresponding input. A digital system can be constructed with one end of the waveguide corresponding to logic one and the other to zero.

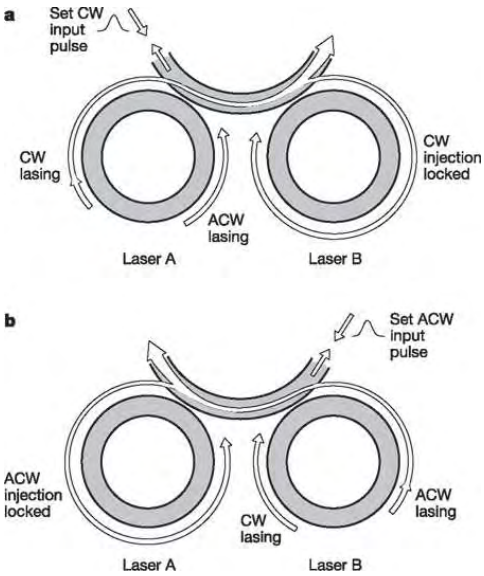

Figure 2.4 Memory device of Hill et al [11]

2.3.5 Reconfigurable circuits

Some of the proposed uses for micro resonators are only achievable with certain types of resonator. Reconfigurable circuits require that the resonators can be physically moved [7, 8], so three-dimensional resonators or microspheres represent the best option. If the group of microspheres are arranged, one next to the other, light can be coupled from one whispering gallery mode to the next and will propagate along the line of microspheres. As the light is propagating in the whispering gallery modes, the straightness of the line of microspheres has no bearing on its propagation. The configuration of microspheres can then be moved to produce an entirely different circuit [9].

2.3.6 Chemical and biological sensors

The field of chemical and biological optical sensors is well established [73] and the property of a resonator to increase the accuracy of these sensors is widely used [23]. These sensors

work on the principle that light interacts with material on the surface of the resonator through the evanescent field [23, 74], if the material in the evanescent field changes this will affect the refractive index, which will alter the resonance. GLS does not respond well to contact with water [75], however it could be used in some hostile environments such as in oil or solvents. For a resonator to operate it must have a higher refractive index than its surroundings. The high refractive index of GLS would allow it to operate in a high refractive index environment such as in oil.

2.3.7 Micro barcodes

Micro barcodes also rely on the mobility of small glass particles, unlike previous uses, they do not necessarily rely on their resonant properties. Micro barcoding is a system of tagging using glass microspheres [12, 13] doped with rare earth ions, to produce unique spectra. It can be used in areas as diverse as microbiology [13], for tagging and tracking samples, and anti-counterfeiting measures for currency and goods, by using them to print marks which would not normally be visible.

The fluorescence and absorption spectra of rare earth ions are sufficiently sharp that a combination of ions can be put into one sphere to produce a spectrum with a series of peaks, analogous to a barcode (Figure 2.5), hence making each sphere identifiable and distinguishable from one another.

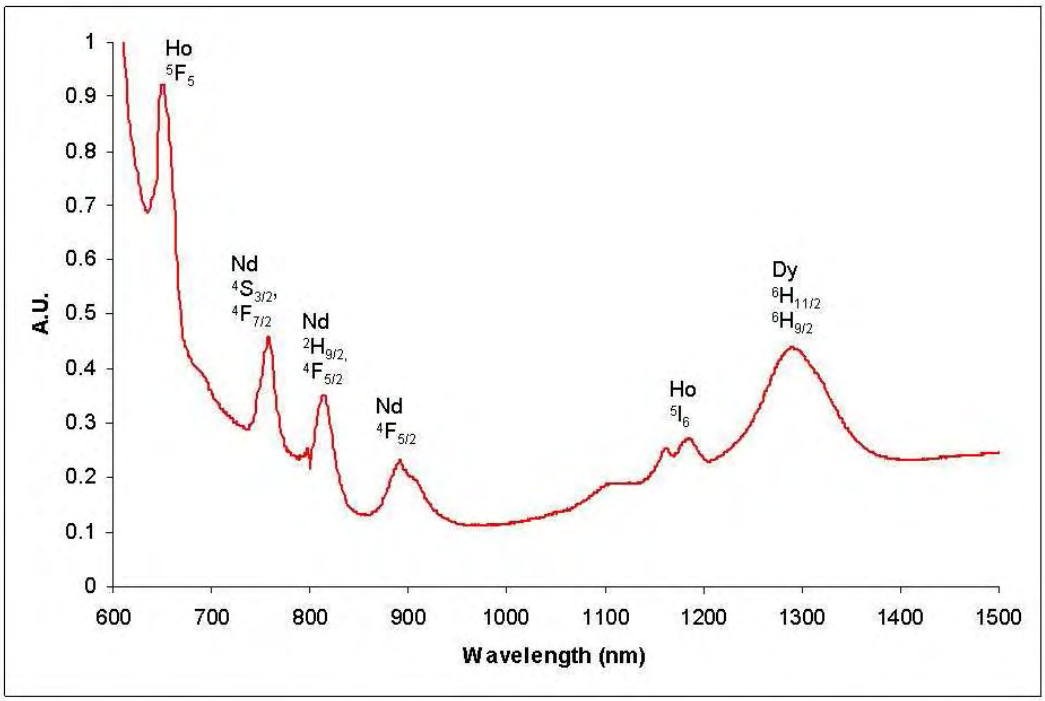

Figure 2.5 Possible absorption spectra for a combination of Nd, Ho and Dy. Labels show peak origins [47]. This spectrum was produced by combining absorption spectra for each dopant.

2.3.8 Photonic crystals

Photonic crystals are highly interesting materials that could prove important in replacing electronic components with photonic components [76]. Crystals are made up of a regular periodic repeating pattern of their basic components. In true crystals, this is on the atomic or molecular level. However, in photonic crystals, this pattern is artificially built into the structure, typically by producing a material with regularly spaced holes.

It has been suggested that a photonic crystal could be constructed from regularly spaced spheres. Microspheres would have the advantage that they will naturally form a close packing structure (Figure 2.6) [76, 77]. It has been suggested that such a structure could be made by holding microspheres in suspension in the solvent, then allowing it to evaporate on a flat surface. The surface tension would pull the spheres together into a close packing structure as the solvent evaporates, producing a self assembled photonic crystal [78, 79].

The properties of chalcogenide glass, combined with the characteristics of a photonic crystal would make the fabrication of such a structure highly interesting avenue of investigation.

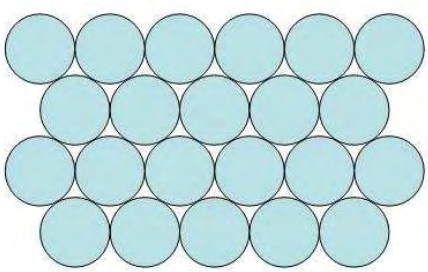

Figure 2.6 Close packing structure of spheres, which results in an artificial crystalline structure.

2.3.9 Ball lenses

It has been suggested [80] that ball lenses could be used to improve the coupling efficiency of pigtailed laser diodes. The material that laser diodes are made from has a high refractive index, which causes the beam to diverge as it leaves the diode and this makes it difficult to couple it to a standard fibre with a much lower index. A ball lens made from a high index glass (Figure 2.7) could be used to couple the light from the diode to the fibre.

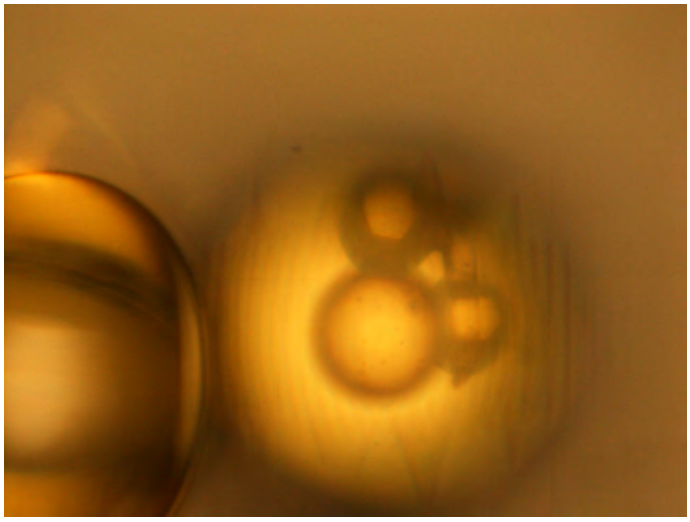

Figure 2.7 Microsphere lens. A microsphere is visible on the left. In the centre the reflection of the three spheres attached to a fibre can be seen focussed through a microsphere, with the striped background of a graticule.

2.4 Summary

The study of chalcogenide microspheres has potential to impact on a number of areas. The high Q factors associated with microspheres and the readiness of GLS to accept rare earth ions, will allow narrow linewidth laser action at low pump thresholds. Whilst a number of other application are possible due to the properties associated with the Q factor.

Some of these devices have been demonstrated or worked towards in this work, whilst others have not been attempted. They have been included here as it is considered helpful to understand the wider potential of these resonators.

3 Theory

This chapter looks at the theory of circular micro-resonators and chalcogenide glass, and presents calculations that show the potential of chalcogenide micro-resonators in a variety of applications.

The most significant aspects of a resonator are its discrete pattern of transmission and its capacity to build up high circulating intensities. The Airy function describes the basic transmission characteristics through a resonator and from this it is possible to determine the internal circulating intensity.

The Airy function only describes a simple resonator such as a Fabry-Perot etalon or a thin circular ring resonator. It is possible to derive a more accurate depiction of the resonances of a cylindrical or spherical cavity, but these will not be examined as the description given by the Airy function is sufficient to understand the principles and possibilities involved.

In order to make calculations regarding the potential uses of a resonator it is necessary to quantify its quality. This is done using the quality factor (or Q-factor), which is a measure of mode damping, and calculations have been made here on the potential Q of a GLS / GLSO resonator.

The Q-factor and the intensity of light circulating inside the resonator can be influenced by many effects such as coupling, scattering and bending loss. For many applications of resonators there will be a trade off between a number of aspects to produce the optimal system and this optimisation will be discussed. One interesting area of application for micro-resonators involves combining nonlinear material such as a chalcogenide into a resonator, this gives rise to effects such as modal movement, bistability and switching. Such all-optical-switches could be used in a number of devices.

Micro-lasers are another exciting area of applications for micro-resonators. They have the potential to produce lasers with low threshold and narrow linewidth. Calculations are made here based on previous GLS lasers and will be looked at from an experimental point of view in chapter 6.

3.1 Airy function

The Airy function gives a simple picture of the transmission through a resonator and the interference that occurs. Here we will look at the derivation of the Airy function and apply it to circular resonators.

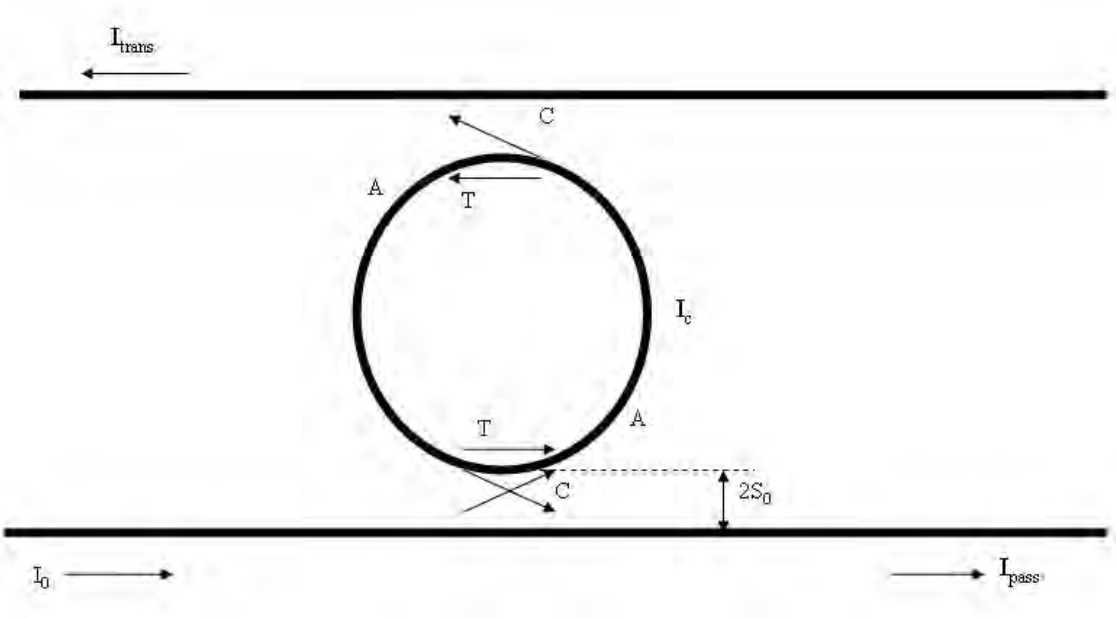

Figure 3.1 Schematic of a ring resonator showing intensities and energy coefficients.

In a circular body, it is possible for light to propagate in a mode of near continuous near total internal reflection, such that the light effectively travels round the perimeter of the circle. When light propagates in this fashion, it is said to exist in a whispering gallery mode (WGM). Whispering gallery modes occur when the effective circumference of the sphere is equal to an integer multiple of wavelengths, allowing the propagating fields to build up constructively. The nature of this interference can be derived mathematically. Following the method of Hecht [51] it can be shown that, by starting with a wave coupled into the resonator with intensity I_0 , it is possible to calculate the intensity of the light that is transmitted through the resonator I_{trans} (Figure 3.1). This is similar to the derivation of resonance in a Fabry-Perot cavity [51].

As the wave propagates it is subject to losses, due to a range of factors such as internal absorption, surface scattering and coupling to any nearby waveguide. This will cause the amplitude of light in the resonator to decay as it propagates.

The wave will also be subject to a phase shift (δ) due to the optical path length of a circuit. If k is the wave vector, p is the path length of one complete circuit and n is the refractive index, then the phase shift is given by

Equation 3.1

$$\delta = kpn$$

Each time the field circulates around the resonator part of it will be coupled out, therefore the total transmitted electrical field (E_t) will be a sum of the waves that propagate around the resonator.

Equation 3.2

$E_t=E_1+E_2+……..+E_N$

Where E_1 is the electrical field to be coupled out of the resonator which effectively passes straight through, E_2 is the second field out (the field that is coupled out after one circuit) and E_N is the Nth electric field coupled out (having undergone N-1 circuits).

If t is the electric field transmission coefficient around half of the ring then all of the calculations can be taken to occur at the point of coupling and, if we assume a lossless system, conservation of energy dictates that T+C=1. Where T is the energy transmission coefficient (t^2=T) and C is the coefficient of energy coupled in or out. Here κ^2=C, κ' is the coefficient of field coupled out of the resonator and κ is the coefficient of field coupled into the resonator and should not be confused with k in Equation 3.1.

$$E_1 = E_0\kappa\kappa' e^{i\omega\cdot time}$$
$$E_2 = E_0\kappa\kappa' t^2 e^{i(\omega\cdot time-\delta)}$$
$$E_3 = E_0\kappa\kappa' t^4 e^{i(\omega\cdot time-2\delta)}$$
$$\ldots$$
$$E_N = E_0\kappa\kappa' t^{2(N-1)} e^{i(\omega\cdot time-(N-1)\delta)}$$

Therefore the transmitted electric field (E_t) becomes

Equation 3.3

$$E_t = E_0\kappa\kappa' e^{i\omega\cdot time} + E_0\kappa\kappa' t^2 e^{i(\omega\cdot time-\delta)} + \ldots.$$
$$= E_0\kappa\kappa' e^{i\omega\cdot time}\left\{1 + t^2 e^{-i\delta} + t^4 e^{-i2\delta} + \ldots\ldots\right\}$$
$$= E_0 e^{i\omega\cdot time}\left\{\frac{\kappa\kappa'}{1-t^2 e^{-i\delta}}\right\}$$

As t is a coefficient with a magnitude less than 1, therefore $t^2 e^{-i\delta} < 1$.

Giving

Equation 3.4

$$\left|E_t\right|^2 = I_{trans} = I_0\left\{\frac{(\kappa\kappa')^2}{\left(1-t^2 e^{i\delta}\right)\left(1-t^2 e^{-i\delta}\right)}\right\}$$

Assuming that the system is lossless ($1 = t^2 + \kappa^2$) this becomes

Equation 3.5

$$I_{trans} = I_0 \left\{ \frac{(1-t^2)^2}{1+t^4-2t^2+4t^2\sin^2(\delta/2)} \right\}$$

Leading to the Airy function

Equation 3.6

$$\frac{I_{trans}}{I_0} = \frac{1}{1+F\sin^2(\delta/2)}$$

Where F is the coefficient of finesse.

Equation 3.7

$$F = \left(\frac{2t}{1-t^2} \right)^2 = \frac{4T}{(1-T)^2}$$

Where t is the electrical field transmission around half of the ring, or the coefficient of the field that is not coupled out at each waveguide port and T is the corresponding coefficient of energy transmission. This does assume that the system is lossless and will not be the case if the resonator incurs loss.

Equation 3.6 will have a maximum value of 1 and a minimum value of $\frac{1}{1+F}$ (Figure 3.2).

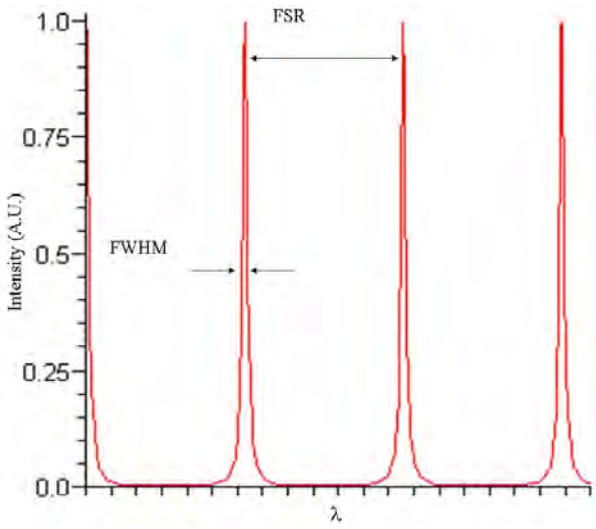

Figure 3.2 Plot of intensity transmitted through a ring resonator, with a transmission value T=0.9.

If a more realistic system is now considered which includes losses, the coupling coefficient is no longer C=1-T, and becomes C=1-T-A, where A is the fractional power loss in half a revolution of the ring. Equation 3.5 then becomes

Equation 3.8

$$\frac{I_{trans}}{I_0} = \frac{C^2}{1+T^2-2T+4T\sin^2(\delta/2)}$$

or

Equation 3.9

$$\frac{I_{trans}}{I_0} = \left(\frac{C}{A+C}\right)^2 \frac{1}{1+F\sin^2(\delta/2)}$$

The coefficient of finesse can now be defined as

Equation 3.10

$$F = \left(\frac{2t}{1-t^2}\right)^2 = \frac{4T}{(1-T)^2} = 4\frac{1-A-C}{(A+C)^2}$$

By similar reasoning to Equation 3.3 [51]

Equation 3.11

$$\frac{I_{pass}}{I_0} = \left|t - \frac{t\kappa\kappa' e^{-i\delta}}{1-t^2 e^{-i\delta}}\right|^2$$

following a process similar to that used from Equation 3.3 to Equation 3.6 using C=1-T-A instead of C=1-T, it follows that

Equation 3.12

$$\frac{I_{pass}}{I_0} = \frac{(1-A)F\sin^2(\delta/2) + \frac{A^2F}{4}}{1+F\sin^2(\delta/2)}$$

This means that the minimum and maximum values are altered. Considering Equation 3.12 in the form

Equation 3.13

$$\frac{I_{pass}}{I_0} = 1-A+\left(\frac{A^2F}{4}-1+A\right)\frac{1}{1+F\sin^2(\delta/2)}$$

It becomes clear that as Equation 3.6 tends to 0, Equation 3.13 will tend to 1-A and when Equation 3.6 = 1, Equation 3.13 = $\frac{A^2F}{4}$. These will be the minimum and maximum respectively provided $A+\frac{A^2F}{4}<1$, otherwise this situation will be reversed. This will be the case for any useful system as A<<1.

Resonant properties can give a value of circulating intensity much higher than input intensity because of the build up of light in the resonator. This does not contravene conservation of energy as the resonator is storing the light. The fact that the maximum value is larger than 1 does mean this function differs from a typical Airy function and is better modelled as for a Fabry-Perot etalon [51].

3.2 Q factor

In order to accurately compare resonators and calculate their usefulness for a particular purposes it is necessary to be able to quantify their ability to resonate, this is known as the quality factor or Q factor. The Q-factor is a measure of mode damping in a resonator and can be affected by any source of loss from the resonator such as material losses or coupling.
The Q factor of the resonator is defined as

Equation 3.14

$$Q = \tau\omega$$

Where τ is the decay time and ω is the angular frequency of the light. This implies that Q represents the number of radian cycles of light before the intensity decays to 1/e of its original level [21]. Here we mean the cycles of the EM field of the light, which should not be confused with circuits around the resonator.
Defining a system where q is the number of circuits of the resonator required for the energy to fall to 1/e, and V is the coefficient of energy transmitted through one circuit of a resonator ($V=T^2$), then decay will be

Equation 3.15

$$\frac{1}{e} = V^q$$

Hence

Equation 3.16

$$\frac{-1}{\ln V} = q$$

Therefore the distance travelled (d), before decay to 1/e, is

Equation 3.17

$$d = 2\pi Rq = pq$$

Using the definition of the speed of light, c, in a medium with refractive index, n.

Equation 3.18

$$\frac{c}{n} = \frac{d}{\tau} = \frac{pq}{\tau}$$

By combining Equation 3.18 and Equation 3.16

Equation 3.19

$$\frac{c}{n} = -\frac{p}{\tau \ln V}$$

Substituting into $Q = \tau\omega$

Equation 3.20

$$Q = -\frac{p\omega n}{c \ln V}$$

Or

Equation 3.21

$$Q = -\frac{\delta}{\ln V}$$

This means that Q can be defined in terms of phase shift and transmission per circuit, alternatively if linear decay distance is considered a similar equation can be derived for loss.

Equation 3.22

$$d = -\frac{p}{\ln V} = -\frac{1}{\ln(1-\alpha)} \approx \frac{1}{\alpha}$$

Where α is the fractional loss and ln(1-α) will be the logarithmic attenuation.

As Q is the number of radian cycles to decay, this gives the equation often quoted [81] equation for Q due to attenuation

Equation 3.23

$$Q \approx \frac{2\pi n}{\alpha\lambda}$$

lnV is a logarithmic attenuation, similar to dB, however a conversion factor is needed in order to use units of dB in these equations (Equation 3.28). As logarithmic values of attenuation can be added, the inverse of Q can be added to give a total Q from the Q factors due to individual sources of loss [81, 82].

Equation 3.24

$$Q^{-1} = Q_1^{-1} + Q_2^{-1} + Q_3^{-1}$$

This means that Q for the system defined in the previous section is

Equation 3.25

$$Q \approx \frac{kpn}{2(A+C)}$$

the factor of 2 occurs because A and C relating to half of the resonator and therefore appear twice in one round trip, see Figure 3.1.

If A and C are measured using a logarithmic scale (e.g. dB), which may be more convenient experimentally, then Equation 3.25 will become an exact equation.

The quantity A incorporates all forms of loss from the ring, other than the coupling, therefore the equation can be expanded to explicitly include other forms of loss. The intrinsic quality factor of a resonator is limited by three main factors, the radiation loss due to the curved nature of the resonator (Q_{curv}), the surface scattering (Q_{surf}), and the internal or material losses (Q_{mat}) this term will include the Rayleigh scattering, electronic absorption and multiphonon absorption. In addition to these three factors, the observed Q will be influenced by interaction with the coupler (Q_{coupl}). These terms are related as below [82].

Equation 3.26

$$Q^{-1} = Q_{mat}^{-1} + Q_{surf}^{-1} + Q_{curv}^{-1} + Q_{coupl}^{-1}$$

Examining the contributions, we note that if the diameter of the resonator is sufficiently large then losses due to curvature will be small [22]. The surface quality can be controlled by the production process and the impact from this should be minimized with improvements in technique. Therefore, as discussed in [22], for a sufficiently large sphere it may be possible to reach the ultimate limit where only the material loss limits the value of Q.

3.3 Maximum possible Q in GLS microspheres

It is possible to calculate the ultimate value of Q from the material losses, these calculations have been published as part of [83]. The attenuation of a material can be reduced by purification of the glass, minimizing contamination during the melting process and processing the spheres in a clean, dry environment. With control of these extrinsic impurities, there comes a point when an ultimate limit for attenuation is reached. This limit is a combination of electronic absorption, multiphonon absorption and Rayleigh scattering. The point at which this ultimate limit on attenuation occurs has been examined in detail for gallium lanthanum sulphide based glasses (GLS/GLSO) [84] and this data can be used to predict an ultimate Q for GLS and GLSO spheres.

According to [84] the loss of GLS is given by

Equation 3.27

$$\alpha = 1.81\times10^{-7}\exp\left(\frac{1.22\times10^{5}}{\lambda}\right)+5.06\times10^{6}\exp\left(\frac{-8.01\times10^{5}}{\lambda}\right)+\frac{5.89\times10^{-20}}{\lambda^{4}}$$

The numbers are derived experimentally and a similar equation is given for GLSO (Figure 3.3).

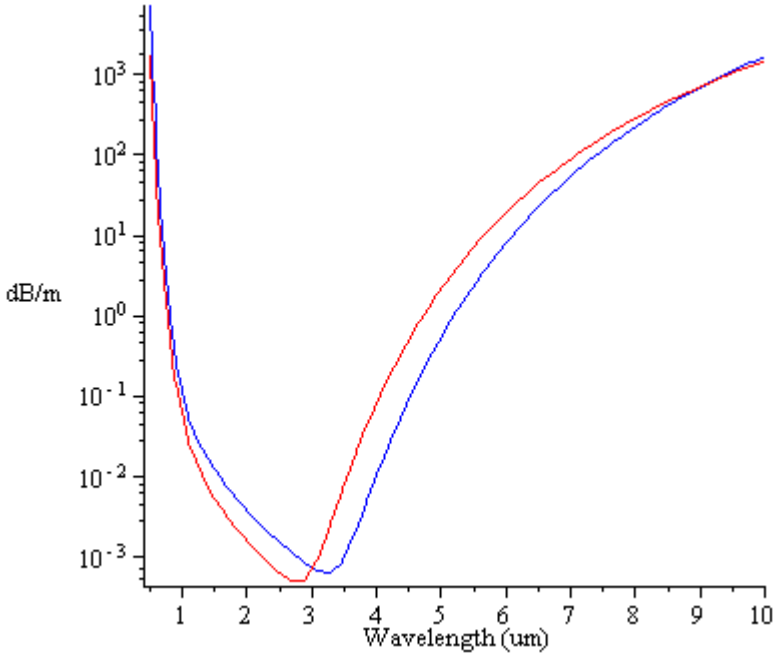

Figure 3.3 Minimum theoretically achievable attenuation of GLS/GLSO. GLS = blue, GLSO = red

This loss is given as dBm^{-1}, as this is a common unit of measurement, an equation for Q can be derived from Equation 3.23 in terms of dBm^{-1} following the reasoning of [22].

Equation 3.28

$$Q = \frac{10\log_{10}(e)kn}{\alpha_{dB/m}}$$

Note that the absorption is logarithmic therefore no approximation has been made in this equation, while k must be in the same units of length as the absorption coefficient (i.e. meters).

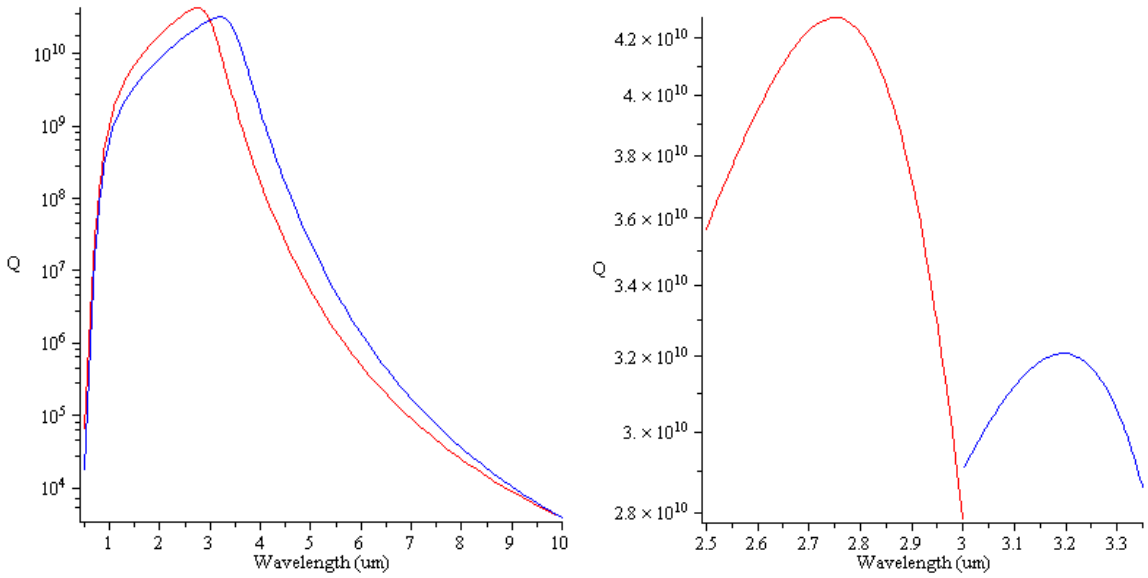

Figure 3.4 (a) Maximum theoretically possible value of Q for a range of wavelengths, with (b) a close-up on the peak, showing the wavelength dependence of the maximum Q. Here GLS = blue, GLSO = red.

With Equation 3.28 and the minimum attenuation data for GLS/GLSO (Equation 3.27) we can predict that in GLSO it is possible to have a maximum Q value of over $4x10^{10}$ at 3µm and 10^9 at 1µm (Figure 3.4). The values quoted here for GLS/GLSO are for specific compositions in [84], but these are typical of GLS/GLSO in general.

In a micro-resonator such values of Q would represent a significant enhancement of the circulating intensity, which would, in turn, significantly reduce the input power needed to observe nonlinear effects.

The minimum attenuation data given in [84] are calculated values, while these low values of attenuation are theoretically possible, they relate to a glass quality that has not been achieved. The current state of the art for minimum attenuation, measured in GLS / GLSO glass fibres, is detailed in [75].

Optical fibres drawn from bulk glass preforms are processed in an environment and manner not dissimilar to our sphere fabrication methods and are therefore more representative of the true Q which could be experimentally achieved. Using this data to calculate a theoretical maximum Q gives a value of 10^7 at 1µm (Figure 3.5).

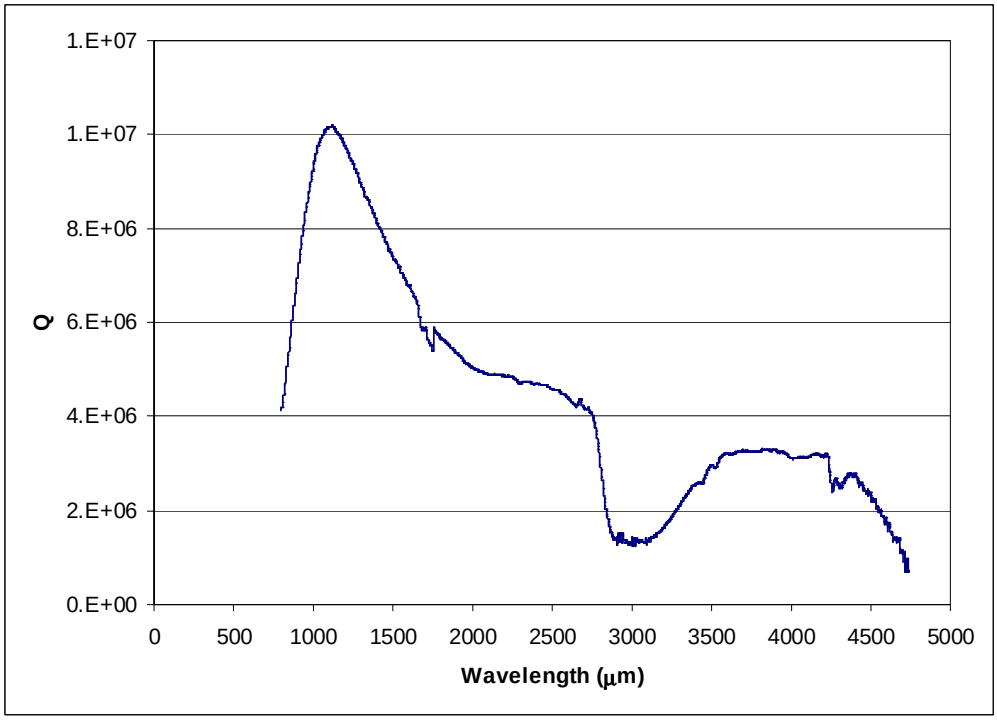

Figure 3.5 Q values calculated from attenuation of chalcogenide (GLSO) fibre. One can see the prominent dip due to OH absorption (water contamination) is observed.

The shape of the Q curve is significantly altered from the maximum theoretical value due to a number of other loss mechanisms such as absorption and scattering. A significant drop in Q can be seen at ~ 3μm due to OH absorption.

Again these values take no account of bending, coupling and surface scattering.

3.4 Methods of Q measurement

In order to understand the quality and therefore potential usefulness of a resonator it is necessary to have a physical measure of its Q factor. A value for the Q of a resonator can be obtained by measuring the full width half maximum (FWHM = $\Delta\lambda$) of each transmission peak (as shown in Figure 3.2) and comparing it to the resonant wavelength [82, 85].

Equation 3.29

$$Q \approx \frac{\lambda}{\Delta\lambda}$$

As Q increases the peaks will remain in the same position, but the width of the peaks will reduce.

As Q increases the cavity losses are reduced, this means that a pulse of light is able to circulate for a longer time before its intensity decays. This can be observed directly by measuring the change in intensity with time. As the circulation time for a photon is affected by the Q, so is the number of times it circulates and this in turn will affect the nature of the inference pattern. An increase in the number of circuits will increase the intensity at the resonant peak, but the point at which destructive interference occurs will move closer, making the resonant peaks become narrower and higher.

The two equations for Q (Equation 3.14, Equation 3.29) represent the two basic methods of measuring Q. Firstly by measuring the width of the spectral peaks and secondly by measuring the decay, or ring-down lifetime of the cavity [22]. This first method is described in more detail in the following section.

The cavity ring down can be measured by exciting a mode with a pump, then shutting off the mode and observing the decay in cavity emission.

The cavity lifetime is given by

Equation 3.30

$$\tau = \frac{Q\lambda n}{2\pi c}$$

Therefore a cavity with a Q of 10^5 and n=2.1, would have a ring-down time of 0.16ns at 1.5μm.

Because of the difficulties involved with measuring very short decay times or very narrow linewidths, it is most practical to use linewidths for cavities with low Q and ring-down for cavities with a high Q.

3.5 Full width half maximum (FWHM)

One of the most common methods for measuring a Q value from experimental data is to divide the resonant wavelength by the full width half maximum of the resonance peak (Equation 3.29) [82, 85].

Starting with the resonance/Airy function, defined earlier, then the minimum normalized value of transmission is given by

Equation 3.31

$$\frac{(I_{trans})_{\min}}{(I_{trans})_{\max}} = \frac{1}{1+F}$$

Where F is the coefficient of finesse defined earlier. For any useful system F>>1, therefore we can say that at half maximum.

Equation 3.32

$$\frac{1}{1+F\sin^2(\delta/2)}=1/2$$

Hence

Equation 3.33

$$\delta=2\arcsin\left(\frac{1}{\sqrt{F}}\right)$$

As the resonance pattern has a maximum at $\delta=0$, the above equation gives half width half maximum.

The finesse *(f)* is defined in [51], and this should not be confused with the coefficient of finesse (F).

Equation 3.34

$$f=\frac{\delta_{FSR}}{\delta_{FWHM}}$$

And

Equation 3.35

$$Q=\frac{pn}{\lambda}f \quad [85]$$

Where δ_{FSR} and δ_{FWHM} are the free spectral range (FSR) and FWHM in units of δ. If we are working in units of δ then the FSR is always 2π [51], therefore

Equation 3.36

$$f=\frac{2\pi}{4\arcsin\left(\frac{1}{\sqrt{F}}\right)}$$

Equation 3.37

$$f\approx\frac{\pi\sqrt{F}}{2}$$

Therefore it is possible to calculate a value of Q from knowledge of all loss mechanisms from a resonator, including coupling.

3.6 Coupling

For a circular resonator to be incorporated into a system such as an optical chip, light will have to be coupled in and out. This coupling will degrade the Q of the resonator, and it will therefore be necessary optimise the level of coupling for the resonator and the application in question.

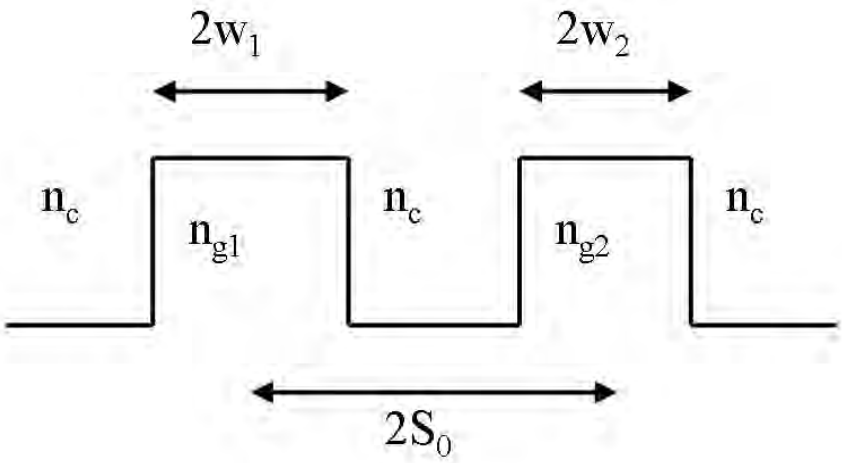

Figure 3.6 The geometry and index of the waveguide coupling system.

The coupling between two curved waveguides, or a curved waveguide and a straight waveguide, has been derived in [6]. The coupling constant is given by;

Equation 3.38

$$\kappa = \frac{\omega^2\left(n_g^2 - n_c^2\right)\cos(k_2 w_2)\sqrt{\pi R}e^{(\gamma_2(w_2-2s_0))}}{c^2\left(k_1^2+\gamma_2^2\right)\sqrt{\gamma_2\beta_1\beta_2\left(w_1+\frac{1}{\gamma_1}\right)\left(w_2+\frac{1}{\gamma_2}\right)}}\left(\gamma_2\cos(k_1 w_1)\sinh(\gamma_2 w_1)+k_2\sin(k_1 w_1)\cosh(\gamma_2 w_1)\right)$$

Where w_1 and w_2 are half the width of waveguide 1 and 2 respectively, n_g the refractive indices of the waveguides, R is the radius of curvature, S_0 is half the distance between the waveguide centres at their closest point (Figure 3.6), k_1 and k_2 are the transverse propagation constants in the waveguide 1 and 2 respectively, γ_1 and γ_2 define the transverse decay constants in the cladding of waveguide 1 and 2 respectively and β_1 and β_2 are the propagation constants in waveguide 1 and 2 respectively. This can then be used to give a value of Q due to coupling (Q_{coupl}).

Equation 3.39

$$Q_{coupl} = \frac{kpn}{2\kappa^2}$$

The factor of 2 occurs because there are two coupling points on the standard ring resonator, the input and output points. (Figure 3.1).

3.7 Bending loss

When light travels in a waveguide a certain proportion of the power will travel outside of the waveguide, in the evanescent tail which extends into the cladding material. At a bend in the waveguide, light at the outer edge of the bend must travel faster. As the evanescent tail extends out into the waveguide cladding, a point is reached where it would have to travel faster than the speed of light in the medium in order to keep up with the light propagating in the waveguide, but this is not possible and the light is radiated away. As this is a source of loss it will affect the Q-factor according to Equation 3.23 and this will in turn have an impact on the potential uses of a resonator.

The attenuation of the curved waveguide can be calculated from the equation;

Equation 3.40 [86]

$$\alpha_{bend} = \frac{\lambda \cos^2(k_1 w_1)\exp(2\gamma_1 w_1)}{4{w_1}^2 \gamma_1 n_c \left\{ \frac{w_1}{2} + \frac{\sin(2w_1 k_1)}{2k_1} + \frac{\cos^2(k_1 w_1)}{\gamma_1} \right\}} \exp\left(-2\gamma_1 \left(\frac{\lambda \beta_1}{2\pi n_c} - 1 \right) R \right)$$

This equation refers specifically to a channel waveguide, but the principles that it outlines can be applied to other geometries. This means that for high index materials such as chalcogenides bending loss will be lower than it would be for lower index materials. Therefore tighter bends may be a practical, allowing a reduction in size.

3.8 Surface scattering

Scattering from surface roughness at a waveguide cladding interface can be considerable even for relatively smooth surfaces. This will be accentuated for circular resonators as a greater proportion of the travelling power will be at the surface, compared to a straight waveguide. As this is a source of loss from the resonator it will affect the Q-factor (Equation 3.23). The attenuation due to scattering can be calculated from the equation;

Equation 3.41 [86]

$$\alpha_{scatter} = \frac{\cos^3\theta}{\sin\theta}\left(\frac{4\pi n_g \sigma}{\lambda}\right)^2\left(\frac{1}{2w_1 + \frac{2}{\gamma_1}}\right)$$

Where θ is the propagation angle with respect to the waveguide direction, σ is the rms roughness of the surface.

3.9 Optimisation

There are several factors, described in previous sections, which will have an impact on the Q-factor and circulating intensity in a resonator. To demonstrate issues in the design of a planar resonator waveguide system (Figure 3.1), these factors have been brought together to show how they interact. Each application of a resonator will have differing priorities and these will determine the balance that is struck between these factors.

Whilst these calculations are for a planar ring resonator, the principles will remain the same for other geometries.

The following graphs model a 100μm diameter ring with a refractive index of 2.1 and cladding index of 2, at a wavelength of 600nm. The fractional attenuation is 0.007, taken from a minimum attenuation [84]. As these calculations are based on waveguide structures and not solid microspheres, it is necessary to define the waveguides. They were defined as w1 and w2 = 0.2μm (Figure 3.6) to make the waveguides single mode.

This represents a realistic planar waveguide design and shows its potential usefulness. Microspheres are more likely to have cladding index of 1, but the principles shown here will remain the same for microspheres. The graphs show various characteristics of the resonator and how they vary with coupling distance.

The desired use of the resonator will determine the coupling distance. Clearly for a high nonlinear effect, the maximum possible internal intensity is desirable, whereas a system which requires a very high Q factor may use a much larger coupling distance and a device that requires a high transmission rate, such as a channel dropping filter, may have a shorter coupling distance.

In this system the transmission does not reach the input intensity as there are internal losses, the maximum value of transmission is

Equation 3.42

$$T_{Max} = \left(\frac{I_{trans}}{I_0} \right)_{Max} = \left(\frac{C}{A+C} \right)^2$$

The maximum transmission is therefore a function of coupling distance for a given value of A (Figure 3.7).

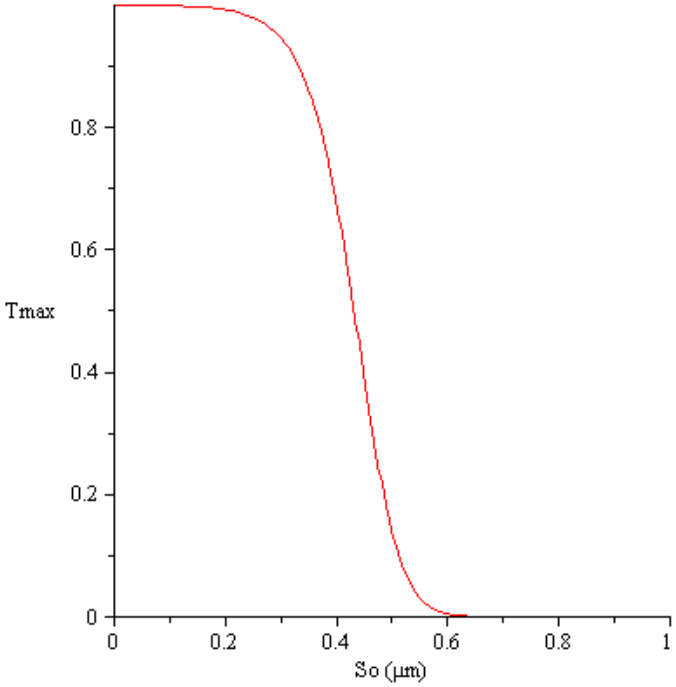

Figure 3.7 Variation of normalised transmission through a resonator as a function of coupling distance using Equation 3.42 and Equation 3.38. Showing the rapid change from the over-coupled to the under-coupled regime.

The intensity transmitted through the resonator is highly sensitive to the coupling distance (Figure 3.7). In the over coupled regime, where the coupling dominates the internal losses of the resonator, transmission will remain high and Q will be mainly dependent on the coupling distance, as can be seen by combining Equation 3.25 and Equation 3.39 (Figure 3.8). This lower Q value will have broader peaks, as described by (Equation 3.29), therefore any designs such as add/drop multiplexes that require narrow linewidth and high transmission will have to balance these two opposing requirements.

In the under coupled regime the internal losses of the resonator dominate over the coupling. This means that the transmission becomes very low (Figure 3.7) and Q will reach its maximum value (Figure 3.8).

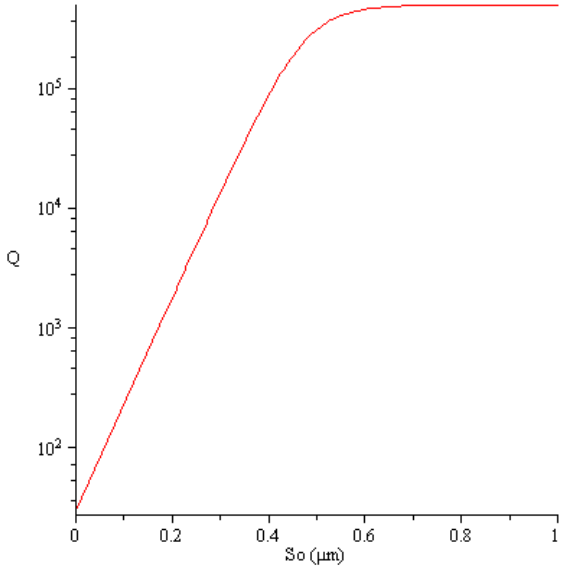

Figure 3.8 Variation of Q with coupling distance shown here on a log scale. The Q value is dependent on coupling distance in the over-coupled region, but plateaus in the under-coupled region, where Q is determined by the resonators intrinsic properties.

Examining the intensity of light circulating inside the resonator a different picture emerges. When the resonator is in the over-coupled regime, light is coupled out too quickly to allow a build up and in the under-coupled regime only a small amount of light is coupled into the resonator. Therefore it is at the balance point of these two regimes that a high intensity builds up inside the resonator (Figure 3.9). The transmitted intensity is related to the circulating intensity by the coupling constant, therefore from Equation 3.42 the circulating intensity is

Equation 3.43

$$\left(\frac{I_c}{I_0}\right)_{\max} = \left(\frac{I_{trans}}{I_0}\right)_{\max} \frac{1}{C} = \frac{C}{(A+C)^2}$$

For many applications, such as lasers and switches, it is the amount of light inside the resonator not the light passing through that is of interest.

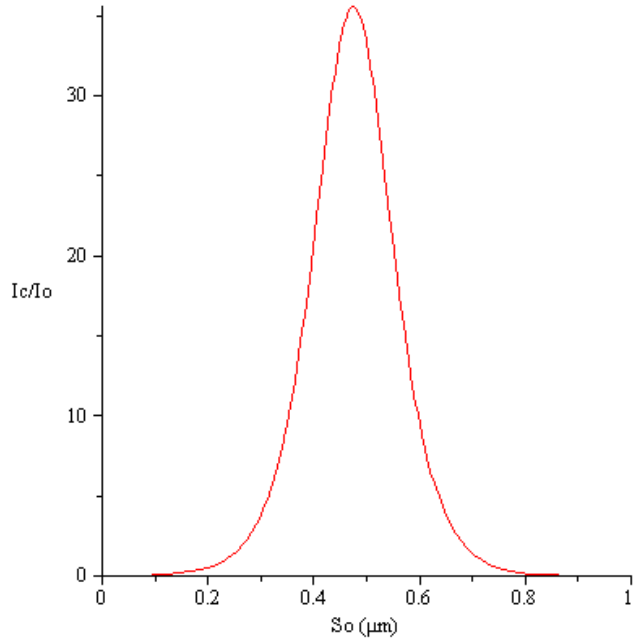

Figure 3.9 Circulating normalised intensity inside the resonator as given in Equation 3.43, showing the sharp peak at the point of optimal coupling. Note that the circulating intensity is higher than the normalised input intensity due to the storage of light.

Comparing the internal intensity of two different resonators with different internal losses (Figure 3.10) it becomes clear that the initial rise in intensity as the coupling distance increases is the same, but the point at which the internal losses come to dominate is different and therefore the optimal coupling distance is also dependent upon internal losses.

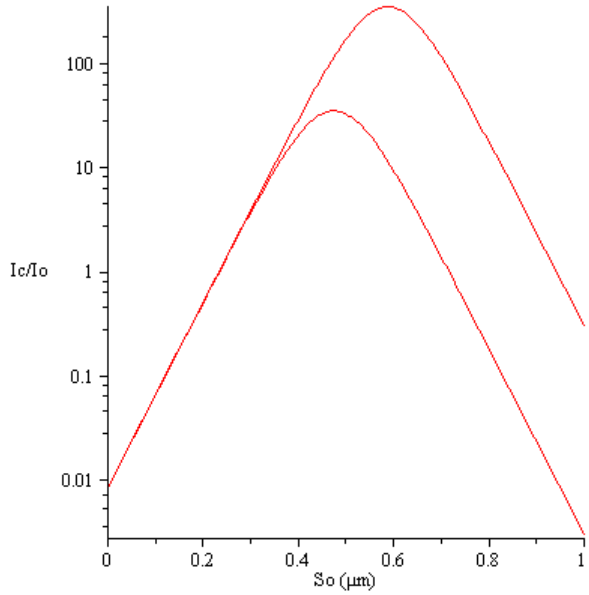

Figure 3.10 Normalised circulating intensity on log scale, with the same value of attenuation as previous (0.007) and second line with the higher peak value corresponds to attenuation an order of magnitude lower (0.0007). The rise in circulating intensity is the same for both, but the point at which it falls away is defined by the attenuation.

By differentiating Equation 3.43 with respect to C the peak intensity is found to occur when A=C [87]. Therefore, given knowledge of the losses of a particular material, it is possible to calculate the distance of optimal coupling / max internal power (Figure 3.11) from Equation 3.38.

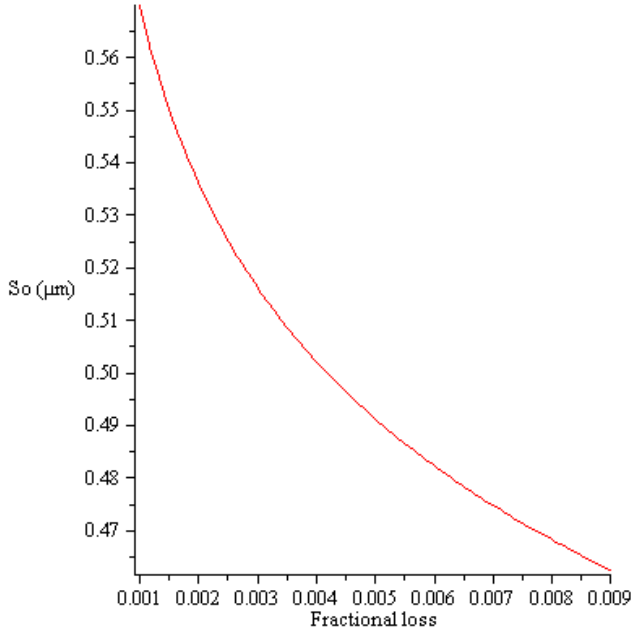

Figure 3.11 Optimal coupling as a function of fractional loss from the resonator. As the loss is reduced the distance of optimal coupling becomes larger.

Therefore at the point of optimal coupling

Equation 3.44

$$T_{Max} = \left(\frac{I_{trans}}{I_0} \right)_{Max} = \left(\frac{C}{A+C} \right)^2 = \frac{1}{4}$$

Equation 3.45

$$\left(\frac{I_{pass}}{I_0} \right)_{Min} = \frac{A^2 F}{4} = A^2 \frac{1-A-C}{(A+C)^2} = \frac{1}{4} - \frac{A}{2}$$

This means that if A<<1, at the point of maximum internal intensity, loss will equal ½ (Figure 3.12) unless some gain were incorporated, this may be rather high for many uses.

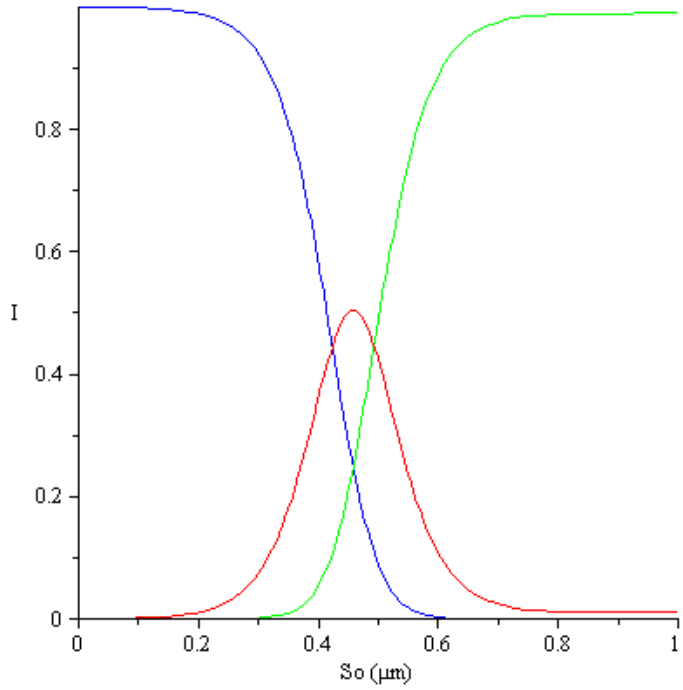

Figure 3.12 Intensity leaving the resonator system. Transmission = blue, pass = green, loss = red.

If a different transmission or loss is required, a position can be calculated that would have these characteristics (Figure 3.12). However it is worth noting that loss will be proportional to internal intensity; therefore if the maximum internal intensity is required the maximum loss must be accepted.

The distance required for critical coupling of a resonator system varies in an approximately linear fashion with wavelength. This assumes that attenuation is constant across the wavelength spectrum, while this is unlikely to be the case in a real system; it is also unlikely that attenuation will conform to the ideal system and other sources of loss are likely to dominate over the fundamental sources of loss.

3.10 Calculated nonlinear movement of mode peaks

One area where the circulating intensity is critical is the observation of nonlinear effects. Because of the high intensities inside resonators it is possible to observe nonlinear effects at relatively low input intensities. The nonlinear effects cause the refractive index to change (Δn) as a function of the circulating intensity (I_c) [52] which will in turn cause the position of the resonance peak to move ($\Delta\lambda$). From the condition for resonance [85] it follows that

Equation 3.46

$$N\Delta\lambda = 2\pi R\Delta n = p\Delta n$$

Where p is the perimeter length and N is an integer representing the number of wavelengths per round trip of the perimeter. Using the initial condition for resonance again gives

Equation 3.47

$$\frac{\Delta\lambda}{\lambda_0} = \frac{\Delta n}{n}$$

Where λ_0 is the original peak wavelength

or

Equation 3.48

$$\frac{\Delta\lambda}{I_c} = \frac{\lambda_0 n_2}{n}$$

This is experimentally useful as I_c will usually be the independent variable and $\Delta\lambda$ the dependent variable. Therefore this equation will give the gradient of the plotted experimental data. These equations are concerned only with the resonator itself and therefore take no account of the coupling.

The peak resonance wavelength can be calculated for a given circulating intensity by the following

Equation 3.49

$$\frac{\lambda}{\lambda_0} = \frac{n_2 I_c}{n} + 1$$

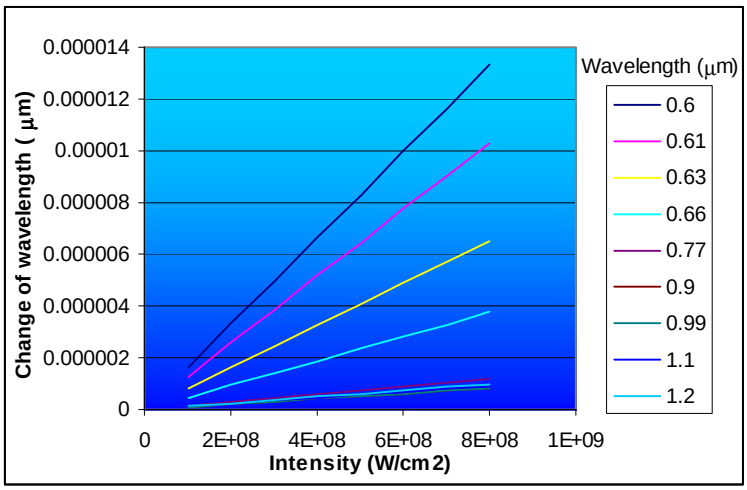

Figure 3.13 Change of wavelength (Δλ) as a function of circulating intensity in a resonator for a range of wavelengths.

As the nonlinear refractive index is a function of wavelength it is possible to plot the shift of the resonance peak for different wavelengths as a function of circulating intensity (Figure

3.13) using Equation 3.48 and published values of nonlinearity [19]. The non-linearity gives rise to a number of potential uses such as switching and memory.

It is worth noting that when looking for nonlinear effects of this nature experimentally it is easy to confuse them with thermal effects. The intensities required to observe nonlinear effects will also heat the material and this will cause a thermal index change and thermal expansion [53, 88], which will physically change the dimensions of the resonator. Both these effects will cause the resonance to alter, but in general these changes occur slower than the changes associated with the nonlinearity and this can be used to tell them apart [89].

3.11 Bistability & switching

One of the most exciting areas where nonlinearity in resonators has the potential to be used, is in all-optical-switching devices. These devices would typically utilise bistability, which is defined as having two stable states for a given input. This is essential for memory devices and is often used in switching devices, but it is not a necessary property for optical switching. A switching device only requires two distinguishable states for two distinct inputs, which may be easier to achieve at lower powers, whereas bistability has two possible outputs for one input. Bistability occurs in systems that have nonlinearity and a feedback mechanism, such as micro-resonators [54, 90].

The switching occurs because of the change in refractive index inside the resonator caused by the high intensity circulating in the resonator. Therefore as Q increases, the threshold power above which bistability occurs, will decrease, but the switching time of the resonator will increase. Therefore in the design of such a switch there has to be a trade off between speed of switching and the power required for switching. A relatively low Q resonator could be switched fast, but would require a high power, whilst a high Q resonator would require little power but would have a longer switching time.

The intensity dependent non-linear refractive index change means that Equation 3.9 will become

Equation 3.50

$$\frac{I_{trans}}{I_0} = \left(\frac{C}{A+C}\right)^2 \frac{1}{1+F\sin^2\left(\frac{kpn_0 + kpn_2 I_c}{2}\right)}$$

By varying the intensity circulating in the resonator (I_c), an interference pattern will be seen, similar to that for varying wavelength (Figure 3.14).

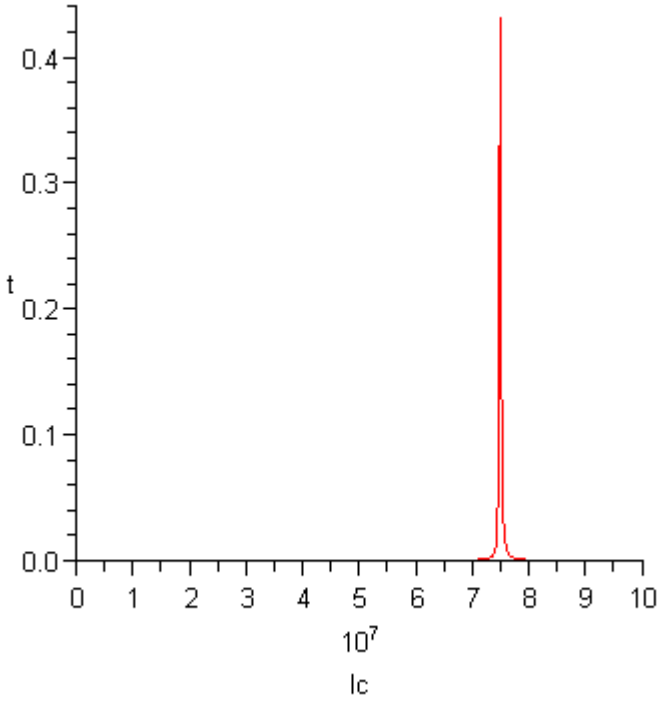

Figure 3.14 An example of transmission dependent on circulating intensity. Showing the peak in transmission as I_c is increased, similar to that seen as wavelength is varied.

Transmission is defined as $t = \frac{I_t}{I_0}$ and the coupling constant C is the fraction of the power that tunnels between the resonator and the waveguide, therefore $I_t = CI_c$, hence

Equation 3.51

$$t = \frac{CI_c}{I_0}$$

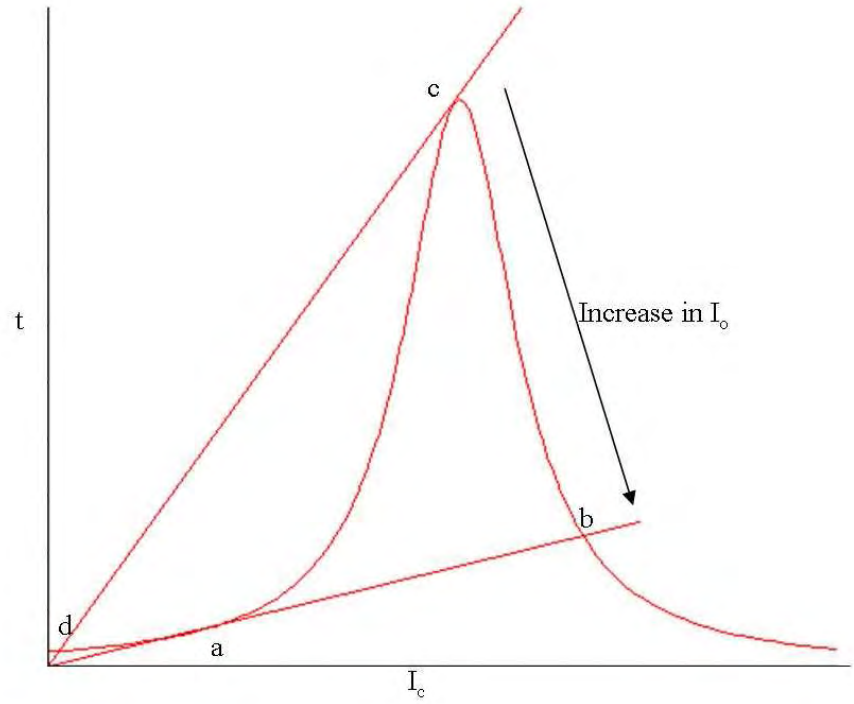

Figure 3.15 Transmission in a bistable system. The curved line represents the intensity dependant nonlinear index (Equation 3.50) while the straight line represents the intensity dependant tunnelling (Equation 3.51). Transmission will only occur where the two lines cross. If the system is transmitting at (a) and the I_o is increased, transmission will jump to point (b); if I_o is then reduced transmission will follow the curve to point (c) then jump down to point (d)

If Equation 3.50 and Equation 3.51 are plotted on the same graph (Figure 3.15), the intersection of the two lines will give the transmission. If the value of I_0 is increased steadily from 0 the circulating intensity will increase, and the transmission for a given I_0 will be given by the intersection point of the two lines on the graph. There will come a point when the I_0 line will intersect the interference pattern more than once, the transmission will follow the lower value (a) as the circulating intensity will not have built up. As I_0 increases there will come a point where there is only one intersection at a higher value of transmission. At this point the circulating intensity will rapidly increase to the stable higher value (b).
If the input power is then decreased, the circulating intensity will remain and the transmission will follow the upper line of the curve (to c), until there is once again only one intersection, when it will fall back to the lower transmission value (d).

The threshold at which bistability occurs can be defined in two ways, firstly it occurs when the mode detuning (due to the nonlinear effects) is larger than the mode width [81] or secondly as the gradient at the point of inflection on the transmission vs. circulating intensity curve [54]. The first definition is true of a system with a separate pump and probe, while the second will be true of a system where the pump and probe are the same.

If one is following the pump / probe approach then the mode detuning ($\Delta\lambda = \frac{n_2 Ip}{N}$ from Equation 3.46) must equal the mode width ($\Delta\lambda \approx \frac{\lambda}{Q}$ from Equation 3.29) at the threshold of bistability. By combining these equations with other standard equations for intensity, speed and volume it follows that;

Equation 3.52

$$W \approx \frac{V\omega n_0^2}{n_2 Q^2 c}$$

Where V is the mode volume, W is the threshold power, c is the speed of light, n_2 is the nonlinear refractive index, n_0 is the refractive index, and ω is the angular frequency [81]. This does assume that the mode diameter is small relative to the resonator diameter.

Using published data for the nonlinearity of GLS [19] Equation 3.52 has been plotted. Firstly a circular resonator with diameter of 100μm was examined for a range of wavelengths and Q values (Figure 3.16, Figure 3.17). Then the Q value was held constant at 10^5 in order to examine the dependence on diameter. In all cases the modal diameter was assumed to be the same as the input diameter to give an input intensity.

Equation 3.53

$$I \approx \frac{kpn_0^2}{n_2 Q^2}$$

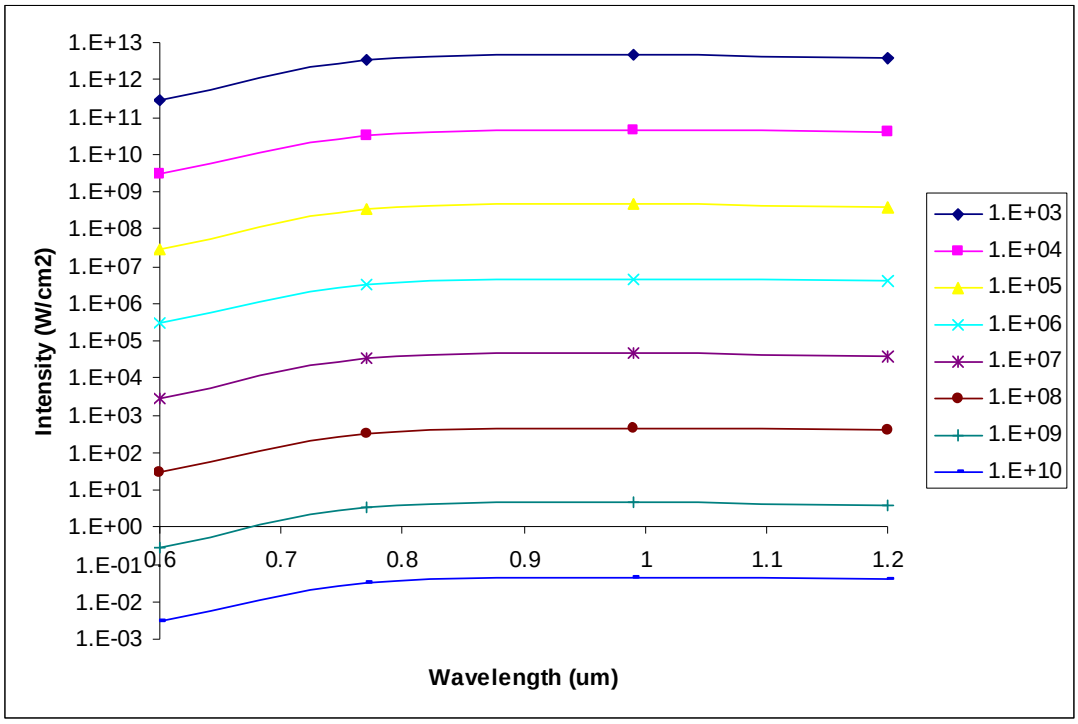

Figure 3.16 Input intensity required to observe bistability in a pump-probe system, in a 100µm diameter ring, examined for a range of Q values (inset). This assumes that the input waveguide and mode have the same cross-sectional area.

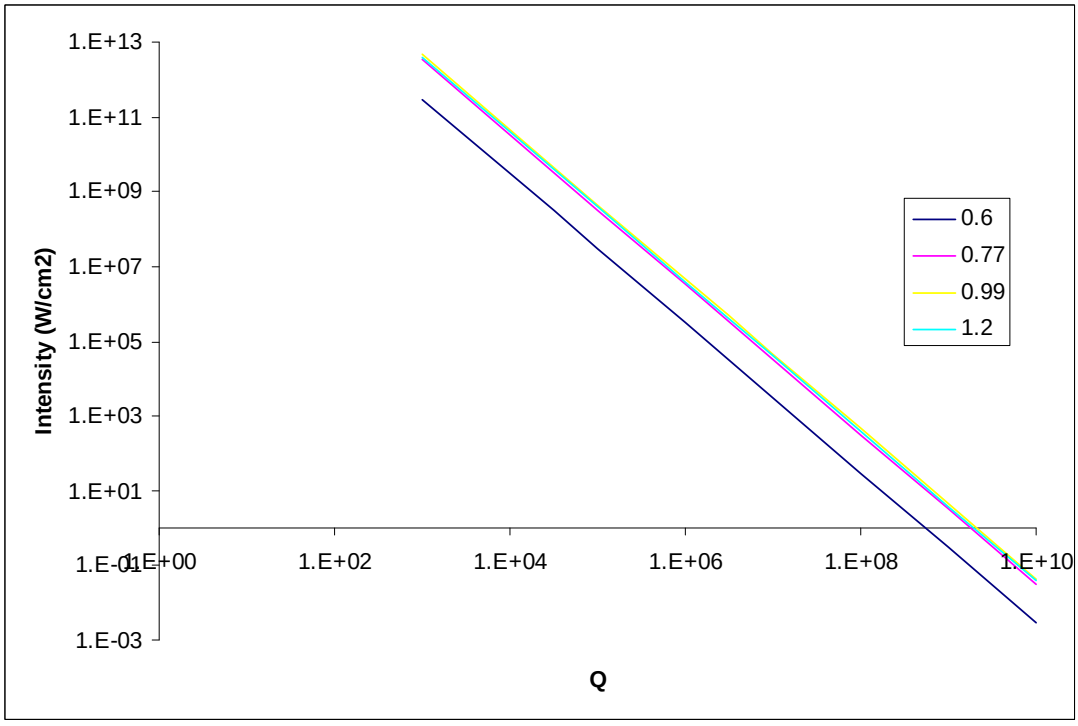

Figure 3.17 Input intensity required for bistability in a pump-probe system as a function Q, with a number of values of wavelength. Resonator diameter is 100µm.

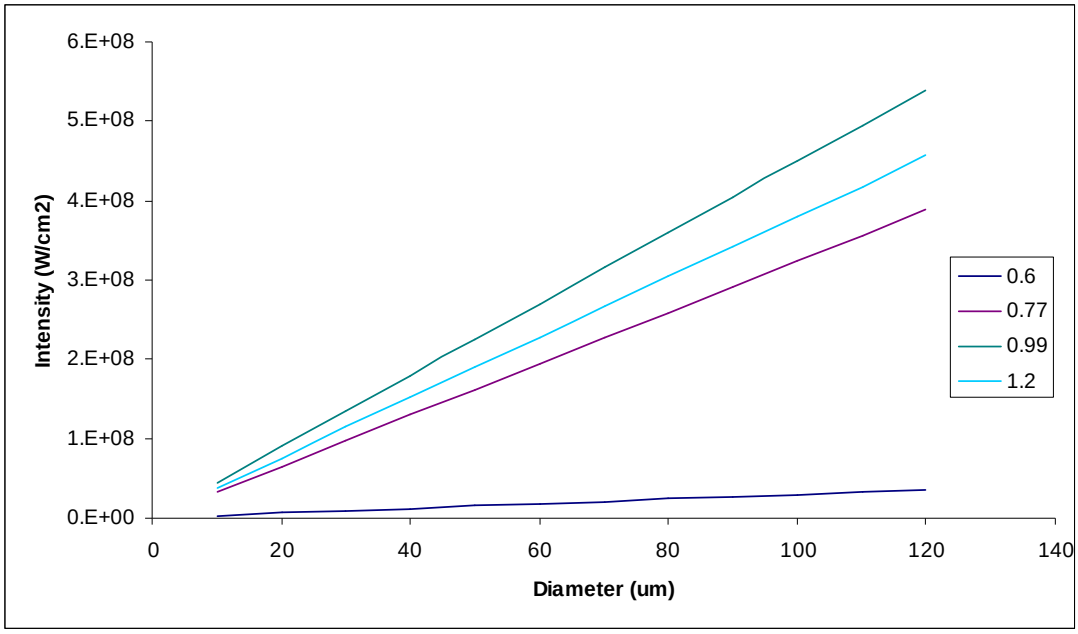

Figure 3.18 intensity required for bistability as a function of diameter with a range of values of wavelength (inset). Q value was held constant at 10^5.

The alternative definition is that bistability occurs at the point of inflection on the curve of transmission vs. circulating intensity and has a tangent that runs through the origin (Figure 3.19). The system could be tuned (e.g. by changing the refractive index through temperature control) to make this happen, therefore the only critical factor is the gradient at the point of inflection [54].

The point at which bistability occurs is when the intensity jumps from point (a) to point (b) (Figure 3.15). If the peak moves towards the origin then this jump will become smaller and occur at lower powers. This will continue until the point of inflection becomes tangent with the origin, when bistability will cease to occur (Figure 3.19). Therefore this is the threshold power. This will correspond to the point at which the hysteresis loop becomes infinitely small. The tangent will correspond to an input power according to Equation 3.51.

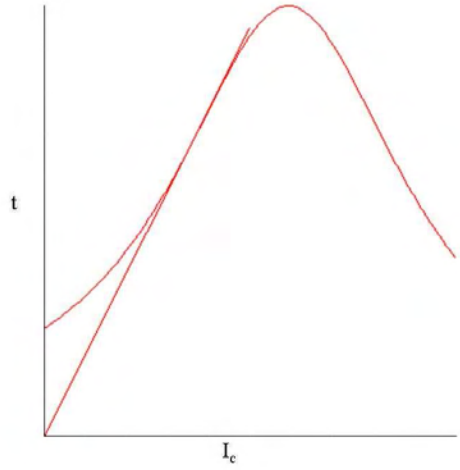

Figure 3.19 Transmission characteristics of a resonant cavity at the limit of bistability, the tangent at the point of inflection passes through the origin.

Following the method of [54], if we define

Equation 3.54

$$b = \frac{kpn + kpn_2 I_c}{2}$$

Then the Airy function becomes

Equation 3.55

$$t = \left(\frac{C}{C+A}\right)^2 \frac{1}{1+F\sin^2 b}$$

Differentiating once to get the gradient

Equation 3.56

$$\frac{dt}{dI_c} = -\left(\frac{C}{C+A}\right)^2 \frac{Fkpn_2}{2} \frac{\sin(2b)}{\left(1+F\sin^2 b\right)^2}$$

Differentiating a second time gives

Equation 3.57

$$\frac{d^2t}{dI_c^{\,2}} = \left(\frac{C}{C+A}\right)^2 \frac{F}{2} \frac{F\sin^2(2b) - \left(1+F\sin^2 b\right)\cos(2b)}{\left(1+F\sin^2 b\right)^3}$$

At the point of inflection the second derivative is equal to zero, which gives

Equation 3.58

$$F\sin^2(2b) = \left(1+F\sin^2 b\right)\cos(2b)$$

Using trigonometry identities this becomes

Equation 3.59

$$0 = \cos^2(2b) + \left(1+\frac{2}{F}\right)\cos(2b) - 2$$

This can be solved by the standard quadratic formula as follows and is called G for ease of use

Equation 3.60

$$\cos(2b) = \frac{1+\frac{2}{F} \pm \sqrt{\left(1+\frac{2}{F}\right)^2 - 8}}{2} = G$$

Therefore the gradient at the point of inflection is

Equation 3.61

$$\frac{dt}{dI_c} = -\left(\frac{C}{C+A}\right)^2 \frac{Fkpn_2}{2} \frac{\sqrt{1-G^2}}{\left(1+\frac{F}{2}-\frac{FG}{2}\right)^2}$$

And therefore using Equation 3.51 the input intensity at the threshold of bistability is

Equation 3.62

$$I_0 = -\frac{(A+C)^2}{C} \frac{2}{kFpn_2} \frac{\left(1+\frac{F}{2}-\frac{FG}{2}\right)^2}{\sqrt{1-G^2}}$$

This equation will give a value for the threshold of bistability [54], but if more explicit information is required about the nature of transmission related to the input, this can be achieved by controlling the resonance position. In order to control the position of the resonance a tuning parameter (I_x) is introduced into Equation 3.50.

Equation 3.63

$$\frac{I_{trans}}{I_0} = \left(\frac{C}{A+C}\right)^2 \frac{1}{1+F\sin^2\left(\frac{kpn_0 + kpn_2(I_c + I_x)}{2}\right)}$$

It is possible to get an explicit equation relating the input intensity (I_0) to the transmission, by combining Equation 3.63 and Equation 3.51. This calculation would usually be solved graphically by plotting Equation 3.63 and Equation 3.51 together as this equation does not give a one to one mapping, but the explicit equation will give its primary solution up to the top of the first peak, and provided the hysteresis loop is not too large this will be sufficient. If the hysteresis loop is too large for this equation it will also mean that peak transmission cannot be reached directly by increasing the power, but will only be reached when the power starts to be reduced again.

Equation 3.64

$$t = \left(\frac{C}{A+C}\right)^2 \frac{1}{1+F\sin^2\left(\frac{kpn_0 + kpn_2\left(\frac{tI_0}{C} + I_x\right)}{2}\right)}$$

Rearranging

Equation 3.64 for input intensity;

$$I_0 = \frac{C}{t}\left(\frac{2\left(-\arcsin\left(\sqrt{\frac{\frac{C^2}{t}-(A+C)^2}{4(1-A-C)}}\right)\right)}{\frac{kp}{n_2}} - n_0\right) - I_x$$

Equation 3.65

From Equation 3.59 and Equation 3.60 a value for I_x can be calculated such that the threshold can be seen.

As t appears twice in Equation 3.65 I_0 has to be a function of *t*, which produces the following graph (Figure 3.20);

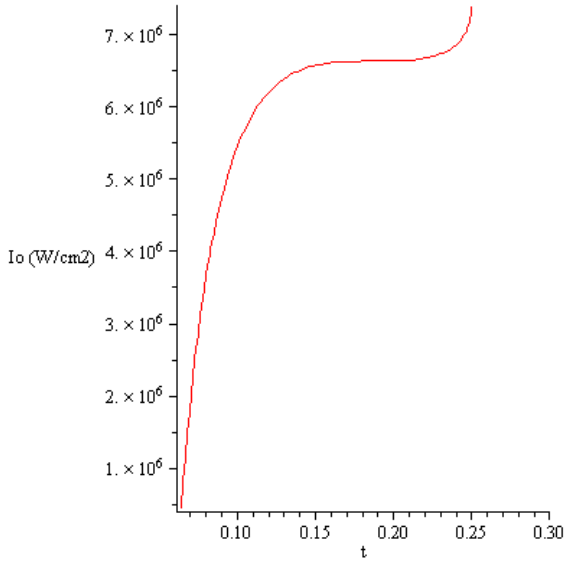

Figure 3.20 Bistable threshold with critical coupling for a 100µm diameter GLS resonator with a Q value of 10^5. The threshold power is the point where the curve is horizontal.

This method gives a slightly lower value for the threshold than the pump-probe method. For a GLS resonator 100µm in diameter, this method gives the critically coupled threshold as 6.63×10^6 W/cm^2, whereas the pump-probe method gave a value of 8.52×10^6W/cm^2. This is due to the simplifications in the pump-probe method, which fails to take account of the interference pattern in its calculation.

A combination of a bistability threshold and critical coupling will represent the lowest input power to achieve bistability (Figure 3.20), but the transmission will only be ¼, which may

also be too low for many applications. The desired transmission can be set using Equation 3.42 or Figure 3.7. For some applications further deviations from the idealised system may be desirable. A system exactly at the threshold may not be ideal if a high degree of definition is required between the ON and OFF states. If the value of I_x is perturbed slightly (Figure 3.21) from its calculated value, the threshold will be moved slightly and the definition between the ON and OFF states will be altered. If I_x is increased (Figure 3.21 Blue line) the system will move out of the bistable region and there will no longer be a switching threshold, however the maximum t will appear at lower intensity input. The value of t at zero intensity will increase, but as the definition between the states may be suitable for applications that only require distinct states this option will represent a lower switching power.

If I_x is decreased slightly, the system (Figure 3.21 green line) will move further into the bistable region, the switching power will move up and the minimum value of t will decrease, making a stronger definition between the ON and OFF states.

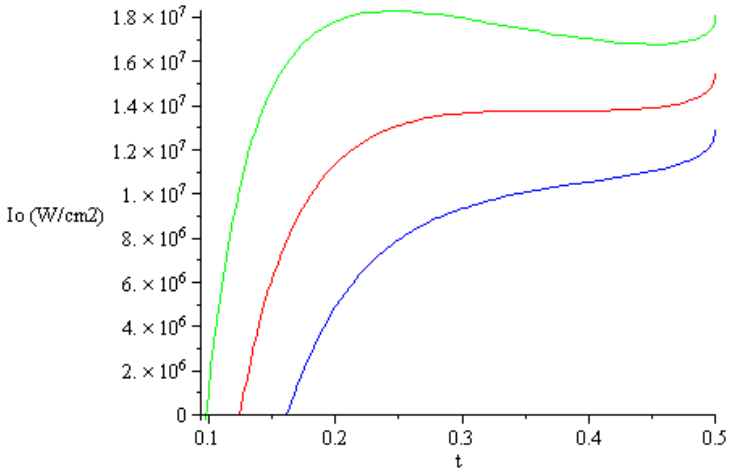

Figure 3.21 Perturbed tuning of the bistable threshold with t_{max} = 0.5. Red = I_x, blue = I_x*1.005, green = I_x*0.995, based on a GLS resonator, 100μm in diameter with the coupling set such that transmission will be 0.5 with at Q of 10^5.

If we define a system similar to that in Figure 3.1, but have the input as a combination of two independent inputs then we can start to define a digital switching system.

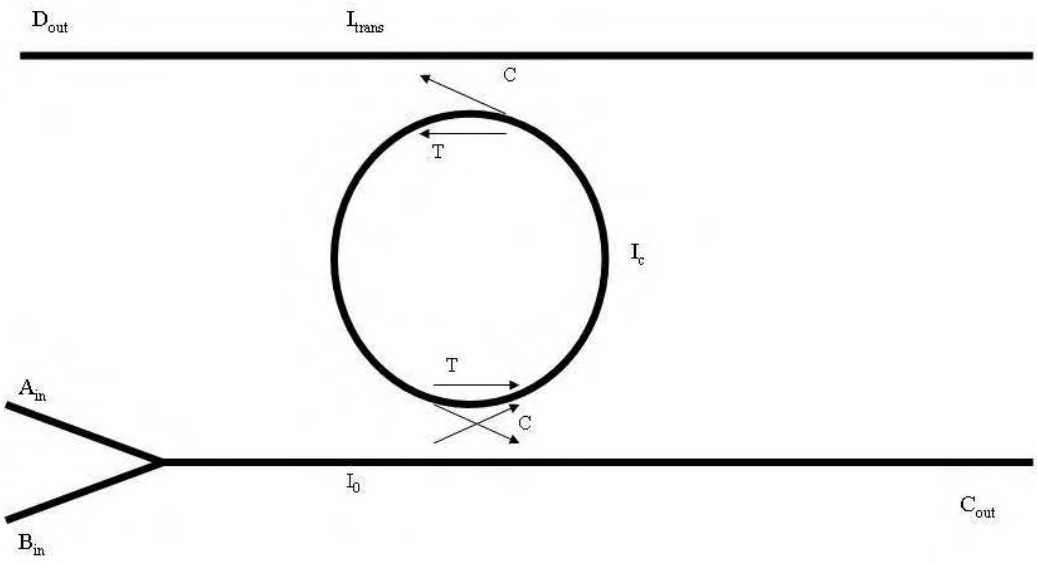

Figure 3.22 Configuration of a switching resonator.

If an ideal resonator system could be designed such that peak transmission occurred at twice the power of minimum transmission and the maximum transmission were 0.5, then this system would work as a combination of an XOR (D_{out}) and an AND (C_{out}) gate (Table 3.1). If the switching threshold is assigned the value 2 then A_{in} and B_{in} each deliver half the switching threshold when on. Therefore switching only occurs when both channels are on.

A_{in}	B_{in}	I_0	C_{out}	D_{out}
0	0	0	0	0
1	0	1	1	0
0	1	1	1	0
1	1	2	0	2

Table 3.1 Inputs and outputs for an ideal system.

However this idealised system is unlikely to be practical, as it takes no account of loss, although this could be counteracted by introducing gain. In a more realistic system, such as Figure 3.21 and Table 3.2, a trade off will have to be made between the power and the distinction between ON and OFF states.

A_{in}	B_{in}	I_0	C_{out}	D_{out}
0	0	0	0	0
1	0	1	~0.74	~0.14
0	1	1	~0.74	~0.14
1	1	2	~0.16	1

Table 3.2 Inputs and outputs for the system described in Figure 3.21

If large resonators are used, the free spectral range will be small and it may become difficult to tell successive peaks from one another.

3.12 Free spectral range (FSR)

In order to be able to differentiate clearly between on and off states, or the Boolean 1 and 0, it is necessary that modes have a sufficient gap between them. This gap is called the free spectral range and is defined as the distance (wavelength) between two adjacent resonance peaks ($FSR = \lambda_2 - \lambda_1$). Examination shows that for resonance to occur $\lambda N = pn$ [85] where p is the round trip path length of the resonator and N is an integer representing the number of optical peaks in one round trip of the resonator. Given that the resonance peaks are adjacent the number of wave peaks in a round trip will differ by one. Therefore

Equation 3.66

$$FSR = \frac{pn}{N} - \frac{pn}{N+1}$$

$$FSR = \frac{2\pi Rn}{N(N+1)}$$

By substituting $\lambda N = pn$ back in it follows that

Equation 3.67

$$FSR = \frac{\lambda}{N+1}$$

$$FSR = \frac{\lambda}{\frac{pn}{\lambda}+1}$$

$$FSR = \frac{\lambda^2}{pn+\lambda}$$

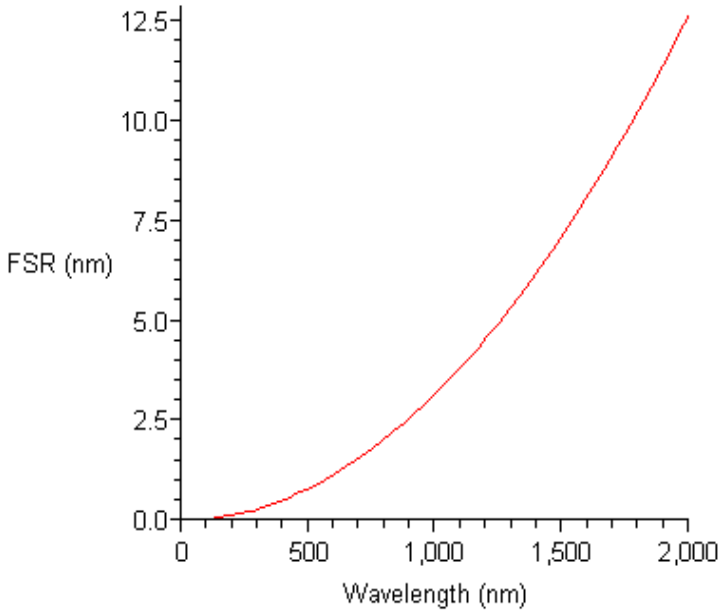

Figure 3.23 Free spectral range for a ring with radius of 100 microns

At large radius or short wavelength the FSR will be very small and peaks may become obscured. This will have to be traded off against the higher powers required for nonlinearity at longer wavelengths and in larger spheres.

3.13 Curve fitting

The nature of the measured spectra makes it favourable to identify families of peaks in order to understand the mode structure. A family of peaks is a set of peaks that can be described by a single Airy function. From this the free spectral range can be measured.

If the light in a given mode is considered to be travelling around a ring inside the sphere then it is possible to fit an Airy function to the data. To do this four numbers are required; λ_p the wavelength at which a peak occurs, N the number of wavelengths that fit into one round trip at wavelength λ_p, Q and the relative intensity. All values are arrived at from an initial estimate via an iterative process, λ_p and N combine to give the peak position, Q gives the shape of the peak and the relative intensity gives the height.

From the definition of free spectral range for a thin ring;

Equation 3.68

$$FSR = \lambda_p - \lambda_{p-1}$$

Where λ_p and λ_{p-1} are the wavelengths at two consecutive peaks. But from Equation 3.67

Equation 3.69

$$N_2 = \frac{\lambda_p}{FSR} - 1$$

Equation 3.70

$$N_2 = \frac{\lambda_p}{\lambda_p - \lambda_{p-1}} - 1$$

By measurement and simple calculation, values for N and λ_p can be achieved. These are the only values that determine the position of the airy function peaks. Once a family of peaks has been identified the values of wavelength are extracted from the data, a value of N can be calculated.

From Equation 3.23 Q can be given as

Equation 3.71

$$Q = \frac{kpn}{2L}$$

Where k is the wave vector, p is the perimeter of the ring, n is refractive index and L is loss of half one round trip of the ring. Using the definition of the wave vector, the perimeter and the condition for constructive interference in a thin ring it follows that,

Equation 3.72

$$kpn = \frac{2\pi\lambda_p N}{\lambda}$$

Note that λ_p will be a constant while λ will be a variable.

Equation 3.73

$$Q = \frac{\lambda_p N\pi}{\lambda L}$$

λ_p and λ will approximately cancel provided they are close in value

Equation 3.74

$$L \approx \frac{N\pi}{Q}$$

Equation 3.75

$$F = \frac{4(1-L)}{L^2}$$

We can therefore obtain a version of the Airy function that is dependent on λ_p, λ, N and Q.

Equation 3.76

$$Airy = \frac{1}{1 + F\sin^2(\frac{\pi\lambda_p N}{\lambda})}$$

This can then be used to match the data. A multiplication factor is applied to take account of the relative intensity of different families of peaks.

3.14 Ring laser calculations

Microsphere lasers have received much attention as they represent a potential low threshold narrow linewidth laser source. In a microsphere, pumping will occur along the mode, approximately in the same place as the laser action. This means that the threshold calculation should be the same as for an end pumped laser. The absorbed pump threshold is given by Equation 3.77 [32].

Equation 3.77

$$P_{th} \approx \frac{\pi h \upsilon_p (L + C)(w_p^2 + w_L^2)}{4\sigma\tau_f}$$

Where h is Planks' constant, ν_p is the pump frequency, L is the round trip loss, C is the fraction of light coupled out per round trip, w_p is the pump beam radius, w_L is the radius of the laser beam, σ is the absorption cross-section, and τ_f is the fluorescence lifetime.

The components of Equation 3.77 can be separated into glass properties and resonator properties, such that all glass properties are contained in a factor X.

Equation 3.78

$$P_{th} \approx (L + C)(w_p^2 + w_L^2)X$$

Laser action has been observed in Nd:GLS 1.5mol% glass before [15] and therefore the factor X will remain the same. The spot sizes here w_L = 9μm and w_p = 7μm.

In previous experiments two different mirrors were used in two different setups, giving different values of absorbed threshold power.

Coupling (unit less)	Absorbed threshold power (P_{th}) (mW)
0.05	18
0.01	8

This give X($w_p^2 + w_L^2$) as 250. As L + C is the loss Equation 3.25 can be rewritten as

Equation 3.79

$$L + C = \frac{kpn}{Q}$$

This leads to

Equation 3.80

$$P_{th} = \frac{kpn}{Q}\left(w_p^2 + w_L^2\right)X$$

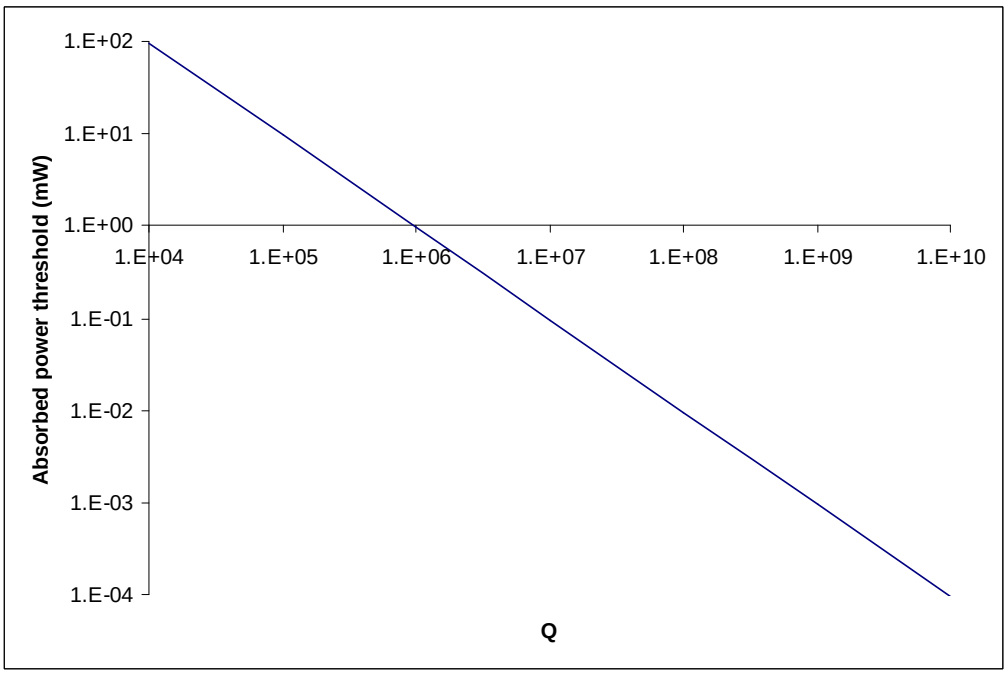

Figure 3.24 Absorbed power threshold for a circular resonator (diameter = 100um) with pump and laser spot sizes the same as for the previous laser

If spot size remains the same as [15] then absorbed threshold power becomes a simple function of Q (Figure 3.24). In reality the mode diameter is likely to be different and this will change the pump threshold. The radius of the pump and lasing modes are assumed to be proportional to their wavelength to build up a picture of how pump threshold is affected Figure 3.25. The quoted mode radius in Figure 3.25 is for the pump, the laser mode is assumed to be proportionally larger.

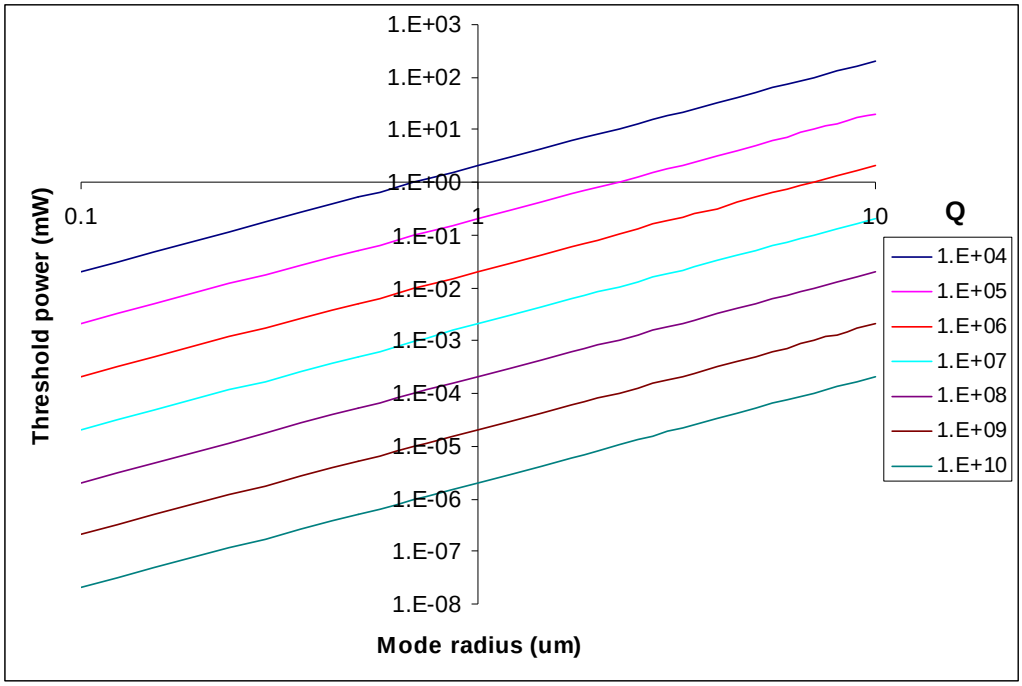

Figure 3.25 Threshold pump power as a function of mode radius for a range of Q values

As lasing has been observed in this glass before, a picture of the threshold potential can be built up. It is not possible to accurately quantify the threshold without knowing which mode will dominate laser action, but it can be seen how threshold is affected by mode size and Q. A variation of several orders of magnitude is predicted in the absorbed power threshold, although it is worth noting that this is not the incident power, and therefore does not take into account the coupling into the resonator and absorption in the resonator.

3.15 Conclusion

In this chapter various aspects of theory surrounding chalcogenide microspheres has been examined. Much of this will inform the experiments that are discussed in later chapters. The potential of GLS microspheres is apparent. Many of the possible uses discussed in the last chapter rely on the principles that have been examined in more depth in this chapter.

In particular many applications would rely on the Q factor, the potential high Q value of over $4x10^{10}$ at 3µm and 10^9 at 1µm that has been calculated here is of particular interest.

A derivation has been given for the threshold of bistability in resonators and nonlinear transmission through a resonator, and these have been applied to a typical GLS resonator. Comparison with a more simplistic threshold calculation found that our calculations gave a lower predicted threshold than those for a pump-probe system.

The potential for GLS micro-resonators to be used in all optical switches and lasers has been examined and shows great promise because of the high Q combined with high nonlinearity or fluorescence that are possible in GLS. In both cases their properties would be heavily dependent on their modal structure and design, but an illustration of the possibilities has been given.

4 Microsphere fabrication

In this chapter the fabrication process of microspheres is discussed along with the ideas behind it. Developing the fabrication process has been an iterative process with many stages, leading to a successful result. These stages are outlined here along with the ideas and the experimental data that informed them.

4.1 Overview

Microspheres can be made from a number of materials such as glasses and plastics (both available commercially), and can be produced by a number of methods, these include polishing [61], chemical etching [61], rapid quenching of liquid droplets [70], by pouring molten glass onto a spinning disk to produce droplets[58, 59], passing crushed glass through a plasma [60], optical fuses [91] and flow control nozzles [92, 93]. These approaches can fabricate great numbers of microspheres in parallel. Individual microspheres can also be formed by melting the tip of an optical fibre or filament [22, 55-57] and allowing surface tension to pull the molten glass into a sphere, which remains attached to the fibre. However this approach means that only one microsphere can be produced at a time and the size is partially determined by the fibre size.

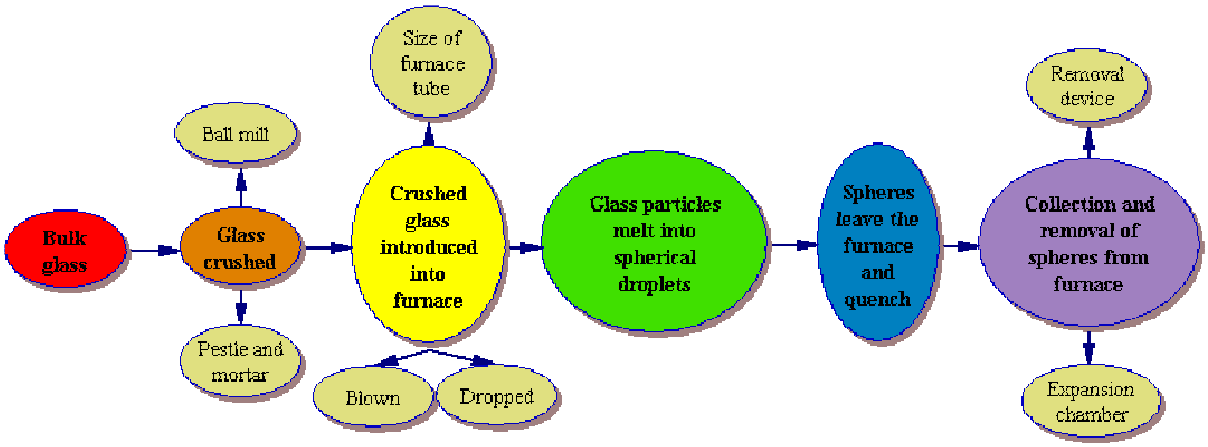

Figure 4.1 Flow diagram of melt process developed in this work.

In the fabrication process developed in this project (Figure 4.1), the crushed glass melts as it passes through a vertical tube furnace. Surface tension pulls the molten particle into a sphere, which then quenches into an amorphous state as it leaves the furnace. The spheres are then collected. Several stages in this process can be conducted by more than one method (indicated in Figure 4.1). In any case we call this the in-flight melt-quenching method.

In this process the glass could either be crushed with a pestle and mortar or a ball mill. The crushed glass then passes through the furnace by one of two methods, firstly by being dropped

(Figure 4.2) from the top to the bottom of the tube or secondly by being blown (Figure 4.3) from the bottom to the top of the tube. This and the other parameters (such as tube size) have a significant impact on the efficiency of production and size of microspheres produced.
The work of Hesford [61], established that GLS microspheres could be produced by dropping particles of glass through a furnace. This was the starting point for the first method, which has been developed and improved in this project. The second method of microsphere production was conceived and developed as part of this work because of a desire to produce smaller spheres than were produced by the first method.

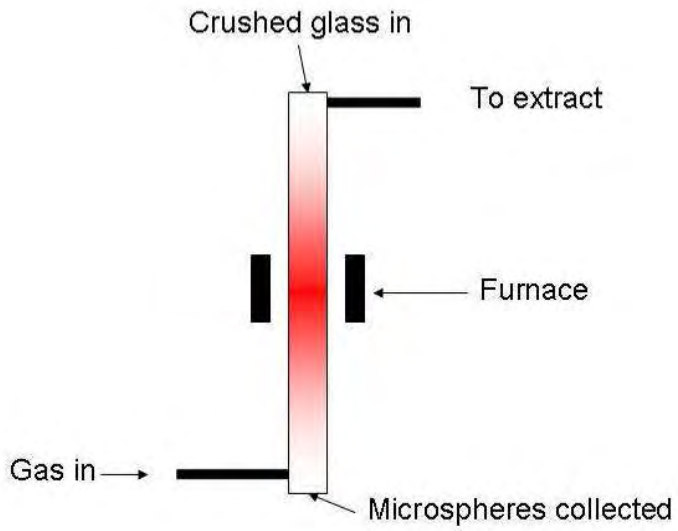

Figure 4.2 Basic schematic of dropped glass microsphere production

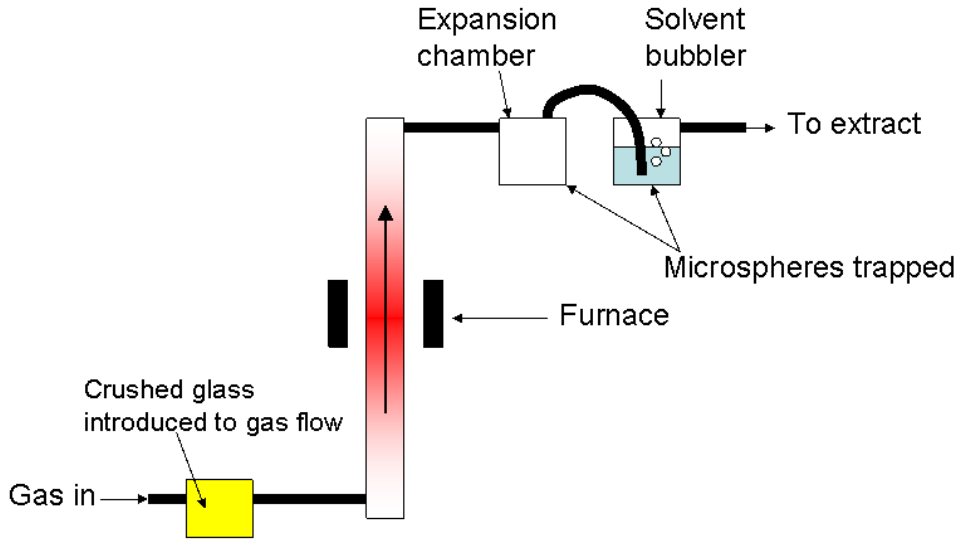

Figure 4.3 Experimental setup for blown dust experiments

Figure 4.4 The author with the fibre drawing tower where initial experiments were carried out

Early trials were performed on an optical fibre drawing tower (Figure 4.4), which provided proof of principle for the free flight method, after which a dedicated vertical furnace (Lenton 16/25/180 1600^{o}C) was utilized.

Due to the reactive nature of molten chalcogenide, glass melting must take place in an inert atmosphere. If GLS is melted in an air atmosphere it will react with the oxygen and water in the air, which will produce a poor surface and increase attenuation [75]. Therefore chalcogenide microspheres are produced in a continually purged inert atmosphere, typically argon.

4.1.1 Preparation

In order to assert control over the size of microspheres produced, crushed particles are separated according to size before they are put into the furnace. Large particles can be separated by sieving, but for small particles sieving was found to be impractical due to clogging. It has been found that small particles of GLS are strongly attracted to surfaces and each other, when placed in solvent (typically isopropanol or methanol) this problem is over come. As an alternative to sieving, a process of sedimentation has been used, taking advantage of the slow terminal velocity of small particles in liquids. The best results were obtaining using a method of particle separation which combines sedimentation and sieving. The smallest particles are separated by sedimentation, the larger particles of crushed glass can then be sieved.

4.1.2 Sphere formation

The terminal velocity of small particles also has an influence on the sphere formation process within the furnace as they will be buoyant in the flows of gas used. In a tube running vertically through a furnace the gas will rise due to convection, when there are no external pressures or flows are acting upon it. If a flow were applied to the furnace in a downward direction, there would be a point where the applied flow would compete with convection and may set up regions of opposing flow. To avoid convective currents being set up inside the furnace the flow of inert gas was applied in an upwards direction. This way the applied flow and convective flow would complement each other. However, according to Stokes' law, small particles on a similar scale to the microspheres being produced (typically <30um) will be buoyant in this gas flow. Therefore to make the smallest spheres it is necessary to introduce the GLS with the gas at the bottom of the tube and collect at the top (Figure 4.3). The size at which this transition takes place is dependent on the size of tube and the flow passing through.

4.1.3 Post-production sorting and storage

The melt process is not perfect and material that has passed through the furnace will typically contain a mixture of particles that have melted into spheres and particles that have not (Figure 4.5, Figure 4.6). This material can be separated according to the quality of the spheres by repeatedly rolling the material down progressively shallower slopes. This was achieved by placing the spheres in a glass container, such as a Petri dish, tilting the container and allowing the spheres to roll down the incline. Each time the material is rolled down a slope, the non-spherical material will be left behind, the steepness of the slope will determine how precisely spherical the particle has to be in order to roll down the slope. As the GLS particles stuck to the dry glass surface they were immersed in solvent to ensure that the spheres were able to roll freely.

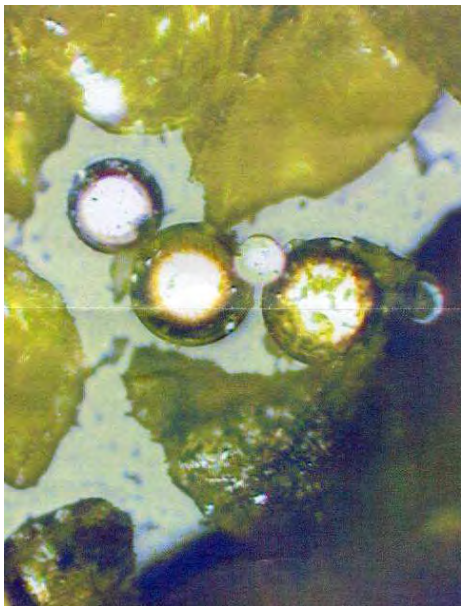

Figure 4.5 Microspheres made with un-washed crushed glass. Shows evidence of dust and un-melted particles.

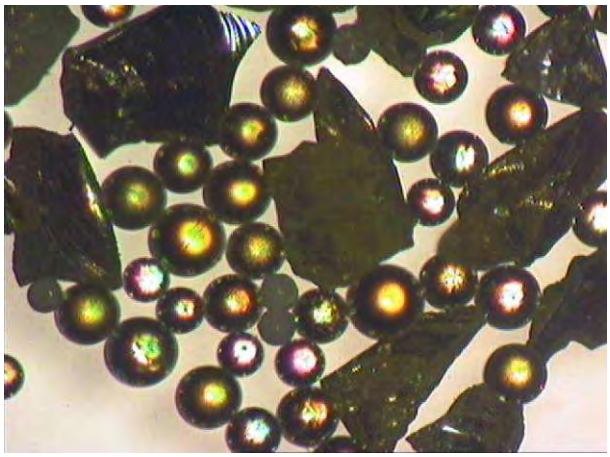

Figure 4.6 Microspheres made from washed, crushed glass at 1600^{o}C, yielding particles between 150 μm and 300 μm in size.

4.2 Preliminary trials

The very first GLS microspheres were produced by dropping crushed GLS by hand into a silica tube which ran vertically down through a furnace and catching the spheres in a Petri dish at the bottom [61]. The furnace used was part of a fibre drawing tower (Figure 4.4) and had a 25mm long carbon heating element, heated by RF induction. The furnace was set to a range of temperatures from 1300 to1600^{o}C. The only form of atmospheric control was a nitrogen line which ran into the bottom of the silica tube at a maximum of 1 l/min and an extract hood, which took away any fumes from the top of the tube. The silica furnace tube was 27mm I.D., 1.6m long.

Spheres were successfully produced (Figure 4.5), however only a small fraction of the particles leaving the furnace had melted.

4.2.1 Problems

These preliminary trials gave a proof of principle and identified certain shortcomings, in particular, spheres below 30μm were not seen and fumes were apparent and seen inside the tube. The latter indicates the presence of a reactive atmosphere and would be likely to result in a poorer quality of glass [75].

Also, at all stages of production there were problems with particles sticking to surfaces and each other and large quantities of particles did not melt when passed through the furnace.

4.3 Theory

In order to make improvements to the melting procedure it is necessary to understand some of the processes that come into play. This includes the flow of gas, the melting and cooling of the glass.

4.3.1 Differential thermal analysis of GLS powder

Analysis of the thermal characteristics was carried out in order to inform the wider sphere production experiments of where the phase changes occur in a stable environment. This gives a comparison with the temperatures that are required in the sphere melting setup. A sample of GLS from the same glass batch as used for sphere production experiments (see section 4.4.3.4) (LD984) was placed in the differential thermal analyser (Perkin Elmer diamond TG/DTA). Differential thermal analysis works by having a reference sample and the sample to be analysed heated in a furnace together. The temperature of both is measured and the temperature difference can be used to identify the heat flow in the sample and its thermal properties such as change of phase.

The heat flow was characterised as the temperature was raised by 50°C/hour up to 1200°C.

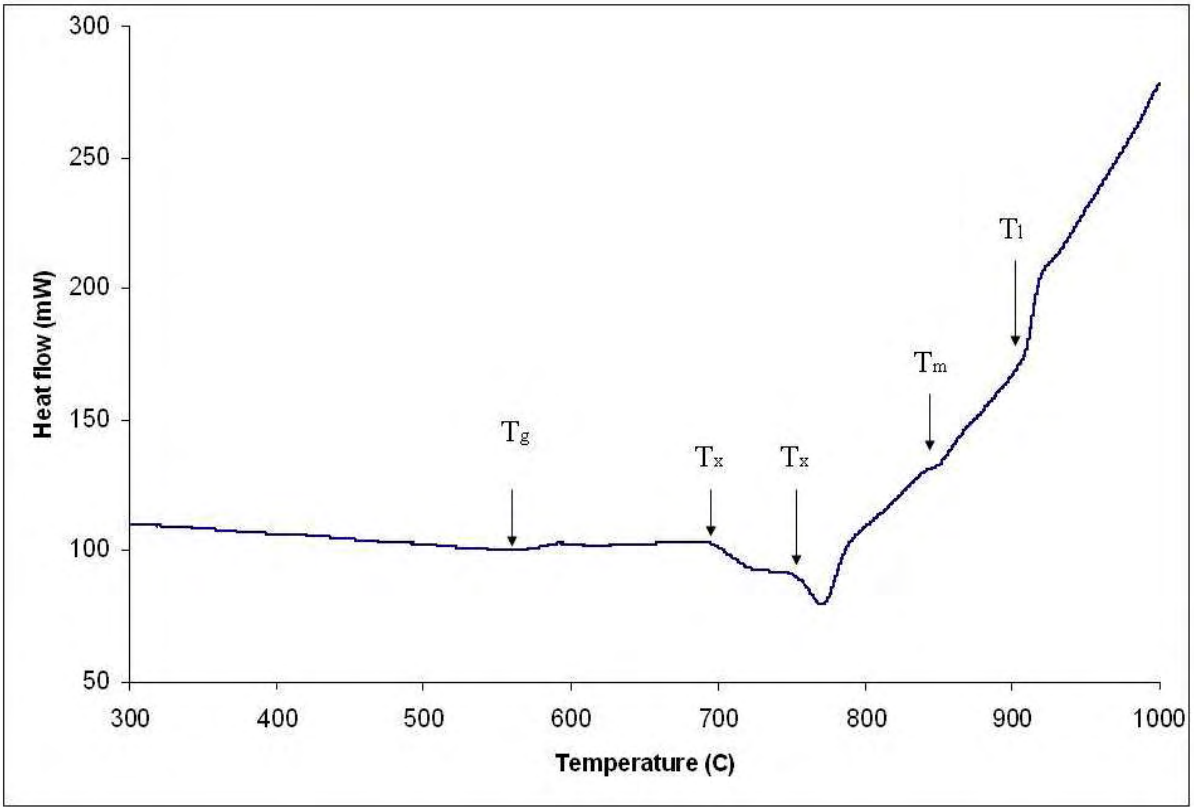

Figure 4.7 Differential thermal analysis of LD984 GLSO powder.

Changes in the heat flow were observed (Figure 4.7) corresponding to a glass transition temperature (T_g) at 560°C, an onset of melting temperature (T_m) of 850°C, a liquidus temperature (T_l) of 900°C and onset of crystallisation temperatures (T_x) of 680°C and 770°C. It is believed that the two crystallisation peaks relate to oxide and sulphide sites within the glass matrix [31, 32].

The liquidus temperature will be of critical importance in the microsphere production process as the particles must become molten to form into spheres. The liquidus temperature is lower than the temperature used to melt microspheres in the preliminary experiments, which suggests that the temperature needs to be notably higher to melt microspheres in the short time they will take to pass through the furnace.

4.3.2 Kelvin cooling of spheres

The speed at which the spheres cool is of critical importance to determine whether the spheres become glass or crystalline. Thus it is also important to the free fall distance below the furnace that is required for cooling. The simplest method of establishing a cooling time is to use the Kelvin cooling calculation.

In order to prove that a source of heat exists in the centre of the earth, Lord Kelvin derived an equation, from Newton's law of cooling, to determine the time taken for the earth to go from a molten state to its current temperature with no internal source of heat [94]. This same equation can be used to determine the time it takes for a sphere to cool as it leaves the furnace. This does assume an instantaneous change in surrounding temperature and a value of 1 for emissivity.

GLS is made up of 30% La_2O_3 and 70% Ga_xS_y which is a mixture of Ga_2S_3 and GaS [32]. La_2O_3 has a molar mass of 325 and Ga_2S_3 and GaS have molar masses of 101 [95] and 235 [95] respectively. This combination can be said to produce a combination of either $La_6O_9Ga_7S_7$ or $La_6O_9Ga_{14}S_{21}$, which have molar masses of 1682 and 2622 respectively. As GLS is a mix of these two the molar mass is taken to be approximately 2000. This can then be used to calculate the number of molecules (N) in a body of GLS, using the equation

Equation 4.1

$$N = \frac{mN_A}{M}$$

Where m is the mass of the body, N_A is Avogadro's number and M is the mol mass. GLS has a density of 4000 kg/m^3 [32].

The cooling time can be calculated from the Kelvin cooling equation [94]

Equation 4.2

$$t_{cool} = \frac{Nk}{2\varepsilon\sigma A}\left[\frac{1}{T_{final}{}^3} - \frac{1}{T_{hot}{}^3}\right]$$

σ is the Stefan-Boltzmann constant, ε is emissivity (taken to be 1), A is the surface area, k is the Boltzmann constant and T is the temperature. If a sphere of GLS is cooled from above its melting temperature (1500 K) to below its glass transition temperature (800 K) this gives a cooling time for a sphere (shown in Figure 4.8). Once below the glass transition temperature the spheres will not undergo crystallisation.

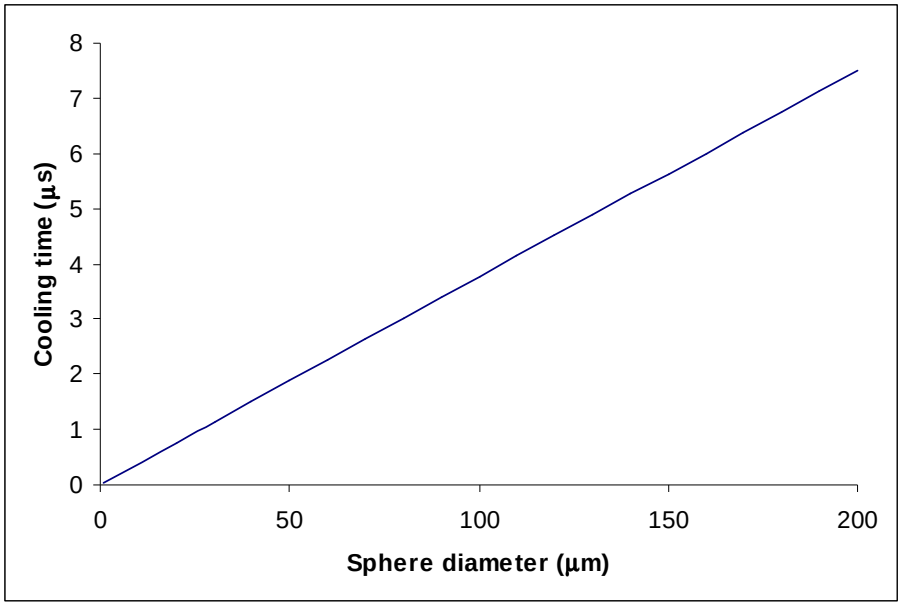

Figure 4.8 Cooling time for a GLS sphere, cooling from 1500K to 800K

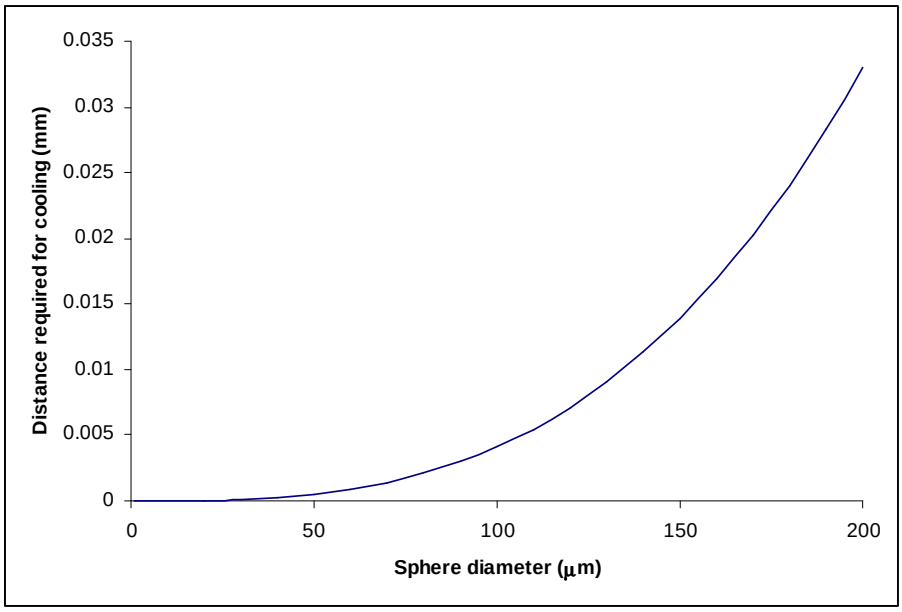

Figure 4.9 The distance in cool argon required for cooling GLS particles from molten to quenched glass, whilst in free fall. This assumes that particles are already at terminal velocity and the gas that they are falling though is not moving.

If the quench rate is too low the microspheres will be polycrystalline. It may then be necessary to incorporate a cooled zone into the microsphere production apparatus after the furnace.

The time it takes a particle of GLS to crystallise is variable so it cannot be determined if this cooling regime would produce crystals [96]. However it can be said that if the assumptions made are reasonable the spheres would be completely solid before they reach the end of the tube (Figure 4.9).

4.3.3 Heat transfer

To exert effective control over the production of microspheres it is helpful to understand the mechanism that causes the particles to melt. The mechanisms by which heat can be transferred are convection, conduction, and radiation. As the heat has to pass through the tube convection cannot be the only mechanism. Convection may be able to transfer heat to the outside of the tube, but only conduction or radiation can transfer heat through the tube. Conduction from the furnace tube to the inert gas inside the tube would result in a hotter zone at the edge of the tube. Whilst radiation would cause approximately uniform heating, as it is incident from all sides. However for radiation to transfer heat from the element to the glass particles, they would have to be efficient absorbers of the radiation.

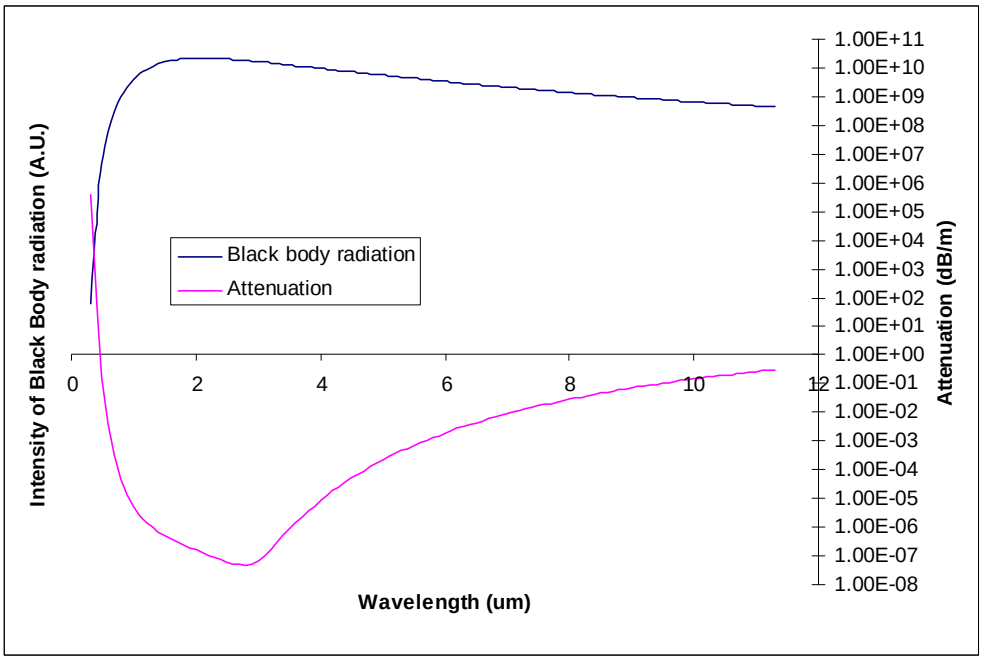

Figure 4.10 Theoretical black body spectrum expected inside the furnace and the theoretical absorption of GLS (both plotted on a logarithmic scale).

A furnace can reasonably be thought of as a black body emitter, and a comparison of the absorption of GLS with a black body shows that the lowest absorption of GLS coincides with the peak emission of a black body at the temperatures used in sphere production (Figure 4.10). Therefore it is unlikely that the dominant method of heat transfer from the furnace to the glass particles is via radiation. This leaves conduction as the method of heat transfer through the furnace liner. This means that the furnace liner would have to heat up the gas inside it, which would result in non-uniform heating, with a temperature gradient running from the edge to the centre of the tube. The presence of melted and un-melted particles in the preliminary experiments would also suggest non-uniform heat or heating in the tube.

4.3.4 Effects of flow

The flow of gas will have a significant effect on the production of microspheres. As heat passes through the tube by conduction, the particles must be heated by the gas through conduction. Therefore flow of gas will have a major impact on the heat that reaches the particles. Some particles will float in the flow of gas, which changes the way they are produced.

The fact that the flow of glass into the furnace is controlled by the flow of gas makes the process significantly more reproducible. The gas flow can be quantified and hence repeated in a different experiment.

It is possible to calculate the size of particles held buoyant in a flow of gas, from Stokes' law of terminal velocity [97]. By rearranging Stokes' law, the following equation can be derived

Equation 4.3

$$d = \sqrt{\frac{18\eta v}{g(\rho_s - \rho_l)}}$$

This can be used to calculate the size of the particles that are buoyant in the gas stream. Where d is the diameter of the particle, v is the terminal velocity, although in this case that will be the velocity of the gas flow rather than the particle velocity, ρ_s is the particle density, ρ_l is the density of the gas, and η is the viscosity of the medium.

Stokes' law assumes a uniform flow of gas across the tube, however this is unlikely to be the case in this system. Friction will cause a lower flow at the surface of the tube and at higher input flows turbulence will occur. These effects will cause the velocity in the tube to differ from the idealised version, but the effect this has on the buoyant particle size will be reduced by the fact that particle size is dependent on the square root of the velocity.

The uniformity of flow can be determined by calculating its Reynolds number. A Reynolds number is a dimensionless number related to the ratio of inertial forces. The point at which flow in a tube becomes turbulent occurs when its Reynolds number reaches ~2000 [98]. However it can be lower if there are inconsistencies in the surface, such as roughness or a sudden expansion of the tube.

The Reynolds number for an infinite tube is calculated from Equation 4.4

Equation 4.4

$$R = \frac{v\rho d}{\eta}$$

Where *v* is velocity, *d* is the diameter of the tube, ρ is the density of the fluid, and η is the viscosity the fluid. However, considering the velocity in terms of a volumetric flow (F), this becomes.

Equation 4.5

$$R = \frac{4F\rho}{\pi d\eta}$$

The density of argon at 0°C is 1.784 Kg/m^3 [95] and this was extrapolated to higher temperatures by approximating it as an ideal gas (Figure 4.11). The viscosity of argon was found in [99] (Figure 4.11). From this data and Equation 4.4, the Reynolds number in the tubes can be calculated (Figure 4.12).

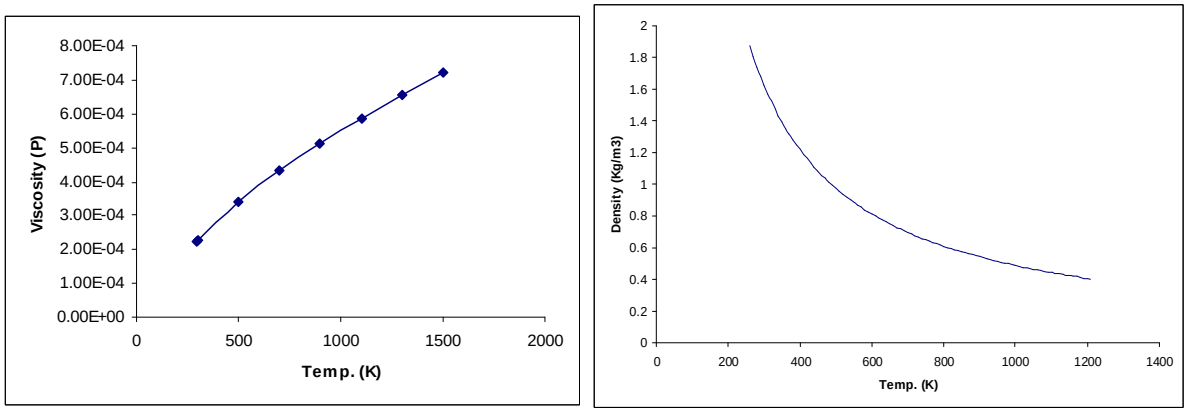

Figure 4.11 Basic properties of argon. Viscosity (left) and density (right).

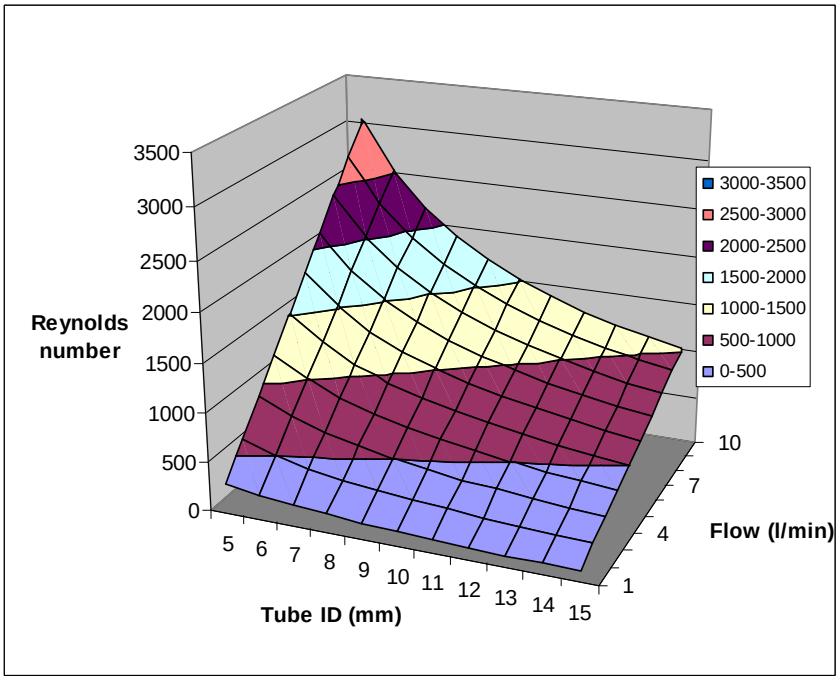

Figure 4.12 Reynolds number for argon at 300K flowing through a variety of tube diameters and at a variety of velocities.

The density of argon is likely to have significant errors further from the calibration point. But this will not have a major impact on the terminal velocity/buoyancy calculation as only the difference between densities contribute, and the density of the glass is three orders of magnitude greater than the density of argon. However it could have a significant impact on the calculated Reynolds number at high temperatures, this will be discussed later.

The viscosity of argon is quoted as having an uncertainty in the range of +/- 1%

The largest source of uncertainty is likely to be the measurements of the system, as follows. The uniformity of the internal diameter of the tube is unknown, but it is likely to be accurate to 0.5-1mm. Gas flows will only be accurate to 1l/min for the range1-10 and 0.1 for the range 0-1.2. The argon is pure to 99.999% (BOC Cryospeed), therefore impurities are not enough to affect its viscosity or density to any significant extent. The presence of the particles of glass in the gas will alter the density and viscosity of the gas as a whole, altering the real system from any calculations which involve only argon. There is some uncertainty regarding the temperature inside the furnace.

In measurements of the temperature in the furnace liner it was found that the temperature was not uniform through the furnace (Figure 4.13). Measurements were taken with a furnace liner in place and with an argon flow of 1 l/min upwards, to duplicate real experimental conditions.

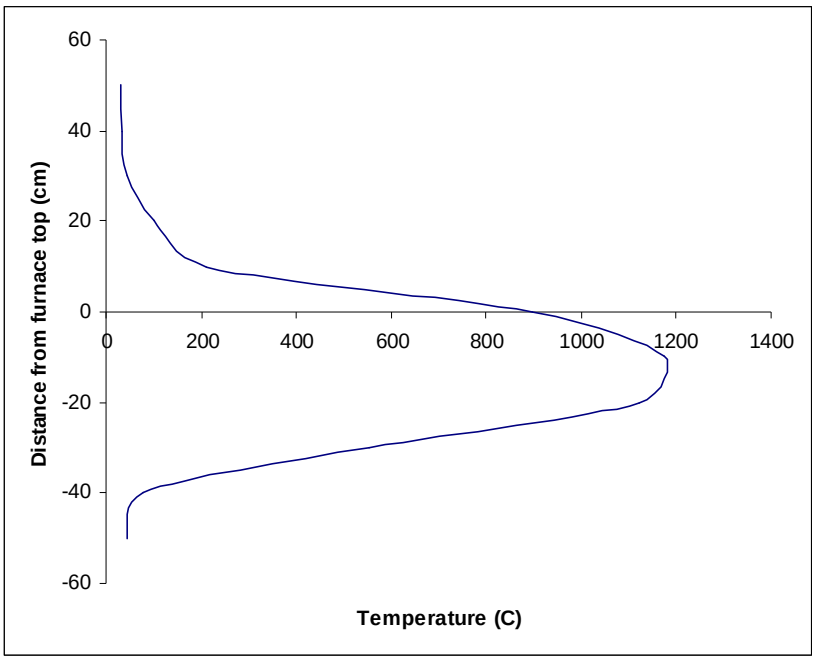

Figure 4.13 Temperature in the furnace tube with furnace set to 1100°C, the 0 point is the top of the furnace, which extends down to -38cm. The heating element runs along its entire length.

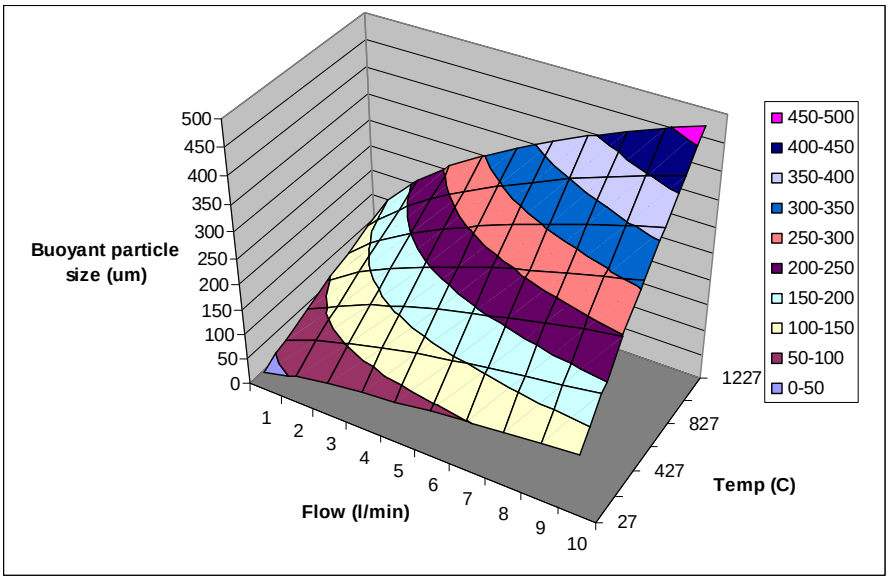

Figure 4.14 The buoyancy of particles in the carrier gas will increase with temperature and flow. (calculations based on a 12mm I.D. tube)

The temperature increase in the carrier gas will cause the particles to become more buoyant on average (Figure 4.14), if the localised effects of turbulence is ignored. This is true if a steady state is assumed, which does not take account of expansion of the gas once it has entered the furnace, however the expansion in the furnace will increase the trend towards turbulence (that is already apparent). Expansion in an enclosed space will cause the flow experienced to be higher than that measured at the input and cause particles to be more buoyant whilst the gas remains hot.

For particles that are blown vertically upwards, only the carrying potential of the room temperature gas is important; as the particles must be carried into the furnace by room temperature gas and the gas leaving the furnace quickly cools down to room temperature.

The calculated Reynolds number only predicts the onset of turbulence in an infinite tube. In a real system other effects will come into play, such as expansion, and inconsistencies in the surface. This means that the onset of turbulence in a real system cannot be calculated precisely.

The flow in the tube will have an impact on the characteristics of the system. Higher flows will result in turbulence, which will cause mixing, but may cause the calculated buoyancy to become inaccurate.

4.3.4.1 Terminal velocity within the furnace

When particles are dropped through the furnace the maximum size supportable by the hot gas will be critically important, as particles below this size they will not be able to pass through the furnace. If a particle were not buoyant at the (cool) top of the tube, but became buoyant in the hot gas of the furnace, it would effectively be trapped. This would increase its chance of hitting the side of the furnace liner and sticking to it, or hitting another sphere and merging with it. In that case the new larger sphere may be able to fall out of the hot zone.

With the spheres competing against the flow of gas there are likely to be rising and falling zones appearing, particularly in larger tubes that have more space for such mechanisms to occur. This has been observed in 30mm and 12mm tubes. This could be because larger tubes will have a larger Reynolds number for a given linear flow. But for a given volumetric flow the Reynolds number will reduce because the reduction in linear flow will dominate over the increase in radius. Therefore if the velocity of gas in the tube is due to convection then this would explain the observed phenomena, if velocity is due to volumetric flow it would not.

It is also worth noting that the convective movement is probably due, in some extent, to the change in temperature across the width of tube. This is likely to be more in larger tubes because linear flow will be lower, meaning that the heat will be less efficiently carried and will be less likely to dominate over the convection.

It is therefore important to choose parameters that will minimise the possibility of particles becoming buoyant when falling through the furnace (Figure 4.15).

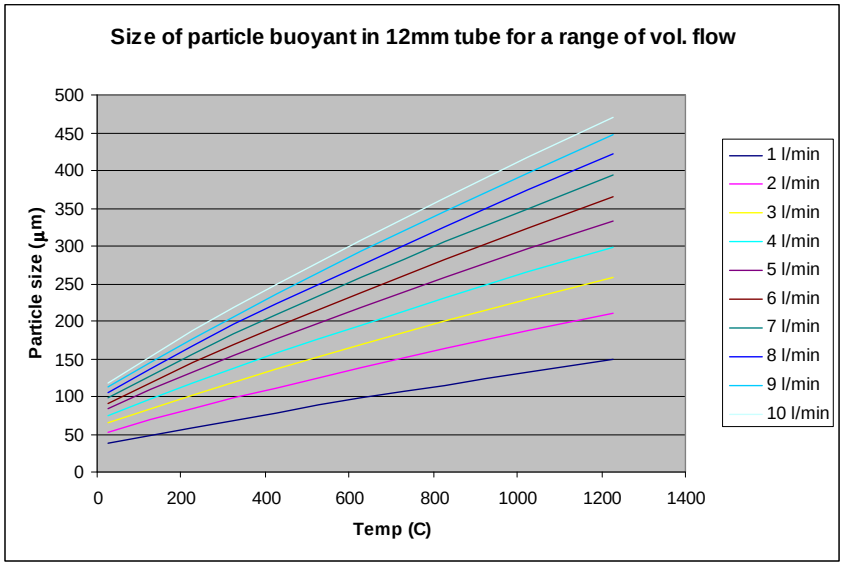

Figure 4.15. Size of particles of GLS that will be buoyant in a 12mm I.D. tube at a given temperature with a given input flow.

4.3.5 Theory conclusion

The thermal properties of the glass used in sphere production has been measured (section 4.3.1) and the time taken for a GLS microsphere to cool from above its melt temperature (900^{o}C) to below its glass transition temperature (560^{o}C) has been calculated (section 4.3.2). The time is dependent on the size of the microsphere, but would typically be 10^{-5}s. This suggests that cooling will occur significantly quicker than the time taken to fall to the bottom of the tube, neglecting buoyancy.

The mechanism by which particles are heated has been examined (section 4.3.3). The theory and the presence of melted and un-melted particles in the preliminary experiments suggests that heat passes through the furnace liner tube by conduction and is then carried to the particles by the gas.

As the heat reaches the particles via the gas, the flow of gas is critical to the production of microspheres. It will have a major impact on the heat profile in the tube by causing mixing of hot and cool gas (section 4.3.4) and it can also cause particles to float (section 4.3.4.1). This can be used as a way of moving smaller particles, but could cause particles being dropped through the furnace to become trapped in a flow of more buoyant gas.

To produce a uniform temperature, and therefore uniformity in the melting of the particles, will be an advantage to the microsphere production. Turbulent flow in the furnace will result in greater mixing of the gas than would occur in a laminar flow and would therefore produce a more uniform temperature. Turbulent flow can be formed by increasing the flow of the gas or decreasing the diameter of the tube.

4.4 Optimizing fabrication

Following the preliminary experiments and guided by the theoretical understanding developed, significant advances have been made in the techniques and apparatus used in GLS microsphere production (Table 4.1), introducing more control and reproducibility into the processes, and improving the quality of the atmosphere.

There have been several stages contributing to the design of the inert atmosphere equipment (Table 4.1). The first system used was a simple tube open at both ends with gas introduced at the top. This produced a very poor inert atmosphere, and fumes were produced when the crushed GLS particles were added. The fumes were taken away by the extract. In all

subsequent melt systems the inert gas was introduced at the bottom of the system and flowed up the tube through the furnace, to an extract system at the top.

Table 4.1 Showing the stages of development of the microsphere production process

	Initial trials /stage 1	stage 2	stage 3	stage 4	stage 5
Method of Glass input	Drop	Blown	Drop	Blown	Blown
Collection	Base of tube	Expansion chamber / Bubblers	Base of tube	Expansion chamber / Bubblers	Expansion chamber / Bubblers
Typical flow (litre/min)	1	1	1-10	1-10	1-10
Tube diameter (mm)	30	30	12	12	5
Tube length (cm)	160	160	120	120	100
Hot zone length (cm)	2.5	2.5	38	38	38
Typical temperature (C)	1200-1500	1200-1500	1100-1200	1100-1200	1100-1200
Range of spheres sizes (microns)	50-300	5 - 50	30-500	0.5-50	0.5-50

Since its original conception, the production apparatus has gone through several stages of development and these fumes are no longer seen in the tube, which would suggest that the atmosphere has been improved.

Subsequent designs of furnace liner concentrate on three main points, achieving a highly inert atmosphere, introducing glass to the furnace without degrading its atmosphere, and being able to collect / remove the spheres without degrading its atmosphere.

4.4.1 Microsphere collection

4.4.1.1 Tube base

In early trials it was important to be able to remove spheres whilst maintaining an inert atmosphere, as time on the equipment was limited. This also allowed microspheres to be produced in batches and inspected during the run without breaking the inertness. Therefore a number of different types of spheres could be produced in series with different production parameters.

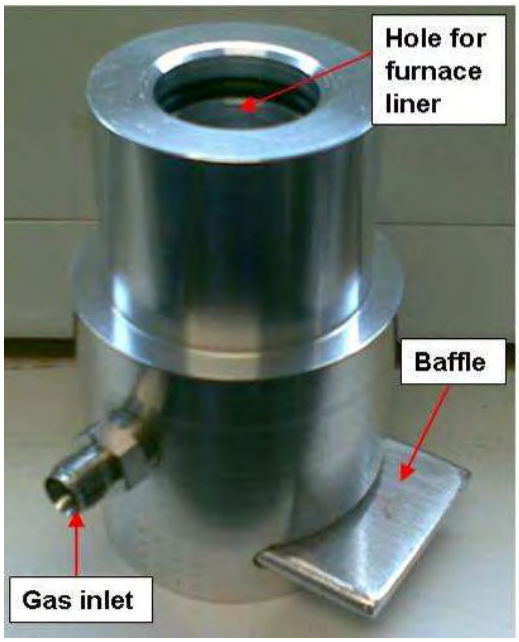

Figure 4.16 First tube base for microsphere removal, with baffle to reduce contamination during removal of spheres

In order to maintain the inert atmosphere, and remove the spheres, it was necessary to have a device at the base of the tube that would allow inert gas to flow in and particles to be removed without atmospheric gasses entering the furnace tube. There were two tube bases produced to achieve this (designed in collaboration with Edwin Weatherby). The first (Figure 4.16) had a baffle which had to be opened before each batch was produced. However this did not offer a complete seal and the quality of the atmosphere therefore relied on a constant flow of gas to prevent atmospheric gas from entering. The baffle was also prone to jamming. For these reasons a second tube base was produced (it is not shown as it was lost in the 2005 fire). It

had a tap at the output to prevent atmospheric contamination whilst in use. The lower part was made of Teflon to reduce the number of particles sticking.

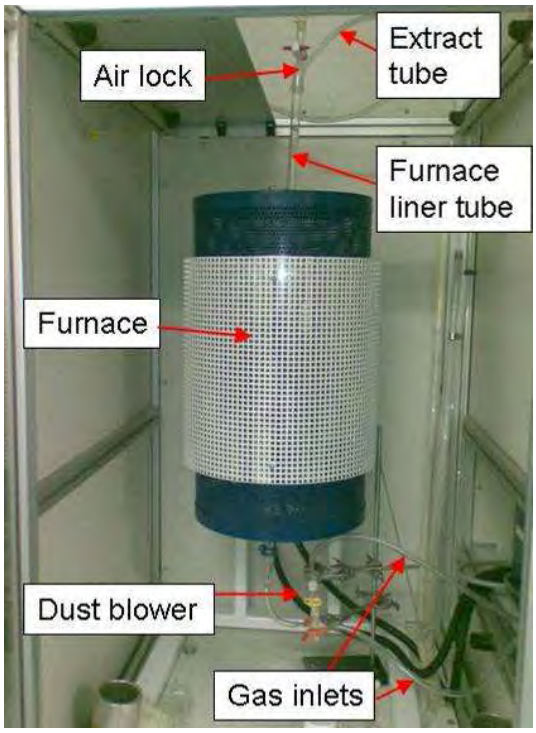

Figure 4.17. The dedicated microsphere production furnace in a unit designed by the author, showing essential components.

However spheres and small particles stuck to this and to the full length of the furnace liner and caused cross contamination of samples. It was therefore not viable to continue producing microspheres in this way. Once a dedicated furnace facility (Figure 4.17) was set up for microsphere production, time in use became less of a constraint and the equipment could be cleaned after each production run to avoid cross contamination. It was therefore no longer necessary to remove spheres whilst maintaining an inert atmosphere, as they could be removed at the end of the experiment when the apparatus was dismantled. For this reason the tube only needed a flat base to collect the spheres (Figure 4.18).

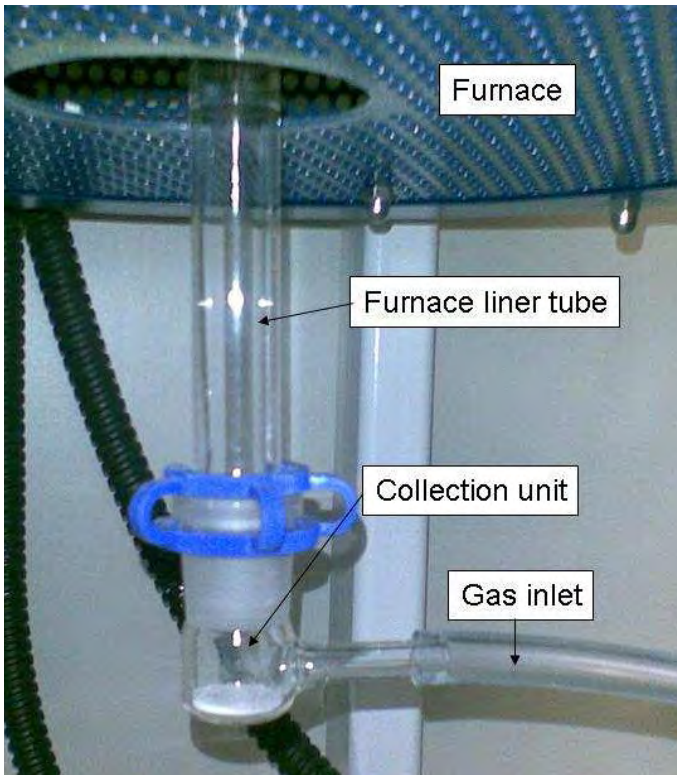

Figure 4.18 Flat glass base unit for collecting microspheres.

The design of the microsphere collecting mechanism has gone through several stages. Initially it allowed particles to be removed while the system was in use, but due to re-designing the whole system, the unit only needed to collect and hold the particles until the system was dismantled.

4.4.2 Glass input

4.4.2.1 Tube top

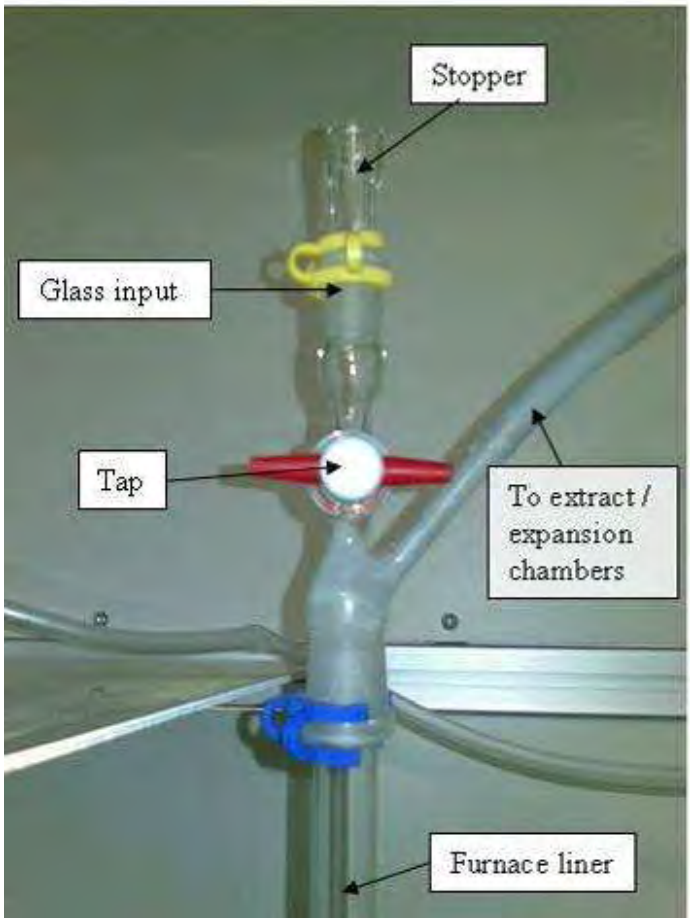

Figure 4.19 Furnace top airlock for introducing glass

In all stages of development the glass needs to be introduced to the furnace whilst maintaining an inert atmosphere. The method used when dropping glass from the top of the furnace tube, is a glass 'stopper and tap' airlock (Figure 4.19, designed by the author and Roger Moore) attached to the top of the furnace liner via a ground glass joint. The glass is put into the system with the tap closed, the stopper is then replaced and secured. To drop the glass into the furnace the tap is opened. This method is used for particles with diameter greater than ~30um.

This method of introducing glass into the furnace has been highly successful (see section 4.6).

4.4.2.2 'Egg timer' flow controller

To make the microsphere production process more reproducible, it may be favourable to regulate the flow of glass into the furnace. One method that was considered was to use a system similar to an egg timer. The GLS dust that is dropped into the top of the furnace is

similar in particle size to sand that would be found in an egg timer [100]. By putting the GLS dust into a tapered tube the flow of material could be regulated.

Initial experiments were carried out (Figure 4.20) to establish the viability of this method of flow regulation. They were found to be broadly successful. However, the GLS dust did sometimes tend to clog up and form threads or flowers of dust, particularly around the nozzle, (Figure 4.21) like iron filings on a magnet. The cause of the static clogging was assumed to be influenced by atmospheric moisture as identical experiments run on different days, produced different results. It was not obvious what was different in the atmosphere on the specific days, but it was assumed that on top of a furnace in a clean-room the atmospheric effects would be minimised.

A new top to the microspheres drop tower was produced and was successfully used to produce microspheres. Clogging remained an issue for this method of flow regulation, especially for smaller particles.

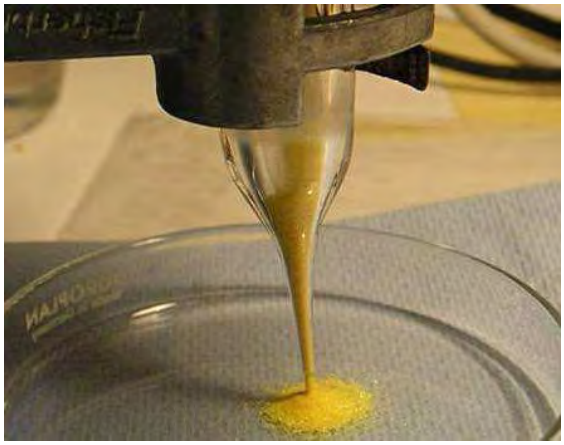

Figure 4.20 GLS flowing through the nozzle

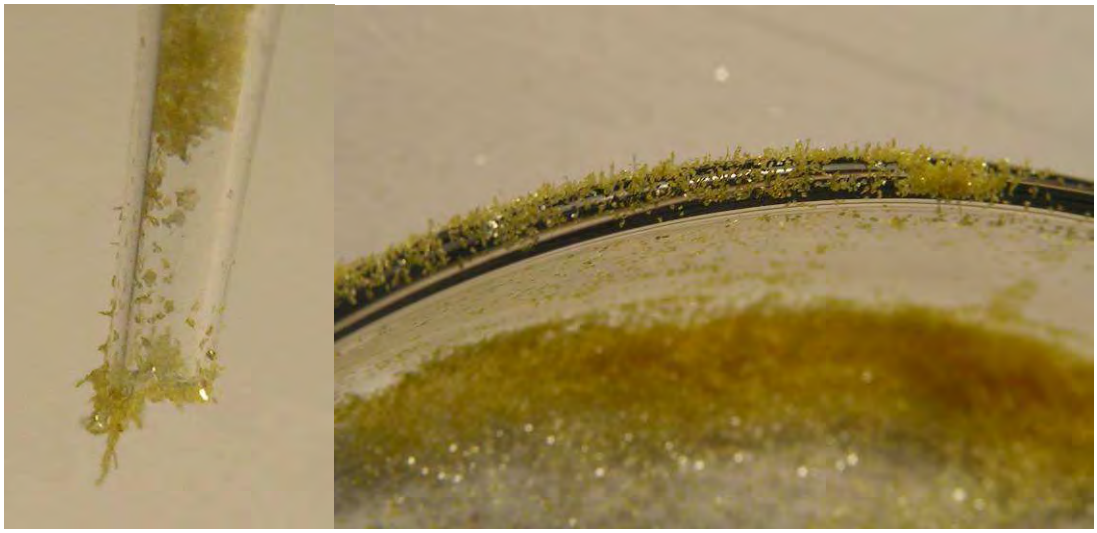

Figure 4.21 Crushed GLS sticking to the tip of the nozzle (left) and the edge of a Petri dish (right)

Ultimately the purpose of the egg timer was to regulate and limit the flow of crushed GLS. It did regulate the flow, but only at relatively large flow rates. When thinner nozzles were used to try to produce a smaller flow they clogged. Meaning that the experiment failed on the second aim and for this reason this method of flow regulation was abandoned. Flow regulation in subsequent experiments was achieved by manually controlling the tap on the top of the furnace liner.

4.4.2.3 Dust blowers

In comparing the two methods of introducing crushed glass into the tube furnace, as shown in Figure 4.2 and Figure 4.3, it became clear that regulating the flow of blown dust is relatively simple (compared to dropping crushed glass) as the flow of gas will control the flow of particles.

In the preliminary experiments, microspheres were only produced by dropping particles through the furnace, but this only produced particles down to ~ 30μm in diameter. After one experiment some glassy dust was found in the extract tube, it was washed out with solvent and examined under the microscope. It was found to contain spheres with a diameter of less than 30 μm. Producing spheres with a diameter <30μm had previously been a problem in that none could be found at the bottom collection area but it transpired that the spheres of 30 microns and less had been buoyant in the gas flow in the furnace, so they had all been carried up the extract in the gas stream, as predicted by the theory (section 4.3.4 and 4.3.4.1). The problem was not making small spheres, but collecting them. As they were buoyant in the gas it was necessary to have the gas carry the particles through the furnace. It was therefore apparent that, in order to produce smaller spheres, it would be necessary to alter the production process.

The first method of introducing particles into the gas flow that was tried, had GLS powder on a mesh with gas blowing from underneath (Figure 4.22), however, the GLS dust did not become airborne and remained on the mesh. After some experimentation, it was found that a relatively high flow of gas was necessary to get the particles airborne, whilst a much smaller flow of gas would keep the particles in suspension. A nozzle was used to achieve the high velocities required to get particles airborne (Figure 4.23), a relatively small flow/ velocity of gas could then blow the GLS dust into the gas stream entering the bottom of the furnace and carry it through.

Figure 4.22 First dust blowing system, containing a mesh. It did not work because the velocity of gas was not high enough

Figure 4.23 Dust blowing system consisting of a flask containing dust through which gas can flow and a nozzle to lift the dust

As particles were being carried through the furnace by the gas, it became necessary to devise a way of removing and collecting them. Spheres above 30 µm in diameter had been collected at the bottom of the tube, therefore spheres close to 30 µm, would only just be buoyant in the gas flow, which means it is very easy to remove them from the gas stream. This is how they came to be deposited on the glass of the extract tube.

The simplest way to remove the particles from the gas stream is to allow the gas stream to expand, thus slowing it down, and the particles will then fall out of suspension. This will only work down to a certain size, beyond which the particles will remain in suspension; to

overcome this problem the gas is then passed through a bubbling system to clean it. The bubbler has a sintered glass head to produce the smallest possible bubbles of carrier gas, and hence the maximum contact with the solvent to maximise the cleaning effect (Figure 4.24). Due to safety concerns about solvent vapour tracking back up the tube to the furnace, an expansion chamber and a solvent bubbler are used together in series. In practice the solvent bubbler removes very little from the gas stream, as most of the particles are taken out by the expansion chamber.

Figure 4.24 The system to remove particles from the flow of gas, consisting of an expansion chamber and a bubbler with a sintered glass head.

Small particles (typically <50µm, dependent on gas flow) can be blown through the furnace. It has been found to be practical to use a nozzle to get the particles into the gas flow. Once they have passed through the furnace they are collected in an expansion chamber and bubbler.

4.4.3 Experiments designed to study and optimise microsphere production

4.4.3.1 Effects of temperature on Sphere Quality

Spheres were produced at a range of temperatures to investigate its effect on the spheres produced. Particles are crushed, washed and sieved to between 52 and 62µm. They were then blown into the furnace, using the glass nozzle (Figure 4.23) blower. A 12mm diameter

silica furnace liner was used. The spheres were collected in the expansion chamber and bubbler described earlier (Figure 4.24).

When the furnace was set to 900°C very little melting occurred, as the temperature increased so did the percentage of particles that melted into spheres.

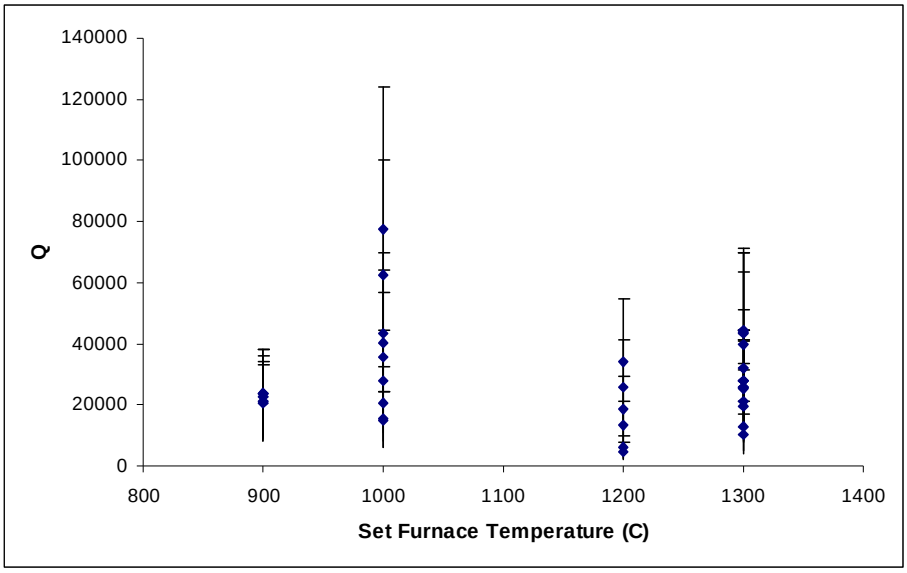

Figure 4.25 Q of spheres produced at a range of temperatures.

The Q value (see theory chapter) of the spheres was measured using the scattered spectrum technique (see next chapter). Some variation in Q was observed. The spheres produced at 1000°C had the highest Q values, however these values were only due to one family of modes and the width was close to the limit of resolution of the apparatus. Therefore the uncertainty is significant and it is quite possible that similar peaks were missed in the other spectra due to the peaks overlapping. The rest of the observed Q values are similar for all temperatures (Figure 4.25), implying that temperature does not have a significant impact on the Q of the sphere.

4.4.3.2 Heat transfer experiments

To establish the method of heat transfer, samples were produced to examine the effect of temperature and gas flow, on the yield of spheres produced. All were produced using the dedicated microsphere furnace, from LD1261(02) GLSO crushed and sieved to between 35 and 53 microns, were blown in an upwards direction through a 12mm I.D. tube.

It was found that increasing the melt temperature increased the percentage of particles that melted to form microspheres, as would be expected (Figure 4.26). However, as the flow was increased the melt percentage increased (Figure 4.27).

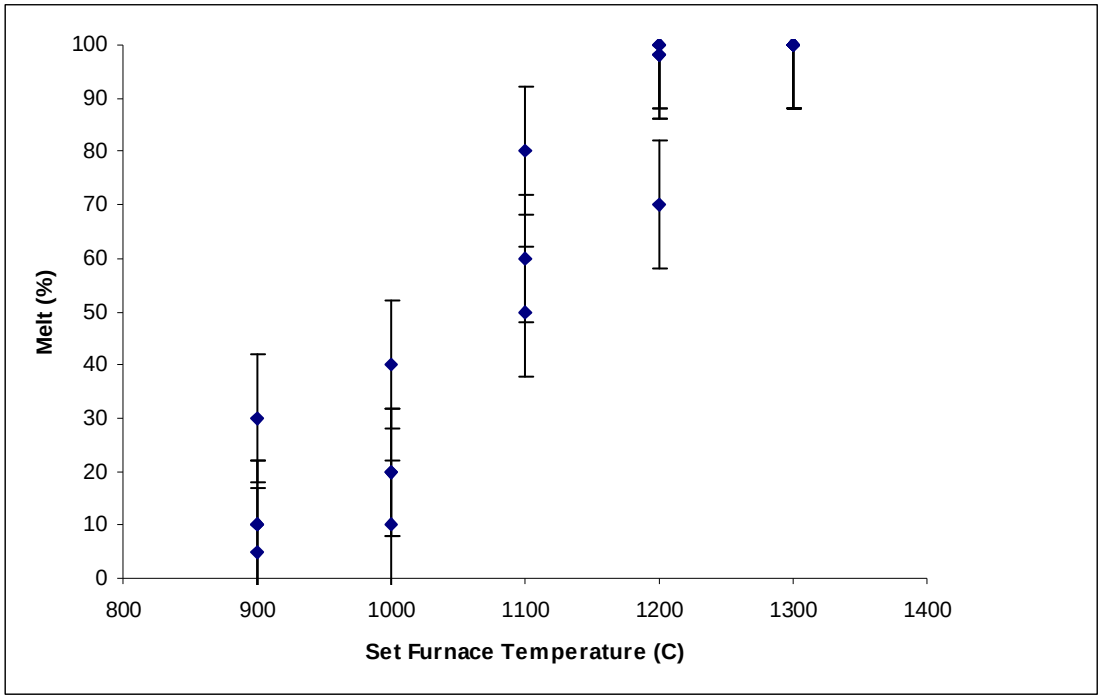

Figure 4.26 Effect of furnace temperature on melt percentage

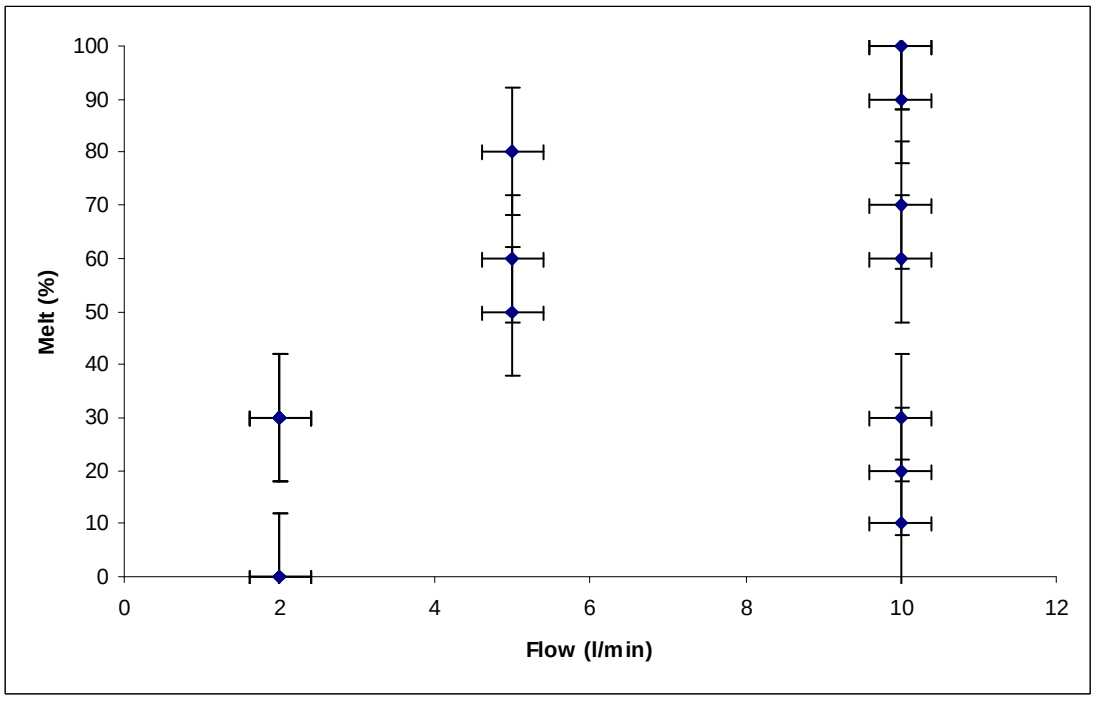

Figure 4.27 Variation in melt of particles as carrier gas flow changes. As flow increases the maximum melt (%) increases.

This seems to run counter intuitive, as the longer transit times associated with lower carrier gas flows would be expected to produce high yields of spheres. A possible explanation could be turbulence in the furnace, causing the pattern of flow to change resulting in a more uniform melt. If a linear laminar flow was occurring the melt rate would be expected to increase at lower flows, as the time spent in the hot zone would be higher, but in a laminar flow the gas

temperature will not be uniform across the tube inside the furnace. If heating was occurring by radiation then uniform heating would be expected. If heating is occurring by conduction, not radiation, there will be a temperature gradient from the tube edge to centre, this will allow the particles in the centre of the tube to remain cooler avoiding melting and forming spheres. A turbulent flow will mix as it flows along the tube, resulting in a more uniform temperature distribution across the diameter of the tube. The melt characteristics seen suggest that flow becomes turbulent at the higher flows used.

The flow in the 7mm I.D. hose before it joins the 12mm I.D. furnace liner will be turbulent at 10l/min, as the Reynolds number (Figure 4.12) is 2262. At this flow rate the Reynolds number in the furnace liner is calculated to be 1319, but flow is unlikely to become laminar for a number of reasons. The area the gas flows in expands sharply. There is a small rim approximately 10cm into the tube caused by joining two pieces of glass. This will act as a trip and cause turbulence to occur.

A laminar flow will not re-form because non-uniform heating will cause a non-uniform expansion of gas. The non-uniform heating of gas in the tube can be inferred from the presence of melted and non-melted particles.

Flow in the furnace is likely to be turbulent at the higher flow rates used in sphere production, and will remain laminar at lower flow rates. This has resulted in a higher percentage of material being melted into spheres at higher flow rates. This suggests that turbulent flow is desirable to produce a high yield of spheres, in agreement with theoretical calculations (section 4.3.4).

4.4.3.3 Utilisation of turbulence

In order to take advantage of the effects of turbulence, a smaller tube was required in the sphere melting process (Figure 4.12). A new tube was used which had an internal diameter (I.D.) of 5mm, compared to the 12mm I.D. of the previous tube. As it was not designed to have material dropped down from the top, it did not require the removable airlock and base units and could be connected directly to the hose carrying the gas.

It has been observed, in all systems, that the points where expansion or compression of the flow occur, (such as joints) caused the particles to drop out of suspension in the gas. Connecting the tube directly to the gas hoses, will cause the gas to be subject to less expansion and compression as it passes through the system and reduce the likelihood of particles being deposited.

The reduction in tube size will also cause larger particles to be buoyant in the gas flow (Figure 4.28). This will give greater control over a larger size range.

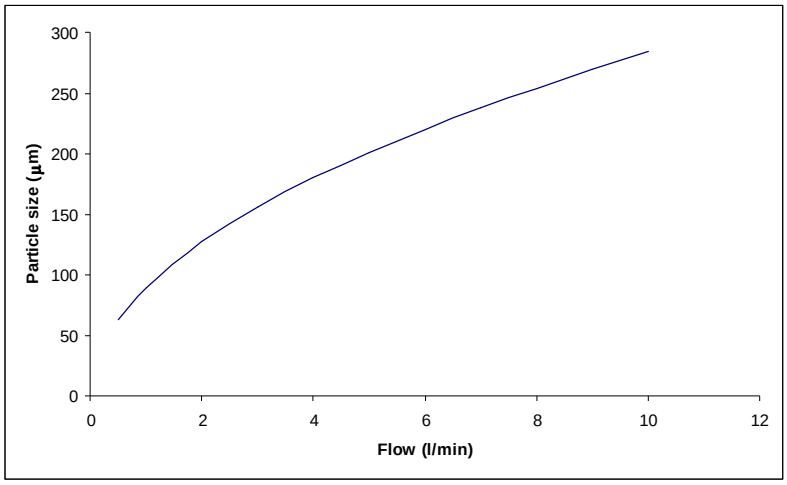

Figure 4.28 Size of particle buoyant in a 5mm tube at 20C.

To demonstrate the effects of the smaller tube size, experiments were conducted with the same volumetric flow and temperature, but using the different glass systems (12mm and 5mm I.D.).

A significant difference was noted between these runs (Figure 4.29). Material that passed through the 12mm tube was found to have a large percentage of un-melted glass, whilst material that had been passed through the 5mm tube was nearly all melted, with a small percentage (<5%) being fire polished but irregular in shape.

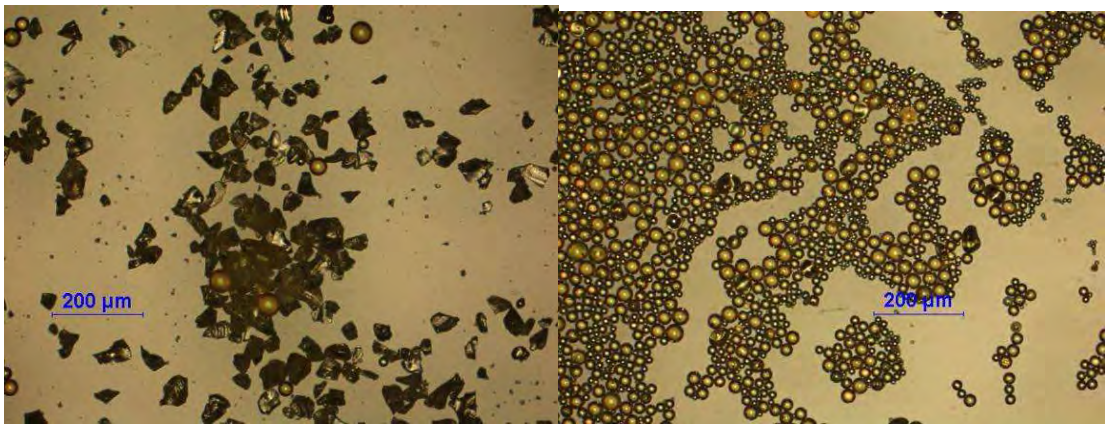

Figure 4.29 Two samples produced with the same vol. flow and temperature, but with different glassware designed to take advantage of turbulence. The sample on the left was produced in a 12mm I.D. tube, the sample on the right was produced in a 5mm I.D. tube.

The thinner tube produced a higher yield of spheres for the same input parameters. Naturally the same volumetric flow in both tubes does not correspond to the same velocity in both tubes; however the melt yields from the thinner tube are looked at in more detail in a later section and are found to agree with intuitive expectations.

4.4.3.4 Effects of temperature and flow on blown sphere production

The aim of this experiment was to investigate how gas flow and temperature affected the production of spheres. Using the thin furnace liner, particles were blown upwards through the furnace to the expansion chamber and bubblers. In all runs, no notable quantity of material was found in the methanol filled bubbler, however significant quantities did come to rest in the hose linking the furnace liner and the expansion chamber. For this reason, the only material taken was from the hose (denoted by H suffix) and the expansion chamber (denoted by B1 suffix). Some batches had to have the expansion chamber washed several times and these are denoted by a decimal point after B1 and the number of the wash, so B1.1 denotes the first wash of the expansion chamber.

To avoid possible confusion, caused by differing melt characteristics, only one size and composition of glass particle was used as the input. The glass (LD984 GLSO) was originally made for fibre production, so has low attenuation. The thermal properties of this glass were measured (see section 4.3.1). It was crushed and washed in methanol, to remove smaller particles, and filtered to between 20 and 35 microns.

A number of batches of spheres were then produced with varying gas flow rates and furnace temperatures (Figure 4.30 - 38). All runs had the same flow through the nozzle (1 litre/min). Quoted values of flow are the flow past the nozzle, therefore total flow in the furnace will be the quoted flow value plus the flow through the nozzle.

Once the particles had passed through the furnace and been collected, they were examined under a microscope (Nikon eclipse LV100) and photos were taken.

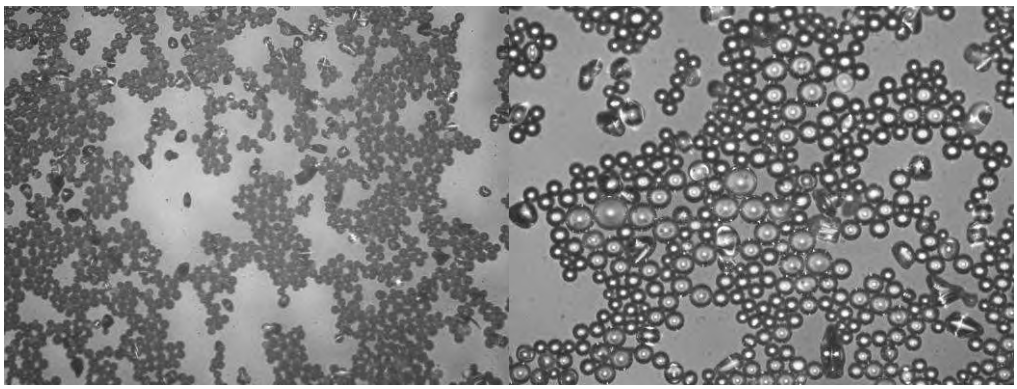

Figure 4.30 M118 H, 1150^{o}C 2l/min, seen through x10 (left) and x20 (right) lens.

Figure 4.31 M119 H 1100°C 2l/min, seen through x10 (left) and x20 (right) lens.

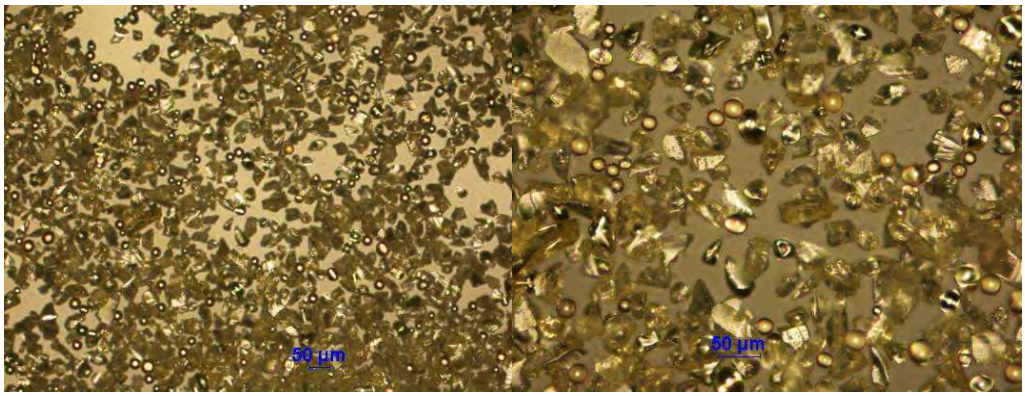

Figure 4.32 M122 H 1100°C 5l/min, seen through x10 (left) and x20 (right) lens.

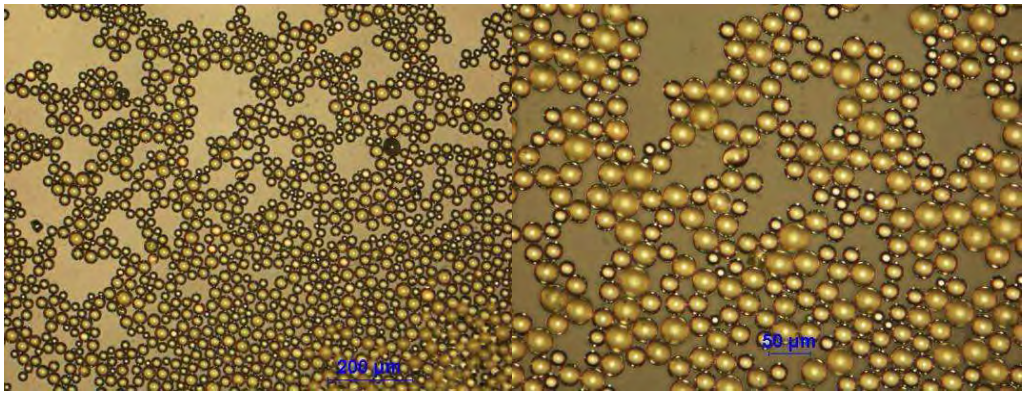

Figure 4.33 M123 H 1200°C 2l/min, seen through x10 (left) and x20 (right) lens.

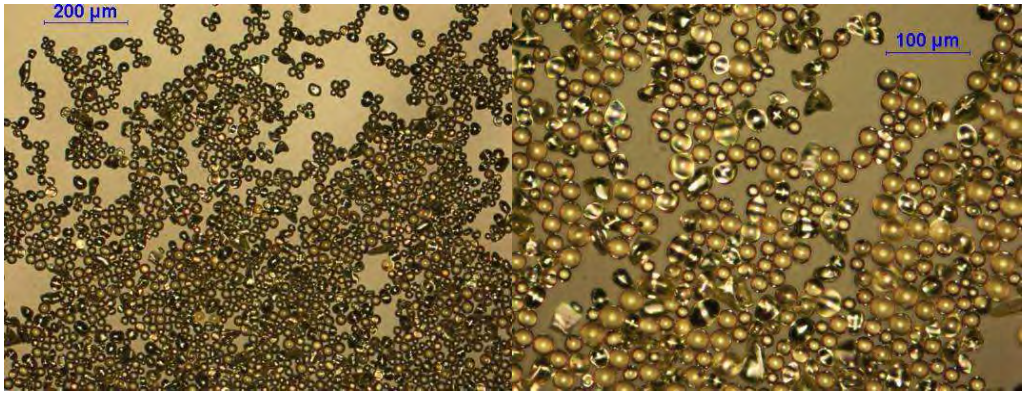

Figure 4.34 M124 H 1000°C 2l/min, seen through x10 (left) and x20 (right) lens.

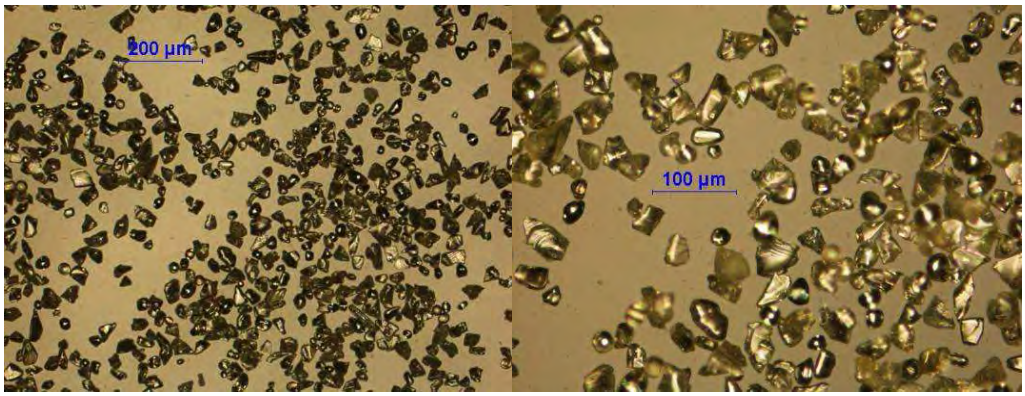

Figure 4.35 M125 H 900°C 2l/min, seen through x10 (left) and x20 (right) lens.

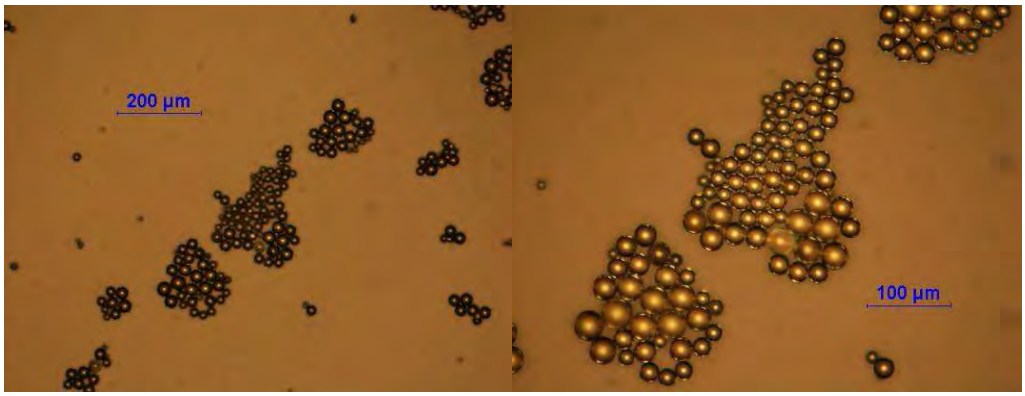

Figure 4.36 M128 H 1100°C 1l/min, seen through x10 (left) and x20 (right) lens.

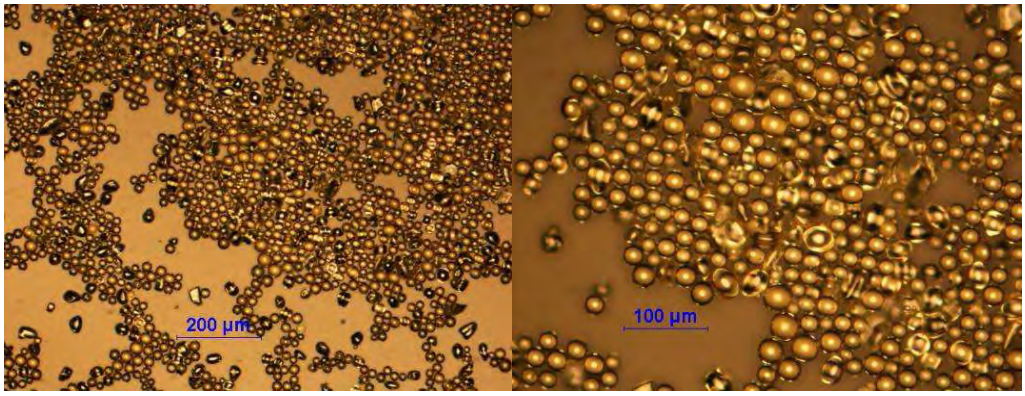

Figure 4.37 M129 H 1100°C 3l/min, seen through x10 (left) and x20 (right) lens.

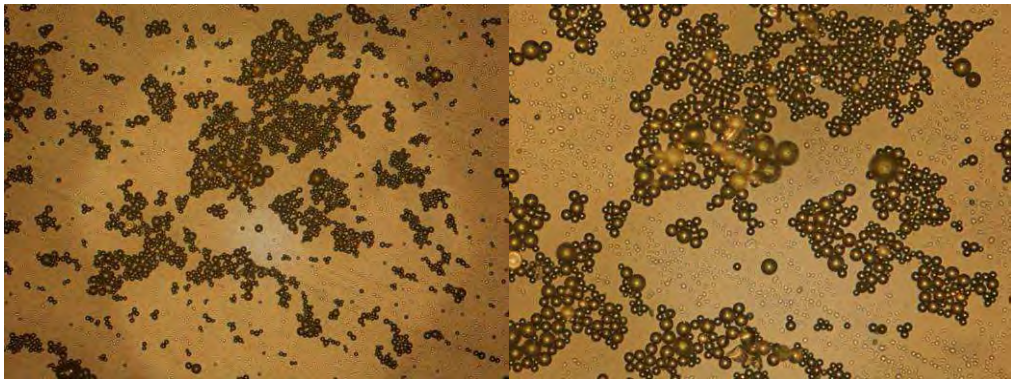

Figure 4.38 M131 H 1200°C 3l/min, seen through x10 (left) and x20 (right) lens.

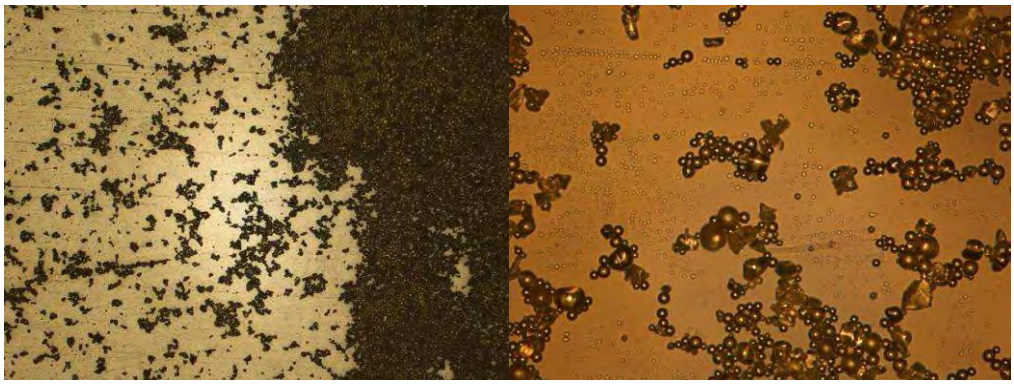

Figure 4.39 M132 H 1200°C 5l/min, seen through x10 (left) and x20 (right) lens.

It is clear that the difference in melt percentage / yield between many of these batches is large. A value of melt percent can be estimated from the pictures and used to build up a more quantified picture of the melt characteristics. As the values range from 0-100% the inaccuracies of estimation will be small compared to the large variation in melt percent seen in the batches.

This data does not represent the yield in terms of the amount produced relative to the amount put into the melt system. This has been largely ignored in this study as the total quantities are so small that it would be very difficult to give any kind of quantified value. There are significant losses of material from particles sticking to the sides of the tubes before, after and inside the furnace. This is in evidence in all batches but its effects are magnified at low flow rates. It is believed that at high temperatures some particles will evaporate completely. Evidence of this has been seen in the form of a thin uniform orange / yellow film deposited on the glass of the furnace liner above the furnace.

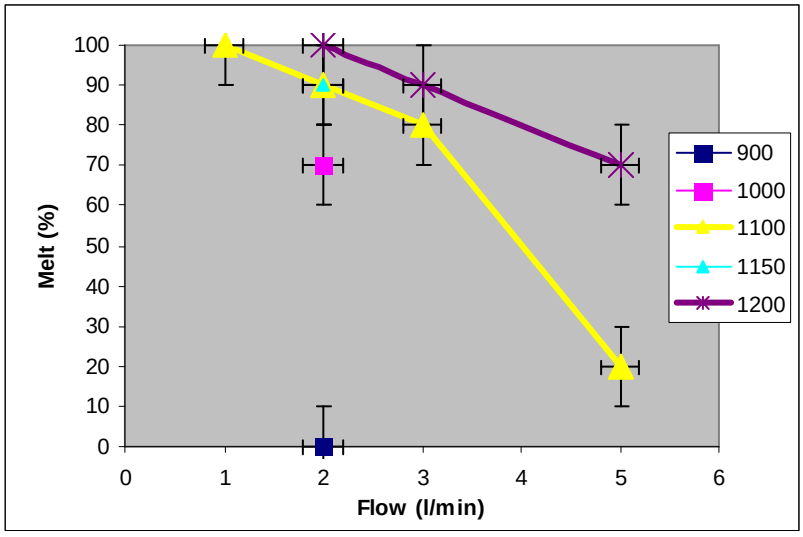

Figure 4.40 Flow vs. melt percentage for different temperatures (shown in degrees C), for a 5mm tube that utilises turbulent flow.

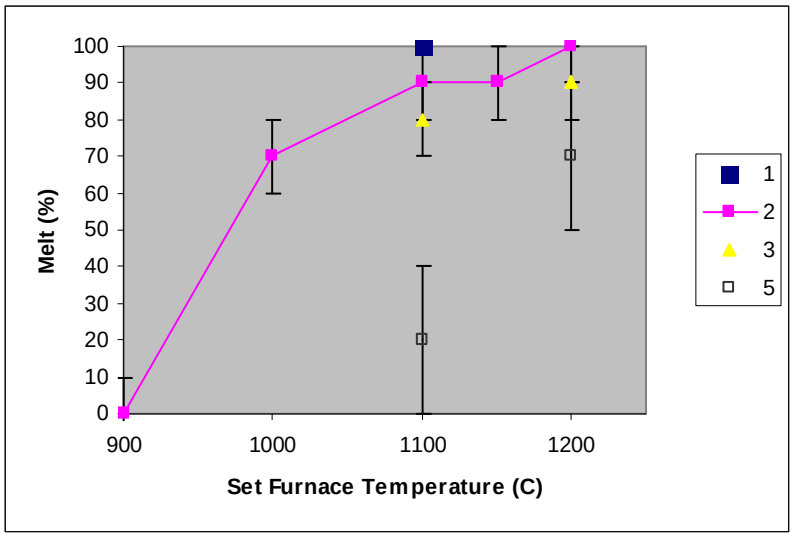

Figure 4.41 Furnace temperature vs. melt percentage for different flows (flows are shown in litre / min), in a 5mm tube system that utilises turbulent flow.

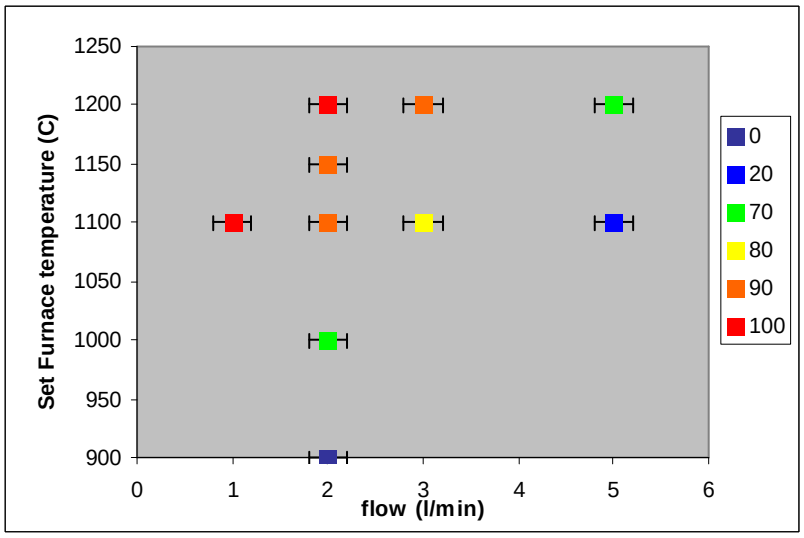

Figure 4.42 Melt percentage vs. furnace temp for different melt percentages, in a 5mm tube, designed to utilise turbulent flow.

The melt rate increases as temperature increases and flow rate decreases (Figure 4.40, Figure 4.41 and Figure 4.42) as intuitively expected. Higher temperature increases the chances of a particle melting and the longer it spends in the furnace the more likely it is to melt. This is contrary to previous results which showed the melt percentage increasing at high flow rates. But this was due to the onset of turbulence which does not play such a major role in this narrow tube system, as all flow rates have a similar or larger Reynolds number than those seen at the onset of turbulence in the larger tube.

This data would seem to suggest that the ideal system would have the highest temperature and lowest flow rate possible, but the system can only cope with a particular temperature range before the glass of the furnace liner melts or the particles passing through evaporate. The

number of particles lost in transit to the collection point will be a function of the flow rate. At 1 litre/min only a very small amount of particles were collected, so this represents a poor production regime even though 100% of particles collected had melted into spheres.
If spheres are only required as examples, then these low yields may be acceptable. However if a large number of spheres were required then the conversion efficiency of input material into spheres may become more important.
Above 1 litre/min the quantity of particles collected were similar. The melt percentage increases as flow decreases and temperature increases, however at low flows the number of particles that get through the furnace becomes small and at high temperatures the furnace liner melts and GLS will evaporate.

4.5 Optimum fabrication technique

Several techniques were integrated to establish an optimum system for microsphere fabrication.

4.5.1 Sphere fabrication

The optimum method of sphere production depends on the size of particle being produced. Smaller particles are blown upwards into a 5mm I.D. silica tube passing through the furnace, whilst larger particles are dropped downwards into a 12mm I.D. silica tube. The blown method can produce microspheres up to 50μm in diameter (Figure 4.33), whilst the dropped method can produce microspheres down to 30μm in diameter. These limits are not fundamental, but could be controlled by making changes to the system, this is also true of the maximum and minimum spheres produced (discussed later in section 4.6.1), however they do represent a convenient crossover point from one system to another.
In both cases the atmosphere in the system is purged with 5 litre/min for 5 minutes prior to sphere melting to produce an inert atmosphere.

4.5.1.1 Blown

The particles are blown into the furnace using the nozzle blower (Figure 4.23). The flow through the nozzle (typically 1liter /min) lifts the particles, which are then carried into the furnace by the carrier flow (typically 2 litres /min). It passes through the furnace in a 5mm I.D. silica tube. After the furnace the flow goes to the expansion chamber where the particles fall out of suspension from the flow. After the expansion chamber the gas passes through a bubbler filled with methanol to remove smaller particles and then goes to the extract.

All parts of the apparatus are connected by plastic hoses and notable quantities of particles are often found in the hose connecting the furnace liner to the expansion chamber.

4.5.1.2 Dropped

Larger spheres are produced by dropping through the furnace. A flow of gas (typically 1liters/min) is maintained throughout to ensure that the atmosphere remains inert. The particles are dropped from the stopper-and-tap airlock (Figure 4.19), into a 12mm I.D. furnace liner tube. At the bottom of the tube the spheres are caught in a flat glass base (Figure 4.18). The airlock, tube and base are all connected by ground glass joints.

4.5.2 Particle handling and processing

4.5.2.1 Glass crushing

Glass particles have to be a suitable size and uniformity before they are melted into microspheres, this allows an amount of control on the spheres produced. We use two different methods of glass crushing, firstly there is a combination of pestle and mortar, and sieve (Figure 4.43) to produce glass particles of the required size. Secondly, we use a Retsch pm 100 ball mill to produce a much finer powder (Figure 4.44) than can be produced with a pestle and mortar.

The ball milling process was to crush 30g of GLS to <300um, which was then placed in the ball mill with 3mm milling balls and topped up with HPLC methanol, the ball mill was set to 25Hz, on for 1 minute and then off for 1 minute continuously running for a total of 40mins. This produced a range of sizes with most material in the 1 to 10 μm range.

Figure 4.43 Metal sieves, pestle and mortar used for crushing and separating particles.

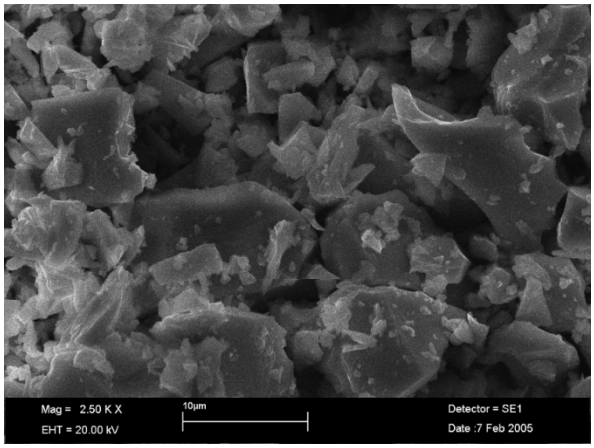

Figure 4.44 SEM picture of GLS that has undergone the ball milling process, but no washing or separation.

Examination of SEM pictures of ball milled powder (Figure 4.44) suggests that a typical particle size produced by this method is in the region of 1 to 10 µm. The only practical method of separation we have at our disposal for particles of this size is sedimentation; cloth sieves were available, but these were found to clog easily.

The steel sieves used ranged from 2mm to 38µm, cloth sieves were also used down to 5µm, but these were impractical.

With both methods a range of particle sizes are produced. These then have to be separated according to size.

4.5.2.2 Handling particles / cleaning dust etc.

Once small particles have been produced, it is necessary to have methods in place for handling them. Small GLS particles stick to surfaces and this can make them difficult to handle. It has been found that when microspheres are placed in a liquid it overcomes the problems associated with their static properties. This means that small quantities of microspheres can be easily and accurately transferred, by means of a pipette. As GLS can react with water [75] an organic solvent is used (typically HPLC methanol).

The spheres are also stored in solvent to limit oxidisation and any dust attaching to their surface.

4.5.2.3 Sphere / particle imaging

It is often useful to be able to examine the spheres under a scanning election microscope (SEM). Preparation for this involves mounting them on a small metal stub with a sticky carbon pad, then coating them in a thin conducting layer. For reasons that will be discussed in chapter 5 it was concluded that the spheres needed to be dry before being placed on the

pad. This was achieved by placing the particles in solvent on a carbon film and allowing them to dry, before placing the film on the pad. A mounting for a transmission electron microscope (TEM) was used, as this had a thin film of carbon suspended on a copper grid (seen in Figure 4.45), which makes it easy to handle. The spheres were dried in an oven to make sure that all the solvent was removed, the sample was then mounted on the pad and coated with gold or carbon in the usual way. This method of preparation and imaging has allowed particles and features of less than 1μm to be observed (see section 4.6.1).

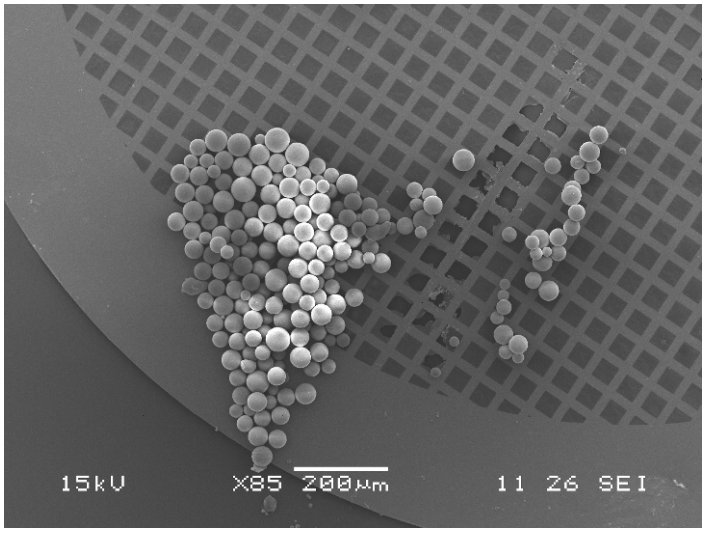

Figure 4.45 Spheres mounted on a TEM grid, on an SEM stub.

4.5.2.4 Separation of particles according to size/sedimentation

The particles of crushed glass can be separated by sieving, this method was found to be inadequate as the only form of particle separation. The steel sieves used were 5% accurate (according to their specification literature) and the differences between sizes were larger than this. When sieving particles of 50 μm or less the sieves had a tendency to clog, making it difficult to be sure of the size. The most significant problem was that smaller particles would stick to larger particles and therefore give false results in experiments. It was therefore necessary to use another method of particle separation.

Sedimentation is a process that is used in the geographical sciences, it utilizes the slow terminal velocity of a particle through a liquid to sort particles according to size. The terminal velocity (v) of a particle can be determined by Stokes' law Equation 4.3.

According to Stokes' law, the terminal velocity of a particle moving through a viscous medium, is determined by the square of its radius. Therefore any method that takes advantage of Stokes' law to separate micro-particles will be more accurate than a method that relies on the radius in a linear fashion (Figure 4.46).

Sedimentation works by having a uniform suspension of particles in a liquid and allowing it to stand for a given time while the particles settle, then pouring off the liquid from the sediment. The time it takes a particle to fall through a given depth of liquid is determined by Stokes' law (Figure 4.46), once this time has elapsed, only particles smaller than this size will remain in suspension. The particles in the sediment will be a mix of sizes because particles that start out lower down the liquid will take less time to reach the sediment. Therefore if complete separation is important the process must be repeated.

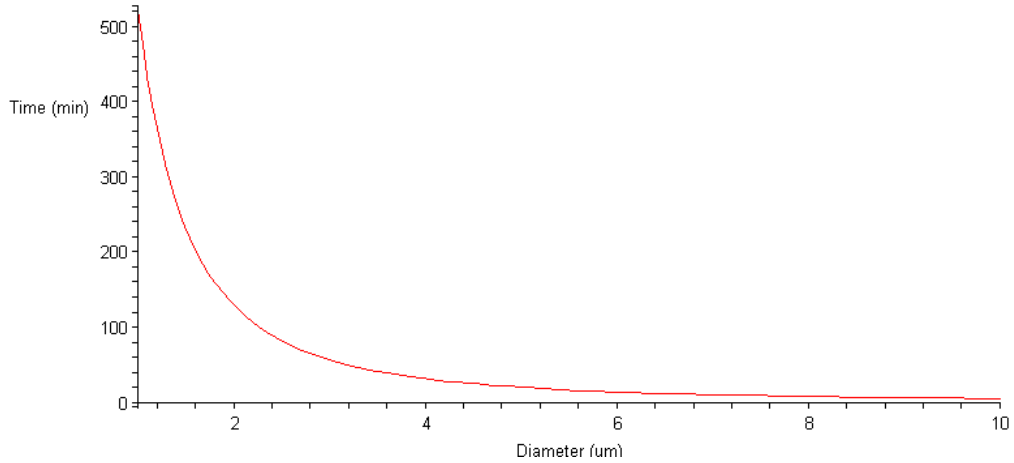

Figure 4.46 Calculated Sedimentation drop time in minutes of 1 to 10 micron particles through 10 cm of methanol at room temperature.

Figure 4.47 Sedimentation apparatus.

A piece of apparatus was designed for sedimentation, consisted of a tube with two taps (Figure 4.47). The distance from the first tap to the tube top was 10cm, the second tap was below that positioned at the base of the tube. A suspension of crushed glass particles in

solvent was placed in the tube with the taps closed, the stopper was replaced and the tube was shaken to ensure a uniform suspension. The tube was then placed in a stand for a specified time, once this time had elapsed the top tap was opened and the liquid was collected. The sediment could be collected by opening the lower tap.

For larger particles sedimentation was impractical, due to the very short time associated with them, it was therefore necessary to separate these particles with a sieve. By this method of sedimentation it was possible to separate the particles to be sieved from the smaller particles.

False measurements of particle size can occur due to flocculation when dealing with high concentrations of particles. Flocculation is the process by which particles come together to sediment as if they were a larger particle. Flocculation can be avoided by using a more dilute suspension of particles or by separating the smaller particles from the larger mix of particles. When dealing only with the particles still in suspension, contamination due to flocculation can be minimised. Evidence of flocculation has been seen, but only in very small particles (<1um).

Previously the procedure for separating particles, prior to melting, involved sieving them and then washing smaller particles through with a solvent. This worked for the most part, but smaller particles than those of the sieve separation were found to stick to the larger particles. One way around this problem is to place all the crushed glass in the sedimenter with solvent and shake to form a suspension, after a designated time the liquid can be drained off. This process is repeated until the liquid drained off becomes clear. This will prevent contamination of larger particles by small particles.

The best method of particle separation combines sedimentation and sieving. The particles are separated in the sedimentation apparatus, starting with the smallest particles. Once the smallest particles have been removed the remaining crushed glass, which cannot be effectively separated by sedimentation, can then be sieved.

Once the crushed particles have been cleaned and sorted into sizes they are ready to be melted into microspheres, however the microspheres produced exhibit a range of sizes larger than the range of input particle size. This may be due to a number of causes, such as non uniform heating, or non uniform flow. Steps could be taken to minimise these effects, but random fluctuations can never be eliminated from the process. Therefore size separation is essential both before and after melting.

4.5.2.5 Static sorting

When microspheres are produced, they have a considerable static charge, which causes them to stick to glass and other surfaces.

Static charges are known to concentrate at edges and corners of objects [98] and it is therefore considered likely that spherical objects will maintain their charge more than non-spherical particles. Experiments into using this as a means of separation were carried out using a pair of parallel horizontal plates (similar to the apparatus used in a Millikan oil drop experiment), but these proved unsuccessful.

If the parallel plates were vertical the particles would need less force acting on them as they fell in order to separate those with charge and those without. Apparatus was designed and built by the author (Figure 4.48), but it was destroyed by fire before it was used and further experiments were not carried out as the following method had been devised.

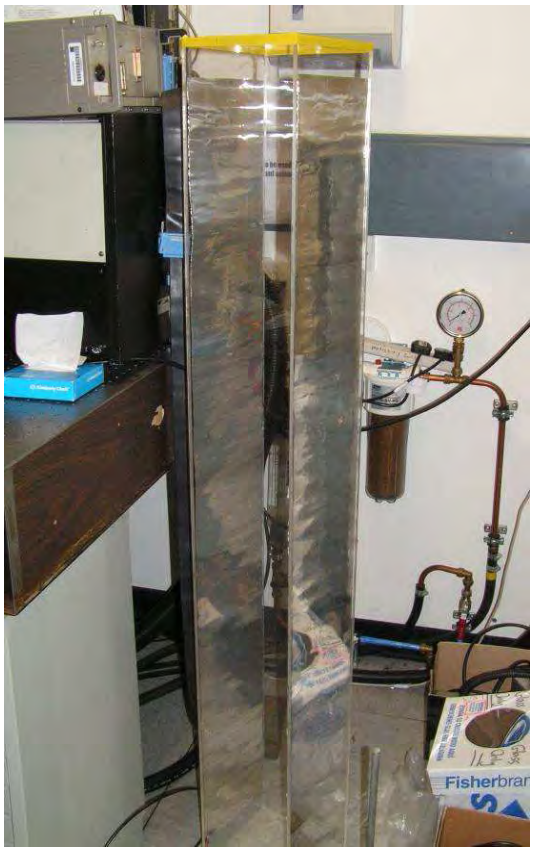

Figure 4.48 Static separation tower, comprising two parallel plates to produce an electrical field which could separate falling particles according to their charge.

4.5.2.6 Rolling separation/Separation of spheres according to quality

The material that is collected at the bottom of the drop furnace is made up of particles that have formed spheres and those that have not. A process was developed to separate particles, according to how spherical the particles are, by repeatedly rolling the material down

progressively shallower slopes. Each time the material is rolled down a slope, the material which is non-spherical will be left behind, the steepness of the slope will determine how precisely spherical the particle has to be in order to roll down the slope. It has been observed that some spherical particles have become trapped by the non-spherical particles, but the spheres that have been successfully rolled can be shown to be spherical (Figure 4.49). The particles will only roll down a glass surface if they are immersed in a solvent, as most small particles will stick to almost any surface.

This method of quality separation has been highly successful (Figure 4.49) for spheres above 30 µm in diameter. No quality separation has been carried out on spheres less than 30 µm, but as spheres of this size have been made with almost no un-melted particles it has been unnecessary.

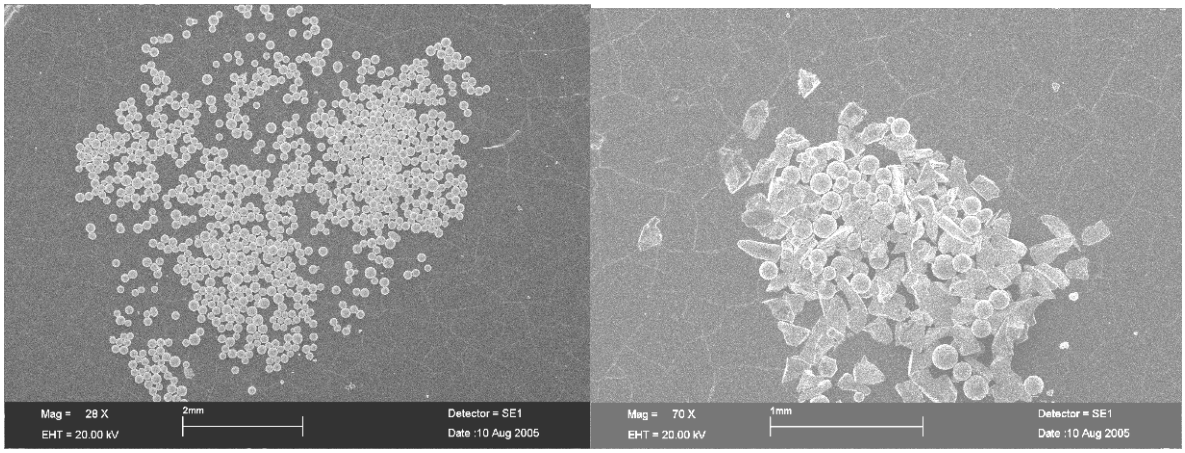

Figure 4.49 SEM pictures of M048 (left) and M049 (right) showing the particles that passed and failed the quality test.

It is theoretically possible that spheres could be separated from non-spherical particles using an internal screw thread, to act in a similar way to an Archimedes screw. The screw would be raised at an angle and rotated slowly. With each rotation, non-spherical particles would travel up the side of the cylinder, before falling and being deposited in the screw thread below, thus stepping downwards with each rotation, whereas spheres would remain at the bottom of the screw groove and roll upwards by the standard Archimedes screw process. Spherical particles would be transported to the top, whilst non-spherical particles would fall to the bottom.

For particles to be able to roll down a surface, the surface must be smooth, on a scale relative to the sphere. Several attempts were made, but it has not been possible to produce such a screw thread in a suitable material, so this theory has not been tested.

4.6 Results

The spheres were analysed to characterise their properties, such as size, surface quality and possibility of crystalline structure. Microspheres were also produced from other material as a demonstration of the transferability of the production method. The production parameters of each microsphere run can be found in the appendix.

4.6.1 Sphere sizes

Spheres have been produced over a significant range of sizes. The method of blowing small particles into the furnace has successfully produced a range of sphere sizes down to approximately 0.5µm in diameter (Fig. 4.50), whilst at the other end of the scale spheres have been produced up to 580µm in diameter (Fig. 4.51), by dropping crushed glass. The failure to confirm spheres of a smaller size than this owes more to the equipment used to analyze the samples rather than a lack of spheres themselves, as this is approaching the smallest size that can be resolved.

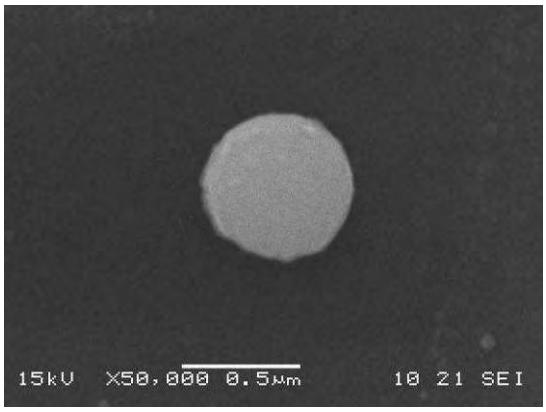

Fig. 4.50 A microsphere 0.5µm in diameter.

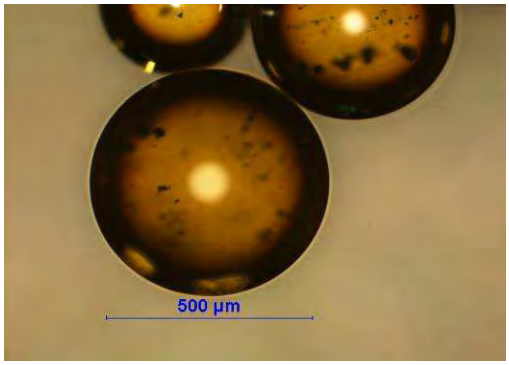

Fig. 4.51. A microsphere with a diameter of 580um.

The most significant controlling factor on the size of spheres produced, is the size of the crushed particles that enter the furnace, however the maximum size is limited by the experimental apparatus. According to Stokes' law, as the diameter of a particle increases, its terminal velocity will increase according to its diameter squared. Therefore, to melt larger particles of crushed glass, a longer hot zone is required. This can be partially overcome by having a large flow of gas passing through the furnace.

However, during the melting process molten particles coalesce, or partially evaporate, increasing the range of particle size, and the longer the particles take to pass through the furnace the stronger these effects will be. The likelihood of molten particles coming into contact with the surface of the tube and sticking will also increase.

In initial experiments a tube of 30mm internal diameter with a flow of 1l/min was used. For the larger particle sizes this flow would have little effect on their terminal velocity and the largest spheres that could be produced were ~300um. When a tube of 12mm internal diameter and a flow rate of up to 10 l/min was used the maximum sphere size produced was >500um. However a significant number of glass particles did become attached to the tube. The furnace hot zone was a similar length in both cases.

4.6.2 Raman spectroscopy scattering data

Raman spectroscopy is used for probing the structure of materials [39], such as to observe the differences between crystals and glass. Raman scattering occurs when incident light interacts with an electron in an atom and the scattered light either gains or loses energy (anti-Stokes Raman scattering and Stokes Raman scattering respectively) [51]. The electron is excited into a virtual state and decays down into an excited state, for Stokes Raman scattering. For anti-Stokes Raman scattering the electron starts in an excited state and decays down to a lower energy state after interacting with the incident photon.

Because Raman scattering interacts with the electrons of atoms and molecules it is a useful way of probing their structure. In a crystal the atomic bonds are clearly defined and only discrete wavelengths of Raman scattering are allowed, in glasses the bond energies are not so well defined and the peaks are broader and smoother.

This difference has been utilised to discern whether the spheres produced are in an amorphous or crystalline state.

Raman data has been taken using a Renishaw Ramanscope with a 633nm HeNe laser. Light from a laser source passes through several notch pass filters to ensure that it has a sufficiently narrow bandwidth, it then passes through a microscope to the sample via some optics. The scattered light is collected by the same microscope lens and passes through notch filters to remove the original laser light. The remaining scattered light is then spectrally analysed. The scattered light is plotted as a shift in wavenumber (cm^{-1}) which is the difference between the wavenumber of incident light and the wavenumber of scattered light.

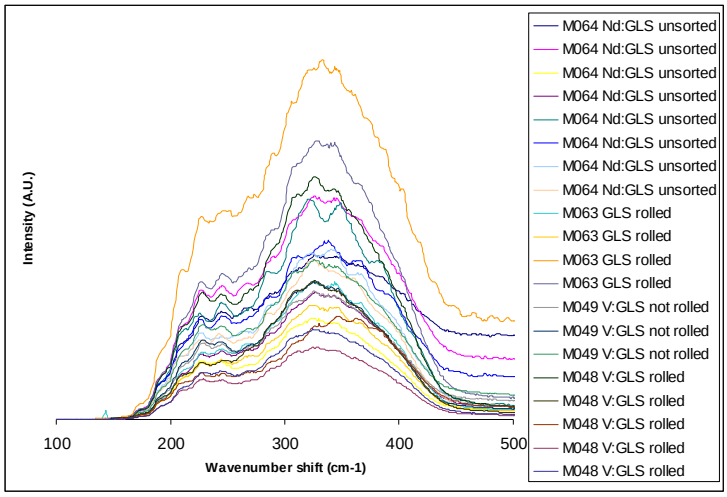

Figure 4.52 'Glassy' spectra for different spheres

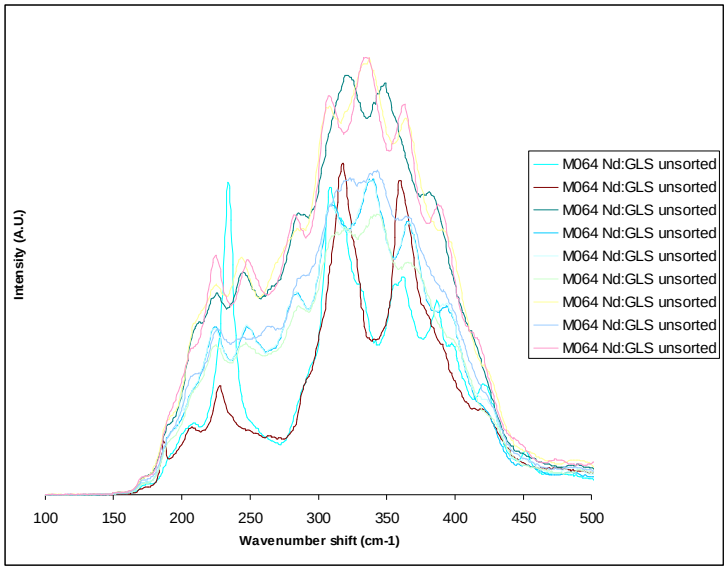

Figure 4.53 Spectra showing increased structure in particles that did not melt.

All of the sorted spherical material has the characteristic smooth double peak of glassy GLS [39] (Figure 4.52). Some particles have more defined peaks in their Raman spectra (Figure 4.53), which would suggest a degree of crystallisation. The particles that exhibit these traits are all from an unsorted sample that contains un-melted particles.

If glassy particles are exposed to the heat, but do not melt, it is quite probable that they will reach the crystallisation temperature and hence undergo some degree of crystallisation. Some particles that have not melted exhibit signs of the onset of crystallisation. However all particles that have passed the quality test and some that have not, have the smooth double peaked Raman spectra associated with glassy GLS. As crystallisation does not appear to be occurring, it is not necessary to add a cooling zone to the microsphere production apparatus. These measurements were taken in collaboration with Daniel Jaques of MUA, Spain.

4.6.3 Surface quality

The surface quality of the spheres is critical to their Q-factor and has been examined using an SEM. The difference between a very poor quality sphere and a high quality sphere can be seen by this method, however the difference between high quality (10^4) and very high quality ($>10^4$) is beyond the resolution of the SEM available. It is therefore of limited use for analysis purposes.

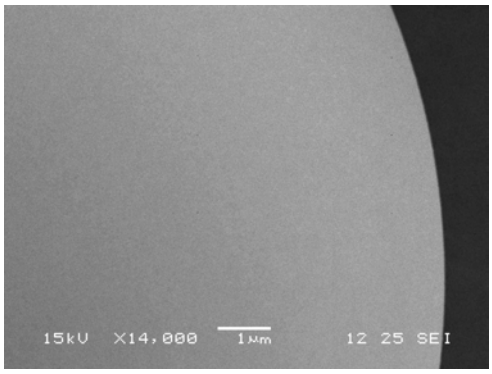

Figure 4.54 M119 spheres from this batch were measured and found to have high Q values

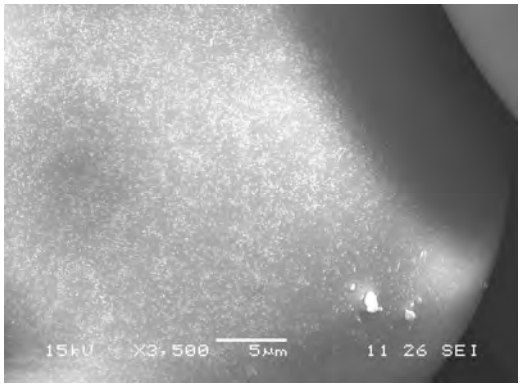

Figure 4.55 M108 spheres from this batch were found to have low Q sphere

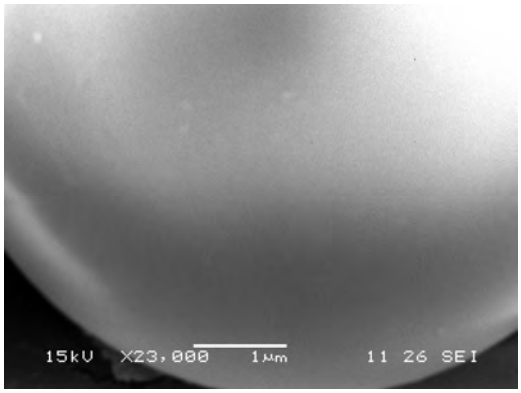

Figure 4.56 spheres from the batch M105 were found to have medium Q sphere, but appear similar to high Q spheres under SEM examination

4.7 Spheres of different compositions

Microspheres have been produced with various compositions of glass other than the simple GLS /GLSO. These include GLS doped with a variety of rare earth ions, which were produced to examine their fluorescent and possible laser properties. Spheres have been made from neodymium doped BK7 borosilicate glass (Figure 4.60) as part of a set of experiments studying microsphere lasers, in collaboration with Yuwapat Panitchob [101].

Work has been carried out by Mark Hughes at the ORC on the fluorescent properties of vanadium doped GLS [36]. From his work, it appears that the ideal lasing length for a vanadium doped GLS laser is of the order of hundreds of microns. This is a similar figure to the circumference of a typical microsphere. So it seemed reasonable to try to produce a

vanadium doped GLS laser using a microsphere, and V:GLS microspheres were produced for this (Figure 4.57, Figure 4.58). A solid-state vanadium laser has never been produced before, as far as we are aware. Vanadium has fluorescence over the entire telecoms window, so if a laser were produced, it could be potentially very useful. However is has not yet been possible to observe fluorescence from a vanadium doped GLS microsphere.
Experiments were also carried out into the possibility of producing microspheres from F1 Schott glass, by blowing crushed particles through a hydrogen flame (Figure 4.59). A small number of spheres were produced, but preliminary experiments were not as successful as those using a furnace.

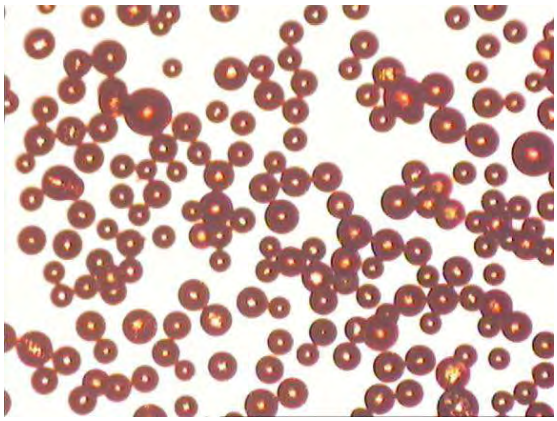

Figure 4.57 Optical microscope picture of vanadium doped GLS spheres (M040) 105um<pre-melt diameter<150um, 1300oC.

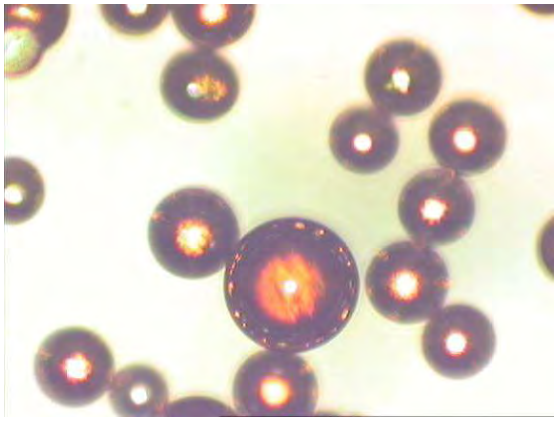

Figure 4.58 Optical microscope picture of vanadium doped GLS spheres (M039) 53um<pre-melt diameter<105um, 1300oC.

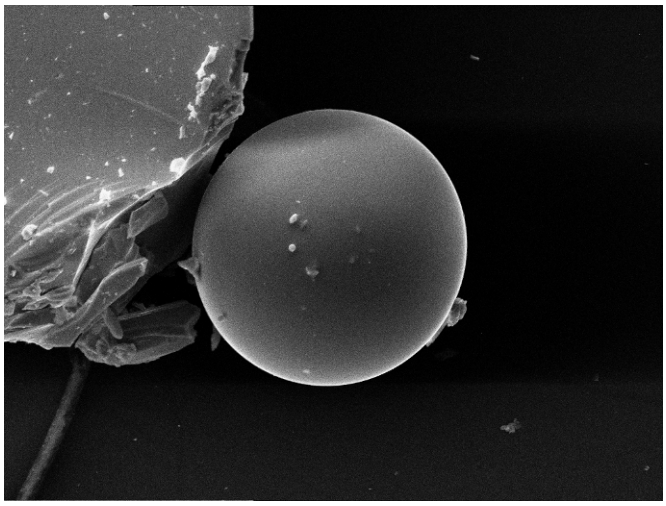

Figure 4.59 SEM image of F1 glass sphere 70μm in diameter.

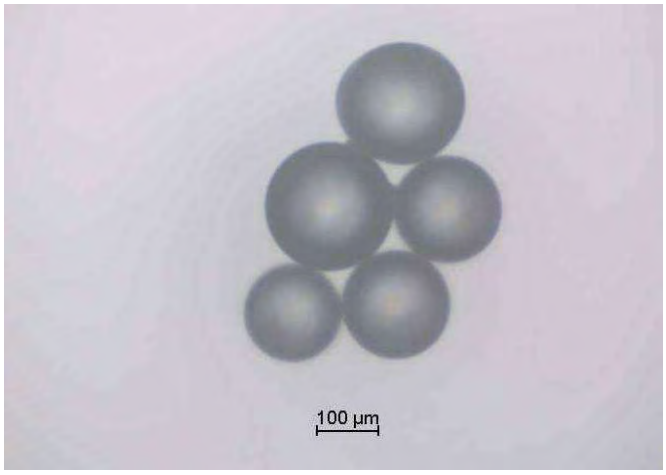

Figure 4.60 BK7 sphere doped with neodymium

4.8 Conclusions

The production of GLS microspheres has been reported on here. They have been produced over a range of diameters from 0.6 to 580μm in GLS and GLSO, un-doped and doped with rare earth ions, as well as in BK7 and F1 Schott glass.

The microspheres are produced by melting, and then quenching, particles of glass whilst in free flight. This is achieved by passing particles of crushed glass through a furnace where they will melt and surface tension will cause them to form spheres. There are two methods used here to pass the crushed glass through the furnace, blowing and dropping. Small particles can be blown through the furnace, this has been carried out in an upward direction and produced microspheres up to 50μm in diameter. Larger particles are dropped through the furnace, which has produced microspheres down to 30μm in diameter. A variety of pieces of apparatus has been developed as part of this project. The most important items are used to introduce crushed glass into the furnace without letting the atmospheric air in. For

the glass dropping system the ‘stopper-and-tap’ airlock has been devised and for the blown system a nozzle dust blower has been developed.

GLS will react if melted in air and this will affect the optical properties of the glass. It is therefore important to maintain an inert atmosphere wherever GLS is being melted and thus avoid reactions. To achieve this, the microspheres are melted in a silica tube which runs through the furnace and is purged with argon. For spheres that are dropped the flow does not appear to be critical once an inert atmosphere is achieved, as long as the flow is sufficiently low not to blow the particles upward. By contrast, when particles are intentionally blown upwards through the furnace, the flow is critical to the efficiency of microsphere production. It has been found that creating a turbulent flow increases the number of particles leaving the furnace that have melted, compared to particles leaving the furnace that have not melted. This is because the heat is transferred through the furnace liner tube by conduction, meaning that the gas heats up from the edge of the tube. A turbulent flow will cause more mixing to occur than would occur in a laminar flow and thus creates a more uniform temperature. To utilise this, a tube with a 5mm internal diameter was used when blowing particles through the furnace, this causes turbulence at flows similar to those required for carrying the particles through the furnace. When this tube was in use it was observed that the transit time through the furnace had a positive relationship with the fraction of particles leaving the furnace that had formed into spheres, relative to those leaving the furnace that had not. At 1 litre/min nearly all particles leaving the furnace were spherical and at 5 litres/min significantly fewer were spherical. However at flows of 1 litre/min or less a very small fraction of the material that was put in, reached the collection point, most was deposited at various points in the tube. The optimum flow is therefore a question of balancing the efficiency of material passing through the furnace, with the efficiency of turning that material into microspheres. A flow of 2 litres/min is considered to give good results.

There was a positive relationship between the melting percentage and temperature. At 900^{o}C, close to the melting temperature of GLS, very few particles melted into spheres, but as the temperature increased so did the percentage that melted.

As particles that pass through the furnace, do not all melt, it is necessary to separate spherical particles from non-spherical particles. The method developed here involves rolling the particles down a slope, typically a Petri dish set at an angle. The main problem with this is that small particles will stick to most surfaces due to static and Van der Waals forces. These forces can be overcome by submerging the particles in a liquid (HPLC methanol was used here). The spherical particles are then able to roll down the slope.

The issue of particles sticking to surfaces, and each other, appears at all stages of microsphere production and it has been found that the most efficient method of handling microspheres is to submerge them in a solvent and move them by means of a pipette.
For microspheres to be produced, certain preparations have to be made. Bulk glass has to be crushed to form the particles that will become microspheres, this is done using a pestle and mortar or a ball mill. Once the particles are crushed they are separated according to size, as the size of the particles into the furnace has the largest impact on size of the microspheres produced. This is done by washing the crushed material with solvent until the solvent becomes clear. The remaining particles are then dried and sieved.

5 Measurements / characterisation

Microspheres can be used for a number of purposes. In order to be able to compare resonators and understand their potential capabilities, it is necessary to quantify their properties.

The first part of this chapter investigates Q measurements, to characterise the microspheres quality as resonators, this has been published as part of the paper [83]. The second part of the chapter examines the effect that environmental factors, such as dust and water, can have. Nonlinear measurements that have been made with the spheres are then discussed. Possible uses in the form of micro ball lenses are also studied.

5.1 Q measurement

As previously described, the quality of a resonators such as a microsphere is quantified by the Q-factor, this can be measured by observing the spectra of the whispering gallery modes (WGM). Here these spectra were taken by observing the scattered light from a microsphere when its WGM were excited with a narrow line-width source.

The experimental apparatus used to observe the WGMs is shown in Figure 5.1. Here, a sphere was placed on an ion-exchange channel waveguide in BK-7 glass [102], which evanescently coupled the light into the microsphere. The waveguide was single mode at 1550nm, the mode was 7.2μm wide by 5.5μm high, with a substrate index of 1.50 and a peak core index of 1.52.

The microsphere was placed on top of the waveguide and the position of the sphere was observed from the side and top using microscopes equipped with CCD cameras. The top microscope also housed an InGaAs detector to measure the scattered power directly. WGMs were excited using a narrow-line tuneable laser source (1440-1640nm at 8dBm), coupled into the waveguide with TM polarization using a polarization maintaining single mode fibre. The throughput of the waveguide was measured with another InGaAs detector. The sphere was placed in contact with the substrate and moved horizontally along the surface perpendicular to the waveguide to achieve the required separation between sphere and waveguide.

In some experiments the sphere was attached to a fibre taper, so that its position could be controlled across the waveguide, in other experiments the sphere was positioned by pushing it with an optical fibre. The taper was made from standard telecoms fibre and was attached to a fibre taper with UV curable resin (with a refractive index of 1.42), its only purpose was as a positioning device (Figure 5.2).

The spectra were taken by exciting the WGM of the microsphere at one wavelength. The scattered intensity was observed via the microscope and InGaAs detector. This was repeated

for a range of wavelengths. The Q can then be calculated from this spectrum using Equation 3.29 (see section 3.4)

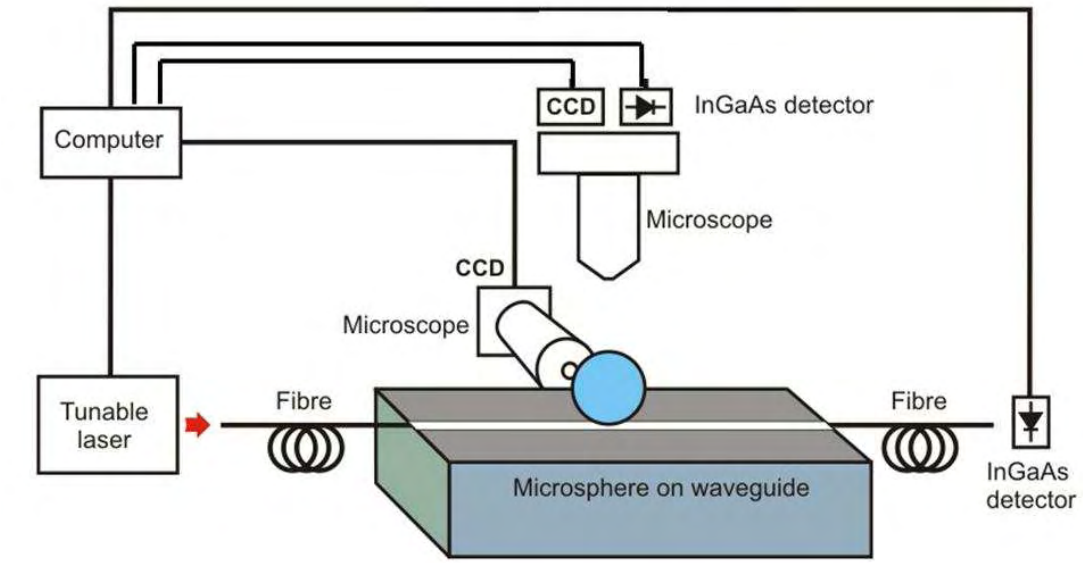

Figure 5.1. Experimental apparatus used for Q measurements.

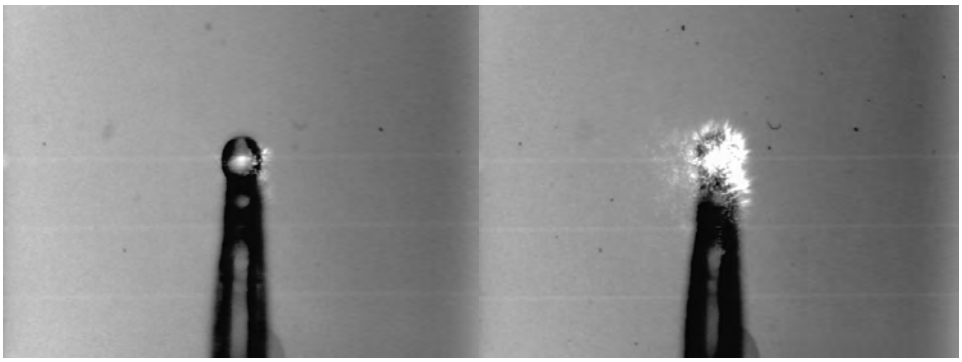

Figure 5.2 A microsphere on a fibre taper. Showing scattering at resonance (right) and off resonance (left).

5.1.1 Q values and curve fitting

Spheres of the order of 100µm in diameter were fabricated from GLSO glass. From these a representative sphere was selected for the Q measurement. The sphere was selected by hand using an optical microscope, therefore no quantitative assessment of surface quality or impurities was made prior to the Q measurement. It is likely that, from amongst all the suitable spheres, a range of Q values would be achieved.

Spectra were taken with the apparatus in Figure 5.1. The sphere was held in two different positions, a strongly coupled position where the sphere was placed directly on top of the waveguide and a weaker coupled position, where the sphere was moved to one side of the waveguide to increase the coupling distance and therefore reduce evanescent coupling. Due to the attractive forces, between the sphere and the substrate/waveguide surface, it was not

possible to accurately position the sphere away from the surface, therefore it was moved across the surface away from the waveguide in order to achieve the required coupling.
A set of Airy functions have been fitted to the measured spectra (Figure 5.3, Figure 5.4) by the method described earlier (section 3.13) in order to clarify the mode 'family' structure. The data that makes up the calculated curve are tabulated in the Table 5.1 and Table 5.2, and from this data, a diameter is calculated for each Airy function.
An Airy function diameter is the quantity, d, defined by the simple resonance condition $\lambda N = \pi dn$ [85], N and λ define the peak positions and d. These values are first fitted to the observed data to define the peak positions for the fitted data. Once the peak position has been fitted, the shape of the peaks is then fitted to the data. Q and relative intensity affect the shape of the peaks, but not the peak position and, whilst they affect each other and are affected by the N and λ through the vernier effect, they have no affect on N, λ, or the peak position .
It was found that an accuracy of more than one significant figure in Q was unnecessary as small variation in any of the other parameters would dominate over this small variation in Q. The periodic nature of the spectra is visible, although the number of peaks corresponding to several of the possible whispering gallery modes does complicate the picture. The weaker coupled spectrum (Figure 5.3) has narrower peaks, implying higher Q values than the same sphere in the stronger coupled position (Figure 5.4). This is because the component of Q due to coupling (Q_{coup}) is dominating the observed Q. Light will also be coupled into the substrate, as the sphere remains in contact with the surface.

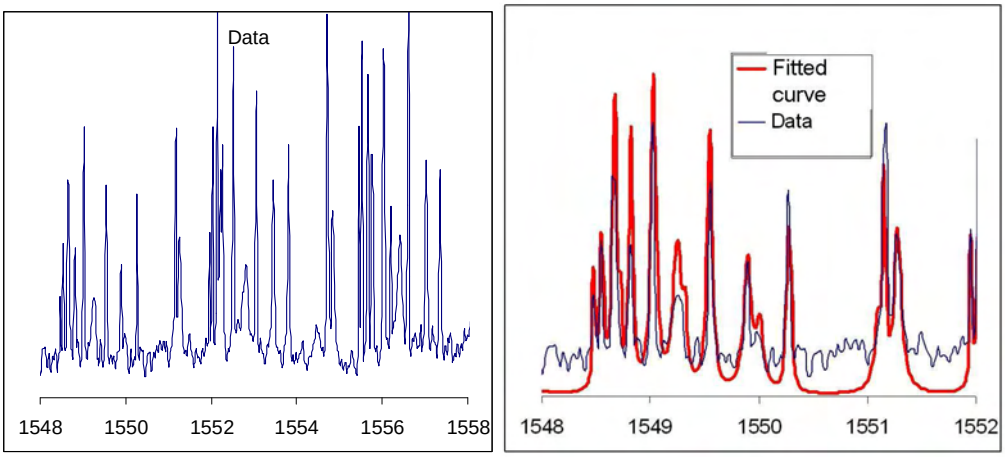

Figure 5.3. Weakly coupled spectra from a 100µm diameter sphere plotted with the fitted spectra. Showing the periodic nature of the spectrum (left) and a close up of the fitted curve (right).

Table 5.1. Parameter values which make up the fitted spectra in Figure 5.3

N	λ (nm)	Q	Relative intensity (a.u.)	Airy function diameter (µm)
449	1548.82	40000	0.8	100.6
447	1548.48	80000	0.5	100.1
446	1548.66	40000	0.5	99.93
444	1549.03	30000	1	99.51
442	1549.55	30000	0.8	99.10
441	1550.26	50000	0.4	98.92
440	1550.26	50000	0.4	98.69
438	1551.16	60000	0.7	98.30
438	1548.68	40000	0.5	98.14
436	1549.90	20000	0.4	97.77
436	1547.72	20000	0.5	97.63

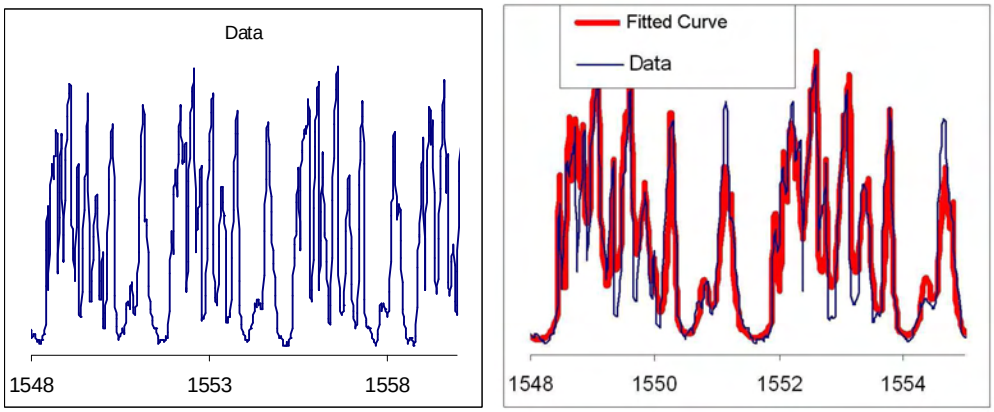

Figure 5.4. Strongly coupled spectra from a 100µm diameter sphere plotted with the fitted spectra. Showing the periodic nature of the spectrum (Left) and a close up of the fitted curve (right).

Table 5.2 Parameter values which make up the fitted spectra in Figure 5.4

N	λ (nm)	Q	Relative intensity (a.u.)	Airy function diameter (μm)
451	1550.01	50000	0.2	101.1
450	1549.32	40000	0.5	100.87
448	1548.85	40000	0.4	100.39
448	1548.62	40000	0.5	100.38
448	1548.47	40000	0.5	100.37
446	1548.73	10000	0.7	99.94
444	1549.10	50000	0.5	99.51
444	1549.03	10000	0.8	99.51
443	1549.62	30000	0.5	99.32
443	1549.54	10000	0.7	99.31
441	1550.29	50000	0.5	98.91
441	1550.25	20000	0.7	98.91
439	1551.14	10000	0.6	98.52
438	1549.85	10000	0.5	98.21
437	1551.25	30000	0.3	98.08
435	1550.80	10000	0.2	97.60

The Airy functions approximate the path of light as a one dimensional loop. This will not be the case in a sphere, but it is a reasonable first approximation as all fitted peaks coincide with their fitted counterparts to within experimental tolerances of 0.25nm. Here N is an approximation of the azimuthal mode number, however the Airy function takes no account of the shape of the sphere or other mode numbers. This leads to several modes having the same azimuthal mode number and slightly different values of diameter (Table 5.1, Table 5.2). In reality these modes could differ in either the radial or angular direction, but in this model that difference is only absorbed into the diameter of the ring. The Airy function diameter must vary in order to take account of the position and free spectral range of the families of peaks. The highest order modes will be those with the largest radius, with a reduction in radius representing a reduction in mode order.

The actual diameter of the spheres, as measured by the microscope, is within the bounds of accuracy of the Airy function diameters, this is to be expected as the modes will be circulating close to the surface of the sphere. The different modes will have a Q associated with them individually, this relates to the various causes of degradation interacting with them differently. For example the high order modes will be closest to the surface and will therefore scatter from the surface more strongly.

The highest value of Q used in the fit of Figure 5.3 was $8x10^4$. Whilst Q values of up to $1.2x10^5$ have been observed. This is several orders of magnitude lower than the ultimate

value of $7x10^9$ at 1.55µm calculated earlier which assumes negligible surface scattering and material loss introduced during fabrication. It has been observed through scanning electron microscope images that some surface roughness exists on these spheres, this will degrade the potential Q of the sphere. It will be further degraded by the resin and contact with the tapered fibre on its surface, which will cause scattering. It is therefore likely that incremental improvements to all aspects of this experimental work will be mirrored by improvement of the measured Q.

It would also be preferred that evaluation of the Q factor takes place using spheres that have been produced minutes or hours earlier, as has been the case in studies made on spheres in other materials [22]. However, in this study, this was not practical and the spheres were produced weeks or months before their Q values were measured. In this time they were stored in solvent to prevent contamination from the air, but it is still likely that some degradation will have occurred.

Finally it is possible that there will be a significant mode mismatch between the BK-7 waveguide used in Q measurements and the sphere. The exact extent of this is not known as the effect of the sphere production process on the refractive index is not known. It is likely that some elements in the glass will have partially evaporated while molten, thus altering the refractive index.

5.1.2 Mode identification

The position of modal peaks can be predicted using Mie scattering. An asymptotic equation for the positions exists, given knowledge of the mode parameters [103, 104] (it should be noted that the paper by Schiller contains a sign error in its prediction). However these mode parameters are not known, so a program was written to compare observed peak positions with a number of calculated positions using the equations in the paper. The position of the theoretical family and the measured family was compared and the square of the difference at each point was taken, to give an absolute value of variation between the two. This was repeated for all parameters as it was expected that a minimum would appear in the error. However this was not observed. It is not clear if this was due to rounding errors in the computer program or due to the high level of complexity of the modal structure of the spheres being examined. As modes overlap this could cause false positions to appear. The model also assumes a perfect spheroid, if it was slightly off spherical it would alter the positions of the modes and this would not be accounted for in the model. However it appears that some computational errors were occurring as it was not possible to perfectly repeat the data in the papers.

5.2 Environmental degradation of spheres

It is known that water has a detrimental effect on GLS [75] and that microspheres exposed to air will degrade [22] as dust becomes attached to their surface. In order to better understand these two effects in GLS microspheres, a number of experiments were carried out.

5.2.1 Water damage

It is often useful to be able to examine the spheres under a scanning election microscope (SEM). Preparation for this involves mounting them on a small metal stub with a sticky carbon pad, then coating them in a thin conducting layer. It is critical that this conducting layer is as thin as possible, otherwise it will obstruct the view of the item in question. As has been mentioned previously, in order to handle small particles effectively they are held in an organic solvent.

When a droplet of solvent containing microspheres is placed on an SEM stub, the solvent will dissolve some of the carbon pad. The carbon is then deposited on the microspheres as a thick layer and obscures all fine detail (Figure 5.5). In an attempt to overcome this problem, spheres in solvent were placed in deionised water, using a pipette, then immediately removed to wash away the solvent. They were then placed on a SEM pad to dry. The extent of the damage to the surface of GLS caused by water was not known in detail before this work.

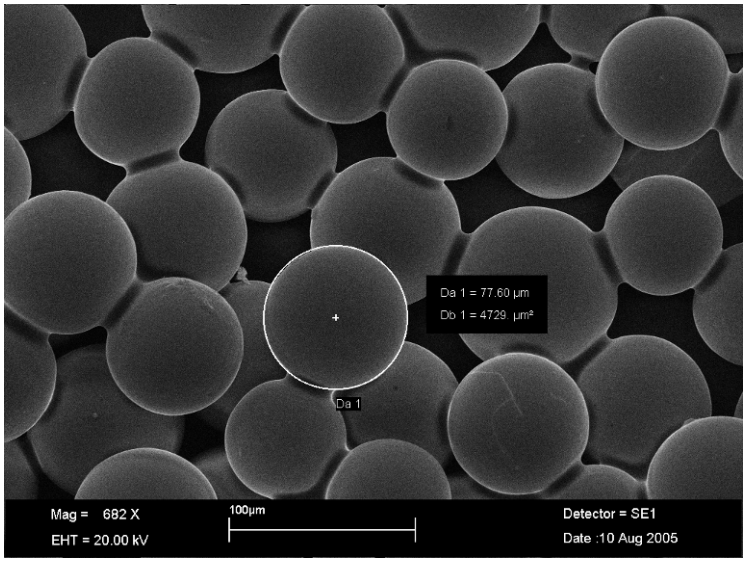

Figure 5.5 Spheres that have a coating due to deposition in solvent onto the sticky carbon pad

It was thought that a short exposure to water would not have a seriously detrimental effect. This view was supported by the ability of bulk glass to withstand prolonged submersion in water. However the spheres showed significant signs of surface degradation in the time it took the water to dry (Figure 5.6). It is even possible to see the way the water receded by examining the pattern of the degradation. A circle can be seen on the top of the spheres where the initial level of the water was and below that is evidence of degradation. As these

circles all face upwards on the SEM pad they must have been formed after being placed there, which would suggest water damage.

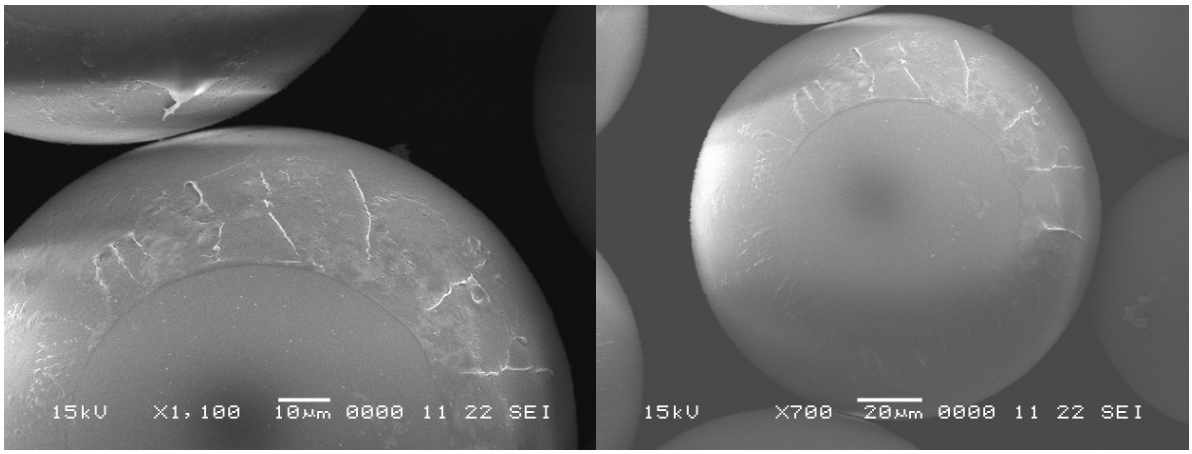

Figure 5.6 Surface damage caused by water. Variation in damage is due to differing levels of exposure as the water evaporated.

The damage observed was far more extensive than expected. It was therefore of interest to examine further the effects of water damage on GLS microspheres.

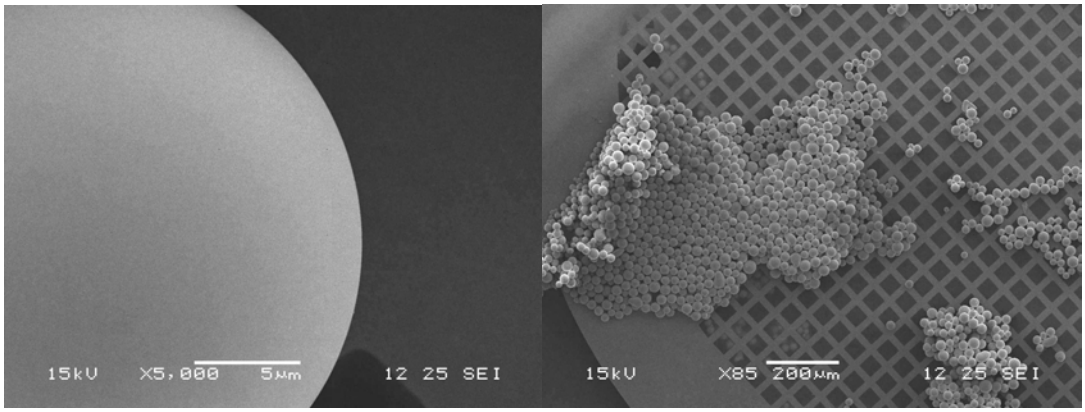

Figure 5.7 Original spheres which were stored in HPLC methanol.

A quantity of M119 GLSO spheres were placed in a tube of tap water, another quantity was placed in tube of deionised water whilst the original sample remained in HPLC methanol. Some spheres were dried out on TEM grids after 24 hours in the water and after 1 week. At this point it was noted that the particles in the water no longer moved like spheres. The spheres remaining in methanol were observed to move smoothly when the tube they were in was moved, as expected of a large number of spherical particles that can move independently, but spheres in water appeared to have agglomerated and showed evidence of sticking to the side of the tube.

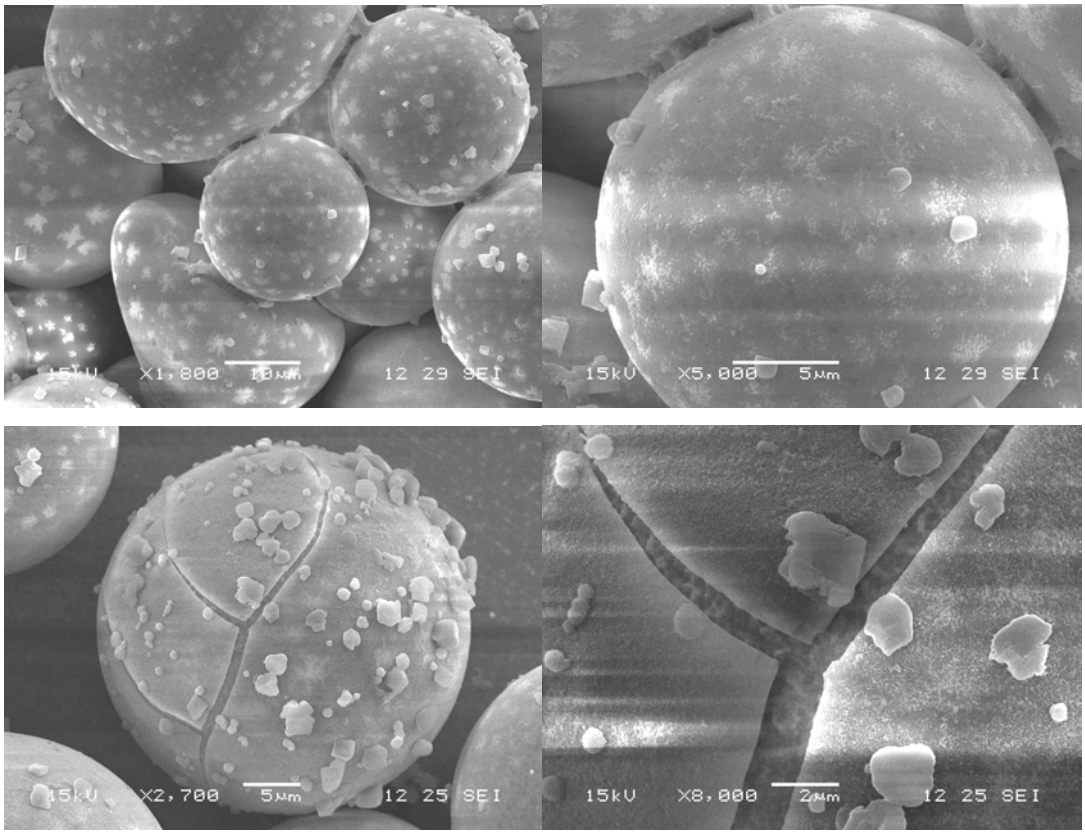

Figure 5.8 spheres after 24 hours in tap water.

When examined under the SEM, the spheres that had remained in methanol had a smooth surface down to the resolution of the SEM (Figure 5.7). There were few un-melted particles and there was no sign of dust contamination. The spheres that had been in tap water for 24 hours showed a pattering on the surface (reminiscent of crystals of frost) (Figure 5.8), there were also particles of about a micron that appeared on their surface and some material had been deposited at the point where two spheres meet (consistent with deposition by a receding layer of water). A small number of spheres showed signs of cracking on the surface and a whole surface layer appeared to be cracking away. It is not clear where these particles and deposits came from. As the original sample was clear of dust this must be due to the presence of the water. They could be particles deposited by the water, in the form of dissolved salts or small particles suspended in the water, or they may be GLS particles that had come off of the spheres.

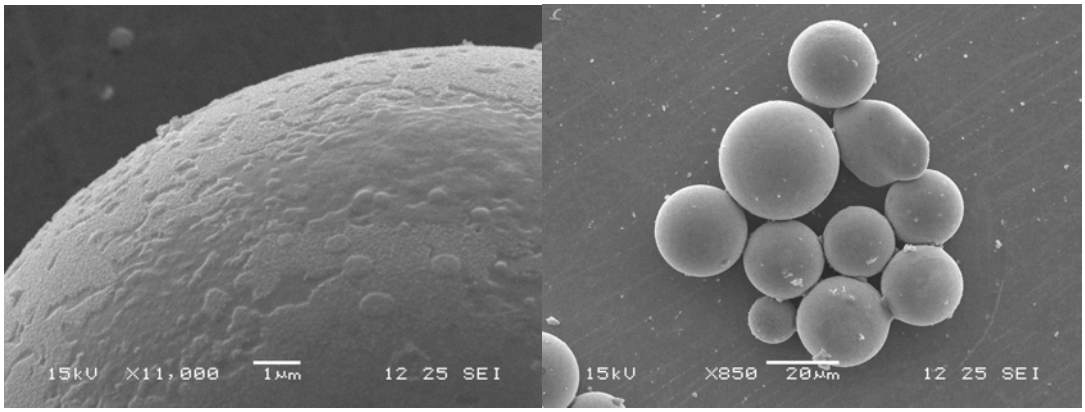

Figure 5.9 Spheres after 24 hours in deionised water.

The spheres that had been in deionised water for 24 hours (Figure 5.9) had developed a rough surface, but not in the pattern that was evident on the spheres in tap water. They also had fewer particles on their surface and did not have the deposits between the spheres. This suggests that the small particles found on the tap water sample are due to impurities found in the water. From a distance, the effects are less obvious than with tap water, but at greater magnification it can be seen to be considerable. The degradation of the surface is fairly uniform and appears on most spheres.

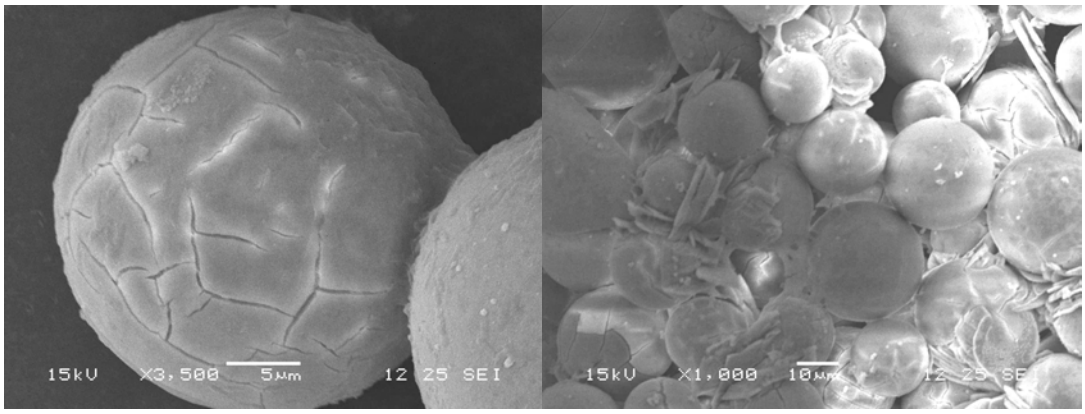

Figure 5.10 after 1 week in tap water.

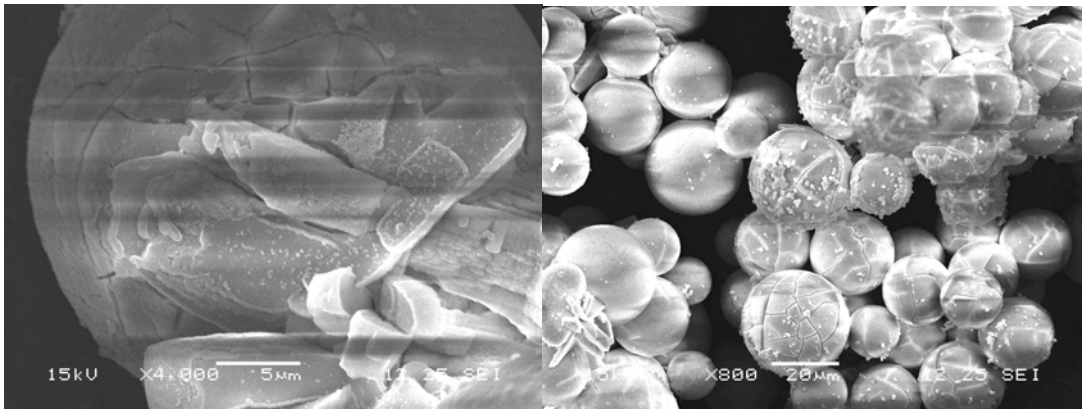

Figure 5.11 after 1 week in deionised water.

After a week both the tap water (Figure 5.10) and deionised water (Figure 5.11) samples had surface cracking on many spheres. Non-spherical particles that were not in evidence in the original sample had appeared. The non-spherical particles were large relative to the spheres

themselves and appeared to be consistent with a surface layer that had cracked off. It is apparent that after one week in water the spheres are starting to crumble. As bulk GLS does not disintegrated in water some kind of surface layer was expected to form, but this does not seem to be the case on this scale. It was noted at the time of removing them from the water that the spheres no longer moved independently and had agglomerated into large lumps.

Before this experiment it was expected that both kinds of water would attack the spheres with deionised being more aggressive. This has been borne out by experiment, although the difference between the two types of water has been less considerable than was expected. Uniform degradation was expected across the surface spheres, it therefore came as a surprise to see cracks appearing. It appears that the cracks only resulted in a surface layer being broken away. This is borne out by the close-up of a crack after 24 hours, and the slab-like nature of particles observed after one week. The agglomeration of broken spheres was also unexpected.

5.2.2 Q measurements after water immersion

In order to quantify the degradation, measurements of the Q-factor were taken, and naturally these could only be taken from spheres that remained intact.

After one week in the water Q measurements were taken by coupling the spheres with a BK7 ion exchanged waveguide. The original sample (stored in methanol) was found to have a Q value of $4x10^4$, the sphere that had been in tap water for one week had a Q value of $1.5x10^3$ and the sphere that had been in deionised water had a Q of $1x10^3$. The peaks from the deionised water treated sphere could barely be distinguished from noise of the reading.

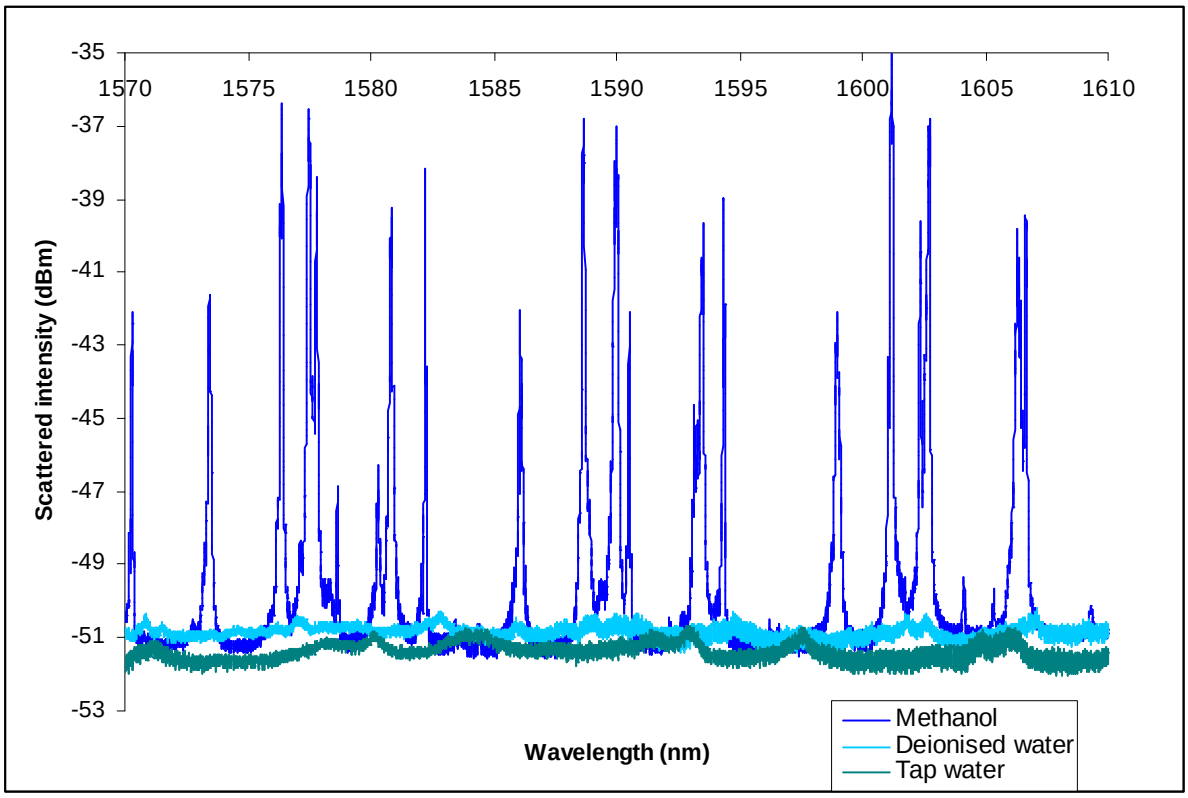

Figure 5.12 Resonance spectra after one week in water compared to those stored in methanol.

It has been found that water can attack GLS spheres aggressively. It is unclear why some spheres are attacked more aggressively than others. Water can cause the total breakdown of some spheres, whilst others show a far more moderate degree of degradation. Even in the spheres that have remained intact, the Q factor has been considerably degraded.

5.2.3 Degradation in air

It has been observed in spheres that the Q changes with exposure to air [22], due to dust attaching to the surface and reactions with the air. It was therefore necessary to investigate how our spheres changed with prolonged exposure to air.

A sphere that had been stored in HLPC methanol for almost four months was placed on a waveguide and its Q was measured in the way described before. The same sphere remained on the waveguide without being moved for a month and scattered spectrum measurements were taken to measure its change with time.

The peak wavelength and Q factor changed over the course of the experiment. The rate of these changes was consistent with an exponential decay. Considering that the sphere starts in an initial state and then approaches a new stable state in air, it seems likely that

measurements of this change will follow an exponential decay, analogous to Newtonian cooling.

By observing the change in peak wavelength and Q, some information about the changes in the sphere can be inferred. The nature of the sphere is expected to change in two main ways, an increase in attenuation, possibly due to the affects of atmospheric water on the surface of the sphere and a change in refractive index as the oxygen content of the surface changes.

The peak position is defined in simple terms by $\lambda N = 2\pi Rn$. If the sphere size and mode number remain the same, only the peak wavelength and refractive index can vary, and the division of one by the other will remain constant. Therefore, considering the change in position of one peak of a sphere over time, the change in refractive index can be found from;

Equation 5.1

$$\frac{\lambda_{initial}}{n_{initial}} = \frac{\lambda_{final}}{n_{final}} = const$$

The Q factor is governed by $Q \approx \frac{2\pi n}{\alpha\lambda}$; therefore as a first order approximation the change in Q is only due to a change in attenuation, as the relationship between wavelength and refractive index is invariant for any given peak. This means that the attenuation and refractive index changes can be observed separately by studying the Q and peak position change.

The excited modes in the sphere have remained the same (Figure 5.13) throughout the course of this experiment, and the size of the sphere has not been observed to alter. Therefore change in refractive index and attenuation must be responsible for any change in Q and position of any given modal peak.

From the data (Figure 5.14) the change in attenuation is $2cm^{-1}$, or as a fractional increase it is 0.77.

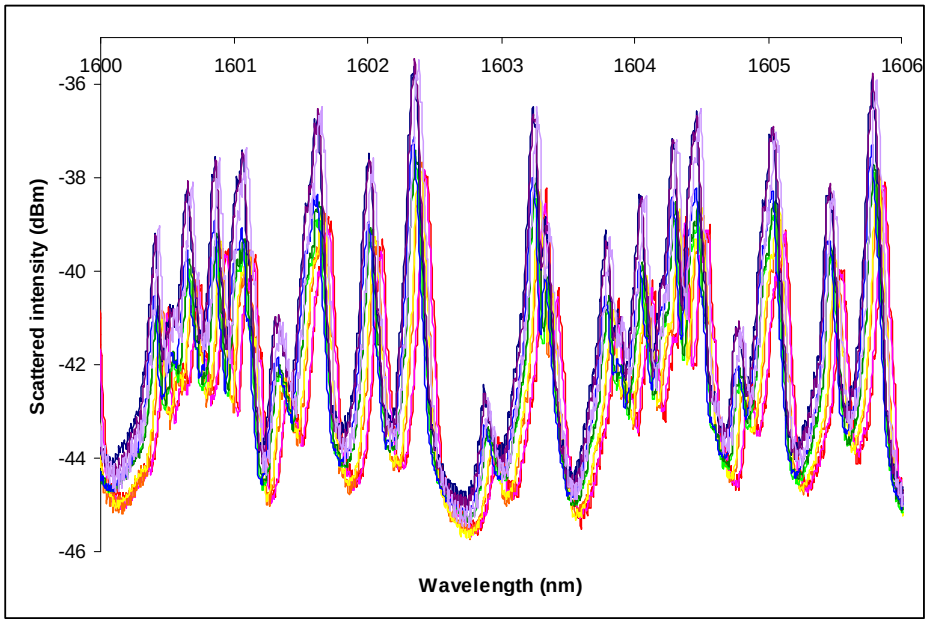

Figure 5.13 Spectra from a sphere over the course of a month.

Changes have been observed in Q factor and peak position in a sphere over the course of 23 days. From this data a first order approximation of the change in attenuation and refractive index can be inferred. Both refractive index and attenuation show some change, which suggests that the surface is indeed being altered by its exposure to normal atmospheric conditions. The fact that both variables show an exponential decay tends to support the view that the surface is being altered to a new stable state.

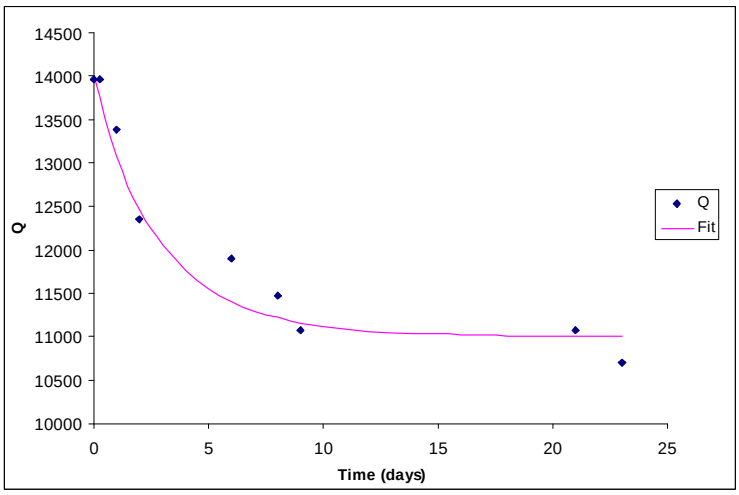

Figure 5.14 Change of Q with time, showing the exponential decay to the new state.

5.2.4 Effects of air on spheres

It has been observed [22] that the Q of a sphere in air will start to degrade from the moment it is made. This suggests that some change is happening to the surface over time.

Previously, when bulk glass had been placed in water and not dissolved, it had been exposed to the air for a prolonged period beforehand. It was therefore theorised that a layer may be built up by exposure to air that protected the glass when subsequently soaked in water.
To test this theory (and to compare the effects of air to the effects of water) an experiment was set up whereby spheres that had been in air were placed in water to see if the same degradation was observed as for the spheres that had been stored in methanol. As the Q seems to become largely stabile after two weeks spheres were left in air for two weeks (Figure 5.15, Figure 5.16), and then placed in deionised water for one week (Figure 5.17). The spheres used were from the same batch as used in the previous two sections (M119). In order to be sure that there was not another longer term effect in play, a separate sample (M056, Figure 5.18) that had been stored in air since its production (2.5 years ago) was also placed in deionised water for the same length of time (Figure 5.19).

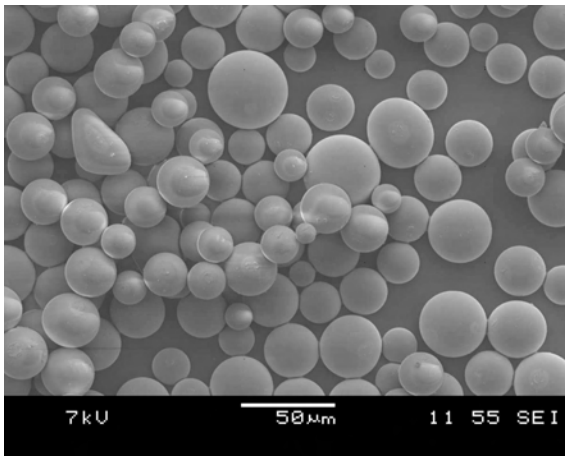

Figure 5.15 M119 spheres after exposure to air for two weeks.

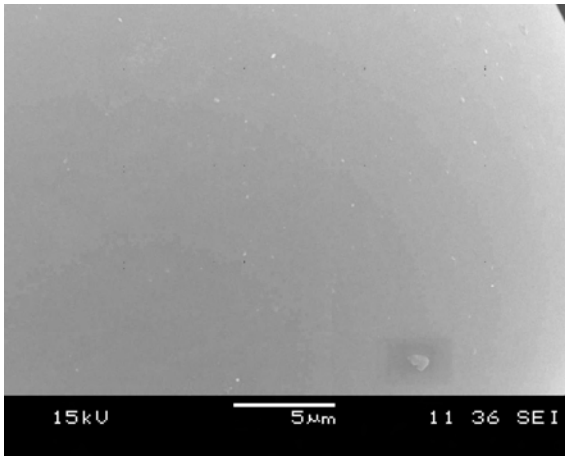

Figure 5.16 Close up of M119 sphere surface after exposure to air for two weeks.

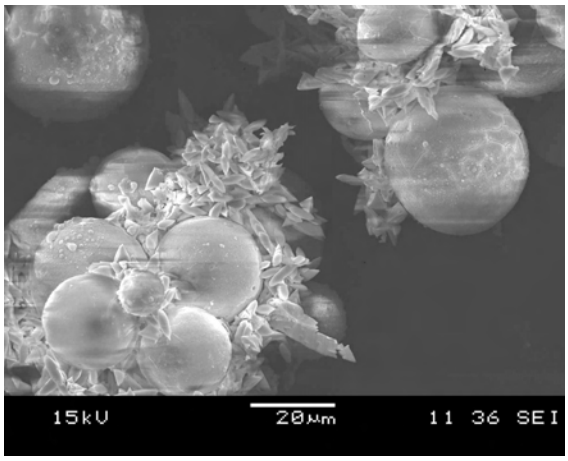

Figure 5.17 M119 spheres after being in air for two weeks then in water for one week. Picture shows agglomeration of particles.

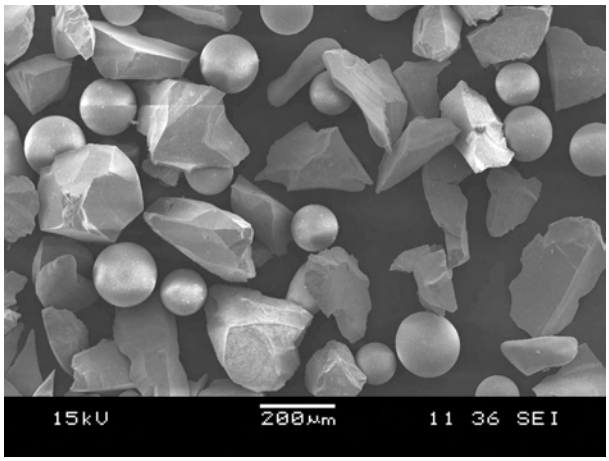

Figure 5.18 M056 in air for 2.5 years

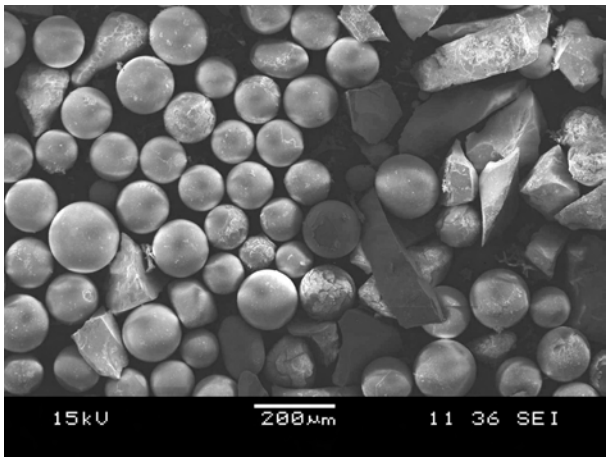

Figure 5.19 M056 after being in water for one week

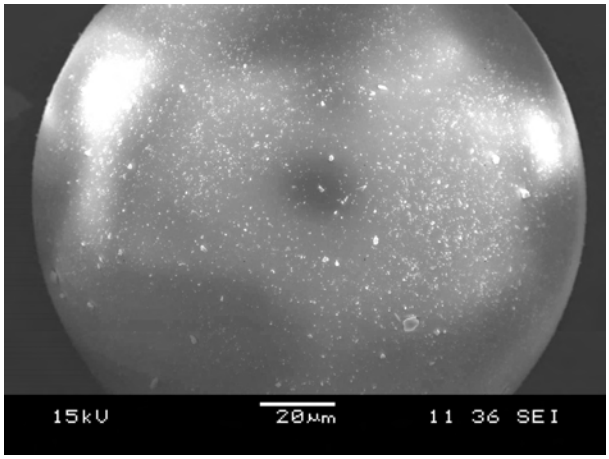

Figure 5.20 Dust on the surface of M056 sphere after being in air for 2.5 years

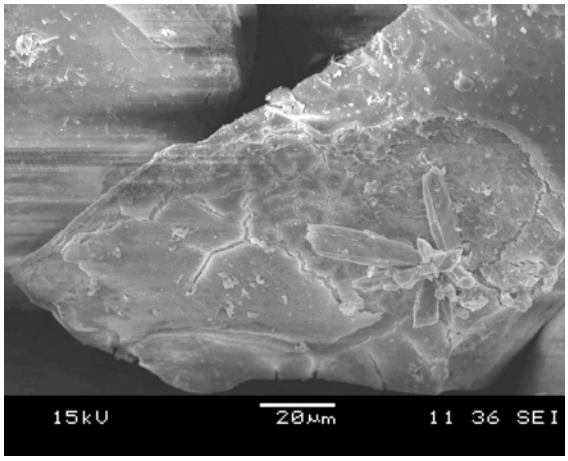

Figure 5.21. Close up of bulk glass piece of M056 after being in water for one week.

The spheres that had been stored in air for two weeks show signs of dust particles attaching to the surface (Figure 5.16); however SEM / EDX experiments showed no signs of the surface layer changing in composition or texture. This suggests that the degradation due to air contamination is due only to dust, or that the surface effects cannot be seen by this method of measurement. The spheres in sample M056 that have been stored in air for 2.5 years (Figure 5.20) show a greater amount of dust on the surface, but also show no sign of degradation of the surface itself.

As with the previous tests, the spheres that had been stored in water for a week appeared to have agglomerated and stuck to the sides of their container.

The same type of degradation seen in the previous test was seen in both samples when the spheres were submerged in water for a week. This suggests that the exposure to air did not have a significant impact on the degradation of glass. Sample M056 contained pieces of un-melted glass (Figure 5.21) that will have all the characteristics of a bulk sample. They are large relative to their surface and they have not been re-melted. It is possible that the re-melting process causes the composition to the glass to change, particularly the surface composition, the un-melted particles offer an opportunity to compare the original material with re-melted material. Surface degradation was observed on these bulk samples in a style similar to that observed in the spheres.

5.2.5 EDX measurements

A compositional measurement of the spheres, that were in water, was taken using an SEM / EDX (JOEL JSM 5910). A number of measurements were taken of the flaky material and of the spheres that had remained intact.

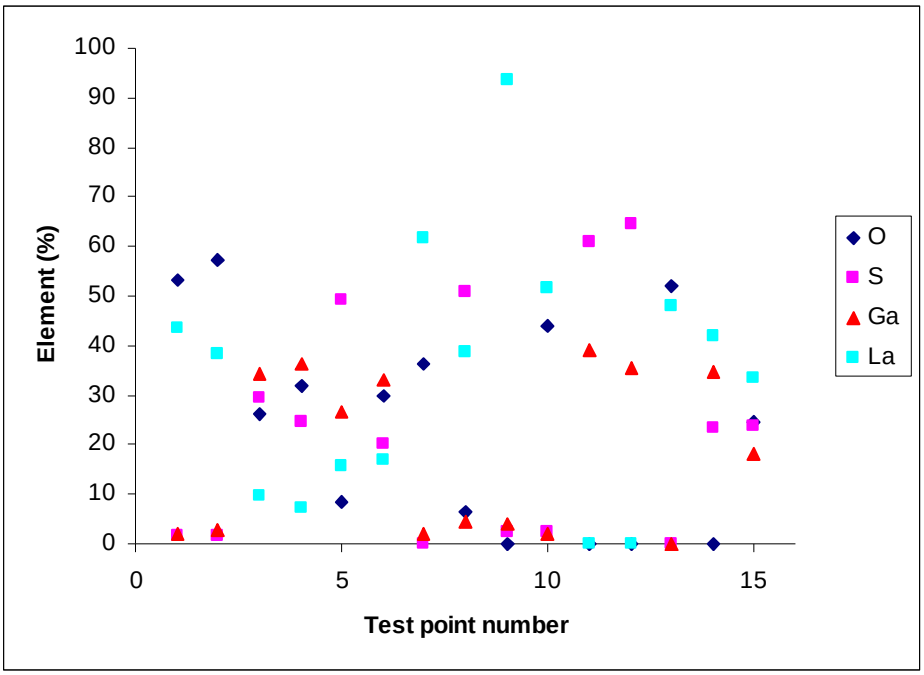

Figure 5.22 Elemental compositions of M119 remnants after two weeks in water, showing that the material remaining does not have a typical GLS composition. The test points represent the variation from spheres that remained whole to those that crumbled completely.

When placed in the water many spheres crumbled, while others only cracked and some spheres remained whole. If the change in the glass structure that causes this cracking and crumbling is due to one or more of the elements leaching out into the water, then it is to be expected that any variation in macroscopic structure would correspond to variations in the elemental composition of the material. This variation in composition is reflected in the variation in the sites measured (Figure 5.22).

The M119 spheres were made from LD984 glass which was made with elements in the proportions oxygen 16%, sulphur 36%, gallium 37%, and lanthanum 11%. At no test site were these proportions maintained, at all sites the composition has been altered in some way by being immersed in water.

It appears that all elements have been affected, but with considerable variation across the sample points. However in general some leaching has occurred to the Gallium or the sulphur or both, and this has resulted in a lanthanum level considerably higher than its original level. The environmental abundance of oxygen may cause some percentages of the other elements to be reduced when no leaching has occurred, but the same is not true for lanthanum. Therefore where lanthanum levels are elevated this represents a loss of one or more from the other elements. In all but two data points lanthanum levels are up relative to sulphur and / or gallium, which means they must have leached out into the water.

If material is being leached out of the glass into the water this would alter the structure of the glass and explain why the spheres have crumbled. It also explains why the spheres exposed to air showed such different degradation to spheres exposed to water. The spheres in air could only be altered by the addition of material, such as dust on the surface and possible water and oxygen absorption, whereas the spheres in water had part of their glass matrix removed. It is not clear why some spheres have remained intact in the water while some have had their gallium leached away and crumbled. It is also not clear why large bulk samples of glass remain whole in water. It is possible that the surface degradation is self limiting, but there is not convincing evidence of this in the experiments carried out here.

5.3 Nonlinear effects

Because of the relatively high intensities that circulate inside resonators it is possible to observe nonlinear effects at much lower input intensities than would be required in bulk material. GLS is known for being a highly nonlinear material [18, 19] therefore GLS resonators should exhibit nonlinearity at very low powers.

Experiments have been carried out to observe the nonlinear effects in GLS microspheres. Using the same method as used for Q measurement, a series of spectra were taken with a range of input powers.

A shift in peak positions was observed as power was increased (Figure 5.23). This movement was found to be consistent with a nonlinear effect (Figure 5.24), although it was not possible to determine if this nonlinearity was third order or thermal in origin.

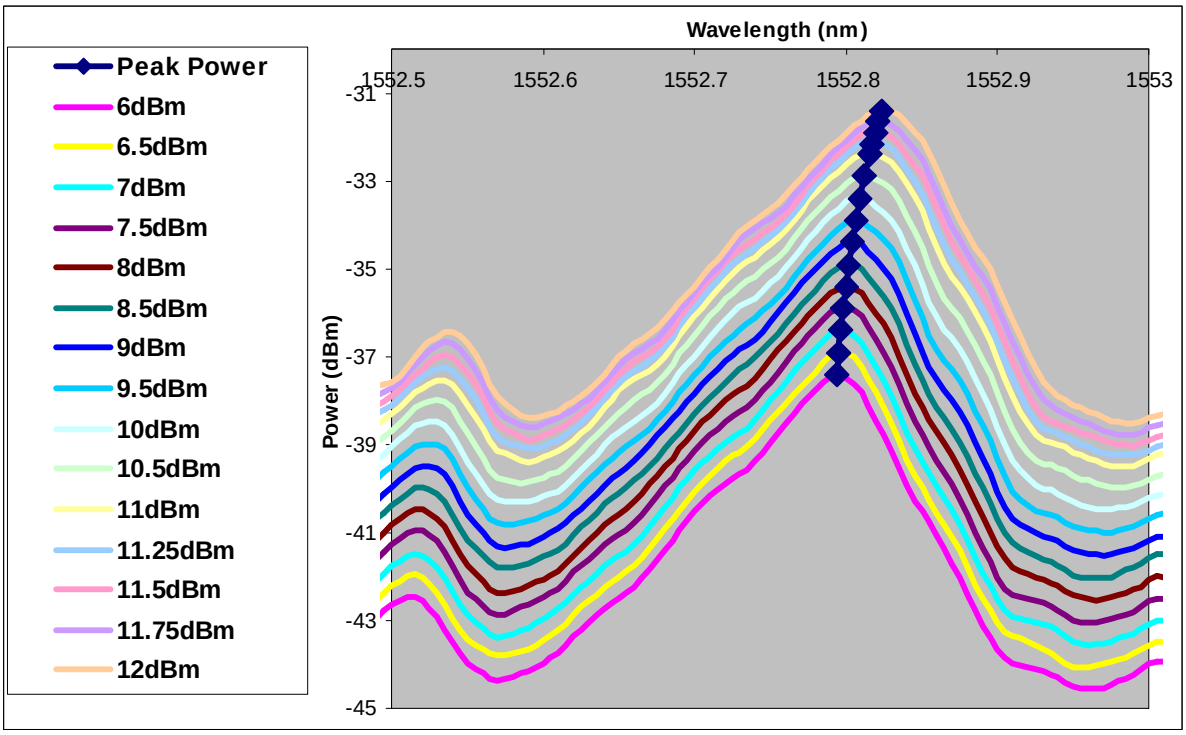

Figure 5.23 Movement of peak position for a range of input powers

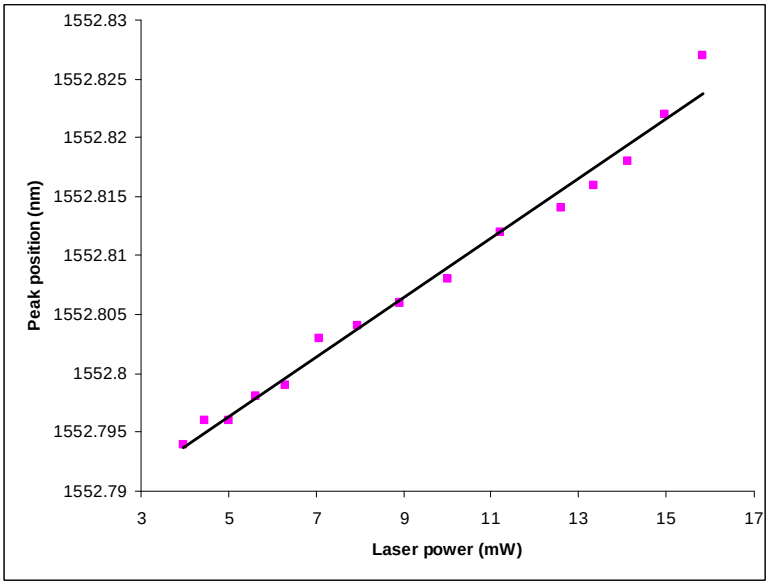

Figure 5.24 Peak position with linear laser power

The change in refractive index due to third order nonlinearity varies linearly with intensity and the change in peak position also varies linearly with refractive index (see section 3.10). Therefore if the area of a mode is assumed to remain constant for any given power, then peak position will vary linearly with power.

However this is also true of thermal change in refractive index and thermal expansion. Previous experiments [89] have overcome this problem by using short pulses to exploit the

difference in response time between thermal and third order nonlinear effects. This represents an interesting experiment to be carried out in the future.

At present it is possible to say that nonlinear effects have been observed in GLS microspheres. It is most likely that these effects are due to a combination of third order nonlinearity, thermal expansion and thermal index change, but their relative contributions cannot be determined at present.

5.4 Microsphere ball lenses

It has been suggested that small ball lenses and microspheres would be useful for coupling light from laser diodes to fibres [80]. It is therefore considered to be of interest to characterise the use of GLS microspheres as ball lenses.

In this experiment, we used the magnification properties of a microsphere under a microscope to ascertain its refractive index. The focal length (f) of a ball lens is determined by its refractive index and its diameter [51] (Equation 5.2), and the focal length determines the magnification (m) (Equation 5.3) [51].

Equation 5.2

$$f = \frac{nd}{4(n-1)}$$

Equation 5.3

$$\frac{1}{m} = \frac{f - x}{f}$$

Where x is the distance between the lens and the object. Equation 5.3 differentiates to

Equation 5.4

$$\frac{dx}{d\left(\frac{1}{m}\right)} = -f$$

A microsphere was attached to a fibre taper to enable it to be positioned. The fibre was mounted on a positioning stage, and the sphere positioned under the microscope. A graticule was placed under the sphere so that it could be observed through the sphere and its magnification measured (Figure 5.25).

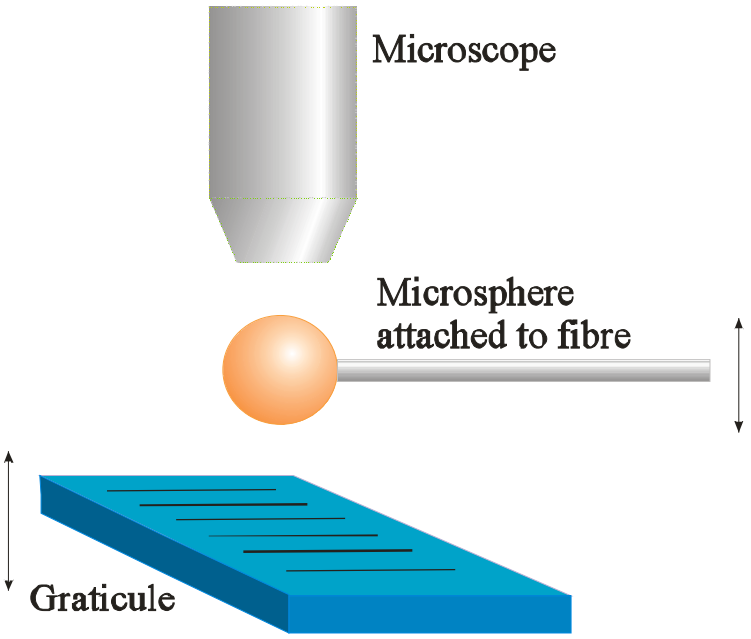

Figure 5.25. Experimental setup for ball lens measurement. The graticule and the sphere can both be independently moved.

The microsphere was brought in and out of focus using the positioning stage and the graticule was moved using the microscope's translational stage. The microsphere was positioned such that a clear image of the graticule could be observed (Figure 5.26).

A value of magnification is then measured by comparing the apparent length of the graticule and its actual length.

This process was repeated a number of times with the graticule at different distanced from the microsphere. As movement of the microsphere alters the magnification measured, it is necessary for the system to be mounted on a vibrationally isolated surface. The microsphere was measured using the software and camera associated with the microscope.

If the inverse of the magnification is plotted against the distance travelled by the graticule a straight line is observed (Figure 5.27), the gradient of which is the focal length (Equation 5.4). From this information, and the observed diameter of the sphere, a value of refractive index can be calculated.

A number of measurements were taken at each position to reduce the error.

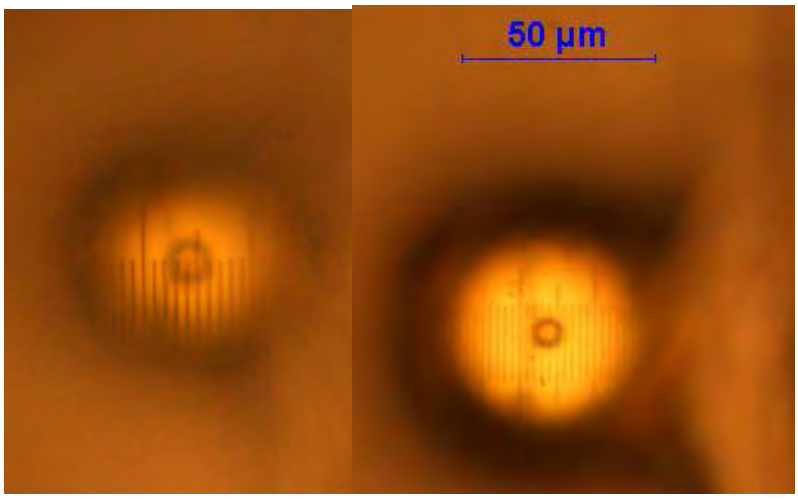

Figure 5.26 Graticule viewed through a microsphere ball lens. Large demarcations on the graticule are 100um. The magnification is apparent when comparing the view of the graticule and the calibrated length.

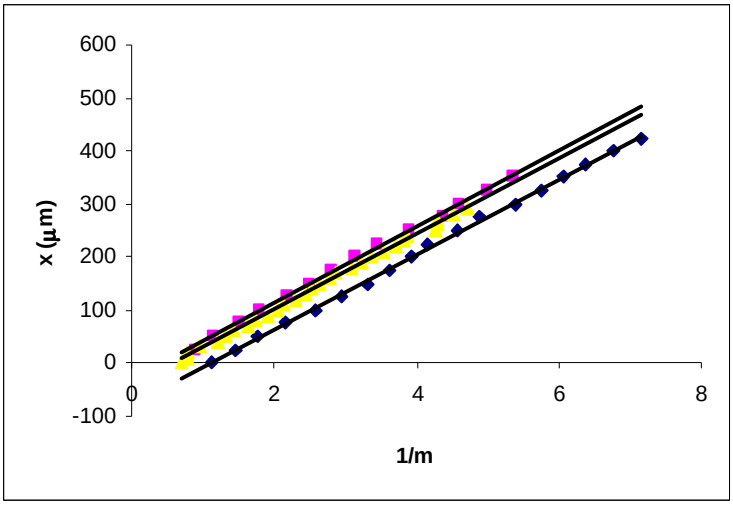

Figure 5.27 The gradient of 1/magnification vs. the change in distance is the focal length of a GLS microsphere ball lens.

From the diameter of the sphere and the measured value of focal length, a value of refractive index can be calculated. The refractive index was calculated to be 2.030+/-0.014 for wavelengths in the visible region. GLS /GLSO has a refractive index of 2 to 2.5 [17], but no data was available on the refractive index of the glass before it was made into microspheres is unknown, so no direct comparison can be drawn. However the value of refractive index calculated here is lower than typical values. This could be due to the process of making GLS into microspheres. Because microspheres are produced in free fall they will experience zero or reduced gravity. This could result in a lower density in the glass, which would result in a lower refractive index.

All of the observed data fits neatly to the theory, however it still results in some considerable uncertainty.

5.5 Conclusion

The Q values of GLS microspheres have been measured and found to range up to a maximum $1.2x10^5$. The modal structure of the microspheres, when light is coupled in using a BK7 waveguide, is very complicated. To better understand its structure a series of simple interference patterns have been overlaid to reproduce the observed pattern.

GLS microspheres have been shown to be sensitive to environmental effects, particularly immersion in water, which results in a severe degradation in Q factor and even catastrophic failure of the glass structure. Particles that have fallen away from the glass structure have been found to be depleted in gallium or sulphur and this is thought to be the cause of the structural failure.

Degradation in the Q factor has been observed when microspheres are exposed to air, but to a much lesser extent. When examined, these spheres were found to have dust attached to their surface, but none of the glass failure associated with immersion in water.

Measurements of the nonlinearity of GLS microspheres have been made by varying the power coupled into them and observing movement in the modes. Some movement was observed, but it was not possible to determine if this was due to third order nonlinearity or thermal effects, such as thermal index change or expansion.

Ball lenses have been demonstrated as one possible application of GLS microspheres.

For many applications the complicated modal pattern could be a drawback. However this complexity could be due to the coupling method, so could potentially be overcome for their application. The sensitivity to environmental effects would preclude GLS microspheres from being used as sensors unless they were coated in a protective material.

Whilst the Q of GLS microspheres is several orders of magnitude lower than silica [22], the properties of GLS make them a viable option for potential switching and laser applications.

6 Chalcogenide microsphere laser

6.1 Introduction

Since their first demonstration, solid state lasers have evolved through many laser geometries and materials. Reducing the threshold power of lasers is an aim that is desired for many applications. This would allow these light sources to be used in applications that could not otherwise afford the power. Miniature high Q cavities allow low power laser action to be achieved along with narrow linewidth, which would make such lasers useful in a range of applications including sensing, communications and computing.

In recent years, microsphere lasers have received much interest because of their extremely low threshold however, to the best of our knowledge, there have been no reports of chalcogenide microsphere lasers to date. Chalcogenide glasses are interesting materials for laser production because of their low phonon energy and infrared transmission. This allows fluorescence in the mid and far infrared to be seen and could result in new lasers at these wavelengths [47].

In this chapter background on previous demonstrations of microsphere lasers is given, then data on chalcogenide microsphere spectroscopy is presented and a laser demonstration in neodymium doped GLS (Nd:GLS) glass. The microsphere laser developed here has a narrower linewidth than all previous GLS lasers. This improvement has been possible because of the high Q microspheres that have been produced in this material [83]. The chapter concludes with a discussion of the possible uses of such a laser.

6.2 Background

Microsphere lasers have been demonstrated in various types of glass, such as silica [22, 56, 57], fluoride[70, 105], phosphate [5, 71] and tellurite [55, 58, 59, 106, 107], using a variety of pumping and coupling methods. Until now, chalcogenide microsphere lasers have not been reported. GLS is a useful chalcogenide host medium for rare earth ions because of the high levels of dopants that can be incorporated into the glass matrix. It is also a low phonon

energy glass which makes the energy transfer from the excited ion to a photon more efficient [15].

GLS has been used for the active laser medium in the form of a bulk glass [15], fibre [50], and planar waveguides [49]. Schweizer et al. [15] produced an Nd:GLS (Nd_2S_3 1.5mol%) bulk glass laser that used a slice of glass 1.42mm thick. This was set in an external cavity formed with two mirrors, one planar and the second with a 50mm radius of curvature. Two different reflectivities were used for the output coupling, one with 1% transmission and the other with 5%. These gave a threshold of 8mW and 18mW respectively.
Schweizer et al. [50] also produced a fibre laser using 22mm of fibre, with a core diameter of 14μm doped with 0.05mol% Nd_2S_3. This produced both a CW and self pulsing laser with a linewidth of 0.2nm. Output coupling of 0.5% and 7% was used to give a threshold of 100mW and 200mW respectively.
Mairaj et al. [49] achieved laser action in a UV written waveguide, 0.2μm deep, 8μm wide and 16mm in length, doped with 0.5mol% Nd_2S_3. This produced laser action with a linewidth of 1nm. Output couplers of 2%, 8% and 12.5% were used and these gave thresholds of 15.1mW, 18.7mW and 33.8mW respectively. It was found that laser action was only achieved with a chopped pump source, because of nonlinear effects due to heating.

Microsphere lasers have gathered much interest because of their low threshold and narrow linewidth. Microsphere lasers were first realised by Garrett et al. [108] in 1961 who produced a pulsed laser from a samarium doped CaF microsphere. Since then lasers have been produced using microdroplets [109, 110], polymer microspheres [111-113], spherical crystals [114] and glass microspheres. Here we will focus on glass microsphere lasers. Table 6.1 summarises a wide selection of glass microsphere laser properties.

To date glass microsphere lasers have been produced by a number of means. The spheres themselves have been produced by various methods and from various materials, with the light coupled in and out by a variety of means.
A frequently used method of producing microspheres is to melt the tip of a glass filament [55] typically an optical fibre [56, 57]. This produces a single sphere which remains attached to the filament. The filament can then be used to position the microsphere wherever it is desired. This method is effective at producing individual high Q [57] microspheres which

can be made into lasers. However as each microsphere has to be individually produced it would be impractical for use in devices where multiple identical spheres are required.
There are three key methods of production that will yield a large number of spheres at once. These include pouring molten glass into liquid nitrogen [55], passing crushed glass through a plasma [60]or onto a spinning disk [58, 59] that then flings out droplets that quench as they fly. It has been reported that when pouring molten glass into liquid nitrogen, a poor quality surface was produced which had to undergo a chemical etch to produce a high Q sphere [55], none of the other sphere production methods examined here had to undergo any kind of etch or polish.
All three methods will produce a large number of spheres with a range of sizes. The spinning disk and plasma methods are similar in principle to the method used in this project.

Table 6.1 Properties of previous microsphere lasers

Glass	Dopant	Production	Sphere size (μm)	Coupling method	Pump (nm)	Threshold	Laser Wavelength	Linewidth	Q	Max power output	Ref.
Tellurite	Nd	Glass coating on metal wire, electrically heated	140	Microscope objective	800	81mW incident	1064nm	-	-	-	[55]
Fluoride	Nd	Liquid glass poured into liquid nitrogen followed by chemical polishing	100 -150	Microscope objective	800	5mW @ 1051nm and 60mW @1334nm	1051nm and 1334nm	<.1nm	-	-	[70, 105]
Tellurite	Er	Liquid glass poured onto spinning disk to produce droplets	1-100s	Fibre taper	975	<2mW	1604nm	.053nm	10^5 10^6	-	[59, 106]
Silica	Nd	Fibre tip melted with CO2 laser	56	Prism	807	200nW absorbed power 1mW incident	1083nm	-	10^6 @ 807nm 10^8 @ 1083nm	-	[57]
Tellurite	Tm	Liquid glass poured onto spinning disk to produce droplets	-	Fibre taper	793	2.5mW @ 1.5μm and 0.7mW @1.9um	1.5μm and 1.9μm	-	-	-	[58, 115]
Silica	Er	Micro torch fusion	150	Angle polished fibre	980	1mW coupled in	1555nm 1530-1560	-	Q_p .5-1x10^6 Q_I 3-8x10^6	-	[72, 116]
Silica	-	Fibre tip melted with CO2 laser	25-120	Fibre taper	1555	Sphere size dependent	1560nm 1670nm	200kHz-1.5MHz	3-8x10^6	4.1 μW	[56]
Phosphate	Er, Yb	-	45	Spliced fibre taper	980	0.4mW	1550nm	<300kHz	-	112u μW	[71]
Phosphate	Er, Yb	-	57	Fibre taper	980	60uW absorbed	1.5μm	-	-	3uW Single Mode 10u μW Multi Mode	[5]
Silica	Er	Microwave plasma torch and ground glass	50-100	Fibre taper	980.8	15mW	1.5 μm				[60]

Microsphere lasers have been produced in a number of geometries to couple light in and out. These can be roughly broken down into three categories; free space, prism and several versions of fibre/taper and hybridisations of these three basic coupling methods (Table 6.1). Fibre taper coupling is the most commonly used method and works by coupling the evanescent field of the taper to the microsphere. It has the advantage that it can be used to excite a limited number of modes at one time, but has the drawback that tapers can be very fragile, which makes them difficult to work with and also precludes integration into a device.

Prism coupling also works by coupling the evanescent field. As it utilises bulk optics it is more robust, but there will be a difference of scale between the prism and the microsphere.

The free space coupling methods use a microscope objective to couple pump light directly into a mode or modes of the microsphere. Miura et al. [70, 105] use the same microscope objective to couple the laser light back out, whilst Sasagawa et al. [55] use a second microscope objective to observe the laser.

Ilchenko et al. [72, 116] used an angle polished fibre as a hybrid of the fibre and prism. This has the advantage of being a similar size to the microsphere, and will be more robust than the fibre taper.

This variety of glass microspheres and coupling methods has produced a selection of lasers and, because of this variety, there are differences in their characterisation methods. For instance where free space coupling has been used it is not trivial to quantify the power absorbed by the microsphere, whereas taper and prism coupling allows an accurate measure of absorption, but threshold values still vary between power coupled in and power absorbed. Therefore no meaningful comparisons have been drawn regarding the spheres themselves.

Of all the microsphere laser papers only one mentioned the movement of modes [59] and this was attributed to thermal effects. However chalcogenide glasses are often noted for their high levels of third order nonlinearity and we have noted modal movement significantly

higher than those observed in [59]. We therefore expect significant differences between the properties of GLS lasers and those demonstrated in the past.

6.3 Experimental method

6.3.1 Sphere fabrication

GLS glass doped with 1.5mol% neodymium was prepared, as described in Chapter 2 and a selection of GLS microspheres were made using the drop technique described in Chapter 4. These spheres were sorted and stored using techniques previously described, in chapter 5, until laser characterization took place. Microspheres produced by this method have been characterised and a Q-factor of up to 10^5 demonstrated.

6.3.2 Basic spectroscopy

In this project a number of methods have been used to observe fluorescence from rare earth doped GLS microspheres. These preliminary experiments allowed the observation of WGM of the fluorescence and provided insight into the eventual demonstration of laser action. Issues with the size of the spheres and the amount of light given off by such a small object meant that standard lenses could not be used effectively. A system of standard lenses was used to measure fluorescence from bulk samples and arrays of spheres, but for single spheres coupling through a fibre or microscope objective was necessary. Experiments have been carried out using a confocal microscope to pump and collect light, and using a microscope objective to pump a fibre coupled sphere.

Initial attempts to measure fluorescence from microspheres were carried out in collaboration with Richard Curry at the University of Surrey. These trials used standard lenses to focus laser light and collect fluorescence. They were successful in measuring fluorescence from bulk samples and collections of spheres, but detection was not efficient for single microspheres.

Experiments were also carried in collaboration with Daniel Jacques in MUA, Spain, using a confocal microscope (Olympus BX41 Raman) (Figure 6.1). These experiments successfully measured fluorescence from single microspheres (Figure 6.2-Figure 6.6), with some interesting results, but we did not definitely observe laser action. Experiments were carried out at our laboratories using a fibre to collect fluorescence. The sphere was mounted on the end of an angle cleaved fibre (Figure 6.8), which both positioned the sphere and collected the fluorescence. The pump power was focussed onto the sphere with a microscope objective (Figure 6.9). Experiments were also carried out with the sphere on a glass slide, a fibre was then positioned close to the sphere to collect the fluorescence. The pump light was focused onto the sphere with a microscope in the same way as for the fibre mounted sphere.

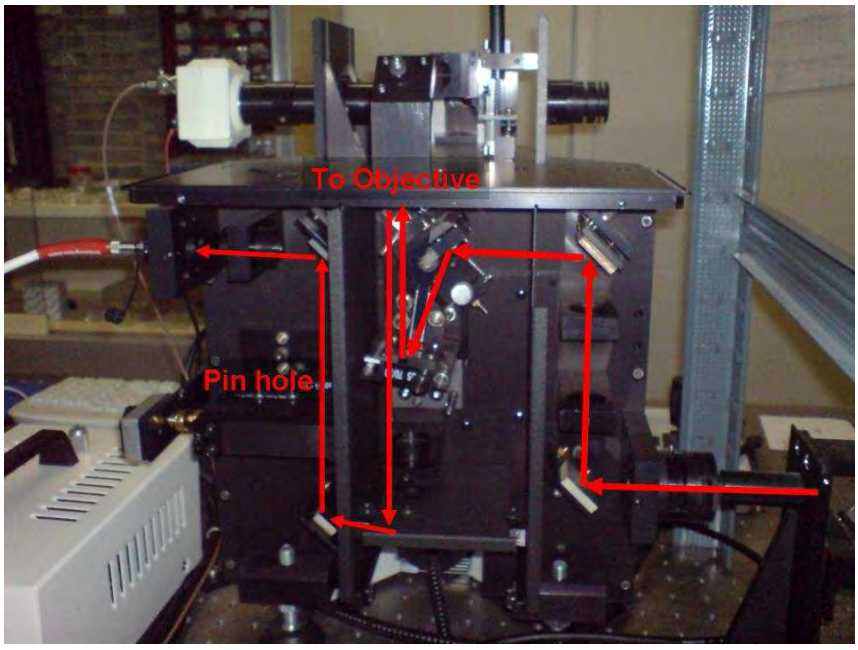

Figure 6.1 The optics in the back of the confocal microscope. Laser light enters from the right, and is passed to the microscope objective. Fluorescence is brought from the objective lens, through a pinhole and is then taken to the spectrometer via the fibre (left). The camera (top left) is for viewing only.

A confocal microscope is able to illuminate a spot with laser light and then collect the fluorescence from that spot. Confocal microscopes differ from standard microscopes in that light collected by the microscope objective is focussed through a pinhole, which blocks stray light coming from anywhere other than the focal point. This means that the depth as well as the x-y plane of a sample point can be specified.

The samples being examined were doped with either Nd or Er, both of which can be pumped with an 808nm laser. The main emission of Nd:GLS is around 1070nm, while Er:GLS has an up conversion to 550nm. The WGM were excited by focusing the confocal microscope to a

spot on edge of the microsphere (Figure 6.2 - Figure 6.4). A series of spectra were taken at regular points on a line from the centre of the sphere to its edge (Figure 6.5) to build up a map (Figure 6.6) of the fluorescence. Although due to technical limitations, this can only be done at one focal distance, as no automatic refocusing could take place. This meant that point of focus could not follow the curve surface of the sphere.

The power of the diode laser was altered to examine the dependence of fluorescence on pump power (Figure 6.3-Figure 6.4). The power was controlled by altering the diode current and calibrated with a detector under the microscope head.
Lifetime measurements were taken using the same confocal microscope set up, but instead of the microscope being coupled to the spectrometer it was coupled to a photo-multiplier, which was in turn linked to an oscilloscope. The diode was driven in square wave pulses, and from the drop off of the fluorescence the lifetime was calculated. The lifetime of Er:GLS was measured at the edge and centre of the sphere and both were found to be 26μsec, which is consistent with previous measurements [47].

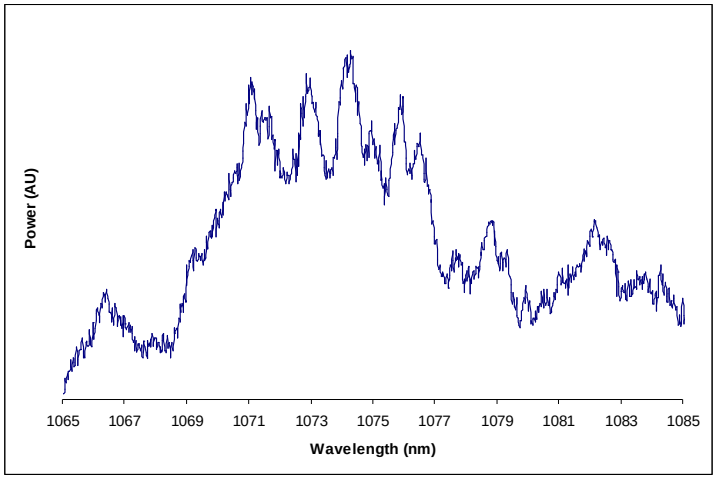

Figure 6.2 Fluorescent spectra taken from the edge of a Nd:GLS sphere (diameter 100um) when pumped at 808nm, taken with a confocal microscope.

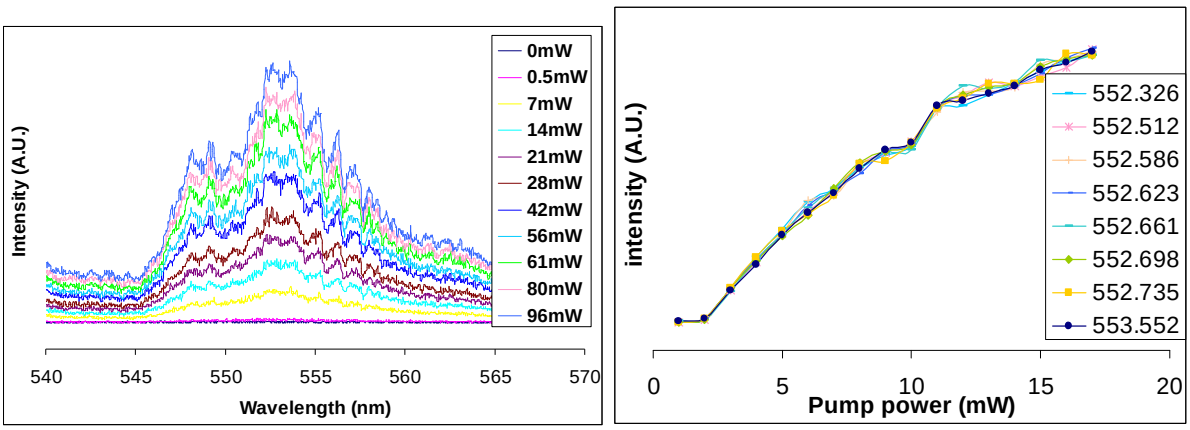

Figure 6.3 Up conversion from the edge of a Er:GLS sphere for a range of incident pump powers, measurements taken with a confocal microscope. Peak power is plotted against pump power. The first two readings are indistinguishable from noise and do not represent a threshold.

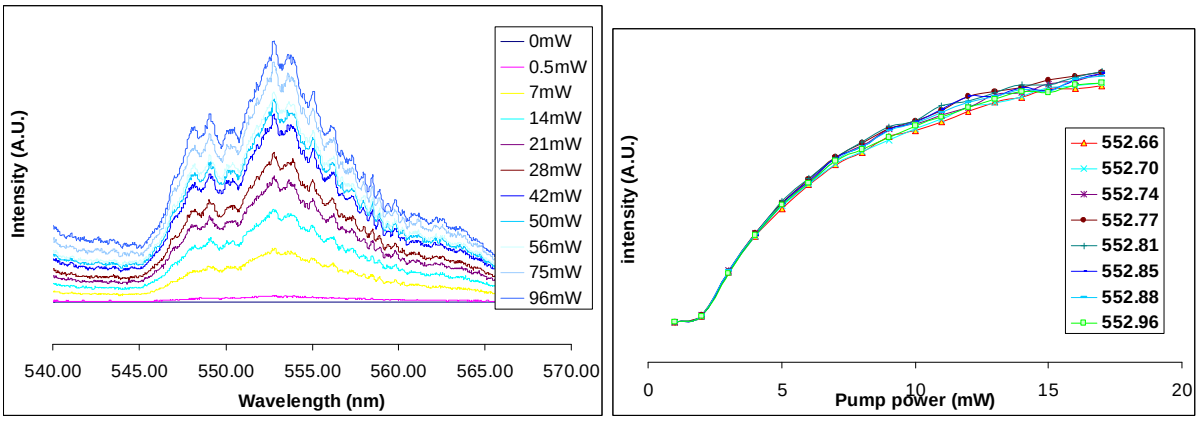

Figure 6.4 Up conversion from the centre of a Er:GLS sphere for a range of incident pump powers, measurements taken with a confocal microscope.

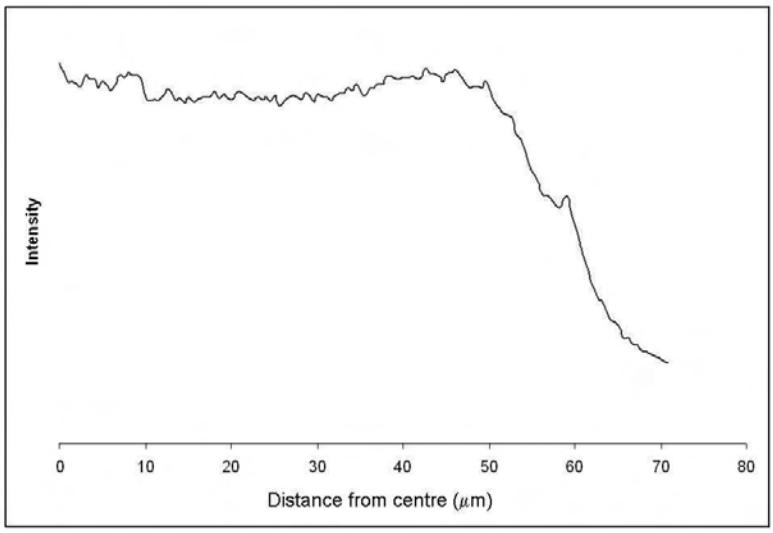

Figure 6.5 peak up-conversion from a Er:GLS sphere as a function of distance from the centre of the sphere, measurements taken with a confocal microscope.

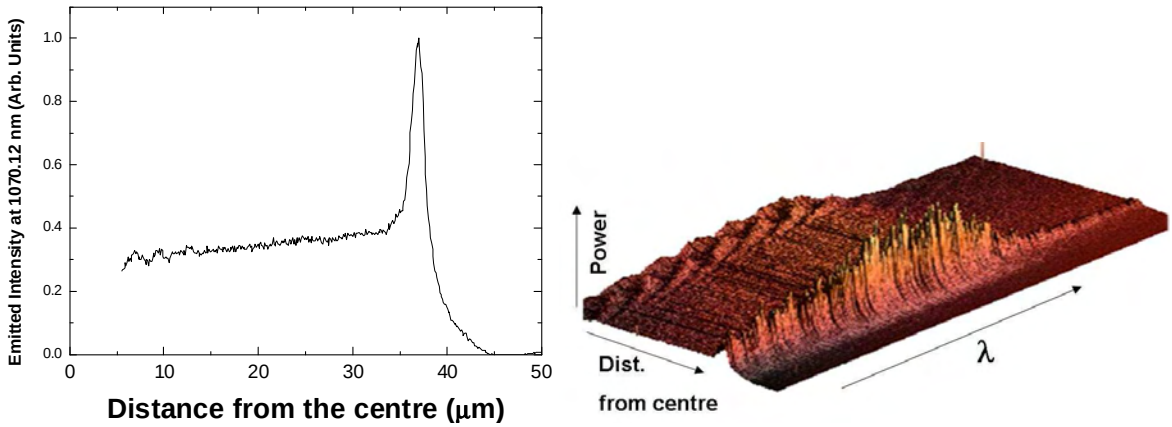

Figure 6.6 Variation of Nd fluorescence at distances from the centre of the sphere (left) and with wavelength (right) showing the WGM at the edge of the sphere. Both plots were taken with a confocal microscope.

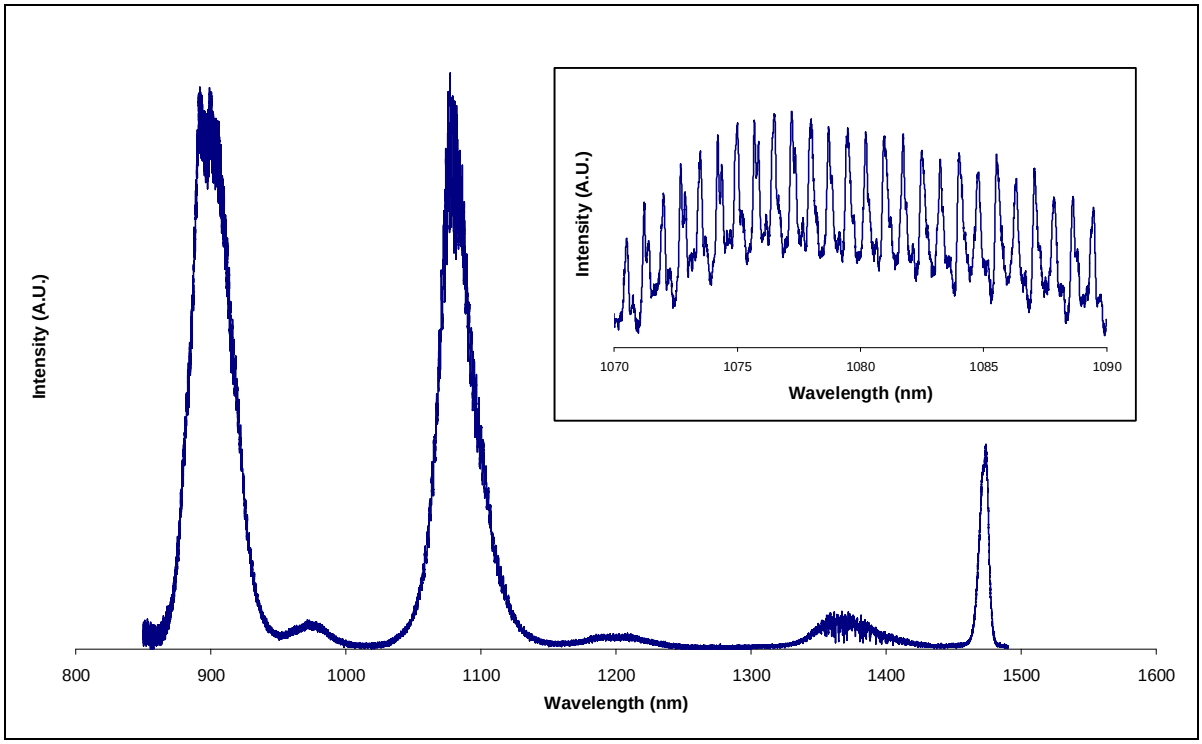

Figure 6.7 Fluorescent spectrum from GLS microsphere doped with 1.5mol% Nd. Inset, close up showing WGM on peak @ 1080nm. This measurement was taken using a fibre coupled microsphere.

Modal structure was observed in Er:GLS up-conversion (Figure 6.3 and Figure 6.4) at a range of pump powers. However the modal peak of the Er:GLS up-conversion (Figure 6.3 and Figure 6.4) showed no threshold in its power dependence and it can therefore be said that no lasing was achieved in this transition. Up-conversion in Nd:GLS is an established

phenomenon [47] and was observed in this study, but modal structure was not observed which indicated that the cavity was not resonating.

When comparing the spectra for the edge and centre of the sphere (Figure 6.5 and Figure 6.6), it can be seen that peaks are more pronounced from the edge spectra, which is most likely due to the spatial positioning of the WGM. It is interesting to note that peaks are still seen on the centre spectra. This suggests that some modal excitement is occurring. However some modal structure is expected from the very centre as light can travel through the centre and reflect off of the opposite surface. The point where modal structure is least likely to be present is between the centre and edge, where there are no direct reflecting modes or WGMs. This theory is supported by the smoother area seen between the centre and edge of the sphere (Figure 6.6). The defined peak at the edge of the sphere (Figure 6.6), is not seen in the Er:GLS up-conversion spectra (Figure 6.5), which is likely to be due to alignment issues in the confocal microscope. The alignment of the confocal microscope components was found to be extremely critical to observing WGM in the fluorescence. Slight adjustments caused WGM to disappear and only bulk type fluorescence would be seen.

WGMs have been seen in the fluorescence using both the confocal microscope (Figure 6.2 - Figure 6.4) and the fibre coupled sphere (Figure 6.7). Using the confocal microscope it is possible to take spectra from specific points on the sphere, this is not possible with a fibre. However when the microsphere was coupled to a fibre, the modal pattern was seen much more clearly (Figure 6.7) than with the confocal microscope setup (Figure 6.2) as the fibre coupling is better able to collect low levels of light from a fluorescing microsphere, which resulted in a much lower noise spectrum. This setup was then adapted for the observation of laser action in a Nd:GLS microsphere.

6.3.3 Laser demonstration

A graded index fibre (GIF625 Thorlabs) was cleaved at an angle (Figure 6.9) and a Nd:GLS microsphere 100µm in diameter was glued to its face with Cyanoacrylate. The fibre and sphere were mounted on a positioning stage and pumped with an 808nm laser diode. The laser diode was pulsed at 2.18kHz using a signal generator and the light from it was focussed on to the microsphere using a 40x objective. The light coupled out through the fibre was split

with one part going to an optical spectrum analyser (Yokogawa AQ6370), while the other was passed through an 850nm long pass filter (Thorlabs FEL0850) to a high speed detector (New Focus 2053), the output from the detector was then passed to an oscilloscope (Tecktronix TDS 2022).

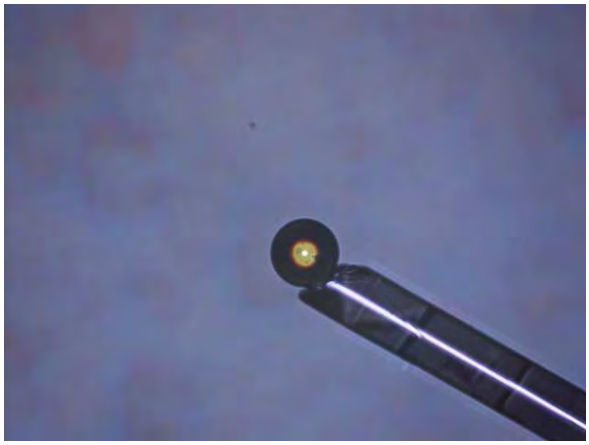

Figure 6.8 Nd:GLS sphere 100µm in diameter mounted on an angled GIF625 fibre.

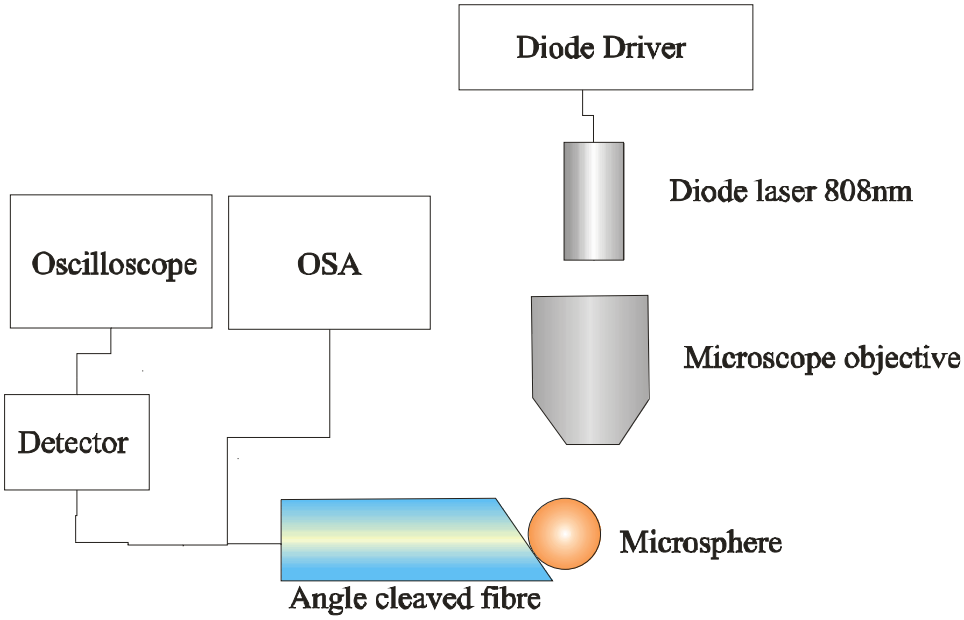

Figure 6.9 angle cleaved fibre coupling for spectroscopy of single sphere.

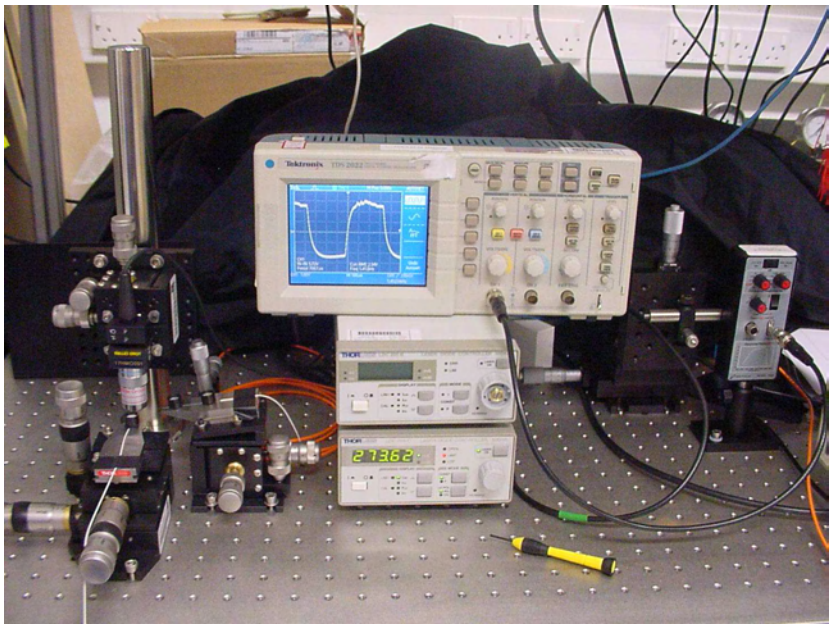

Figure 6.10 Experimental setup used to observe laser action.

Prior to observation of laser action in a chalcogenide microsphere, Y. Panitchob [117] demonstrated laser action in BK7 microspheres doped with 1.5mol% Nd. The first experiments were carried out using a Ti:sapphire laser (808nm) focussed through a standard lens onto a microsphere mounted on a glass plate. A (GIF625) multimode fibre was held close to the microsphere to collect the fluorescence and deliver it to the OSA.

This result was repeated by the author using an 808nm laser diode focussed though a 10x microscope objective lens onto the BK7 microsphere. The light was collected and analysed in the same way.

The alignment and observation of laser action in BK7 microspheres was much simpler than it turned out to be for chalcogenide microspheres. The major difference between these two types of microsphere is their refractive index. Launching into the WGM of the higher index microsphere will be more difficult as refraction will tend to draw light into the body of the microsphere and away from the WGM.

Observing fluorescence in a chalcogenide microsphere was relatively easy, but it took many attempts over a period of 3 months, before laser action was quantifiably observed. The first configuration that was tried had the spheres placed on a glass microscope slide with the 808nm diode pump focussed through a 10x microscope objective and a square cleaved fibre was held close to the microsphere to collect the fluorescence. This was the same setup that had previously been used to successfully observe laser action in a BK7 microsphere. We were able to observe fluorescence but not laser action.

Another configuration had the microsphere glued directly to the end of a non-angle cleaved fibre, with the pump focussed as before. This had the advantage that less alignment was required because there were fewer components, meaning that the microsphere could be brought to the focus of the objective by maximising the fluorescence. This reduces uncertainty over whether the relative position of the microsphere and fibre were failing to couple light out.

Again with this geometry fluorescence was observed. As laser action was not seen there were concerns that sticking the sphere to the fibre could be causing a point of loss, which would make laser action more likely to occur where the sphere surface was not in contact with the fibre. Therefore a second cleaved fibre was positioned close to the microsphere perpendicular to the first fibre. This set up also showed fluorescence but not laser action. Laser action was ultimately observed by using an angle cleaved fibre and a 40x objective lens. Even then it was extremely sensitive to small adjustments in the position of the microsphere. The positioning stage had a relative accuracy of 20nm, but the sphere had to be positioned with the smallest possible movement, significantly smaller than the positioning stages increments.

Once the position where laser action could occur had been found and fixed, measurements were taken over a period of several hours. On several consecutive days when the system was turned on it was found to have relaxed and required some repositioning to successfully reinstate laser action.

6.4 Results

Using the method described in the previous section, the position of the sphere was altered under the objective until a jagged top associated with time dependent emission was observed at the top of each fluorescence pulse (Figure 6.11). The output of the fibre was then transferred to an optical spectrum analyser (OSA) (Yokogawa AQ6370) to observe any sharp lasing peaks (Figure 6.12). By varying the power, the change in the peaks and the threshold can be observed.

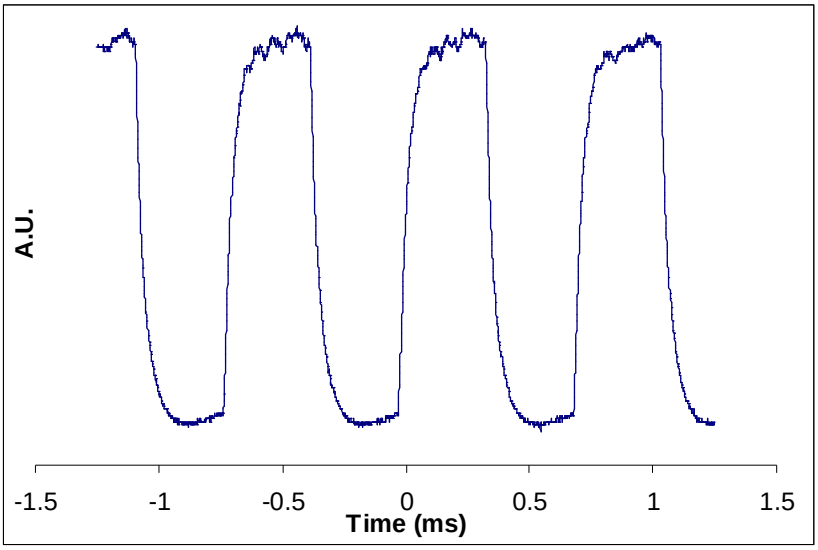

Figure 6.11 Time dependence of fluorescence from 100mm Nd:GLS microsphere pumped at 808nm, showing peaks of laser transitions.

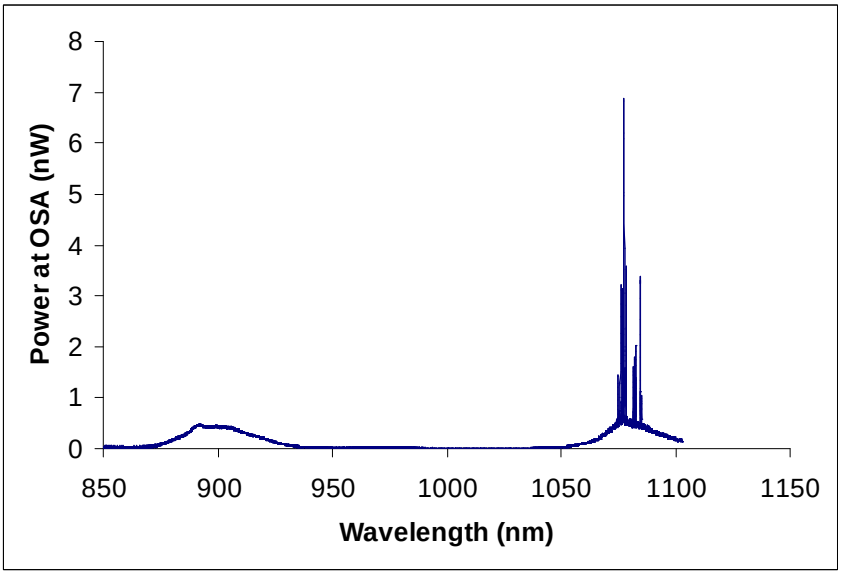

Figure 6.12 Spectra showing bulk fluorescence and lasing (incident pump power 217mW).

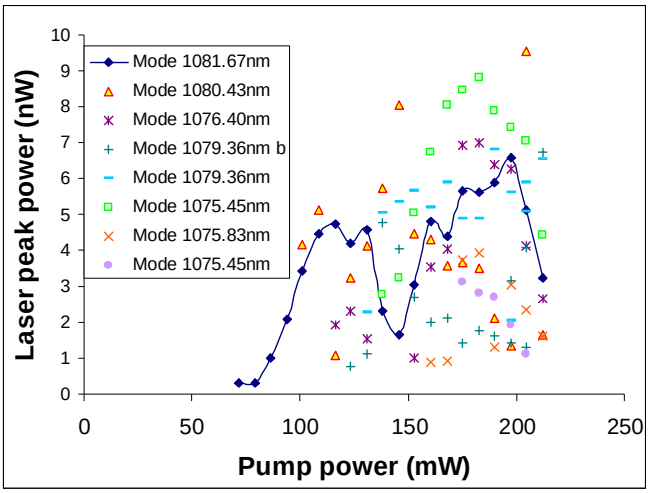

Figure 6.13 Laser modal peak output power showing the eight most dominant modes as a function of pump powers. With the primary mode highlighted to show the threshold at ~82mW incident pump power, initial slope and competing modes. Modes are identified by the wavelength at which they first lase.

Spectra were taken for a number of pump powers in order to observe the threshold pump power (Figure 6.13). However it was also observed that the peaks moved and new peaks started to lase, as the power was increased (Figure 6.13). Laser action was only observed when the pump was chopped and the peaks were also observed to change with pump chopping frequency. All results reported here were taken with the pump chopped at 2.18kHz. As the pump power was increased, the laser output power changed, and moved to longer wavelengths (Figure 6.13, Figure 6.14, Figure 6.15). The dominant lasing mode also changed as the pump power increased (Figure 6.13).

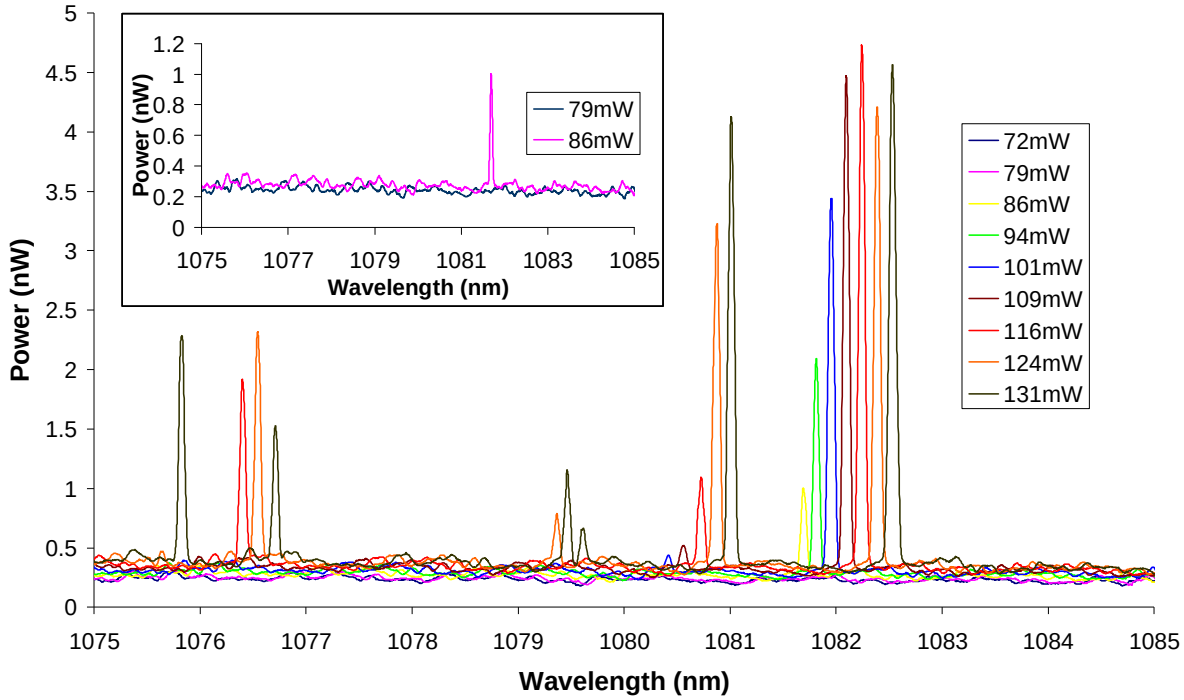

Figure 6.14 Laser peaks, showing the change of mode, movement of peak and increase of laser output with increased pump power. Inset shows power output from the microsphere laser as the threshold is crossed.

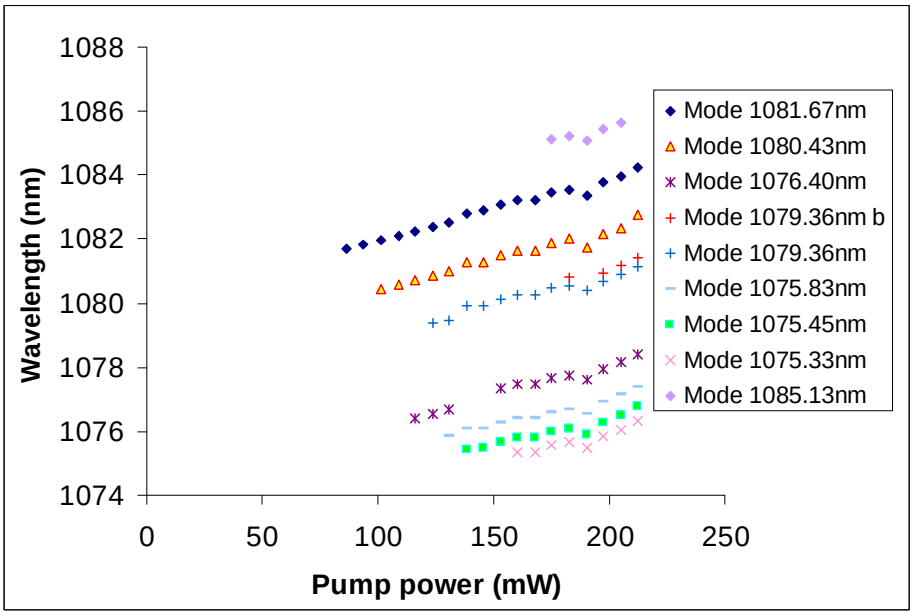

Figure 6.15 Wavelength of laser peaks and their shift as pump power increases. Laser modes move by up to 2.5nm.

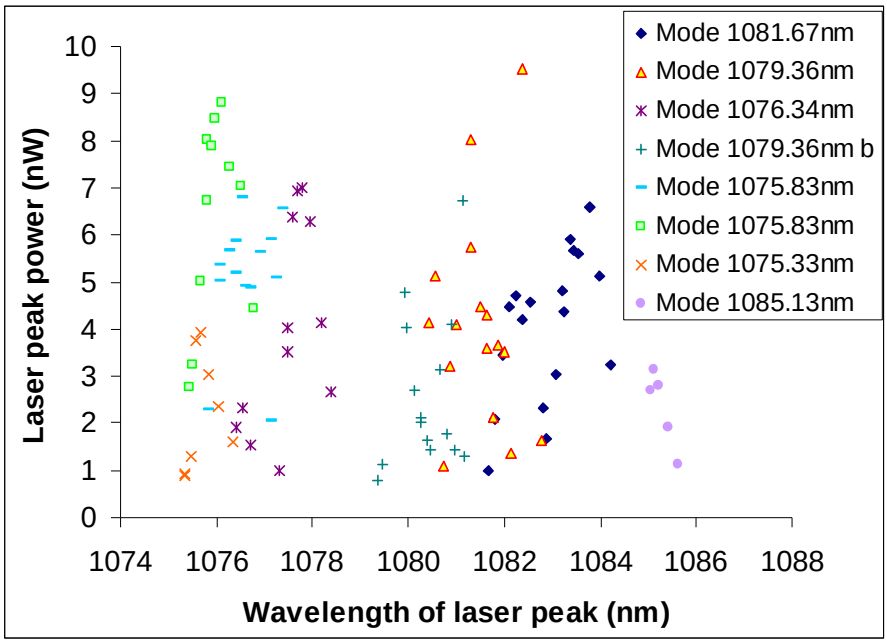

Figure 6.16 Wavelength of laser peaks and their output power showing no clear correlation. The two regions of laser action are visible from 1075 to 1079nm and from 1080nm to 1085nm.

The presence of a threshold (Figure 6.13) and the appearance of a sharp peak (Figure 6.14) in the spectra confirmed that lasing was occurring in the sphere. The microsphere laser has a threshold of ~82mW incident pump power and slope efficiency of 1.6×10^{-7} (Figure 6.13). When this is compared to threshold calculations (see section 3.14) it appears that either the absorption is very low or the modal size is larger than expected. It is not known how much of this power is absorbed, because of the nature of the setup. However it is likely to be only a small fraction of the total incident power.

The movement of the lasing modes are approximately constant with power in (Figure 6.15). Whilst the lasing modes rise and fall, the non-lasing modal structure has remained largely unchanged, so the spectra can be repositioned to remove the effects of movement (Figure 6.17). This shows that laser modes have undergone very little movement relative to each other. Where it appears that there has been relative movement, closer inspection reveals several competing modes very close together (Figure 6.17).

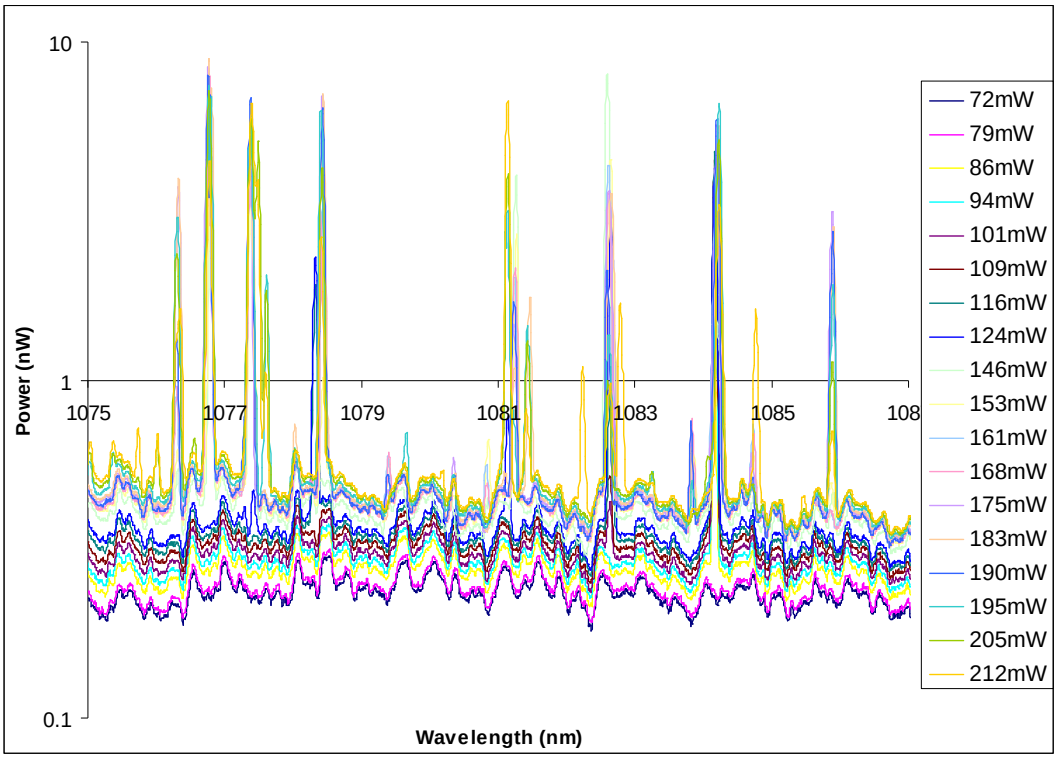

Figure 6.17 Laser spectra repositioned to align modes

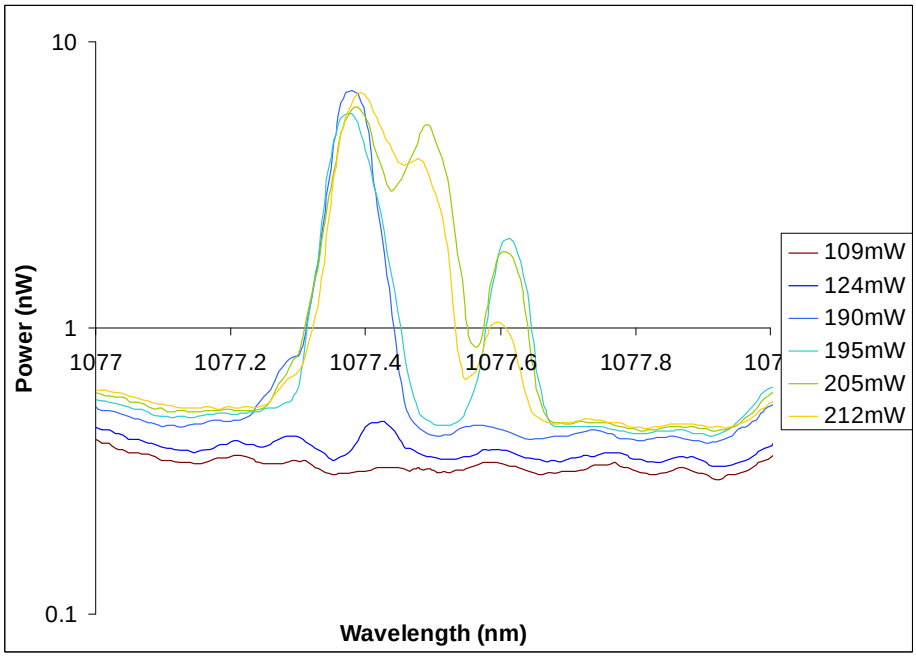

Figure 6.18 Modes close together

The movement of these peaks, as shown in Figure 6.18, suggests that properties of the sphere are being changed by the circulating light. This could represent an interesting property of GLS microsphere lasers if they can have their laser wavelength tuned by an external source of light. It is unclear if the movement of the whole spectrum is due to the third order

nonlinearity or thermal effects such as thermal index change or thermal expansion of the sphere.

Assuming that the shift is due only to index change, either third order or thermal, and using the theory described in chapter 3, it is possible to calculate the change of index to be 0.005. If this were due only to third order nonlinearity it would require a circulating intensity of $2.4 \times 10^{11} W/cm^2$ which is higher than the damage threshold for GLS. However a combination of thermal index change and expansion would account for the wavelength shift with a $30^{o}C$ increase in microsphere temperature. Therefore the thermal effects are likely to dominate over the third order effects.

It is desirable to isolate third order nonlinearity from thermal effects. One method used with passive spheres exploits the difference in response time between third order and thermal effects. A fast pulsed source is used to excite the WGM, the pulse frequency is increased until the thermal effects can no longer take effect [89]. However it would not be possible to use this method in this instance because the pulse speed has a significant effect on the lasing mode and, at sufficiently high pulse speeds, lasing will stop altogether.

As well as the position of individual modes changing, the dominant lasing mode changes as the pump power is increased (Figure 6.13 and Figure 6.15). This could be due to mode saturation causing other modes to become dominant and reduce the available energy. After the onset of multimode operation there does not appear to be any simple relationship between the mode output power and its pump power (Figure 6.13) or position (Figure 6.15).

The Nd:GLS fluorescence spectrum has two peaks (~1077,~1082), but they are not usually very distinct. However they are exaggerated by laser action and show up as two distinct regions of laser action (Figure 6.12, Figure 6.14-Figure 6.16, Figure 6.19).

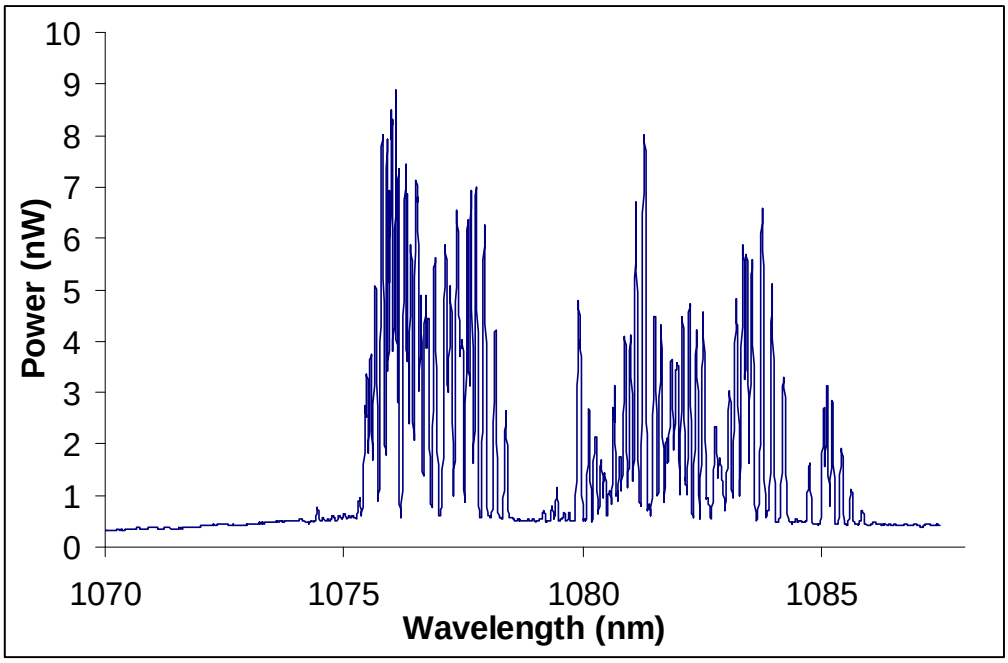

Figure 6.19 Maximum output power from all pump powers, showing the two areas where laser action occurred.

The OSA setup used had a resolution limit of 0.05nm and this was found to limit the measurement of the laser peak widths. Therefore it can only be said that the peaks are <0.05nm wide, this is significantly narrower than other GLS lasers. This linewidth is an order of magnitude narrower than the linewidths associated with dense wavelength division multiplexing (DWDM) [118].

6.5 Discussion

6.5.1 Laser action

It was found that a Nd:GLS microsphere could achieve laser action. A threshold was observed at 82mW (Figure 6.13) of incident pump power for a 1082nm laser line. A sharp spectral peak, or peaks <0.05nm FWHM, were present above this power (Figure 6.14). As the pump power was increased the laser wavelength of each mode moved to longer wavelength (red-shifted) and above 100mW incident pump power the microsphere laser became multimode (Figure 6.15, Figure 6.13). As it increased further the laser became increasingly multimode. Individual modes continued to red-shift (Figure 6.15), but new modes appeared at shorter wavelengths. The exact mechanism by which this shift occurs is unknown, but it may be possible for the laser wavelength to be controlled or altered by the introduction of non-pump light onto the sphere.

Between threshold and the onset of multimode action (Figure 6.13), the power output increased linearly with a slope efficiency of 1.6×10^{-7}, but when the laser became multimode there was no consistent pattern to the peak power of laser modes (Figure 6.16). However the position of the laser peaks did move linearly with the increasing pump power (Figure 6.15) and this shift was the same for all modes. When the incident pump power was increased from 82mW to 220mW, the wavelength was shifted by 2.5nm. It was noted that the chop frequency at which the laser was pumped had an effect on the laser output, but this has not been studied.

It has been shown in a previous study [59] that as pump power is increased the resonant peaks move continuously to longer wavelengths while new shorter wavelengths also start to lase. This has also been found to be the case here (Figure 6.15), individual modes move to longer wavelengths as pump power increases and there is a tendency for new modes to appear at shorter wavelengths, but there does not appear to be any simple relationship that determines how the power is distributed amongst these modes. Peng et al. [59] ascribe the individual modal shift to thermal expansion of the sphere and thermal refractive index change, but do not make any

mention of third order nonlinearity. In a glass such as GLS, nonlinearity is very high and it is possible that this will have some impact on laser action. However thermal and third order nonlinear effects would both cause the resonant wavelength to become longer as they both increase the effective path length, which makes it difficult to separate these effects.
Regardless of which effect dominates, both are likely to play a role and this could be used to control the operation of the laser. Thermal control is widespread [59], but the use of nonlinear control is not. A form of nonlinear control has been demonstrated in a chalcogenide photonic crystal [119], which was tuned with an external laser. The ability to control the wavelength of a laser could be of significant use in optical circuits, where it could be used for fast switching or to work between channels on a wavelength multiplexed system.

6.5.2 Effect of coupling

There are several methods of coupling that have been used with microsphere lasers (Table 6.1). Free space pumping of the microsphere to produce a laser is a well established method [55, 105] however it does mean that it is not possible to ascertain the pump power that is absorbed and this makes it difficult to compare our results with others that have used a different coupling method.

Coupling via a fibre taper is an efficient and frequently used method (Table 6.1), however tapers are fragile. Optical fibres and microscope objective lenses are a well established and stable coupling technology. Because this is the only technology that is used in our coupling system this makes it more robust. Other microsphere laser coupling systems have used microscope objective lenses or fibres, but not both together. Sasagawa et al. [55] used two objective lenses, one to couple in and one to couple light out of the microsphere, whilst Miura et al. [70, 105] used one objective lens to couple in and out. Using microscope objective lenses to couple out as well as in will require the system to be very accurately aligned before the microsphere is introduced for analysis. By comparison, in our scheme the laser and microscope objective do not require critical alignment before the microsphere is then brought to the focus of the laser. This point can be found by observing the fluorescence through

the fibre that is used to position the microsphere. This makes it simple to observe fluorescence, on top of this the system is very robust.

Tellurite glass has a high refractive index and high nonlinearity similar to GLS and it has been used to make Nd-doped microsphere lasers that were also pumped by free space coupling. Sasagawa et al. [55] reported an incident pump power threshold of 81mW with a coupling system. This is very similar to our threshold of 82mW which also coupled the pump with a microscope objective.

Peng et al. [59] used a fibre taper to couple the pump into the microsphere and therefore it is difficult to make a direct comparison with our measurements. Although in both cases the threshold is known. Peng et al. [59] also observed a shift of 1.2nm when the pump power was increased from threshold at 2mW to 7.6mW (280% of threshold power). Our shift was observed to be 2.5nm when the incident pump power was increased from its threshold at 82mW to 212mW (260% of threshold power).

6.5.3 Applications

Whilst Nd:GLS does not produce a laser in the 1550nm telecoms window it is possible that an Er:GLS laser would. This could therefore represent a useful laser in telecoms applications because of its narrow bandwidth and low energy consumption. The narrow bandwidth of this laser and low energy could make it useful in a number of other fields such as optical sensors.
Many optical sensors rely on narrow band lasers for their accuracy. If this could be provided with a low energy requirement it would make these sensors cheaper to use and potentially applicable in more situations. As microspheres have the potential to be used as sensors [23] there exists the possibility to incorporate the microsphere laser into the optical sensor.

It is possible to produce a memory device from two circular resonator lasers with a waveguide between them [11], in principle the two circular resonator lasers could be microsphere lasers if two suitable similar lasers could be identified.

6.6 Conclusion

We have made a GLS microsphere laser and, to the best of our knowledge, this is the first demonstration of a chalcogenide microsphere laser. Microsphere lasers are known to have low thresholds and narrow linewidths. Because of the free space coupling that has been used here it is not possible to compare a GLS microsphere laser with other GLS lasers on an equal basis, but its linewidth is narrower than any previously reported GLS laser.

The threshold of the GLS microsphere laser was found to be 82mW incident pump power, which is similar to other microsphere lasers that have been reported. From 82mW to 100mW there was only one laser mode, but above 100mW the microsphere laser became multimode.

As the pump power was increased the wavelength of each laser mode moved to a longer wavelength and new laser modes tended to appear at shorter wavelengths. It is likely that the movement of individual modes is due to a combination of thermal and third order nonlinear effects. This could be used to make a laser that can have its wavelength controlled by an external laser. The wavelength shift observed in this laser was 2.5nm which is larger than has been demonstrated in other microsphere lasers.

A microsphere laser that could be tuned by an external light source has potential for a number of applications, such as all optical switching or cross channel communication in a wavelength division system, allowing significant advances in optical technology by replacing electronic technology.

7 Conclusion

In this thesis a comprehensive theoretical and experimental study of novel chalcogenide microspheres made by in-flight melt-quenching, the potential of chalcogenide micro-resonators and details of experiments that have been carried out, including evidence of laser action are presented.

The potential of a chalcogenide / GLS micro-resonator has been discussed, particularly the high Q factor of 10^{10} that could theoretically be achieved.

It is also shown that to achieve this potential would require improvement in the manufacturing process of the glass. However with glass currently produced and characterised it should be possible to produce resonators with a Q of up to 1.6×10^{7} at 1µm.

The high Q associated with microspheres has resulted in interest in their use as all optical switches or lasers. All optical switches rely on the high nonlinear refractive index of chalcogenide. This allows the resonant wavelength to be changed by the intensity of light and creates the potential for switching. To calculate the exact power required for switching it is necessary to know many of the details of the resonator, such as Q and modal volume, however it does seem likely that switching could be achieved at low powers.

Microsphere lasers have also attracted attention as low power narrow linewidth laser sources. As GLS can hold high levels of rare earth ions it would seem to be an ideal host medium. In order to accurately calculate the threshold power required it is necessary to know details of their parameters.

GLS microspheres have been produced by a method of in-flight melt-quenching, whereby particles of glass are passed through a furnace, where they melt and surface tension pulls them into a spherical shape, they then pass out of the furnace and quench to form a glass again. There have been many stages in developing and optimising this process and several items of apparatus have been designed and made to achieve this. Microspheres larger than ~30µm are produced by dropping through a furnace, while particles smaller than ~50µm can be produced by blowing the seed particles vertically through a furnace. As GLS will react with air when molten it is necessary to melt the particles in an inert atmosphere. Systems have been designed and produced to allow the glass to be introduced to the furnace and then be collected, whilst maintaining an

inert atmosphere. Using the system developed for blowing glass through the furnace, experiments were run to establish the optimum production parameters. It was found that turbulence played an important part and, at the optimum point, approximately all of the particles collected had been melted into microspheres.

Q measurements, which quantify the quality of the sphere, were carried out and Q values up to $1.2x10^5$ were demonstrated experimentally. The value of Q measured is heavily dependent on the coupling and therefore highly affected by the measurement system.

It is known that the Q value of microspheres will degrade with time exposed to air and also that GLS is adversely affected by water. When the Q value of a sphere was repeatedly measured over a period of time, it was found to exponentially decay from an original Q to a new Q value, however when GLS microspheres were submerged in water for a period of time, in many cases, they were found to disintegrate completely. When their composition was analysed the fragments had very little gallium remaining in their structure. It appears that gallium will leach out of GLS when submerged in water.
One potential use of GLS microspheres is as ball lenses, these could be particularly useful for coupling between laser diodes and optical fibres. Microspheres were characterised as ball lenses and found to work as such.

Fluorescence from GLS microspheres doped with rare earth ions has been observed. Within the fluorescence it is often possible to observe WGMs and laser action has been observed. The laser action took place in a GLS microsphere doped with 1.5mol% of neodymium, with the laser peak appearing at 1082nm. It required 83mW of 808nm applied pump power although it is not possible to determine how much of that was absorbed. The linewidth was found to be less than 0.05nm.
The narrow linewidth could make this type of laser useful for a number of applications, such as telecoms, however the peak wavelength of neodymium would not be suitable and other rare earth dopants would be required.

7.1 Novel contributions

Novel contributions to the field include;

- Predictions of maximum possible Q and maximum achievable Q given current state of the art in GLS / GLSO microspheres
- Calculations of bistability in GLS
- Development of in-flight melt-quenching method of producing microspheres, which can be used on a number of types of glass
- Design and development of apparatus for in-flight melt-quenching method
- Development of method for separating spheres from non-spherical particles
- Produced first GLS microspheres
- Mass produced first GLS microspheres
- First Q measurement of chalcogenide microsphere
- Developed method of fitting Airy functions to complex resonance spectra
- Development of first chalcogenide microsphere laser
- Observations of modal movement in GLS microsphere laser
- Observation of degradation in GLS microspheres in water and air
- First observation of elements leaching from GLS glass
- First observation of catastrophic failure in GLS glass structure when immersed in water.
- Demonstration of the use of GLS microspheres as a ball lens
- Preliminary observations of nonlinear effects in GLS microspheres

8 Future work

The work carried out in this project has highlighted potential avenues for further enquiry. These are laid out here

8.1 Future work on microspheres

8.1.1 Downward flow optimisation

Throughout this project gas has flowed upwards through the furnace. This is because hot gasses will naturally rise, however with a sufficient downward flow this may be overcome and could produce interesting results. It is likely that spheres blown this way may be produced to a larger size than those blown in an upwards direction. This would bring the advantages of turbulence to a larger size range.

8.1.2 Q with respect to flow

No study has been carried out to observe how the flow of gas affects the Q factor of microspheres. Spheres have been produced with various gas flows, but due to time limitations, the study has not been carried out.

8.1.3 Er:GLS Microsphere laser

The Er- doped GLS microsphere laser could represent an interesting opportunity for a telecoms laser. Er has its major emission in the telecoms window and microsphere lasers typically have a very narrow linewidth. Using GLS as a host medium also presents the possibility to utilise nonlinear tuning to control the output [119].

8.1.4 Nonlinear measurements

Although some evidence of nonlinear movement of modes has been shown, it has not been possible to separate thermal effects from third order effects. It would be interesting to carry out experiments to separate these effects, possibly by using a pulsed beam and increasing the repetition rate until the thermal effects no longer exist [89]. This could potentially lead to observation of bistability and all-optical-switching.

8.1.5 Other methods of producing microspheres

The method of microsphere production that has been presented here is effective at producing large numbers of microspheres with high Q factors. However there are areas that could be improved, such as extending the lower and upper limits of microsphere size and improving the uniformity of the microspheres produced.

There are several possible areas that should be explored to efficiently produce microspheres smaller than 1μm. It is believed that spherical particles are produced as a by product in the chemical vapour deposition (CVD) of glass, specifically GeS. Similarly anecdotal evidence suggests that bleeding oxygen into a plasma sputtering system whilst sputtering GLS produced spherical particles. There is also evidence to suggest that spherical particles of less than 1μm are produced when GLS undergoes laser oblation [120].

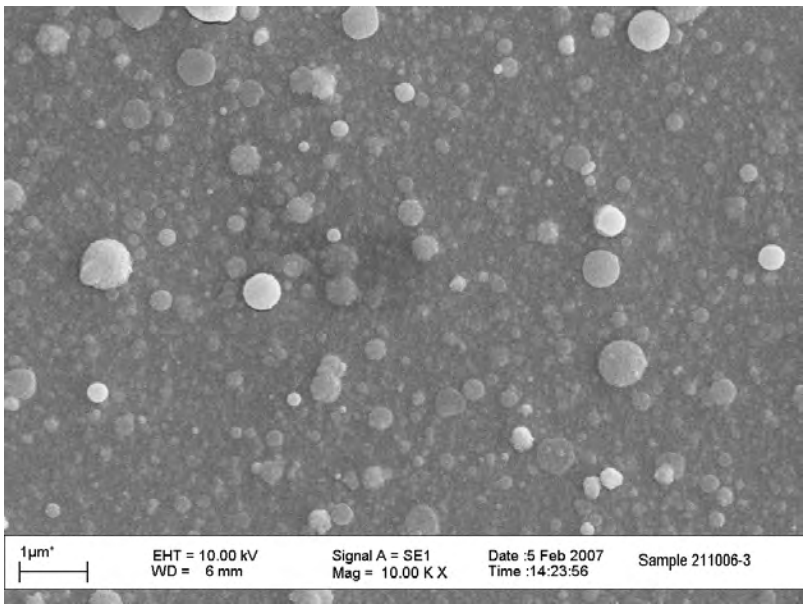

Figure 8.1 GLS particles produced by pulsed laser deposition at the ORC by Mark Darby.

It is possible to produce a stream of small and highly uniform particles, by allowing a liquid to pass through a small hole in conjunction with a flow of gas [92, 93]. It has been considered that this would be possible and advantageous for the production of GLS microspheres. But it has not been realised, as it would require the design of a new system of furnace furniture. It does represent an interesting line of inquiry that could be followed in the future.

Due to various constraints no detailed examination of these methods has been carried out.

8.2 Future work on planar resonators

Planar resonators are a very exciting area for future investigation, because of their potential to be incorporated into integrated optical circuits. It has not been possible to pursue this line of investigation because of a lack of facilities capable of producing the sub-micron structure required to for circular planar resonators.

Planar resonators are similar to microspheres in many ways, but may have some significant advantages in terms of the ability to be integrated into circuits or systems. Microspheres are likely to have a higher Q than integrated planar resonators because of the production methods. As microspheres are melted and quenched in flight the surface roughness should be at a minimum, whereas planar resonators will most likely have to be etched to define their shape.

There are several stages of design that should be considered in order to successfully produce a planar circular resonator and these are outlined below.

8.2.1 Waveguide Design

The process of designing a planar resonator will most likely have to be an iterative process, as the optimal geometry of the system is dependent on the characteristics of the components of the system. Optimal spacing of the waveguide and the resonator depends on the bulk attenuation and the loss due to surface scattering. Therefore it would be necessary to characterise the straight and curved waveguide before designing a resonator as a whole.

The waveguide may not perform in a theoretically perfect way. It is quite likely that the waveguide may appear to be single mode at sizes that should theoretically be multimode, due to surface roughness stripping off higher order modes [121]. However the waveguide needs to be single mode and polarisation maintaining, as different modes and polarisations in the waveguide will produce different peaks in the resonator.

8.2.1.1 Device geometry / Calculate gap

As discussed in the chapter 3 the optimum coupling distance will depend on the loss. Therefore to achieve maximum circulating intensity in the resonator it is necessary to have knowledge of the loss from the resonator before the geometry of the device can be designed. Once this data is known the separation of the waveguide from the resonator can be calculated.

8.2.2 Device fabrication

There are a number of ways of producing planar waveguides and resonators. All will require the pattern/design to be transferred to them and most production methods will also require a thin film to be deposited.

Broadly speaking the options fall into two categories; deposition of a thin film and patterning.

In chalcogenide glass, waveguides have been produced by UV direct writing [26], ion exchange or thin film/etching (rib waveguide) [28, 121]. Waveguides produced by UV direct writing typically have a graded index structure, which gives them diffuse edges. This could cause problems where two guides have to be close to each other for evanescent coupling. It is possible that there would be an area between the two waveguides that would get exposed by the UV twice. This could potentially give it higher refractive index than either of the waveguides, making it the more favourable guiding region.

Ion exchange waveguides could potentially be made by diffusing sulphur or metals into GLS /GLSO. By exposing GLSO to H_2S at a high temperature and allowing the sulphur to diffuse into the GLSO and displace some of the oxygen thus raising the index. Alternatively metals can be diffused into the glass, a similar process has been carried out using silver and GeS [122].

The alternative to a graded index is a step index waveguide. This would require the deposition of a thin film and a patterning process, many of these technologies are well established for GLS. In addition to these it has been suggested that it may be possible to form a film from a sintered chalcogenide coating. This would take the form of something akin to a paint, which could then be sintered to form a film. It is envisaged that finely crushed chalcogenide could be suspended in a high-density solvent (DMF). This could then be spin coated or sprayed on, to produce an even coating, then baked to remove the solvent and join the glass particles together. Currently no work has taken place on the development of this process.

Having established the type of waveguide used for the resonator, it will be necessary to establish the exact method of production. Chalcogenide thin films can be deposited by pulsed laser deposition [14, 120], chemical vapour deposition (CVD) [25, 123], sputtering [124] and hot dip spin coating [27]. The quality and thickness of the thin film produced by each method varies and this will ultimately determine which method is used. The hot dip spin coating method produces a film too thick for single mode

waveguides, sputtered chalcogenide has too high an attenuation to be viable, therefore CVD seems to remain as the favoured option for producing the thin film.

The micro-resonator pattern can also be achieved by a number of methods. These include standard mask-photolithography methods, direct write photolithography, focused ion beam etching and electron beam lithography. Mask based photolithography has advantages in its reproducibility, one mask can hold a lot of device designs, however, this has drawbacks for any kind of one-off or iterative experiment. It may also have issues surrounding resolution. Direct write lithography has the advantage of being quick, which makes it useful for one off production.
To produce a rib waveguide with any photolithography method there has to be some kind of etching process. Previous trials by [28] suggest that ion beam milling is the best method for reproducible rib waveguides, with minimal surface roughness on the etched/milled face. Focused ion beam etching, does not rely on any previous patterning process, it can also achieve higher levels of accuracy than photolithography with very smooth surfaces. Electron beam lithography has been used by others [125] to produce circular micro-resonators.
An important parameter to consider when producing any resonators is the surface quality produced by the etching or fabrication process. The quality of the resonator is heavily dependent on the smoothness of this surface. Therefore, the choice of etching method that could be used for resonator production will depend heavily on the quality that can be produced.
It is possible to overcome the shortcomings of the photolithography process by using a different patterning method. One patterning method that is capable of giving a much higher resolution than that achieved through available photolithography is focused ion beam etching. In collaboration with Bristol University, circular resonators have been produced in chalcogenide films (Figure 8.2) by focused ion beam etching. This project is currently at the feasibility stage and no characterisation or measurements have been made.

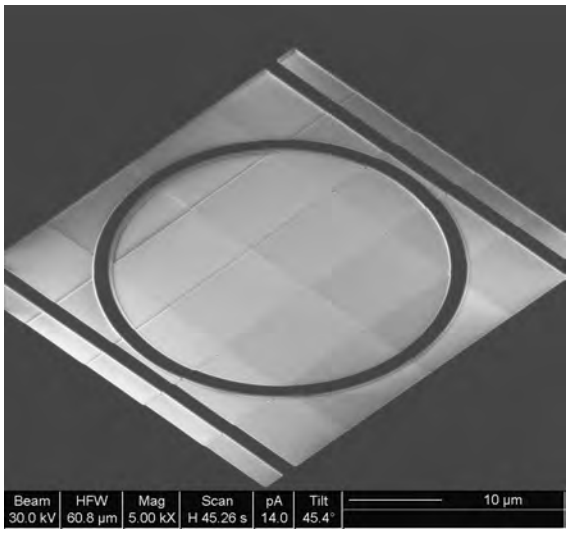

Figure 8.2 Chalcogenide planar resonator produced in collaboration with Bristol University.

9 References

1. Marcatili, E.A.J., "*Bends in Optical Dielectric Guides"*. The Bell System Technical Journal, **48**, 2103-2132, (1969)
2. Ibrahim, T.A., R. Grover, L.C. Kuo, S. Kanakaraju, L.C. Calhoun, and P.T. Ho, "*All-optical AND/NAND logic gates using semiconductor microresonators"*. Ieee Photonics Technology Letters, **15**(10), 1422-1424, (2003)
3. Ibrahim, T.A., K. Amarnath, L.C. Kuo, R. Grover, V. Van, and P.T. Ho, "*Photonic logic NOR gate based on two symmetric microring resonators"*. Optics Letters, **29**(23), 2779-2781, (2004)
4. Blom, F.C., D.R. vanDijk, H.J.W.M. Hoekstra, A. Driessen, and T.J.A. Popma, "*Experimental study of integrated-optics microcavity resonators: Toward an all-optical switching device"*. Applied Physics Letters, **71**(6), 747-749, (1997)
5. Cai, M., O. Painter, K.J. Vahala, and P.C. Sercel, "*Fiber-coupled microsphere laser"*. Optics Letters, **25**(19), 1430-1432, (2000)
6. Little, B.E., S.T. Chu, H.A. Haus, J. Foresi, and J.P. Laine, "*Microring resonator channel dropping filters"*. Journal of Lightwave Technology, **15**(6), 998-1005, (1997)
7. Yin, Y.D., Y. Lu, and Y.N. Xia, "*A self-assembly approach to the formation of asymmetric dimers from monodispersed spherical colloids"*. Journal of the American Chemical Society, **123**(4), 771-772, (2001)
8. Grujic, K., O. Helleso, J. Wilkinson, and J. Hole, "*Optical propulsion of microspheres along a channel waveguide produced by Cs+ ion-exchange in glass"*. Optics Communications, **239**(4-6), 227-235, (2004)
9. Grujic, K., O. Helleso, J. Hole, and J. Wilkinson, "*Sorting of polystyrene microspheres using a Y-branched optical waveguide"*. Optics Express, **13**(1), 1-7, (2005)
10. Poon, J.K.S., L. Zhu, G.A. DeRose, and A. Yariv, "*Polymer microring coupled-resonator optical waveguides"*. Journal of Lightwave Technology, **24**(4), 1843-1849, (2006)
11. Hill, M.T., et al., "*A fast low-power optical memory based on coupled micro-ring lasers"*. Nature, **432**(7014), 206-209, (2004)
12. Officer, S., Prabhu, R., Pollard, P. et al, "*Novel online security system based on rare-earth doped micro glass beads"*. Proceedings of SPIE Vol. #5310, (2005)
13. Dejneka, M.J., A. Streltsov, S. Pal, A.G. Frutos, C.L. Powell, K. Yost, P.K. Yuen, U. Muller, and J. Lahiri, "*Rare earth-doped glass microbarcodes"*. Proceedings of the National Academy of Sciences of the United States of America, **100**(2), 389-393, (2003)
14. Zakery, A. and S. Elliott, "*Optical properties and applications of chalcogenide glasses: a review"*. Journal Of Non-Crystalline Solids, **330**(1-3), 1-12, (2003)
15. Schweizer, T., D.W. Hewak, D.N. Payne, T. Jensen, and G. Huber, "*Rare-earth doped chalcogenide glass laser"*. Electronics Letters, **32**(7), 666-667, (1996)

16. Curry, R., A. Mairaj, C. Huang, R. Eason, C. Grivas, D. Hewak, and J. Badding, "*Chalcogenide glass thin films and planar waveguides*". Journal Of The American Ceramic Society, **88**(9), 2451-2455, (2005)
17. Yayama, H., S. Fujino, K. Morinaga, H. Takebe, D.W. Hewak, and D.N. Payne, "*Refractive index dispersion of gallium lanthanum sulfide and oxysulfide glasses*". Journal of Non-Crystalline Solids, **239**(1-3), 187-191, (1998)
18. Requejo-Isidro, J., A.K. Mairaj, V. Pruneri, D.W. Hewak, M.C. Netti, and J.J. Baumberg, "*Self refractive non-linearities in chalcogenide based glasses*". Journal of Non-Crystalline Solids, **317**(3), 241-246, (2003)
19. Kang, I., T.D. Krauss, F.W. Wise, B.G. Aitken, and N.F. Borrelli, "*Femtosecond Measurement of Enhanced Optical Nonlinearities of Sulfide Glasses and Heavy-Metal-Doped Oxide Glasses*". Journal of the Optical Society of America B-Optical Physics, **12**(11), 2053-2059, (1995)
20. Rayleigh, L., "*Scientific papers*". Vol. 171. 1902.
21. Slusher, R.E., "*Optical Processes in Microcavities*". Semiconductor Science and Technology, **9**(11), 2025-2030, (1994)
22. Gorodetsky, M.L., A.A. Savchenkov, and V.S. Ilchenko, "*Ultimate Q of optical microsphere resonators*". Optics Letters, **21**(7), 453-455, (1996)
23. Vahala, K.J., "*Optical microcavities*". Nature, **424**(6950), 839-846, (2003)
24. West, Y.D., T. Schweizer, D.J. Brady, and D.W. Hewak, "*Gallium lanthanum sulphide fibers for infrared transmission*". Fiber and Integrated Optics, **19**(3), 229-250, (2000)
25. Huang, C.C. and D.W. Hewak, "*High-purity germanium-sulphide glass for optoelectronic applications synthesised by chemical vapour deposition*". Electronics Letters, **40**(14), 863-865, (2004)
26. Mairaj, A.K., P. Hua, H.N. Rutt, and D.W. Hewak, "*Fabrication and characterization of continuous wave direct UV (lambda=244 nm) written channel waveguides in chalcogenide (Ga : La : S) glass*". Journal of Lightwave Technology, **20**(8), 1578-1584, (2002)
27. Mairaj, A.K., R.J. Curry, and D.W. Hewak, "*Inverted deposition and high-velocity spinning to develop buried planar chalcogenide glass waveguides for highly nonlinear integrated optics*". Applied Physics Letters, **86**(9), -, (2005)
28. Huang, C.C., D.W. Hewak, and J.V. Badding, "*Deposition and characterization of germanium sulphide glass planar waveguides*". Optics Express, **12**(11), 2501-2506, (2004)
29. Hughes, M., W. Yang, and D. Hewak, "*Fabrication and characterization of femtosecond laser written waveguides in chalcogenide glass*". Applied Physics Letters, **90**(13), -, (2007)
30. Mairaj, A.K., C. Riziotis, A.M. Chardon, P.G.R. Smith, D.P. Shepherd, and D.W. Hewak, "*Development of channel waveguide lasers in Nd3+-doped chalcogenide (Ga : La : S) glass through photoinduced material modification*". Applied Physics Letters, **81**(20), 3708-3710, (2002)
31. Brady, D.J., "*Gallium lanthanum sulphide based glasses for mid-infrared optical fibres*", 1999, University of Southampton, Thesis (Ph.D.)
32. Mairaj, A.K., "*Optical waveguides and lasers in improved gallium lanthanum sulphide glass*", 2003, University of Southampton, Thesis (Ph.D.)
33. Hughes, M.A., "*Modified chalcogenide glasses for optical device applications*", 2007, University of Southampton, Thesis (Ph.D.)

34. Petrovich, M.N., A. Favre, D.W. Hewak, H.N. Rutt, A.C. Grippo, J.F. Gubeli, K.C. Jordan, G.R. Neil, and M.D. Shinn, "*Near-IR absorption of Ga : La : S and Ga : La : S : O glasses by free-electron laser-based laser calorimetry*". Journal of Non-Crystalline Solids, **326**, 93-97, (2003)
35. Lima, S.M., A.S.S. de Camargo, L.A.O. Nunes, T. Catunda, and D.W. Hewak, "*Fluorescence quantum efficiency measurements of excitation and nonradiative deexcitation processes of rare earth 4f-states in chalcogenide glasses*". Applied Physics Letters, **81**(4), 589-591, (2002)
36. Hughes, M., H. Rutt, D. Hewak, and R. Curry, "*Spectroscopy of vanadium (III) doped gallium lanthanum sulphide chalcogenide glass*". Applied Physics Letters, **90**(3), 31108-1-3, (2007)
37. Choi, Y., R. Curry, B. Park, K. Kim, J. Heo, and D. Hewak, "*Extreme hypersensitivity observed from H-6(15/2)<-> F-6(11/2) transition of Dy3+ in inorganic noncrystalline solids*". CHEMICAL PHYSICS LETTERS, **403**(1-3), 29-34, (2005)
38. de Camargo, A.S.S., S.L. de Oliveira, D.F. de Sousa, L.A.O. Nunes, and D.W. Hewak, "*Spectroscopic properties and energy transfer parameters of Tm3+ ions in gallium lanthanum sulfide glass*". Journal of Physics-Condensed Matter, **14**(41), 9495-9505, (2002)
39. Schweizer, T., R. Goutaland, E. Martins, D.W. Hewak, and W.S. Brocklesby, "*Site-selective spectroscopy in dysprosium-doped chalcogenide glasses for 1.3-mu m optical-fiber amplifiers*". Journal of the Optical Society of America B-Optical Physics, **18**(10), 1436-1442, (2001)
40. Lima, S.M., J.A. Sampaio, T. Catunda, A.S.S. de Camargo, L.A.O. Nunes, M.L. Baesso, and D.W. Hewak, "*Spectroscopy, thermal and optical properties of Nd3+-doped chalcogenide glasses*". Journal of Non-Crystalline Solids, **284**(1-3), 274-281, (2001)
41. Schweizer, T., B.N. Samson, J.R. Hector, W.S. Brocklesby, D.W. Hewak, and D.N. Payne, "*Infrared emission from holmium doped gallium lanthanum sulphide glass*". Infrared Physics & Technology, **40**(4), 329-335, (1999)
42. Schweizer, T., B.N. Samson, J.R. Hector, W.S. Brocklesby, D.W. Hewak, and D.N. Payne, "*Infrared emission and ion-ion interactions in thulium- and terbium-doped gallium lanthanum sulfide glass*". Journal of the Optical Society of America B-Optical Physics, **16**(2), 308-316, (1999)
43. Hector, J.R., J. Wang, D. Brady, M. Kluth, D.W. Hewak, W.S. Brocklesby, and D.N. Payne, "*Spectroscopy and quantum efficiency of halide-modified gallium-lanthanum sulfide glasses doped with praseodymium*". Journal of Non-Crystalline Solids, **239**(1-3), 176-180, (1998)
44. Schweizer, T., D.W. Hewak, B.N. Samson, and D.N. Payne, "*Spectroscopy of potential mid-infrared laser transitions in gallium lanthanum sulphide glass*". Journal of Luminescence, **72-4**, 419-421, (1997)
45. Ye, C.C., D.W. Hewak, M. Hempstead, B.N. Samson, and D.N. Payne, "*Spectral properties of Er3+-doped gallium lanthanum sulphide glass*". Journal of Non-Crystalline Solids, **208**(1-2), 56-63, (1996)
46. Schweizer, T., D.W. Hewak, B.N. Samson, and D.N. Payne, "*Spectroscopic data of the 1.8-, 2.9-, and 4.3-mu m transitions in dysprosium-doped gallium lanthanum sulfide glass*". Optics Letters, **21**(19), 1594-1596, (1996)
47. Schweizer, T., "*Rare-earth-doped Gallium lanthanum sulphide glasses for mid-infrared fibre lasers*", 2000, University of Southampton,

48. Halliday, D., R. Resnick, and K.S. Krane, "*Physics. Vol.2, extended version*". 4th ed. ed. 1992, Wiley, New York ; Chichester. xi,p593-1216,[42]p.
49. Mairaj, A.K., A.M. Chardon, D.P. Shepherd, and D.W. Hewak, "*Laser performance and spectroscopic analysis of optically written channel waveguides in neodymium-doped gallium lanthanum sulphide glass*". Ieee Journal of Selected Topics in Quantum Electronics, **8**(6), 1381-1388, (2002)
50. Schweizer, T., B.N. Samson, R.C. Moore, D.W. Hewak, and D.N. Payne, "*Rare-earth doped chalcogenide glass fibre laser*". Electronics Letters, **33**(5), 414-416, (1997)
51. Hecht, E., "*Optics*". 4th ed., International ed. ed. 2002, Addison-Wesley, San Francisco ; London. vi, 698 p.
52. Boyd, R.W., "*Nonlinear optics*". 1992, Academic Press, xiii,439p.
53. Lima, S.M., A. Steimacher, A.N. Medina, M.L. Baesso, M.N. Petrovich, H.N. Rutt, and D.W. Hewak, "*Thermo-optical properties measurements in chalcogenide glasses using thermal relaxation and thermal lens methods*". Journal of Non-Crystalline Solids, **348**, 108-112, (2004)
54. Miller, D., "*Refractive Fabry-Perot bistability with linear absorption - theory of operation and cavity optimization* ". IEEE Journal of Quantum Electronics, **17**(3), 306-311, (1981)
55. Sasagawa, K., K. Kusawake, J. Ohta, and M. Nunoshita, "*Nd-doped tellurite glass microsphere laser*". Electronics Letters, **38**(22), 1355-1357, (2002)
56. Spillane, S.M., T.J. Kippenberg, and K.J. Vahala, "*Ultralow-threshold Raman laser using a spherical dielectric microcavity*". Nature, **415**(6872), 621-623, (2002)
57. Sandoghdar, V., F. Treussart, J. Hare, V. LefevreSeguin, J.M. Raimond, and S. Haroche, "*Very low threshold whispering-gallery-mode microsphere laser*". Physical Review A, **54**(3), R1777-R1780, (1996)
58. Wu, J.F., S.B. Jiang, and N. Peyghambarian, "*1.5-mu m-band thulium-doped microsphere laser originating from self- terminating transition*". Optics Express, **13**(25), 10129-10133, (2005)
59. Peng, X., F. Song, S.B. Jiang, N. Peyghambarian, M. Kuwata-Gonokami, and L. Xu, "*Fiber-taper-coupled L-band Er3+-doped tellurite glass microsphere laser*". Applied Physics Letters, **82**(10), 1497-1499, (2003)
60. Righini, G.C., et al., "*Integrated optical amplifiers and microspherical lasers based on erbium-doped oxide glasses*". Optical Materials, **27**(11), 1711-1717, (2005)
61. Hesford, R., "*Microspheres*", in *University of southampton Internal report*. 2004.
62. Cai, M. and K. Vahala, "*Highly efficient optical power transfer to whispering-gallery modes by use of a symmetrical dual-coupling configuration*". Optics Letters, **25**(4), 260-262, (2000)
63. Cai, M., P.O. Hedekvist, A. Bhardwaj, and K. Vahala, "*5-Gbit/s BER performance on an all fiber-optic add/drop device based on a taper-resonator-taper structure*". Ieee Photonics Technology Letters, **12**(9), 1177-1179, (2000)
64. Laine, J.P., B.E. Little, D.R. Lim, H.C. Tapalian, I.C. Kimerling, and H.A. Haus, "*Planar integrated wavelength-drop device based on pedestal antiresonant reflecting waveguides and high-Q silica microspheres*". Optics Letters, **25**(22), 1636-1638, (2000)
65. Little, B.E., et al., "*Very high-order microring resonator filters for WDM applications*". Ieee Photonics Technology Letters, **16**(10), 2263-2265, (2004)

66. Ibrahim, T.A., W. Cao, Y. Kim, J. Li, J. Goldhar, P.T. Ho, and C.H. Lee, "*Lightwave switching in semiconductor microring devices by free carrier injection".* Journal of Lightwave Technology, **21**(12), 2997-3003, (2003)
67. Ibrahim, T.A., W. Cao, Y. Kim, J. Li, J. Goldhar, P.T. Ho, and C.H. Lee, "*All-optical switching in a laterally coupled microring resonator by carrier injection".* Ieee Photonics Technology Letters, **15**(1), 36-38, (2003)
68. Wu, Y. and P.T. Leung, "*Lasing threshold for whispering-gallery-mode microsphere lasers".* Physical Review A, **60**(1), 630-633, (1999)
69. Ilchenko, V., X. Yao, and L. Maleki, "*Pigtailing the high-Q microsphere cavity: a simple fiber coupler for optical whispering-gallery modes".* Optics letters, **24**(11), 723-725, (1999)
70. Miura, K., K. Tanaka, and K. Hirao, "*CW laser oscillation on both the F-4(3/2)-I-4(11/2) and F-4(3/2)-I-4(13/2) transitions of Nd3+ ions using a fluoride glass microsphere".* Journal of Non-Crystalline Solids, **213**, 276-280, (1997)
71. Cai, M. and K. Vahala, "*Highly efficient hybrid fiber taper coupled microsphere laser".* Optics Letters, **26**(12), 884-886, (2001)
72. Maleki, L., X. Yao, and V. Ilchenko, "*Fiber-coupled microsphere laser",* in *United States patent office,* U.S.p. office, Editor. 2002: United States.
73. Soref, R.A. and B.E. Little, "*Proposed N-wavelength M-fiber WDM crossconnect switch using active microring resonators".* Ieee Photonics Technology Letters, **10**(8), 1121-1123, (1998)
74. Nitkowski, A., L. Chen, and M. Lipson, "*Cavity-enhanced on-chip absorption spectroscopy using microring resonators".* Optics Express, **16**(16), 11930-11936, (2008)
75. Curry, R., S. Birtwell, A. Mairaj, X. Feng, and D. Hewak, "*A study of environmental effects on the attenuation of chalcogenide optical fibre".* Journal Of Non-Crystalline Solids, **351**(6-7), 477-481, (2005)
76. Tarhan, I. and G. Watson, "*Photonic band structure of fcc colloidal crystals".* Physical Review Letters, **76**(2), 315-318, (1996)
77. Vlasov, Y., X. Bo, J. Sturm, and D. Norris, "*On-chip natural assembly of silicon photonic bandgap crystals".* Nature, **414**(6861), 289-293, (2001)
78. Denkov, N., O. Velev, P. Kralchevsky, I. Ivanov, H. Yoshimura, and K. Nagayama, "*Mechanism of Formation of 2-Dimensional Crystals from Latex-Particles on Substrates".* LANGMUIR, **8**(12), 3183-3190, (1992)
79. Rakers, S., L. Chi, and H. Fuchs, "*Influence of the evaporation rate on the packing order of polydisperse latex monofilms".* LANGMUIR, **13**(26), 7121-7124, (1997)
80. Wilson, R., "*Ball-lens coupling efficiency for laser-diode to single-mode fiber: comparison of independent studies by distinct methods".* Applied Optics, **37**(15), 3201-3205, (1998)
81. Braginsky, V.B., M.L. Gorodetsky, and V.S. Ilchenko, "*Quality-Factor and Nonlinear Properties of Optical Whispering-Gallery Modes".* Physics Letters A, **137**(7-8), 393-397, (1989)
82. Yariv, A., "*Universal relations for coupling of optical power between microresonators and dielectric waveguides".* Electronics Letters, **36**(4), 321-322, (2000)
83. Elliott, G., D. Hewak, G. Murugan, and J. Wilkinson, "*Chalcogenide glass microspheres; their production, characterization and potential".* Optics Express, **15**(26), 17542-17553, (2007)

84. Brady, D.J., T. Schweizer, J. Wang, and D.W. Hewak, "*Minimum loss predictions and measurements in gallium lanthanum sulphide based glasses and fibre*". Journal of Non-Crystalline Solids, **242**(2-3), 92-98, (1998)
85. Siegman, A.E., "*Lasers*". 1986, University Science Books.
86. Reed, G.T. and A.P. Knights, "*Silicon photonics : an introduction*". 2004, John Wiley, Chichester. 255 p.
87. Cai, M., O. Painter, and K.J. Vahala, "*Observation of critical coupling in a fiber taper to a silica-microsphere whispering-gallery mode system*". Physical Review Letters, **85**(1), 74-77, (2000)
88. Steimacher, A., A.N. Medina, A.C. Bento, J.H. Rohling, M.L. Baesso, V.C.S. Reynoso, S.M. Lima, M.N. Petrovich, and D.W. Hewak, "*The temperature coefficient of the optical path length as a function of the temperature in different optical glasses*". Journal of Non-Crystalline Solids, **348**, 240-244, (2004)
89. Rokhsari, H. and K.J. Vahala, "*Observation of Kerr nonlinearity in microcavities at room temperature*". Optics Letters, **30**(4), 427-429, (2005)
90. Abraham, E. and S. Smith, "*Optical Bistability and Related Devices*". Reports on Progress in Physics, **45**(8), 815-885, (1982)
91. Grillet, C., S.N. Bian, E.C. Magi, and B.J. Eggleton, "*Fiber taper coupling to chalcogenide microsphere modes*". Applied Physics Letters, **92**(17), 171109, (2008)
92. Ganan-Calvo, A.M., "*Generation of steady liquid microthreads and micron-sized monodisperse sprays in gas streams*". Physical Review Letters, **80**(2), 285-288, (1998)
93. Ganan-Calvo, A.M., "*Perfectly monodisperse microbubbling by capillary flow focusing: An alternate physical description and universal scaling*". Physical Review E, **69**(2), 027301, (2004)
94. http://hyperphysics.phy-astr.gsu.edu/Hbase/thermo/cootime2.html. "*Kelvin cooling time for the earth*". 2008 [cited 2008 16/06/08].
95. Lide, D.R., "*CRC handbook of chemistry and physics : a ready-reference book of chemical and physical data*". 84th ed. / editor-in-chief, David R. Lide. ed. 2003, CRC, Boca Raton, Fla. ; London. 1 v (various pagings).
96. Takebe, H., D.J. Brady, D.W. Hewak, and K. Morinaga, "*Thermal properties of Ga2S3-based glass and their consideration during fiber drawing*". Journal of Non-Crystalline Solids, **258**(1-3), 239-243, (1999)
97. Lamb, H.S., "*Hydrodynamics*". 6th ed. ed. 1993, Cambridge University Press, Cambridge. 738p.
98. Resnick, R., D. Halliday, and K.S. Krane, "*Physics. Vol.1*". 4th ed. ed. 1992, Wiley, New York ; Chichester. xi,592,[44]p.
99. Dawe, R. and E. Smith, "*Viscosity of Argon at High Temperatures*". Science, **163**, 675-676, (1969)
100. Mills, A.A., S. Day, and S. Parkes, "*Mechanics of the sandglass*". European Journal of Physics **17**(3), 97-109, (1996)
101. A.Benayas, G.S.Murugan, Y.Panitchob, D.Jaque, and J.S.Wilkinson, "*Time resolved confocal luminescence of Nd3+ doped BK7 glass microspheres*", in *ICL '08* 2008: Lyon.
102. Panitchob, Y., G. Murugan, M. Zervas, P. Horak, S. Berneschi, S. Pelli, G. Conti, and J. Wilkinson, "*Whispering gallery mode spectra of channel waveguide coupled microspheres*". Optics Express, **16**(15), 11066-11076, (2008)

103. Lam, C.C., P.T. Leung, and K. Young, "*Explicit Asymptotic Formulas for the Positions, Widths, and Strengths of Resonances in Mie Scattering*". Journal of the Optical Society of America B-Optical Physics, **9**(9), 1585-1592, (1992)
104. Schiller, S., "*Asymptotic-Expansion of Morphological Resonance Frequencies in Mie Scattering*". Applied Optics, **32**(12), 2181-2185, (1993)
105. Miura, K., K. Tanaka, and K. Hirao, "*Laser oscillation of a Nd3+-doped fluoride glass microsphere*". Journal of Materials Science Letters, **15**(21), 1854-1857, (1996)
106. Peng, X., F. Song, M. Kuwata-Gonokami, S.B. Jiang, and N. Peyghambarian, "*Er3+-doped tellurite glass microsphere laser: optical properties, coupling scheme, and lasing characteristics*". Optical Engineering, **44**(3), -, (2005)
107. Peng, X., F. Song, S.B. Jiang, M. Gonokami, and N. Peyghambarian, "*Signal enhancement in Er3+ doped tellurite glass microsphere*". Glass Science and Technology, **75**, 27-38, (2002)
108. Garrett, C.G.B., W. Kaiser, and W.L. Bond, "*Stimulated emission into optical whispering modes of spheres*". Physical Rreview **124**(6), 1807-1809, (1961)
109. Lin, H.B., A.L. Huston, B.L. Justus, and A.J. Campillo, "*Some Characteristics of a Droplet Whispering-Gallery-Mode Laser*". Optics Letters, **11**(10), 614-616, (1986)
110. Lin, H.B., A.L. Huston, J.D. Eversole, B.L. Justus, and A.J. Campillo, "*Some Characteristics of a Droplet Whispering Gallery Mode Laser*". Journal of the Optical Society of America B-Optical Physics, **3**(8), P250-P251, (1986)
111. Kuwatagonokami, M., H. Yasuda, K. Ema, and K. Takeda, "*Observation of Intermode Correlation in Whispering Gallery Mode Laser with Dye Doped Polystyrene Micro Sphere*". Tenth International Conf on Laser Spectroscopy, 234-235, (1992)
112. Kuwatagonokami, M., K. Takeda, H. Yasuda, and K. Ema, "*Laser-Emission from Dye-Doped Polystyrene Microsphere*". Japanese Journal of Applied Physics Part 2-Letters, **31**(2A), L99-L101, (1992)
113. Kuwatagonokami, M., K. Ema, and K. Takeda, "*Lasing and Intermode Correlation of Whispering Gallery Mode in Dye-Doped Polystyrene Microsphere*". Molecular Crystals and Liquid Crystals, **216**, 21-25, (1992)
114. Baer, T., "*Continuous-Wave Laser Oscillation in a Nd-Yag Sphere*". Optics Letters, **12**(6), 392-394, (1987)
115. Wu, J.F., S.B. Jiang, T. Qua, M. Kuwata-Gonokami, and N. Peyghambarian, "*2 mu m lasing from highly thulium doped tellurite glass microsphere*". Applied Physics Letters, **87**(21), -, (2005)
116. Ilchenko, V.S., X.S. Yao, and L. Maleki, "*A fiber-coupled erbium-doped microsphere laser*", in *Conference on Lasers and Electro-Optics (CLEO 2000). Technical Digest. Postconference Edition. TOPS Vol.39*, S. Electro-Opt, A. Opt. Soc, E. Quantum, S. Opt. Div. Eur. Phys, and G. Japanese Quantum Electron. Joint, Editors. 2000, Opt. Soc. America: San Francisco, CA. p. 600-600.
117. Panitchob, Y., "*BK7 Microsphere laser*". 2008, Southampton University.
118. ITU. "*http://www.telecomengineering.com/downloads/DWDM%20ITU%20Table%20-%20100%20GHz.pdf*". [cited 4/11/08].
119. Faraon, A., D. Englund, D. Bulla, B. Luther-Davies, B.J. Eggleton, N. Stoltz, P. Petroff, and J. Vuckovic, "*Local tuning of photonic crystal cavities using chalcogenide glasses*". Applied Physics Letters, **92**(4), -, (2008)

120. Darby, M., R. Simpson, M.-S. TC, D. Hewak, and R. Eason, "*influence of deposition parameters on composition and refractive index of femtosecond and nanosecond pulsed laser deposition gallium lanthanum oxysulphide"*. Journal of non-Crystalline Solids (2007)
121. Ruan, Y.L., W.T. Li, R. Jarvis, N. Madsen, A. Rode, and B. Luther-Davies, "*Fabrication and characterization of low loss rib chalcogenide waveguides made by dry etching"*. Optics Express, **12**(21), 5140-5145, (2004)
122. Huang, C. and D. Hewak, "*Silver-doped germanium sulphide glass channel waveguides fabricated by chemical vapour deposition and photo-dissolution process"*. Thin Solid Films, **500**(1-2), 247-251, (2006)
123. Huang, C., K. Knight, and D. Hewak, "*Antimony germanium sulphide amorphous thin films fabricated by chemical vapour deposition"*. Optical Materials, **29**(11), 1344-1347, (2007)
124. Frantz, J., J. Sanghera, L. Shaw, G. Villalobos, I. Aggarwal, and D. Hewak, "*Sputtered films of Er3+-doped gallium lanthanum sulfide glass"*. Materials Letters, **60**(11), 1350-1353, (2006)
125. Xiao, S., M.H. Khan, H. Shen, and M. Qi, "*Multiple-channel silicon micro-resonator based filters for WDM applications"*. Optics Express, **15**(12), 7489-7498, (2007)

10 Appendix A – Publications

G.R.Elliott, D.W.Hewak, G.S.Murugan, J.S.Wilkinson, “Chalcogenide glass microspheres; their production characterization and potential”, Optics Express 2007 Vol.15 pp.17542-17553

G.R.Elliott, D.W.Hewak, “Chalcogenide microspheres”, OECC/ACOFT 2008 Sydney 7-10 Jul 2008

A.Joyce, G. R. Elliott, D.M.Kane, D.W.Hewak, “Laser cleaning of chalcogenide glass microspheres and shard particles”, EMRS-DTC Technical Conference 2006 Edinburgh 13-14 Jul 2006

D.W.Hewak, G.R.Elliott, J.S.Wilkinson, M.N.Zervas, G.S.Murugan, Y.Panitchob, “Chalcogenide glass microspheres and their applications”, 8th Pacific rim conference on Ceramic and Glass Technology Vancouver May 31-Jun 5 2009

A.Benayas, G.R.Elliott, D.Jaque, D.W.Hewak, “Spatially resolved luminescence characterisation of rare earth doped chalcogenide glass microspheres”, ICL '08 Lyon 7-11 Jul 2008

Photonic Glasses and Glass-Ceramics
Ed.: G. Senthil Murugan
Research Signpost, India (In Press) 2009
Chalcogenide Glasses for Photonics Device Applications
Daniel W Hewak,Dominic Brady, Richard J Curry, Greg Elliott, Chung-Che Huang, Mark Hughes, Kenton Knight, Arshad Mairaj, Marco Petrovich, Rob Simpson, Chris Smith and Chris Sproat

G.R.Elliott, D.W.Hewak, J.S.Wilkinson, M.N.Zervas, G.S.Murugan, Y.Panitchob, Invention notice; ‘Chalcogenide microsphere laser’

G.R.Elliott, D.W.Hewak, J.S.Wilkinson, M.N.Zervas, G.S.Murugan, Y.Panitchob, Chalcogenide microsphere laser (paper in progress)

Y.Panitchob, G.S.Murugan, D.W.Hewak, G.R.Elliott, J.S.Wilkinson, M.N.Zervas, “Nd:BK7 microsphere laser” (paper in progress)

11 Appendix B - Microsphere production runs

	Glass					Equipment set up				Furnace		Gas flow		
ID	No.:	Type :	Crush me	Cleaned:	Sizes of particle	Top:	Tube i.d.:	Bottom:	Bubblers	Type :	Tempera	Gas:	in tube:	at nozzel through blower:
M001	LD984(2)	GLS	P/M	no	d<106um	bung	27mm	pipe and petri dish		silica	1300	N2	100mb	- -
M002	LD984(2)	GLS	P/M	no	d<106um	bung	27mm	pipe and petri dish		silica	1300	N2	100mb	- -
M003	LD984(2)	GLS	P/M	no	d<106um	bung	27mm	pipe and petri dish		silica	1300	N2	100mb	- -
M004	LD984(2)	GLS	P/M	no	d<106um	bung	27mm	pipe and petri dish		silica	1300	N2	100mb	- -
M005	LD984(2)	GLS	P/M	no	d<106um	bung	27mm	pipe and petri dish		silica	1300	N2	100mb	- -
M006a	LD984(2)	GLS	P/M	no	105um<d<150um	bung	27mm	pipe and petri dish		silica	1300	N2	100mb	- -
M006	LD984(2)	GLS	P/M	no	105um<d<150um	bung	27mm	pipe and petri dish		silica	1300	N2	100mb	- -
M007	LD984(2)	GLS	P/M	no	105um<d<150um	bung	27mm	pipe and petri dish		silica	1300	N2	100mb	- -
M008	LD984(2)	GLS	P/M	no	105um<d<150um	bung	27mm	pipe and petri dish		silica	1300	N2	100mb	- -
M009	LD984(2)	GLS	P/M	no	105um<d<150um	bung	27mm	pipe and petri dish		silica	1300	N2	100mb	- -
M010	LD984(2)	GLS	P/M	no	150um<d	bung	27mm	pipe and petri dish		silica	1500	N2	100mb	- -
M011	LD984(2)	GLS	P/M	no	150um<d	bung	27mm	pipe and petri dish		silica	1300	N2	100mb	- -
M012	LD984(2)	GLS	P/M	yes	53um<d<106um	bung	27mm	alu fitting		silica	1300	N2	100mb	- -
M013	LD984(2)	GLS	P/M	yes	106um<d<150	bung	27mm	alu fitting		silica	1300	N2	100mb	- -
M014	LD984(2)	GLS	P/M	yes	150um<d<300	bung	27mm	alu fitting		silica	1300	N2	100mb	- -
M015	LD984(2)	GLS	P/M	yes	300um<d<600	bung	27mm	alu fitting		silica	1300	N2	100mb	- -
M016	LD984(2)	GLS	P/M	yes	600um<d<1mm	bung	27mm	alu fitting		silica	1300	N2	100mb	- -
M017	LD984(2)	GLS	P/M	yes	150um<d<300	bung	27mm	alu fitting		silica	1600	N2	100mb	- -
M018	LD984(2)	GLS	P/M	yes	300um<d<600	bung	27mm	alu fitting		silica	1600	N2	100mb	- -
M019	LD984(2)	GLS	P/M	yes	1mm<d<2mm	pyrex	27mm	alu fitting		large bore	1200	N2	7lt/min	- -
M020	LD984(2)	GLS	P/M	yes	1mm<d<2mm	pyrex	27mm	alu fitting		large bore	1300	N2	7lt/min	- -
M021	LD984(2)	GLS	P/M	yes	600um<d<1mm	pyrex	27mm	alu fitting		large bore	1300	N2	7lt/min	- -
M022	LD984(2)	GLS	P/M	yes	600um<d<1mm	pyrex	27mm	alu fitting		large bore	1300	N2	4lt/min	- -
M023	LD984(2)	GLS	P/M	yes	600um<d<1mm	pyrex	27mm	alu fitting		large bore	1400	N2	4lt/min	- -
M024	LD984(2)	GLS	P/M	yes	300um<d<600um	pyrex	27mm	alu fitting		large bore	1400	N2	4lt/min	- -
M025	LD984(2)	GLS	P/M	yes	300um<d<600um	pyrex	27mm	alu fitting		large bore	1400	N2	4lt/min	- -
M026	LD984(2)	GLS	P/M	yes	150um<d<300um	pyrex	27mm	alu fitting		large bore	1400	N2	4lt/min	- -
M027	LD984(2)	GLS	P/M	yes	300um<d<600um	pyrex	27mm	alu fitting		large bore	1450	N2	4lt/min	- -
M028	LD984(2)	GLS	P/M	yes	300um<d<600um	pyrex	27mm	alu fitting		large bore	1500	N2	4lt/min	- -
M029	LD984(2)	GLS	P/M	yes	300um<d<600um	pyrex	27mm	alu fitting		large bore	1500	N2	2lt/min	- -
M030	LD984(2)	GLS	P/M	yes	300um<d<600um	pyrex	27mm	alu fitting		large bore	1550	N2	2lt/min	- -
M031	LD984(2)	GLS	P/M	yes	300um<d<600um	pyrex	27mm	alu fitting		large bore	1600	N2	2lt/min	- -
M032	LD984(2)	GLS	P/M	yes	600um<d<1mm	pyrex	27mm	alu fitting		large bore	1650	N2	2lt/min	- -
M033	LD984(2)	GLS	P/M	yes	600um<d<1mm	pyrex	27mm	alu fitting		large bore	1650	N2	2lt/min	- -
M034	LD984(2)	GLS	P/M	yes	300um<d<600um	pyrex	27mm	alu fitting		large bore	1650	N2	2lt/min	- -
M035	LD984(2)	GLS	P/M	yes	600um<d<1mm	pyrex	27mm	alu fitting		large bore	1675	N2	2lt/min	- -
M036	LD984(2)	GLS	P/M	yes	300um<d<600um	pyrex	27mm	alu fitting		large bore	1675	N2	2lt/min	- -
M037	LD984(2)	GLS	P/M	yes	600um<d<1mm	pyrex	27mm	alu fitting		large bore	1700	N2	2lt/min	- -
M038	LD1257(02)	V:GLS	P/M	yes	150um<d<300um	pyrex	27mm	alu fitting		silica	1300	N2	1lt/min	- -
M039	LD1257(02)	V:GLS	P/M	yes	53um<d<105um	pyrex	27mm	alu fitting		silica	1300	N2	1lt/min	- -
M040	LD1257(02)	V:GLS	P/M	yes	105um<d<150um	pyrex	27mm	alu fitting		silica	1300	N2	1lt/min	- -
M041	LD1257(02)	V:GLS	P/M	yes	105um<d<150um	pyrex	27mm	alu fitting		silica	1500	N2	1lt/min	- -
M042	LD1257(02)	V:GLS	P/M	yes	53um<d<105um	pyrex	27mm	alu fitting		silica	1500	N2	1lt/min	- -
M043	LD1257(02)	V:GLS	P/M	yes	150um<d<300um	pyrex	27mm	alu fitting		silica	1500	N2	1lt/min	- -
M044	LD1257(02)	V:GLS	P/M	yes	150um<d<300um	pyrex	27mm	alu fitting		silica	1500	N2	1lt/min	- -
M045	LD1257(02)	V:GLS	P/M	yes	150um<d<300um	pyrex	27mm	alu fitting		silica	1500	N2	1lt/min	- -
M046	LD1257(02)	V:GLS	P/M	yes	53um<d<105um	pyrex	27mm	alu fitting		silica	1500	N2	1lt/min	- -
M047	LD1257(02)	V:GLS	P/M	yes	53um<d<105um	pyrex	27mm	alu fitting		silica	1500	N2	1lt/min	- -
M048	LD1257(02)	V:GLS	P/M	yes	53um<d<105um	pyrex	27mm	alu fitting		silica	1500	N2	1lt/min	- -
M049	LD1257(02)	V:GLS	P/M	yes	53um<d<105um	pyrex	27mm	alu fitting		silica	1500	N2	1lt/min	- -
M050	LD1257(02)	V:GLS	P/M	yes	53um<d<105um	pyrex	27mm	alu fitting		silica	1500	N2	1lt/min	- -
M051	LD984(2)	GLS	P/M	yes	106um<d<150um	bung	27mm	pipe and petri dish		silica	1300	N2	100mb	- -
M051a	LD984(2)	GLS	P/M	yes	106um<d<150um	bung	27mm	pipe and petri dish		silica	1300	N2	100mb	- -
M052	LD1257(02)	V:GLS	P/M	yes	53um<d<105um	pyrex	27mm	alu fitting		silica	1500	N2	1lt/min	- -
M053	LD1257(02)	V:GLS	P/M	yes	53um<d<105um	pyrex	27mm	alu fitting		silica	1500	N2	1lt/min	- -
M054	LD1257(02)	V:GLS	P/M	yes	53um<d<105um	pyrex	27mm	alu fitting		silica	1500	N2	1lt/min	- -
M055	LD984(2)	GLS	P/M	yes	150<d<300	Egg timer 2	27mm	steel & PTFE		silica	1300	N2	1lt/min	- -
M056	LD984(2)	GLS	P/M	yes	106<d<150	Egg timer 2	27mm	steel & PTFE		silica	1300	N2	1lt/min	- -
M057	LD984(2)	GLS	P/M	yes	63<d<106	Egg timer 2	27mm	steel & PTFE		silica	1300	N2	1lt/min	- -
M058	LD984(2)	GLS	P/M	yes	53<d<63	Egg timer 2	27mm	steel & PTFE		silica	1300	N2	1lt/min	- -
M059	LD984(2)	GLS	P/M	yes	106<d<150	Egg timer 1	27mm	steel & PTFE		silica	1300	N2	1lt/min	- -
M060	LD984(2)	GLS	P/M	yes	106<d<150	Egg timer 1	27mm	steel & PTFE		silica	1300	N2	1lt/min	- -
M061	LD984(2)	GLS	P/M	yes	106<d<150	Egg timer 1	27mm	steel & PTFE		silica	1500	N2	1lt/min	- -
M062	LD984(2)	GLS	P/M	yes	150<d<300	Egg timer 2	27mm	steel & PTFE		silica	1500	N2	1lt/min	- -
M063	LD984(2)	GLS	P/M	yes	150<d<300	Egg timer 2	27mm	steel & PTFE		silica	1500	N2		0 - -
M064	LD571	Nd:GLSO	P/M	yes	150<d<300	Egg timer 2	27mm	steel & PTFE		silica	1500	N2	1lt/min	- -
M065	LD571	Nd:GLSO	P/M	yes	150<d<300	Egg timer 2	27mm	steel & PTFE		silica	1500	N2	1lt/min	- -
M066	LD571	Nd:GLSO	P/M	yes	106<d<150	Egg timer 2	27mm	steel & PTFE		silica	1500	N2	1lt/min	- -
M067	LD571	Nd:GLSO	P/M	yes	63<d<106	Egg timer 2	27mm	steel & PTFE		silica	1500	N2	1lt/min	- -
M068				yes	d<38	Egg timer 2	27mm	steel & PTFE		silica	1300	Ar	1lt/min	- -
M069				yes	d<38	Egg timer 2	27mm	steel & PTFE		silica	1300	Ar	1lt/min	- -

	Glass					Equipment set up				Furnace		Gas flow			
ID	No.:	Type :	Crush me	Cleaned:	Sizes of particle	Top:	Tube i.d.:	Bottom:	Bubblers	Type :	Tempera	Gas:	in tube:	at nozzel	through blower:
M070				yes	d<38	Egg timer 2	27mm	steel & PTFE		silica	1300	Ar	1lt/min	-	-
M071				yes	d<38	Egg timer 2	27mm	steel & PTFE		silica	1300	Ar	1lt/min	-	-
M072	LD1261(02)	GLSO	P/M Ball m	yes	20<d<10um	-	27mm	steel & PTFE		7m	1300	Ar	10 ltr/min	-	-
M073	LD1261(02)	GLSO	P/M Ball m	yes	20<d<10um	-	27mm	steel & PTFE		7m	1300	Ar	11 ltr/min	-	-
M074	LD1261(02)	GLSO	P/M Ball m	yes	20<d<10um	-	27mm	steel & PTFE		7m	1300	Ar	12 ltr/min	-	-
M075	LD1261(02)	GLSO	P/M Ball m	yes	20<d<10um	-	27mm	steel & PTFE		7m	1300	Ar	13 ltr/min	-	-
M076		GeS	CVD	yes	<300um	-	27mm			7m	1300	Ar	5	0.7	5
M077	LD1261(02)	GLSO	P/M Ball m	yes	35<d<53	glass	12mm	glass		diary box	1000	Ar	2x 1/2	-	-
M078	LD1261(02)	GLSO	P/M Ball m	yes	106<d<150		12mm	glass		diary box	1100	Ar	2x 1/3	-	-
M079				yes			12mm	glass				Ar		-	-
M080				yes		glass	12mm	glass			1100	Ar	5+full	-	-
M081	LD1261(02)	GLSO	P/M Ball m	yes	20>d>38	glass	12mm	glass			1100	Ar	5+full	-	-
M082	LD1261(02)	GLSO	P/M Ball m	yes	20>d>38	glass	12mm	glass			1100	Ar	5+full	-	-
M083	LD935	Er:GLS	P/M	yes	106>d>90	glass	12mm	glass			1100	Ar		-	-
M084	LD935	Er:GLS	P/M	yes	90>d>75	glass	12mm	glass			1100	Ar		-	-
M085	LD642	Nd GLS	P/M	yes	90>d>75	glass	12mm	glass			1100	Ar		-	-
M086	LD643	Nd GLS	P/M	yes	106>d>90	glass	12mm	glass			1100	Ar		-	-
M087	LD311	Pr,Ce:GLS	P/M	yes	106>d>90	glass w/tap	12mm	glass	empty	drop	1100	Ar	5ltr/min	0	1ltr/min
M088	LD311	Pr,Ce:GLS	P/M	yes	106>d>90	glass w/tap	12mm	glass	empty	drop	1100	Ar	0	0	0
M089	LD266	Tb	P/M	yes	106>d>90	glass w/tap	12mm	glass	empty	drop	1100	Ar	5ltr/min	0	1ltr/min
M090	LD1261(02)	GLSO	P/M	yes	106>d>63	glass w/tap	12mm	glass	empty	drop	1100	Ar	5ltr/min	0	1ltr/min
M091	LD1261(02)	GLSO	P/M	yes	106>d>63	glass w/tap	12mm	glass	empty	drop	1100	Ar	10ltr/min	0	1ltr/min
M092	LD1261(02)	GLSO	P/M	yes	106>d>63	glass w/tap	12mm	glass	empty	drop	1100	Ar	5ltr/min	0	1ltr/min
M093	LD1261(02)	GLSO	P/M	yes	106>d>90	glass w/tap	12mm	glass	empty	drop	1100	Ar	10ltr/min	0	1ltr/min
M094	LD1261(02)	GLSO	P/M	yes	106>d>90	glass w/tap	12mm	glass	empty	drop	1100	Ar	0	0	0
M095	LD266	Tb	P/M	yes	106>d>90	glass w/tap	12mm	glass	empty	drop	1100	Ar	1	0	1
M096	LD1261(02)	GLSO	P/M	yes	106>d>90	glass w/tap	12mm	glass	empty	drop	1000	Ar	10	0	1
M097	LD1261(02)	GLSO	P/M	yes	106>d>90	glass w/tap	12mm	glass	empty	drop	1200	Ar	10	0	1
M098	LD311	Pr,Ce:GLS	P/M	yes	106>d>90	glass w/tap	12mm	glass	empty	drop	1100	Ar	1	0	1
M099	LD311	Pr,Ce:GLS	P/M	yes	106>d>90	glass w/tap	12mm	glass	empty	drop	1100	Ar	0.5	0	0.5
M100	LD1261(02)	GLSO	P/M	yes	35<d<53	pointy	12mm	glass	empty	blow	1100	Ar	7	1.2	2
M101	LD1261(02)	GLSO	P/M	yes	35<d<53	tap	12mm	glass	empty	blow	1100	Ar	2	1.2	2
M102	LD1261(02)	GLSO	P/M	yes	35<d<53	tap	12mm	glass	empty	blow	1100	Ar	5	1.2	5
M103	LD1261(02)	GLSO	P/M	yes	35<d<53	tap	12mm	glass	empty	blow	1100	Ar	5	1.2	10
M104	LD1261(02)	GLSO	P/M	yes	35<d<53	tap	12mm	glass	empty	blow	1100	Ar	5	1.2	10
M105	LD1261(02)	GLSO	P/M	yes	35<d<53	tap	12mm	glass	empty	blow	1000	Ar	5	1.2	5
M106	LD1261(02)	GLSO	P/M	yes	35<d<53	tap	12mm	glass	empty	blow	1200	Ar	5	1.2	5
M107	LD1261(02)	GLSO	P/M	yes	35<d<53	tap	12mm	glass	empty	blow	900	Ar	5	1.2	5
M108	LD1261(02)	GLSO	P/M	yes	35<d<53	tap	12mm	glass	empty	blow	1300	Ar	5	1.2	5
M109			ball milled	no		tap	12mm	glass	empty	blow	1100	Ar	5	1	5
M110	Nd:BK7	Nd:BK7	P/M	yes	100	tap	12mm	glass	empty	drop	1250	Ar		0	2/0
M111	Nd:BK7	Nd:BK7	P/M	yes	35-100	tap	12mm	glass	empty	blow	1200	Ar		1.2	10
M112	LF319	GLSO	P/M	yes	20-35	tap	12mm	glass	empty	blow	1100	Ar	5	1	5
M113	LF319	GLSO	P/M	yes	20-35	tap	12mm	glass	empty	blow	1100	Ar	5	1	10
M114	LF319	GLSO	P/M	yes	20-35	tap	12mm	glass	empty	blow	1200	Ar	5	1	10
M115	LF319	GLSO	P/M	yes	20-35	tap	12mm	glass	empty	blow	1200	Ar	5	0.6	10
M116	Nd:BK7	Nd:BK7	P/M	yes	100	tap	12mm	glass	n	drop	1250	Ar	5	-	1
M116/2	Nd:BK7	Nd:BK7	P/M	yes	100	tap	12mm	glass	n	drop	1250	Ar	5	-	2
M117	LF319	GLSO	P/M	yes	20-35	-	5mm	-	e	blow	1150	Ar	5	1.1	2
M118	LF319	GLSO	P/M	yes	20-35	-	5mm	-	2+1	blow	1150	Ar	5	1.1	2
M119	LF319	GLSO	P/M	yes	20-35	-	5mm	-	2+2	blow	1100	Ar	5	1.1	2
M120	LF319	GLSO	P/M	yes	0-		5mm		1+1	blow	1100	Ar	5	1.1	2
M121	Nd:BK7	Nd:BK7	P/M	yes	100	tap	12mm	glass	n	drop	1250	Ar	1	-	1
M122	LF319	GLSO	P/M	yes	20-35	-	5mm	-	1+1	blow	1100	Ar	1	1	5
M123	LF319	GLSO	P/M	yes	20-35	-	5mm	-	1+1	blow	1200	Ar	1	1	2
M124	LF319	GLSO	P/M	yes	20-35	-	5mm	-	1+1	blow	1000	Ar	1	1	2
M125	LF319	GLSO	P/M	yes	20-35	-	5mm	-	1+1	blow	900	Ar	1	1	2
M126	LD1261(02)	GLSO	P/M	yes	35<d<53	-	5mm	-	2 empty	blow	1100	Ar	2	1.2	2
M127	Nd:BK7	Nd:BK7	P/M	yes	30-100	tap	12mm	glass	n	drop	1250	Ar	1	-	1
M128	LF319	GLSO	P/M	yes	20-35	-	5mm	-	1+1	blow	1100	Ar	1	1	1
M129	LF319	GLSO	P/M	yes	20-35	-	5mm	-	1+1	blow	1100	Ar	1	1	3
M130		GLSO	P/M	yes	125-150	tap	12mm	glass	n	d	1200	Ar	5	-	5
M131	LF319	GLSO	P/M	yes	20-35	-	5mm	-	1+1	blow	1200	Ar	1	1	3
M132	LF319	GLSO	P/M	yes	20-35	-	5mm	-	1+1	blow	1200	Ar	1	1	4
M133	Ld165	Nd:GLS	P/M	yes	106-125	tap	12mm	glass	n	d	1150	Ar	5	-	0
M134	ld634	Nd:GLS	P/M	yes	125-150	tap	12mm	glass	n	d	1151	Ar	5	-	0
M135	ld634	Nd:GLS	P/M	yes	125-150	tap	12mm	glass	n	d	1151	Ar	5	1	0
M136		Nd:BK7	P/M	yes	30-100	yes	12mm	glass	yes	d	1250	Ar	5	0	1